In vivo characterization of the mammalian AlkB homologues ALKBH1 and ALKBH4

Anja Nilsen

Thesis for the degree of Philosophia Doctor (PhD)

Supervisor: Professor Arne Klungland
Co-supervisor: Magnar Bjørås

Clinic for Diagnostics and Intervention, Institute of Medical Microbiology,
Oslo University Hospital – Rikshospitalet,
University of Oslo, Norway 2013

Acknowledgements

The work presented in this doctoral thesis has been performed at the Clinic for Diagnostics and Intervention and the Institute of Medical Microbiology at Oslo University Hospital, Rikshospitalet. Financial support has been granted by the University of Oslo (MLS^{UiO} Molecular Life Science) and Oslo University Hospital.

I wish to express my gratitude to my supervisor, Professor Arne Klungland, for letting me be a part of his research group. I appreciate the support and freedom to pursue my own ideas and development of projects during my time as a PhD-student. I am also very thankful for the opportunity to participate in international conferences and meetings and for being able to have a (rather unconventional) research stay at Yungui Yang's lab in Beijing. I would also like to thank my co-supervisor, Professor Magnar Bjørås, for creating an inclusive and supportive work environment, both scientifically and socially, in the department.

I am very grateful to all the co-authors of the papers included in this thesis. Thanks to Professor Yungui Yang and his research group in Beijing for being the driving force behind much of the work. Big thanks to Dr. Markus Fusser for being a great colleague on the ALKBH4-project and for useful discussions and critical reading during the preparation of manuscripts and thesis. Additionally, I would like to thank Dr. Peter Fedorcsák for being very enthusiastic and helpful with analyses and manuscript preparations. Thanks to Hege Wiksén, Linda Tveterås and Guro F. Lien for valuable technical help.

I am also grateful to all the former and present members of the Klungland group, as well as members of the other groups in the lab for help and support. Especially, I would like to thank "B-gjengen". You are the people who have made getting to work a pleasure by being so ever helpful and creating a great working and social atmosphere. The daily "lunch quiz" has been a highlight☺.

Last, but not least, I am forever grateful for all the support, love and patience from my family Andreas, Sondre and Marie.

Oslo, 2013

Anja Nilsen

Table of Contents

List of papers

This thesis is based on the following papers, which will be referred to by the following Roman numbers:

I Li MM*, Nilsen A*, Shi Y*, Fusser M, Ding YH, Fu Y, Liu B, Niu Y, Wu YS, Huang CM,Olofsson M, Jin KX, Lv Y, Xu XZ, He C, Dong MQ, Rendtlew Danielsen JM, Klungland A,Yang YG, ALKBH4-dependent demethylation of actin regulates actomyosin dynamics. *Nat Commun*, 4, 1832 (2013)
* shared first authorship

II Nilsen A, Gregains G, Fusser M, Fedorcsak PZ, Klungland A, ALKBH4 depletion in male germ cells leads to spermatogenic defects. Manuscript.

III Nordstrand LM, Svärd J[#], Larsen E[#], Nilsen A[#], Ougland R[#], Furu K[#], Lien GF, Rognes T, Namekawa SH, Lee JT, Klungland A, Mice lacking Alkbh1 display sex-ratio distortion and unilateral eye defects. *PLoS ONE* 5, e13827 (2010).
[#] shared 2nd authorship

Abbreviations and glossary

1meA	1-methyladenine
2OG	2-oxoglutarate
3meC	3-methylcytosine
3meU	3-methyluridine
6meA	6-methyladenine
ADP	adenosine-di-phosphate
AP	apurine/apyrimidine
ARP	actin related protein
ATP	adenosine-tri-phosphate
BMP	bone morphogenetic protein
BrdU	5-bromo-2-deoxyuridine
chromatin	complex of DNA and histone units (nucleosomes) that forms chromosomes within the nucleus of eucaryotic cells.
DAPI	diamidino-2-phenylindole
DNA	deoxyribonucleicacid
dsDNA	double-stranded DNA
ectoderm	one of the three primary germ cell layers in the early embryo. Differentiates to form the epidermis and nervous tissue.
Er-α	estrogen receptor α
ESC	embryonic stem cell
e.g.	exempli gratia
F-actin	filametous actin
fibroblast	cell of the connective tissue. Synthesize extracellular matrix and collagen.
FTO	fat mass and obesity associated protein
G-actin	globular actin
GFP	green fluorescent protein
GTP	guanosine triphosphate
histone	small, basic eucaryotic proteins that package and order DNA into structures called nucleosomes
Hsp70	heat shock protein 70
JHDM	JmjC-domain containing histone demethylase
JmjC	jumonji-domain containing
mcm5U	5-methoxycarbonylmethyluridine
mcmhm5U	5-methoxycarbonylhydroxymethyluridine
MEF	mouse embryonic fibroblast
MHC	myosin heavy chain
MLC	myosin light chain
MMS	methyl methane sulphonate
mRNA	mesenger RNA
MSUC	meiotic silencing of unsynapsed chromosomes
MSYq	male-specific region of the mouse Y chromosome long arm
MT	methyl transferase
myoblast	embryonic precursor of a muscle cell
NF-kappaB	nuclear factor kappa-light-chain-enhancer of activated B cells
NMI	non-muscular myosin I

NMII	non-muscular myosin II
NOR	nucleolar organizing regions
Nuclear speckles	small subnuclear structures, also called the splicing factor (SF) compartments in the nucleoplasm of mammalian cells with factors that participate in transcription and pre-mRNA processing.
Nucleolus	structure found in the nucleus of cells composed of proteins and nucleic acids. Its function is ribosomal RNA (rRNA) transcriprion and assemblage.
p53	protein 53/ tumor protein 53
PHMT	Protein histidine methyltransferase
pI	isoelectric point
piRNA	PIWI-interacting RNA
PKDM	protein lysine demethylases
PKMT	protein lysine methyltransferases
polygeny	more than one gene affects a given trait
protamines	small, nuclear proteins that replace histones during spermiogenesis.
PTM	post-translational modifications
RhoA	Ras homolog gene family, member A
RNA	ribonucleic acid
RRM	RNA recognition motif
S.pombe	*Schizosaccharomyces pombe*
SAM	S-adenosyl methionine
SC	synaptonemal complex
ssDNA	single-stranded DNA
SUMO	Small Ubiquitin-like Modifier
SYCP3	synaptonemal complex protein 3
TEX14	testis expressed gene 14
tRNA	transfer RNA
trophectoderm	outer layer of the developing blastocyst that will ultimately form the embryonic side of the placenta.
XY-body	structure found in male mammalian spermatocyte containing unpaired sex chromosomes that has become densely heterochromatic.
yH2A.x	H2A histone family, member X, phosphorylated on serine 139

Summary

The *E.coli* DNA repair enzyme AlkB acts by hydroxylating methyl lesions in DNA, such as 1-methylAdenine (1meA) and 3-methylCytosine (3meC), which leads to spontaneous loss of the hydroxymethyl group and recovery of the correct base. Nine different mammalian AlkB homologues have been identified. These proteins belong to the superfamily of 2-oxoglutarate and Fe^{2+}-dependent dioxygenases which include numerous members with a broad assortment of substrates. The aim of this study was to uncover the biological properties of the mammalian *E.coli* AlkB homologues ALKBH1 and ALKBH4.

In paper I we present the first *Alkbh4* knockout mouse. *Alkbh4*$^{-/-}$ mice display embryonic lethality at an early preimplantation stage, and siRNA or Cre-mediated induced ALKBH4 depletion in cell culture results in apoptosis, cytokinesis failure and reduced cell mobility. We provide evidence that ALKBH4 is required for the reversion of mono-methyl modifications on actin lysine-84 (K84me1). ALKBH4 interacts with methylated lysine-84 in actin, and depletion of ALKBH4 in cell culture based studies lead to an increase in the level of actin-K84me1. Methylated K84 is most abundant in F-actin, and when actin-K84 is methylated, the non-muscular myosin II (NMII) displays less ability to bind actin filaments. Based on these findings, we propose a role for ALKBH4 in the regulation of actomyosin dynamics by demethylating actin-K84me1.

In paper II, we investigate the physiological role of ALKBH4 in mice using a tamoxifen-inducible Cre-mediated *Alkbh4* knockout mice to circumvent embryonic lethality. Surprisingly, the ALKBH4 depleted mice displayed overall similar phenotype as the control animals used in this study, except for a striking failure in the development of promeiotic spermatocytes from the pachytene stage and on.

To investigate the role of ALKBH1, we generated mice lacking ALKBH1 by homologous recombination as described in paper III. Lack of ALKBH1 leads to reduced viability during embryonic development, improper development of tissues originating from the ectodermal lineage, sex-ratio distortions and apoptotic haploid cell types in *Alkbh1*$^{-/-}$ testes.

1. Introduction

1.1 *E.coli* AlkB

The first report about the *Escherichia coli* (*E.coli*) gene *alkB* was published 30 years ago. This study showed that *alkB* mutants were sensitive to the methylating agent methyl methane sulphonate (MMS) (Kataoka et al., 1983). However, the enzymatic mechanism of the *alkB* gene product, AlkB, remained unknown for almost 20 years until it was classified as a member of the 2-oxoglutarate (2OG)-Fe^{2+}-dependent dioxygenase superfamily (Aravind and Koonin, 2001). These enzymes use an active iron–oxo intermediate to hydroxylate their prime substrate and they catalyze a wide range of biological oxidations. They use 2OG, which gets decarboxylated yielding succinate and CO_2, as a co-factor (Hausinger, 2004). AlkB was found to catalyze the direct reversion of primarily 1meA and 3meC in DNA to adenine and cytosine by oxidative demethylation, which is a mode of DNA repair (figure 1, upper panel). The hydroxymethylated intermediates decompose to yield formaldehyde, thus restoring the correct bases (Falnes et al., 2002; Trewick et al., 2002). In addition, *E.coli* AlkB can remove methyl lesions in RNA (Aas et al., 2003).

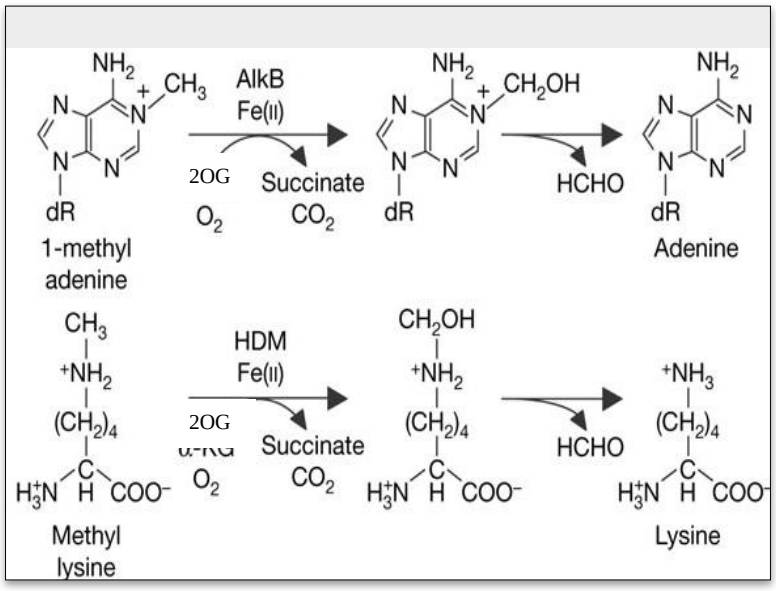

Figure 1. The AlkB mechanism. Upper panel, Hydroxylation of 1meA by AlkB requires O_2, 2OG and Fe^{2+}, and generates CO_2 and succinate. One oxygen atom is transferred to 2OG, which generates succinate and CO_2. The second oxygen atom is transferred to the target substrate. Hydroxylated methyl groups are released as formaldehyde. Lower panel, The AlkB mechanism is utilized by the JHDMs for methyl-lysine demethylation of histones. (Figure adapted from Tsukada et al., 2006).

The similarity between the chemistry of removing a methyl group from 1meA and methyl-lysine (figure 1, lower panel) made Tsukada *et al* to test whether a similar mechanism could be used in histone lysine demethylation. Indeed, they found that Jumonji (JmjC)-domain containing histone demethylases (JHDMs) could catalyze the

equivalent oxidative demethylation mechanism on methylated histones (Tsukada et al., 2006). Thus, the AlkB mechanism is also required for epigenetic regulation.

1.2 Mammalian AlkB homologues

Nine different mammalian AlkB homologues, ALKBH1-8 and the somewhat more distant family member FTO (fat mass and obesity associated protein), have been identified through bioinformatical homology searches (Kurowski et al, 2003; Gerken et al., 2007; figure 2).

Like the *E.coli* AlkB, ALKBH2 and ALKBH3 are DNA repair enzymes that demethylate 1meA and 3meC lesions in nucleic acids (Aas et al., 2003; Ringvoll et al., 2006; Duncan et al., 2002). ALKBH2 exhibit activity on DNA as substrate backbone**,** preferentially on double stranded DNA (dsDNA) (Aas et al, 2003; Falnes et al., 2004). It localizes to the nucleus, and accumulates at replication foci (Aas et al, 2003). ALKBH3 prefers ssDNA and RNA as substrate backbone, and it is evenly distributed in both the nucleus and the cytoplasm (Aas et al, 2003). Mice lacking *Alkbh2* and/or *Alkbh3* are viable and with no apparent phenotype. Yet, *Alkbh2*$^{-/-}$ mice display higher levels of 1meA in genomic DNA, suggesting that this lesion is the main target of ALKBH2 (Ringvoll et al., 2006). *Alkbh3*$^{-/-}$ mice did not display any accumulation of 1meA (Ringvoll et al., 2006). Expression of ALKBH2 and -3 are affected in various human cancers/tumors. Down-regulation of ALKBH2 increases sensitivity towards chemotherapy of non-small cell lung cancer cell lines (Wu et al., 2011). Decreased levels of ALKBH2 have been found in brain tumors and gastric cancers (Gao et al., 2011; Cetica et al., 2009). Aberrant ALKBH3 expression have been found in non-small-cell-lung cancer (Tasaki et al., 2011), rectal carcinoma (Choi et al., 2011) and brain tumors (Cetica et al., 2009).

Recently, ALKBH5 has been shown to remove the methyl group of 6-methyladenine (6meA) from messenger RNA (mRNA) both *in vitro* and *in vivo* (Zheng et al., 2013). 6meA is the most prevalent internal modification of mRNA in mammals (Dominissini et al., 2012). The ALKBH5 protein co-localizes with nuclear speckles where pre-mRNA processing occurs. It is also involved in mRNA export regulation, in which its demethylation activity seems to play an important role. *Alkbh5* knockout mice display impaired male fertility due to compromised spermatogenesis (Zheng et al., 2013).

FTO, as ALKBH5, is an oxidative demethylase targeting the 6mA residues in RNA *in vitro* (Jia et al., 2011). Nevertheless, *in vivo* studies in *Fto*$^{-/-}$ mice have failed to identify increased levels of 6meA. On the contrary, increased ratio of 3-methyl Uracil/Uracil in total RNA from brains was identified (Berulava et al., 2012), suggesting that FTO has multiple RNA substrates. FTO co-localizes with nuclear speckles and probably associates with nuclear pre-mRNA splicing components (Jia et al., 2008). Mice lacking the *Fto* gene display growth retardation, loss of white adipose tissue and increased energy metabolism (Wu, Q. et al., 2010). On the contrary, overexpression of FTO in mice leads to obesity (Church et al., 2010). Similarly, epidemiological studies have established a strong link between certain human FTO variants and obesity (Kilpelainen et al., 2011).

The target substrates of ALKBH6 and ALKBH7 are still unknown. GFP-tagged ALKBH6 fusion proteins show both nuclear and cytoplasmic localization (Tsujikawa et al., 2007). ALKBH7 has been shown to localize to the mitochondria (Solberg et al., 2013; Fu et al., 2013). *Alkbh7*$^{-/-}$ mice have dramatically increased body weight and body fat. There are indications that ALKBH7, directly or indirectly, facilitates the utilization of short-chain fatty acids, which may cause the obesity phenotype (Solberg et al., 2013).

The ALKBH8 protein differs from the other known AlkB homologues due to the fusion of a RNA recognition motif (RRM) and a S-adenosyl-L-methionine (SAM)-dependent methyltransferase (MT) motif to the AlkB domain (see figure 2). It has been shown that ALKBH8 is required for biogenesis of tRNAs that contain 5-methoxycarbonylmethyluridine (mcm^{5}U) in the wobble position, which is required for selenoprotein synthesis (Songe-Moller et al., 2010; van den Born et al., 2011; Fu, D. et al., 2010). The AlkB domain hydroxylates mcm^{5}U into (S)-mchm^{5}U in tRNA (Fu, Y. et al., 2010). *Alkbh8* mutant mice are viable with no apparent phenotype, but have a reduced level of selenoproteins (Songe-Moller et al., 2010). Increased levels of ALKBH8 have been found in urothelial cancers (Shimada et al., 2009).

E.coli AlkB, ALKBH2, 3, 5 and 8 have all a relatively high pI (isoelectric point), positively charged surfaces (figure 2), and they act on nucleic acids. It then seems plausible that the high pI of ALKBH6 could indicate a role in nucleotide/nucleic acid repair or modification (Sedgwick et al., 2006). Based on the low pI of ALKBH1, 4 and 7, an association with nucleic acids cannot be predicted,

indicating that proteins are the main target. ALKBH1 and ALKBH4 will be described in more detail in the following chapters.

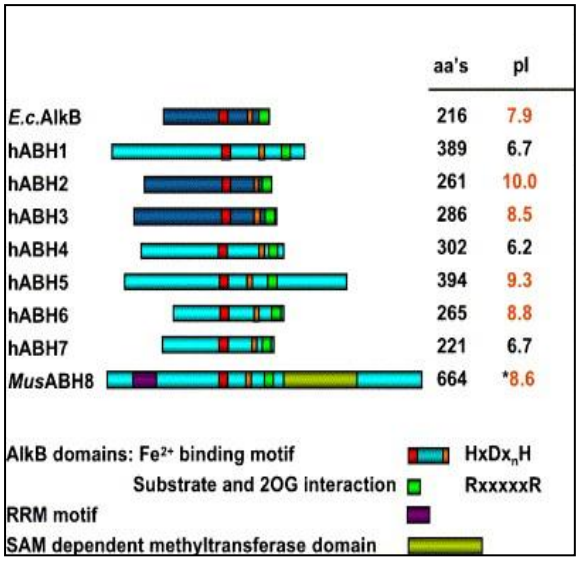

Figure 2. Human AlkB homologues. Sequence homology searches and predicted protein fold analyses revealed members of the mammalian AlkB homologue family. Motifs for Fe2+ binding and substrate interaction are indicated. ALKBH8 also contains a DNA/RNA recognition motif (RRM) and a S-adenosyl-L-methionine (SAM)-dependent methyltranferase domain. pI, isoelectric point. FTO is not included in this overview, as it was first described late in 2007 (Gerken, et al., 2007). Figure adapted from (Sedgwick et al., 2007).

1.2.1 ALKBH1

The first mammalian AlkB homologue to be identified was ALKBH1. It was reported that a methyl-methane-sulphonate-exposed *E.coli alkB* mutant could be partially rescued by over-expression of ALKBH1 (Wei et al., 1996). However, this *in vivo* DNA-repair activity could not be reproduced by others (Aas et al., 2003; Falnes et al., 2004). It has been reported that ALKBH1*in vitro* can repair 3meC in ssDNA and RNA (Westbye et al., 2008). However, several other studies demonstrate no such activity on any DNA or RNA substrate (Duncan et al., 2002; Falnes et al., 2004; Lee et al., 2005). Two reports by Muller *et al* show that ALKBH1 possess apurinic/apyrimidinic (AP) lyase activity, cleaving DNA at abasic sites (Muller et al., 2010; Muller et al., 2013). This activity is not dependent on the co-substrates 2OG and Fe^{2+} and is not affected by mutation of the putative metal binding motif, indicating that the lyase activity of ALKBH1 is dependent on a different active site than the one that executes hydroxylation (Muller et al., 2010). There are also some conflicting reports about the intracellular localization of ALKBH1. Westbye *et al* found ALKBH1 to localize predominantly in the mitochondria of HeLa cell line (Westbye et al., 2008), while other studies report nuclear localization (Pan et al., 2008; Ougland et al., 2012).

In 2008, the first report describing ALKBH1-null mice was published. In this study ALKBH1 was identified predominantly on nuclear euchromatin, and found to interact with Mrj, a histone binding protein which recruits class II histone

deacetylases (HDACs). In addition, this report describes intra-utreine growth retardation and dysregulation of trophoblast marker genes in the developing placenta in ALKBH1 null mice (Pan et al., 2008).

Ougland *et al* established embryonic stem cells (ESCs) from another *Alkbh1* knock-out mouse strain (described in paper III). They report higher expression of the pluripotency factors OCT4, NANOG and SOX2 and delayed differentiation to neural progenitor cells from *Alkbh1*$^{-/-}$ ESCs. In the same report, ALKBH1 is shown to be involved in the demethylation of a novel methyl group on histone H2A (Ougland et al., 2012). In addition, in *S.pombe*, two studies have identified histone H2A dioxygenase activity for Ofd2, a close relative to ALKBH1 (Korvald et al., 2011; Lando et al., 2012).

1.2.2 ALKBH4

So far, there is limited information on the biochemical, physiological and cellular functions of ALKBH4. The sub-cellular localization of ectopically expressed GFP-tagged ALKBH4 fusion proteins has been analyzed, and ALKBH4 is found to localize to both the nucleus, particularly in nucleoli, and the cytoplasm (Tsujikawa et al., 2007; Bjornstad et al., 2012). Expression data based on microarrays show ubiquitous expression of ALKBH4 in mouse organs, and elevated expression in testis and T-cells (GeneExpressionAtlas:www.ebi.ac.uk/gxa/gene/ENSMUSG00000039754). One report describes ALKBH4 interactions with the proteins AF9, ENL and p300, which are proteins associated with transcription and chromatin regulation (Bjornstad et al., 2012).

The potential of ALKBH4 for decarboxylation has also been published. Here, ALKBH4 was identified as a true 2OG/Fe^{2+} dioxygenase, due to its ability to utilize the co-substrate 2OG and O_2 to succinate and CO_2 in the presence of Fe^{2+} (uncoupled reaction), but the prime substrate was not identified (Bjornstad et al., 2011). In this study the predicted 2OG and Fe^{2+} binding motif of ALKBH4, His169-Asp171-His254 (HDH), was found to be required for Fe^{2+} binding and decarboxylation activity (Bjornstad et al., 2011). Other attempts to identify the prime substrate of ALKBH4 have failed (Lee et al., 2005). We find that ALKBH4 is required for demethylation of actin-K84me1 (Paper I).

1.3 Actin

Actin and actin dynamics have been extensively studied for many years, but there are still several aspects that remain to be clarified. Actins are essential components of the cytoskeleton and play critical roles in a wide range of cellular processes, including cytokinesis, cell migration, regulation of transcription, cell shape, vehicle and organelle movement, and cell junctions.

In vertebrates there are six highly conserved actin isoforms (Rubenstein, 1990). Four of these are primarily expressed in striated ($\alpha_{skeletal}$ and $\alpha_{cardiac}$) and smooth (α_{smooth} and γ_{smooth}) muscle cells, and the two cytoplasmic β-actin and γ-actin isoforms are ubiquitously expressed (Rubenstein, 1990). Actin isoforms differ only by a few amino acids, with most of the variations occurring at the N-terminus (Herman, 1993).

Actin belongs to a structural superfamily with sugar kinases, hexokinases and heat-shock 70 (Hsp70) proteins (Bork et al., 1992). Common for these proteins, in addition to structural similarity, is the catalysis of ATP to ADP + γ-phoshate coupled to conformational changes in two subdomains of the protein (Hurley, 1996). In actin, two clefts are formed between the two subdomains. The upper cleft contains the nucleotide binding site, and the lower is called the target binding cleft and makes up the contact point between actin subunits in filaments/polymers (Oda, 2009). Actin participates in more protein-protein interactions than any known protein and is able to convert between monomeric (G-actin) and filamentous (F-actin) states under the control of ATP-hydrolysis and a large number of actin-binding proteins (Domingues and Holmes, 2011). G-actin is, compared to F-actin, not an effective ATPase, and nucleotide hydrolysis by F-actin is one of the main factors regulating the G-actin to F-actin transition. G-actin join the growing barbed (+) end of the filament in the ATP state, hydrolysis takes place in the filament, and ADP-actin monomers dissociate from the pointed (-) end. This mechanism of actin polymerization/depolymerisation is known as actin filament treadmilling (Wegner and Isenberg, 1983), and the dynamics of filament assembly observed in cells are regulated by many actin binding proteins (Pollard and Borisey, 2003). Also, post-translational modifications (PTMs) have been identified in actin, and several are involved in regulation of important cellular events (Terman and Kashini, 2013). Homozygous β-actin knock-out mice display embryonic lethality (Shawlot et al., 1998; Bunnell et al., 2011), and cytoplasmic γ-actin knock-

out mice show reduced viability (Bunnell and Ervasti, 2010). No homozygous actin deletions or nonsense mutations has been described in humans, probably because, like in mice, such deletions or mutations would be lethal. However, several missense mutations in the actin genes have been associated with human diseases including cardiovascular diseases, myopathy, mental retardation and developmental malformations (Mogensen et al., 1999; van Wijk et al., 2003; Procaccio et al., 2006). In mice, mutations in actin coding genes have also been associated with tumourigenesis and metastasis (Taniguchi et al., 1986).

1.3.1 The actomyosin interaction and contraction

Actin-myosin is one of the most studied protein-protein interactions. Myosins are responsible for many motile processes in eukaryotes, and their role in muscle contraction is well studied (Cooke, 1997). However, there are at least 19 classes of myosins with a huge diversity of structures and mechanochemical properties (Hodge and Cope, 2000; Berg et al., 2001). Myosins produce force and displacement through their interaction with F-actin, which act as "tracks" for myosin-driven motility. The system of actin and myosin working together is referred to as actomyosin. Nonmuscle myosins (class II myosins, NMII) are found in both muscle and non-muscle cells, and are involved in cytokinesis, cell motility and formation of cell polarity and shape through the actin-myosin cytoskeleton (Sellers, 2000). Ablation of NMII in mice results in embryonic lethality (Conti et al., 2004; Tullio et al., 1997; Tullio et al., 2001).

Myosin II molecules are composed of myosin II heavy chain (MHC) dimers and two pairs of myosin light chains (MLCs), called the essential and the regulatory MLC (figure 3). The head region of myosin binds reversibly to actin filaments, and hydrolyzes ATP when activated by actin, which converts chemical energy into mechanical force and movement (Clark et al., 2007). Actomyosin contractility results from the action of myosin II motors connected with bundles of actin filaments. Myosin II motors attach and detach from actin filaments in a cyclic manner (Jay et al., 1995). The myosin motor undergoes a conformational change during attachment which is tightly coupled to ATP-hydrolysis that moves the motor along the filament and generates a displacement of the actin filament. One single myosin II molecule is not sufficient for motility but their assembly into mini-filaments, by their rod portion, converts them into processive motor complexes (figure 3; Clark et al., 2007).

The myosin head interacts with four regions on the target binding sub-domain in actin, region 1 involving residues (1-4, 24-25, 99-100, 144), region 2 involving residues 339-354, region 3 with residues 145-148 and 332-227, and region 4 with the residues 79-92 (Schroder et al., 1993).

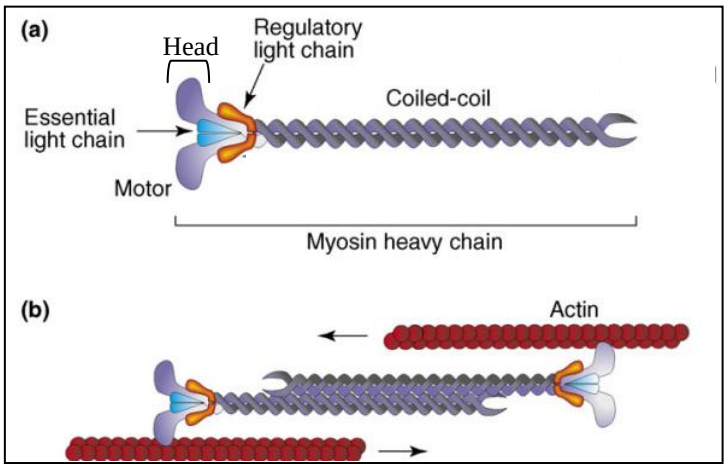

Figure 3. Myosin II and the actomyosin interaction.
(a) Schematic diagram of a myosin II monomer, showing the light and heavy chains.
(b) Myosin II assembles into bipolar filaments at the C-terminus; the N-terminus binds to actin filaments. Activation of the myosin II motor domain leads to the pulling of actin filaments (in the direction of the arrows) to make tension/ contraction (Figure adapted from Clark et al., 2007).

1.3.2 Actomyosin's involvement in cytokinesis and migration

Cytokinesis is the final step in cell division. The process begins during chromosome segregation, when the ingressing cleavage furrow begins to divide the cytoplasm between the developing daughter cells. Simplified, the cytokinesis-process in animal cells uses a contractile ring of actin filaments and NMII to constrict a cleavage furrow. However, the molecular mechanisms of marking the cleavage site and the assembly and organization of the contractile ring are complex, and many aspects of these mechanisms are still unknown (Barr and Gruneberg, 2007; Steigemann and Gerlich, 2009).

The mitotic spindle-machinery communicates with the cell cortex via Rho GTPase-mediated (RhoA) signal transduction pathways to activate the assembly and constriction of the actomyosin contractile ring at the cell equator (Piekny et al., 2005). Anillin is a protein that is highly concentrated in the cleavage furrow in animal cells. It is a scaffold protein that links RhoA, actin and myosin during cytokinesis (Piekny et al., 2008). NMII concentrates in spots, followed by assembly of actin filaments by formin proteins around the equatorial cell cortex at the site of the emerging cleavage furrow (Zhou and Wang, 2008). NMII applies force to these filaments to assemble the

ring (Vavylonis et al., 2008). In animal cells, contractile ring actin filaments have mixed polarities and thus are oriented in both directions in small bundles around the ring (Sanger and Sanger, 1980; Maupin and Pollard, 1986). NMII interaction with antiparallell actin filaments could constrict the contractile ring by a sliding filament mechanism similar to muscle constriction. The actin filaments probably depolymerize as the contractile ring constricts, because the contractile ring decreases in volume as the cytokinesis progresses (Wu and Pollard, 2005), but little is known about the mechanisms that trigger constriction and coordinate the removal of actin and associated proteins from contractile rings as they constrict. A simplified schematic of the postulated organization of the contractile ring is presented in Figure 4. Myosin-II relocates away from the intercellular bridge and F-actin abundance drops when the furrow has ingressed (Sanger et al., 1989), and as the abscission occurs significantly later this is probably achieved via an F-actin independent mechanism (Schweitzer and Souza-Schorey, 2004). In fact, successful abscission requires a cleavage site free of F-actin (Emoto et al., 1996; Emoto and Umeda, 2000; Emoto et al., 2005). Cytokinesis is a highly regulated and complex process, and it is not surprising that cytokinesis can sometimes fail. Cytokinesis failure may lead to both centrosome amplification and production of tetraploid cells (Normand and King, 2010).

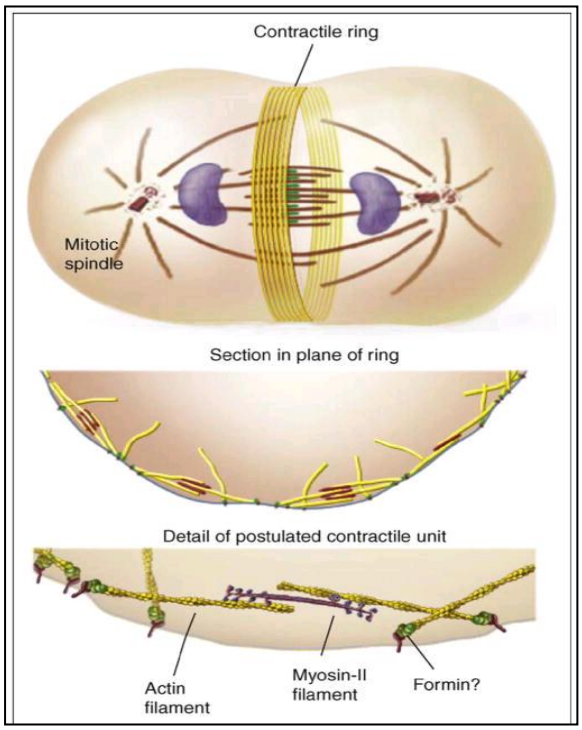

Figure 4. Schematic of the organization of contractile rings (simplified). As myosin-II walks toward the barbed end on an actin filament it applies tension to the plasma membrane (Figure adapted from Pollard, 2010).

Actomyosin dynamics are also essential for cell migration, a central feature for animal cells. Cells of the immune system migrate to find and destroy pathogens and during embryonic development some cells migrate to different locations in the developing body. Cancer cells use similar mechanisms to spread through the body (Vicente-Manzanares et al., 2005).

Assembly of actin filaments can modify the shape of the cell and generate a protrusion, which is often the first step in cell migration. A simplified schematic of actin filament organization in a migrating fibroblast is presented in figure 5. Protrusions generally contain two actin based structures: the lamellipodium and the lamellum (Heath and Holifield, 1991). The actin nucleator Arp2/3 generates the highly dynamic lamellipodium in the leading edge of a migrating cell by assembling a network of short, branched/dendritic actin filaments (Pollard and Borisy, 2003). The network of branched filaments disappears in the lamellipodial-lamellar interface a short distance behind the plasma membrane where the first stable/strong adhesion to the substratum occurs (Gupton and Waterman-Storer, 2006). The lamellar actin filaments are extending from the lamellipodium to the cell body. NMII is not located in, nor seem to play a part in the physical organization of the lamellipodium, but it can affect the rate of cellular protrusion (Vicente-Manzanares et al., 2007; Ponti et al., 2004; Cai et al., 2006). The role of NMII in protrusion formation is probably generation of the retrograde flow of actin in the lamellum, which is associated with the lamellipodium (Ponti et al., 2004; Giannone et al., 2007). Moreover, NMII is involved in the fusion of actin into bundles at the lamellum-lamellipodia interface (Anderson et al., 2008; Nemethova et al., 2008), and in retraction at the rear of the cell (Vicente-Manzanares et al, 2009).

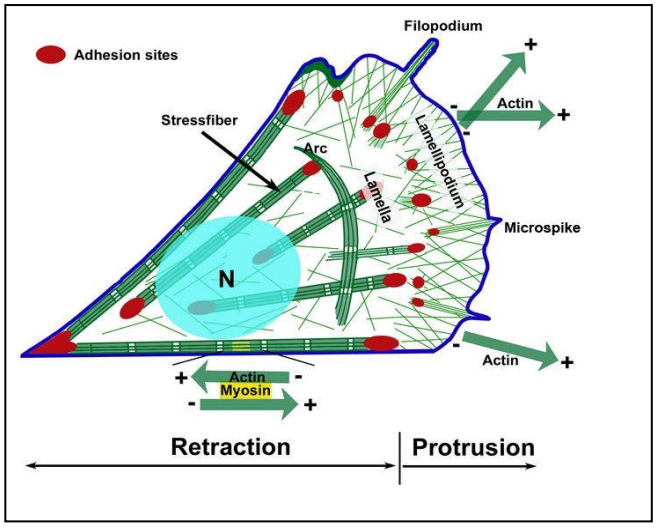

Figure 5: Schematic representation of the actin cytoskeleton in a migrating fibroblast. The different actin filament structures are shown: actin filament meshwork in the lamellipodium, projecting filopodium, contractile bundles of actin (stress fiber) in the lamella, cell body and at the cell edge, and a loose actin network throughout the cell. Sites of adhesion of the cell with the substratum are also indicated, in red. N= Nucleus. (Figure adapted from www.cellix.imba.oeaw.ac.at/3-actin-cytoskeleton

1.3.3 Nuclear actin and myosin

Actin and myosin are also found in the nucleus, and nuclear actin and myosin take part in chromatin remodeling, chromosome movements and gene transcription by recruitment of RNA polymerases to their target promoters, and in mRNA processing and export (de Lanerolle, 2012). Whereas F-actin is a common structure in the cytoplasm, nuclear actin probably exist as monomers (G-actin) or short polymers (Pederson and Aebi, 2002), actin has the ability to form filaments in the nuclei under various pathological conditions in somatic cells (Hofmann, 2009; Munsie et al., 2011). It has been suggested that normal cells limit the formation of F-actin or form short filaments that turn over very quickly in the nucleus. Regulation of these dynamics and structures could go via post-translational modifications in actin (de Lanerolle and Serebryannyy, 2011).

Actin is also connecting the cytoplasm and nucleus. Transcriptional regulation is the major reaction of cells to changes in the external environment. Several transcriptional activators and repressors bind to actin filaments in the cytoplasm and translocate to the nucleus as a response to actin polymerization/depolymerization in the cytoplasm (Haller et al., 2004; Favot et al., 2005; Vartiainen et al., 2007).

Non-muscular myosin I (NMI) was the first myosin to be discovered in the nucleus (Pestic-Dragovich et al., 2000), and has been extensively studied. NMI is implicated in RNA polymerase I/II mediated transcription (Nowak et al., 1997; Fomproix and Percipalle, 2004; Ye et al., 2008; Philimonenko et al., 2004; Pestic-Dragovich et al., 2000; Hofmann et al., 2006). Additionally, actin and NMI are crucial for the functional compartmentalization of the nucleus. The nuclear centre includes early replicating chromosomes, whereas the periphery contains late replicating heterochromatic chromosomal regions. Studies of long-range interphase chromosome movements show dependency on nuclear actin and NMI (Chuang et al., 2006), but the molecular details about the motor activity remain unclear. Actin and actin related proteins (ARPs) are important in recruiting chromatin remodeling complexes (Zhao et al., 1998; Kukalev et al., 2005; Obrdlik et al., 2008; Qi et al., 2011; Blessing et al., 2004), and NMI interacts with the chromatin remodeling complex WSTF-SNF2h (Percipalle and Farrants, 2006).

Other nuclear myosins have been described in addition to NMI. Embryonic myosin II has been found in the nuclei of proliferating myoblasts (Rodgers, 2005),

and adult myosin II is localized to the nucleus in smooth muscle cells where it regulates RNA polymerase II mediated transcription (Li and Sarna, 2009). Myosin VI is detected in the RNA polymerase II complex (Vreugde et al., 2006). Myosin V has been found in nuclear speckles and nucleoli, and is involved in transcription by RNA polymerase I (Pranchevicius et al., 2008; Lindsay and McCaffrey, 2009).

1.4 Lysine methylation

Methyl groups are one of the major post-translational modifications regulating protein function (Bedford and Clarke, 2009). Histone lysine methylations have been extensively studied (Lachner and Jenuwein, 2002). Yet, several non-histone proteins lysine methylations have been reported. The physiological roles of non-histone lysine methylation remain largely unknown, (Cho et al., 2011; Chuikov et al., 2004; Huang et al., 2006; Kunizaki et al., 2007). The number of identified non-histone proteins that are methylated at lysine residues by protein lysine methyltransferases (PKMTs) is growing rapidly. In the last few years, lysine methylations of e.g. the 70 kilodalton heat shock protein 70 (Hsp70) (Cho et al., 2012) and different transcription factors, e.g. p53 (Chuikov et al., 2004), NF-kappaB (Yang et al., 2009), Er-α (estrogen receptor α) (Subramanian et al., 2008) have been reported. Some PKMTs possess methylation activity on both histones and non-histones. Examples are SET7/9 which methylates histone H3 (Wang et al., 2001; Nishioka et al., 2002) and non-histone proteins such as p53 (Chuikov et al., 2004) and Er-α (Subramanian et al., 2008), and SETD8 which methylates histone H4 (Fang et al., 2002) and p53 (Shi et al., 2007).

Similar to several other post-translational modifications, lysine methylations can be enzymatically removed by protein lysine demethylases (PKDMs). Again, enzymes involved in histone lysine-demethylation can also demethylate lysines on non-histone proteins. LSD1 demethylate p53 and E2F1 in addition to its histone target, the dimethylated lysine-4 in histone H3 (H3K4me2) (Shi et al., 2004). The fact that a single PKMT or PKMD may target several substrates, could potentially lead to opposite biological effects (He et al., 2012).

1.5 Spermatogenesis

Male germ cell differentiation, or spermatogenesis, is a complex process that begins with mitotic proliferation of spermatogonia. In the rodent testis, type A spermatogonia, intermediate spermatogonia and type B spermatogonia have been identified. The completion of a series of mitotic divisions results in the conversion of type B spermatogonia to the first stage of primary spermatocytes in the prophase of meiosis I (Phillips et al., 2010).

In the preleptotene stage, cells are tetraploid and enter meiosis with a prolonged prophase consisting of five steps (I-V): (I) In the leptotene stage, the chromosomes begin condensing and axial protein elements of the synaptonemal complex (SC) start to assemble along the chromosomes. The SC is a zipper-like structure mainly composed of meiosis-spesific proteins which mediates synapsis of homologuos chromosomes. (II) In the zygotene stage, the homologous chromosomes become closely paired (called bivalents) and synapse by assembly of the central elements of the SC. This phase is also called the bouquet stage due to the clustering of telomeres at one area of the nuclear membrane. (III) In the pachytene stage, non-sister chromatids of homologous chromosomes exchange segments of genetic material in a process called homologous recombination (Hess and Renato de, 2008). Defects in recombination and/or chromosome synapsis in meiotic prophase I results in meiotic arrest in the pachytene stage. Meiotic arrest is activated by checkpoint mechanisms,"the pachytene checkpoint", which involves a subset of DNA damage response proteins (Roeder and Bailis, 2000). (IV) In the diplotene stage the SC degrades and homologous chromosomes begin to separate, but they remain attached at the chiasmata (the place where crossing-over took place). (V) In diakinesis, the final stage of the promeiotic metaphase I, the chromosomes condense and separate, the nucleoli disappears and the nuclear membrane disintegrates. The spermatocytes then enter two subsequent meiotic divisions to become secondary spermatocytes and spermatides (Hess and Renato de, 2008).

The haploid germ cells go through a differentiation phase called spermiogenesis (Hess and Renato de, 2008). The round spermatid, which arises from the second meiotic division, goes through a series of complex structural remodeling, including nuclear condensation, acrosome and flagellar formation, which transforms the spermatid into mature sperm (spermatozoon). During spermiogenesis histones in

the chromatin are replaced with protamines (Hess and Renato de, 2008). At the end of somatic cell cytokinesis, the midbody structure is abscised and separates the two cells (Glotzer, 2005). However, germ cells do not abscise the midbody, and the cells stay connected through stable syncytium linking the cytoplasm of generations of daughter cells (Fawcett et al., 1959). A picture of a cross section of testicular tubuli with a simplified overview of the spermatogenesis is presented in figure 6.

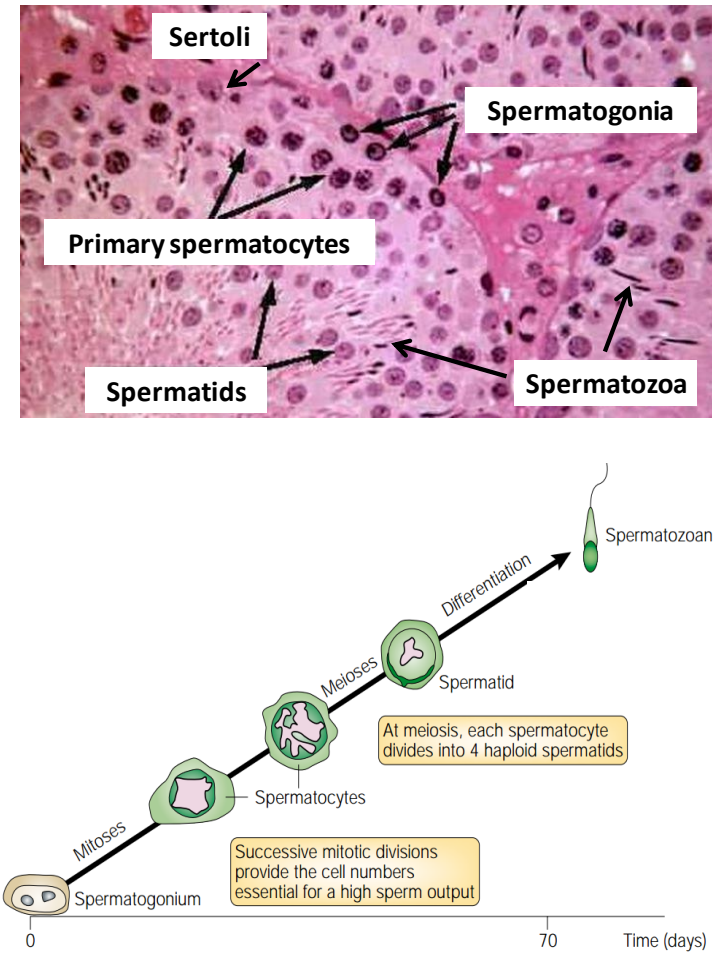

Figure 6. Cross section of testicular tubuli and human spermatogenesis. Upper panel, light micrograph of a HE-stained testicular cross section with tubular cell types indicated (Adapted from http://instruction.cvhs.okstate.edu/histology/mr/himrp3.htm). Lower panel, simplified schematic overview of the spermatogenic stages. The time course shown is that for a human male (75 days) (Adapted from Cooke and Saunders, 2002).

In addition to the germ cell lineage, testicular tubuli have a somatic cell population called Sertoli cells. These cells form the structural support of the epithelium and provide the physiological environment required for the development of sperm cells. Germ cells lie between the Sertoli cells and are attached to them by cell-cell actin based adherence junctions and assist in the translocation of spermatocytes through the seminiferous epithelium (Vogl et al., 2009).

Germ cells are arranged in a highly ordered sequence from the basement membrane to the lumen in the tubules. Spermatogonia lie on the basement membrane, followed by primary spermatocytes, secondary spermatocytes, and spermatids toward the tubule lumen. 12 different germ cell stages have been identified in mice (presented in figure 7). A cycle of spermatogenesis involves the division of primitive spermatogonial stem cells into subsequent germ cells. Several cycles of spermatogenesis coexist within the germinal epithelium at any one time. The cells differentiate synchronized over some distance, e.g. in mice, so that an entire tubule cross section should have cells at the same stage. Stage I is followed by II, followed by III, etc. through Stage XII, which is then repeated by stage I (Hess and Renato de, 2008).

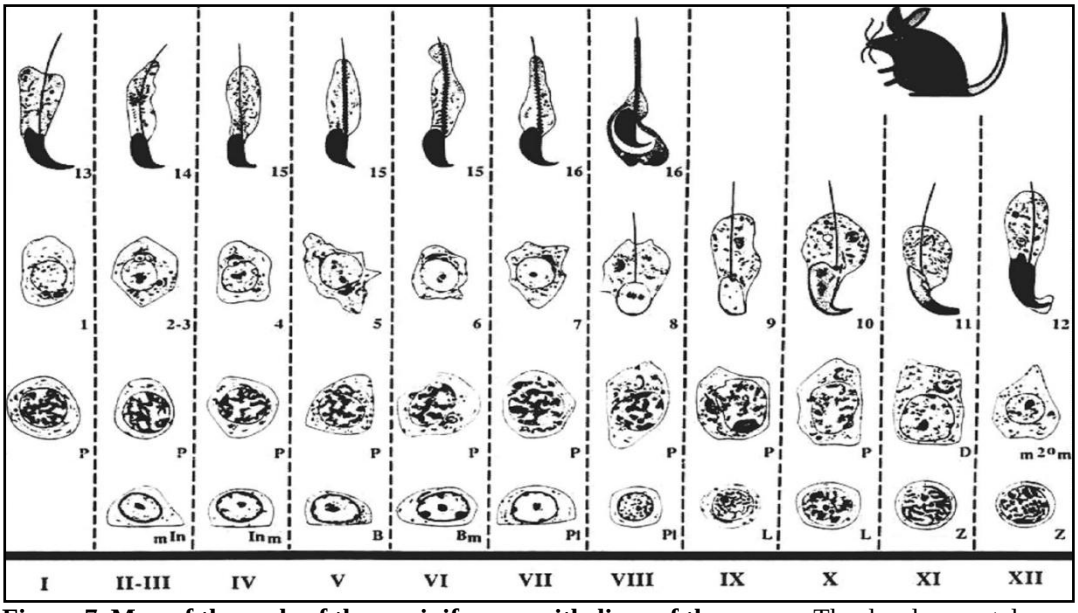

Figure 7. Map of the cycle of the seminiferous epithelium of the mouse. The developmental progression of a cell is followed horizontally until the right hand border of the cycle map is reached. The cell progression continues at the left of the cycle map one row up. The vertical columns, designated by Roman numbers, depict cell associations (stages), meaning the different cell types that can be found in a testis cross section. In, intermediate spermatogonia; B, type B spermatogonia; Pl, preleptotene; L, leptotene; Z, zygotene; P, pachytene; D, diplotene (Figure from Russel et al., 1990. Reprinted with permission of Cache River Science, an imprint of Quick Publishing, LC, 888-PUBLISH, fax 314-993-4485, Email Cacheriverpress@sbcglobal.net)

2. Aims of the study

The projects presented here were initiated to increase our knowledge about the mammalian homologues of *E.coli* AlkB. The DNA/RNA repair activity of *E.coli* AlkB and the functional mammalian homologues ALKBH2 and ALKBH3 have been established. On the contrary, although the endogenous substrates have been found for some AlkB homologues, they are less well described. It appears like these proteins target a rather wide variety of substrates, both proteins and nucleic acids and thereby regulate various cellular functions and pathways. The studies described in this study have focused on ALKBH1 and ALKBH4.

The study was initiated by the generation of *Alkbh4* deficient mice in order to characterize the role of ALKBH4 *in vivo*. Conditional Cre-recombinase *Alkbh4* mice were generated next due to the letality of constitutive *Alkbh4* targeted mice. Conditional ALKBH4 depletion was also studied in cell culture. Moreover, we used ALKBH4 siRNA to generate knockdown cells.

Similarly, the role of *Alkbh1* was studied by generating gene-targeted mice. It was previously suggested that ALKBH1 could have other target substrates than DNA/RNA, and might be involved in epigenetic regulation, based on the lack of activity on nucleic acids and the low pI value of the protein. Gene targeted mice allowed investigation of the phenotype of mice deficient of ALKBH1.

3. Summary of papers

Paper I

Regulation of actomyosin dynamics by post-transcriptional modifications in cytoplasmic actin is still poorly understood. Here we demonstrate that dioxygenase ALKBH4-mediated demethylation of a monomethylated site in actin (K84me1) regulates actin-myosin interaction and actomyosin-dependent processes such as cytokinesis and cell migration. ALKBH4-deficient cells display elevated K84me1 levels. Non-muscle myosin II only interacts with unmethylated actin and its proper recruitment to and interaction with actin depend on ALKBH4. ALKBH4 co-localizes with the actomyosin-based contractile ring and midbody via association with methylated actin. ALKBH4-mediated regulation of actomyosin dynamics is completely dependent on its catalytic activity. Disorganization of cleavage furrow components and multinucleation associated with ALKBH4 deficiency can all be restored by reconstitution with wild-type but not catalytically inactive ALKBH4. Similar to actin and myosin knock-out mice, homozygous *Alkbh4* mutant mice display early embryonic lethality. These findings imply that ALKBH4-dependent actin demethylation regulates actomyosin function by promoting actin-non-muscle myosin II interaction.

Paper II

ALKBH4, an AlkB homologue in the 2OG and Fe2+ dependent hydroxylase family, has previously been shown to regulate the level of monomethylated lysine-84 in actin and thereby indirectly influence the ability of non-muscular myosin II to bind actin filaments. ALKBH4 modulates fundamental processes including cytokinesis and cell motility, and its depletion is lethal during early preimplantation embryo stage.

The aim of this study was to investigate the effect of ALKBH4 deficiency in a physiological context, using inducible *Alkbh4* knockout mice. Here, we report that ALKBH4 is essential for the development of spermatocytes during the prophase of meiosis, and that ALKBH4 depletion leads to insufficient establishment of the synaptonemal complex. We also show that ALKBH4 is localized in nucleolar structures of Sertoli cells and in nuclear foci in spermatogonia and primary spermatocytes.

Paper III

In the present study we show non-Mendelian inheritance of the *Alkbh1* targeted allele in mice. Both *Alkbh1−/−* and heterozygous *Alkbh1+/−* offspring are born at a greatly reduced frequency. Additionally, the sex-ratio is considerably skewed against female offspring, with one female born for every three to four males. Most mechanisms that cause segregation distortion, act in the male gametes and affect male fertility. The skewing of the sexes appears to be of paternal origin, and might be set in the pachythene stage of meiosis during spermatogenesis, in which Alkbh1 is upregulated more than 10-fold. In testes, apoptotic spermatids were revealed in 5–10% of the tubules in *Alkbh1−/−* adults. The deficiency of ALKBH1 also causes misexpression of Bmp2, 4 and 7 at E11.5 during embryonic development. This is consistent with the incompletely penetrant phenotypes observed, particularly recurrent unilateral eye defects and craniofacial malformations.

Genetic and phenotypic assessment suggests that ALKBH1 mediates gene regulation in spermatogenesis, and that ALKBH1 is essential for normal sex-ratio distribution and embryonic development in mice.

4. Results and discussion

4.1 ALKBH4

4.1.1 Phenotype of ALKBH4 deficient mice and cell lines

To investigate the biological function of ALKBH4, we generated conditional *Alkbh4* gene-targeted mice with LoxP sites flanking exons 2 and 3 of the endogenous *Alkbh4* locus. Exons 2 and 3 includes conserved residues presumed to constitute the AlkB-domain (Aravind and Koonin, 2001) and residues required for binding to the Fe^{2+} and 2OG co-substrates (Bjornstad et al., 2011). The resultant $Alkbh4^{+/L}$ (*L* refers to the floxed allele) mice were crossed with mice ubiquitously expressing Cre-recombinase to generate the *Alkbh4* null allele ($Alkbh4^{-}$). Heterozygous $Alkbh4^{+/L}$ and $Alkbh4^{+/-}$ mice develop normally, with no apparent phenotype. However, $Alkbh4^{+/-}$ intercrosses failed to give rise to homozygous $Alkbh4^{-/-}$ offspring, and the Mendelian distribution between wild-type and heterozygous genotypes indicated that disruption of *Alkbh4* results in embryonic lethality. Blastocysts from embryonic day 3.5 from heterozygous intercrosses were genotyped and no $Alkbh4^{-/-}$ embryos were detected, suggesting developmental arrest at an early pre-implantation stage (Paper I).

To circumvent embryonic lethality we generated an inducible Cre-recombinase mediated *Alkbh4*-knockout mouse stain (designated $Alkbh4^{\Delta/\Delta}$ after induction of the Cre-recombinase). Cell culture based studies of ALKBH4 deficient cells, both inducible primary MEF cells and siRNA treated cells, showed increased level of apoptosis and revealed that ALKBH4 plays an important role in cytokinesis. Multiple proteins that normally localize to the midbody failed to localize properly during cytokinesis in ALKBH4 depleted cells, suggesting a role for ALKBH4 in formation of the cleavage furrow. We also observed a dramatic reduction in the migration ability of $Alkbh4^{\Delta/\Delta}$ compared to $Alkbh4^{L/L}$ MEF cells, using the scratch assay method (Paper I).

To reveal the role of ALKBH4 in a physiological context, we decided to induce ALKBH4 depletion in 4-week old mice (Paper II). Considering the embryonically lethal phenotype of the conventional $Alkbh4^{-/-}$ *mice* and increased cell death and cytokinetic failure in cell culture after depletion of ALKBH4 (Paper I), it was surprising that the induced mutant mice were viable with general normal appearance except for disruption of spermatogenesis.

The defects in the germinal epithelium after Cre-mediated ALKBH4 depletion were pronounced after two weeks of tamoxifen treatment. The relatively long treatment period might be necessary because of a potentially high initial level of ALKBH4 protein in testis or a putatively long turnover time of the ALKBH4 protein. The remaining protein might be sufficient for sustainable cell homeostasis until the spermatocytes reach the pachytene stage where the pachytene checkpoint mechanisms are activated (Roeder and Bailis, 2000).

The absolute density of Sertoli cells was increased in *Alkbh4*$^{\Delta/\Delta}$ testicular tubuli, but any proliferative activity in these cells was not apparent in 5-bromo-2-deoxyuridine (BrdU)-labeling experiments. This observation may be due to a lower cellularity of *Alkbh4*$^{\Delta/\Delta}$ tubuli, allowing more precise distinction of Sertoli cells. Intriguingly, the somatic and non-proliferative Sertoli cells, in addition to the spermatogonial cell types, seem unaffected by depletion of the *Alkbh4* gene. These cell types, like the premeiotic spermatocytes, display nuclear localization of ALKBH4, but it is possible that ALKBH4 is involved in other or less essential processes for cell homeostasis in spermatogonia and Sertoli cells.

Many regulators of the meiotic process have been reported, and their absence often leads to prophase arrest and apoptosis. Coordinated execution of cell cycle processes is very important for the production of gametes, especially during the meiotic prophase (reviewed in (MacQueen and Hochwagen, 2011). Defects in formation of the synaptonemal complex (SC) also lead to meiotic silencing of unsynapsed chromosomes (MSUC), a phenomenon normally restricted to the sex chromosomes, and results in transcriptional silencing of the affected chromosomal regions (Kurahashi et al., 2012). As reported in paper II, we discovered impaired localization of the SC component synaptonemal complex protein 3 (SYCP3) and also persistent yH2Ax staining??? in the pachytene stage cells in ALKBH4 depleted male mice, indicating unsynapsed chromosome axes (Mahadevaiah et al., 2008).

4.1.2 Intracellular localization of ALKBH4

ALKBH4 is localized both in the cytoplasm and in the nucleus (Paper I; Paper II; Bjornstad et al., 2012; Tsujikawa et al., 2007). A pronounced accumulation of ALKBH4 at the contractile ring and midbody structures was seen in cell cultures

(Paper I). In interphase cells, ALKBH4 distributes along filaments and in foci in distal parts in the cytoplasm and lamellipodia (Figure 8).

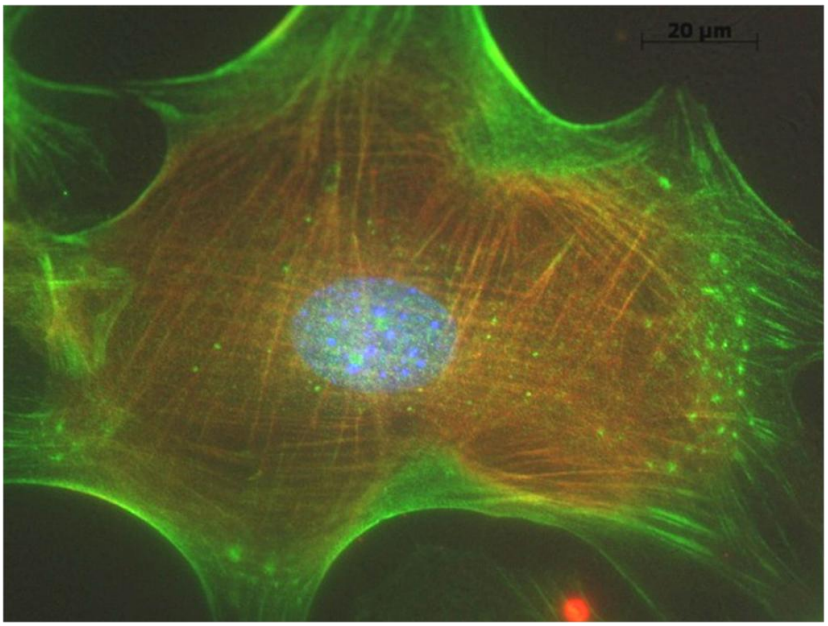

Figure 8. ALKBH4 (green) localization in MEF cell in interphase. Co-immunostaining of ALKBH4 (green) and NMII (red). DNA stained with diamidino-2-phenylindole (DAPI (blue)). (Anja Nilsen, unpublished).

Ectopically expressed green fluorescent protein (GFP)-tagged-ALKBH4 localizes in the nucleolus where it partly co-localizes with the RNA polymerase I complex (Bjornstad et al., 2012). We also find endogenous ALKBH4 to accumulate in the nucleoli of somatic cells, as we have shown in the Sertoli cells in seminiferous tubuli in mice (Paper II) and, in MEF cells in culture (Figure 8). In paper II, we reported the nuclear localization pattern of ALKBH4 in male germ cells. In spermatogonia ALKBH4 localizes to the nuclear periphery in several foci/patches. In the early stages of premeiotic spermatocytes (preleptotene and mid-leptotene) ALKBH4 is found in several threads and patches in the nucleus. The number of patches decreases as the cells from late leptotene stage to mid-pachytene. Interestingly, ALKBH4 does not seem to be present in the nuclei of late pachytene and metaphase cell types, at least not in aggregates. At present, we have not been able to identify what these particular ALKBH4-containing nuclear structures are, and further investigations will be needed. One possibility is that these foci/structures are nucleolar organizing regions (NORs), nuclear structures engaged in ribosome biogenesis (Schwarzacher and Wachtler, 1993) which is associated with several autosomal chromosomal bivalents in meiotic prophase spermatocytes (Kierszenbaum

and Tres, 1974). At middle pachytene the NORs detach from their autosomal bivalents and associates close to the XY chromosomal pair (termed the XY-body), thus rearranging their nucleolar components and forming a new nucleolus at late pachytene. The nucleolus associated to the XY pair appears transcriptionally inactive (Tres, 2005). We could not detect ALKBH4- aggregates nearby the XY-body in pachytene stage spermatocytes (Paper II), which also reflects the possibility that ALKBH4 is only present at transcriptionally active sites in the nucleus.

4.1.3 ALKBH4-dependent actin-K84me1 demethylation

We found that ALKBH4 interacts with actin (Paper I). More specifically, we discovered that the ALKBH4-actin interaction is dependent on monomethylated Lysin-84 in actin (actin-K84me1). Intriguingly, the level of K84me1 in actin increased in ALKBH4 depleted cells (Paper I and figure 9).

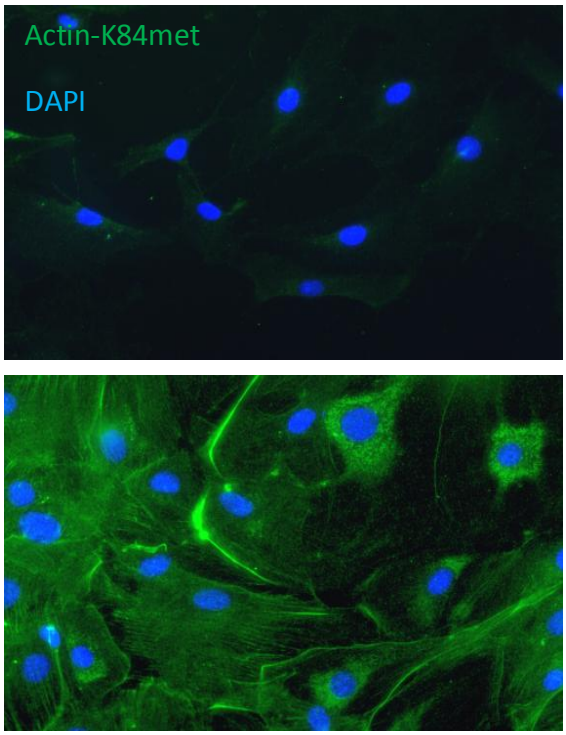

Figure 9. Increased level of Actin-K84me1 in ALKBH4 depleted MEF cells. Immunofluorescence staining (IF) of *Alkbh4*$^{\Delta/\Delta}$ MEFs (lower panel) with higher level of K84me1 (green) than the control (*Alkbh4*$^{+/+}$) MEFs (upper panel). DAPI was used as DNA counterstain (blue). (Figure by Anja Nilsen, unpublished)

In vivo, complementation assays or overexpression with ectopically expressed wild-type ALKBH4 either prevented this accumulation or reduced the level of K84me1, respectively. We attempted to test the *in vitro* demethylase activity of recombinant ALKBH4 expressed and purified from *E.coli* and Flag-tagged ALKBH4 purified from human cells towards a variety of actin substrates, but no vigorous

activity was detected. We speculate that ALKBH4 might need a cofactor, or that actin must be in a particular conformation for demethylase activity. It is possible that ALKBH4 requires a specific scaffolding protein or protein complex to be recruited to its substrate.

The catalytically inactive HDH ALKBH4 mutant showed stronger interaction or binding of K84me1-actin than WT ALKBH4 (Paper I). This finding is an indication that actin-K84me1 is the prime substrate of ALKBH4, based on previous observations that catalytically inactive enzymes can display more persistent binding of their substrates (Mailand et al., 2007).

Lysin-84 in actin is located within the predicted interaction-region for (NMII) (Schroder et al., 1993). Hence, we speculated if methylation of this residue could influence the actin-NMII interaction. In contrast to ALKBH4, NMII does not interact with methylated actin-K84 (Paper I). All together, these findings indicate that ALKBH4-dependent demethylation of actin-K84me1 promotes binding of NMII to F-actin in the actomyosin network. We propose an actin-K84me1 demethylation mechanism by ALKBH4 similar to the mechanism described for the JmjC-dioxygenases on methylated histones (Tsukada et al., 2006).

4.1.4 Post-translational modifications of actin

Actin is a major target for a wide range of different post-translational modifications (PTMs) which regulate the organization of actin. So far, acetylations, arginylations, phosphorylations, ubiquitylations, SUMOylations, sulfations and methylations have been identified at different actin residues which occur through enzymatic mechanisms (Terman and Kashina, 2013). ATP-bound G-actin is the normal substrate for F-actin filament formation. F-actin is an ATPase, such that the filaments soon contain just ADP. ADP F-actin is less stable than ADP G-actin. This enables actin filaments to be readily disassembled, which is important for the actin recycling process in cells (Wegner and Isenberg, 1983). But how this process is controlled, is rather unclear.

Among the methyl modifications identified, the methylated histidine-73 (His-73) residue is the most studied. This modification regulates actin's interdomain flexibility and stability by slowing the inorganic phosphate (Pi) release after ATP hydrolysis, leading to F-actin stabilization (Nyman et al., 2002; Yao et al., 1999; Oda et al., 2009; Murakami et al., 2010). It is tempting to compare the function of methylated His73 with methylated Lys84 in actin. As we show in paper I, K84me1 is

mainly found in F-actin. In addition to the negative effect on NMII interaction, it is possible that methylated K84 helps to stabilize F-actin in ADP state so that it will not depolymerize into G-actin. Another possibility is that methylation of K84 alters the F-actin conformation/helix. Changes in the F-actin conformation might also be the reason why NM II doesn't bind K84me1-actin. K84 in actin is located within the region where NMII binds (Schroder et al., 1993), but mutants of this residue in actin filaments do not alter the NMII-binding capacity (Miller et al., 1995). We show in paper I that K84, via its PTM, is indeed involved in actin-myosin interaction.

"Double PTMs" occurring simultaneously on the same protein site have been seen in actin from nuclear extracts. Lysine-326 is first arginylated, and this modification can be further methylated. It is suggested that this "double PTM" could be involved in chromatin and/or transcriptional control (Saha et al., 2011).

Protein histidine methyltransferase (PHMT) and carnosine N-methyltranferase have been identified as actin methylating enzymes/ methyl transferases, but their specific target histidine residues have not yet been revealed (Vijayasarathy and Rao, 1987; Raghavan et al., 1992). Currently, no lysine methyltransferase have been shown to perform actin methylation, but lysine-methyltransferases have been shown to target a variety of proteins, both histones and non-histones (He et al., 2012). Thus, it is possible that a described lysine methyltransferase is involved in actin-K84 methylation as well. Moreover, no actin demethylating enzyme has been reported to this date, making ALKBH4 the first putative actin-demethylase described (Paper I). Other lysine demethylases have been shown to target various proteins as substrates (He et al, 2012), hence there is a possibility that ALKBH4 targets other substrates in addition to K84 in actin.

The K84, together with several other lysine residues in actin, is also subjected to ubiquitylation (Xu et al., 2010: Kim et al., 2011). Ubiquitinylation (polyubiquitinylation) of proteins is a common feature for proteins that will undergo degradation, and actin levels decrease when actin is ubiquitylated (Kudryashova et al., 2005). On the other hand, monoubiquitylation of actin is thought to confer stability and differential subcellular localization of actin (Dantan-Gonzalez et al., 2001; Field et al., 1993). Whether K84-ubiquitylation leads to degradation, stabilization or specific intracellular localization of actin is not known. How this modification and K84me1 alternate and affect actin dynamics remains to be elucidated.

4.1.5 ALKBH4 in cytokinesis and migration

In paper I we show that ALKBH4-mediated demethylation of actin-K84me1 is important for maintaining actomyosin dynamics in supporting normal cytokinesis and cell migration. Most likely, ALKBH4 also affects a broader range of actomyosin related functions in the cell, by making actin-filaments accessible for NMII interaction, resulting in contraction of the actomyosin network.

If K84me1 stabilizes F-actin, it is plausible to think that the highly dynamic assembly/dissasembly of filaments during cytokinesis fails (Wolfe and Gould, 2005). At late telophase there are no F-actin and NMII localized in the midbody before abscission (Schweitzer and Souza-Schorey, 2004). Yet, ALKBH4 localizes in the midbody also at late telophase (Paper I). It is possible that ALKBH4 prevents new formation of F-actin or destabilizes the remaining F-actin in this structure. In ALKBH4 depleted cells, failure of recruitment of midbody associated proteins even in the early stages of furrow ingression supports a role for ALKBH4 throughout cytokinesis.

Unfortunately, we were not able to characterize the localization pattern of cytoplasmic ALKBH4 in testis sections. Alternative methods for tissue-preparation might solve this problem. We hypothesized that ALKBH4 might locate to the intercellular bridges between germ cells, since ALKBH4 localize to the midbody during cytokinesis. Preliminary investigations by fractionation of intercellular bridges (Greenbaum et al., 2007) and co-localization staining with the intercellular bridge marker TEX14 (Greenbaum et al, 2006) have not been able to substantiate this (unpublished results, Anja Nilsen). An interesting difference between the intercellular bridges of spermatogenic cells and the midbodies of dividing somatic cells is that the stable mammalian intercellular bridges contain F-actin (Russell et al., 1987), as opposed to the more dynamic furrow ingression in somatic cell types which is devoid of F-actin before abscission (Schweitzer and Souza-Schorey, 2004). This strengthens the idea that ALKBH4 plays a role in the regulation of dynamic actomyosin interactions.

ALKBH4 deficient MEF cells show reduced ability to migrate when tested in scratch-wound healing assays (Paper I). In a scratch-wound healing assay the fibroblasts migrate into a region denuded of cells, and the direction of cell motility is promoted by chemotaxis and/or haptotaxis (Carter, 1967; Gauss-Muller et al., 1980).

Cell migration plays a critical role in embryogenesis, wound healing, immune response, and tissue development (Lauffenburger and Horwitz, 1996; Mitchison and Cramer, 1996; Pollard and Borisey, 2003). Abnormal and/or unregulated cell motile behavior may contribute to several illnesses, including vascular disease and cancer (Ridley et al., 2003).

Cells use actin filaments to create protrusive and contractile arrangements that drive cell motility. From the lamellipodium in the protruding front of the cytoplasm into the lamella behind, there is a conversion of the polymerizing actin-meshwork to an assembly of contractile bundles of actin with non-muscular myosin II (Small and Resch, 2005). In the rear (trailing edge) of a migrating cell, actin and myosin mediated contraction pulls the cell body forward to follow the front. NM II is the key regulator of this contractility, generating increased tension at the trailing edge and concurrently reducing tension at the leading edge (Jay et al., 1995; Verkhovsky et al., 1999). Interestingly, cytoplasmic ALKBH4 localize primarily to the distal region of the cytoplasm of cells in interphase (figure 8), probably the protrusive region in the lamellipodium where it is seen in filametous structures and in foci at or near dendritic actin-branches or in focal adhesion points. NMII appears in the transition zone/lamellum along the stess fibres/actin bundles (Vicente-Manzanares et al., 2009). It is plausible that ALKBH4 demethylates actin filaments in the lamellipodium, and possibly at the actin branches or adhesion points, thus making the actin filaments more accessible for NMII for bundling in the lamellum. Alternatively, demethylation of actin-K84 by ALKBH4 might facilitate depolymerization of actin fibers in the lamellipodium. More studies of ALKBH4 related to migration and adheshion dynamics need to be conducted.

4.1.6 Nuclear ALKBH4 and actin-K84me1

Actin exists as monomers and polymers within the nucleus (McDonald et al., 2006). Both actin polymers and myosin are required to drive RNA polymerase transcription, in addition chromatin remodelling and nuclear speckle formation requires polymeric actin. Factors promoting actin polymerization/depolymerisation in the cytoplasm are also present in the nucleus, hence likely to affect actin dynamics there (Gieni and Hendzel, 2009).

Mechanisms that could regulate the dynamics and filament structure of nuclear actin are post-translational modifications. As described above, cytoplasmic actin is

subject to many posttranslational modifications, but SUMOylation, which increases the nuclear retention of actin, is the only PTM that has been described for nuclear actin (Hofmann et al, 2009). Interestingly, immunostaining of ALKBH4 depleted MEF cells show actin-K84me1 accumulation in euchromatic regions in the nucleus (Figure 10). These subnuclear regions may correspond to nucleoli and/or nuclear speckles, and an increase of K84me1 in actin in these compartments may disrupt actomyosin dynamics necessary for driving/orchestrating active gene transcription and/or RNA processing or stabilize actin polymers in euchromatic compartments. Whether K84me1 alters the interaction ability of other myosin isoforms in addition to NMII, e.g. NMI, remains to be explored.

As described above, in paper II we show nuclear distribution of ALKBH4 in male germ cells. Whether the nuclear localization pattern of ALKBH4 in these cells corresponds to nucleolar organization regions (NORs), nuclear speckles and/or chromatin remodelling complexes, is yet unclear. However, it is plausible that ALKBH4 regulates nuclear actomyosin dynamics in these cell structures as well. Nucleoli and nuclear speckles dissociates before a cell enters mitosis, which is a feature also observed in meiotic cells (Schwarzacher and Wachtler, 1993). Interestingly, ALKBH4 aggregates/foci also dissociate in late premeiotic cell types (paper II). Whether ALKBH4 depletion results in transcriptional silencing, affecting genes involved in synaptonemal complex formation, or in other aspects leading to asynapsis of homologous chromosomes remains to be elucidated.

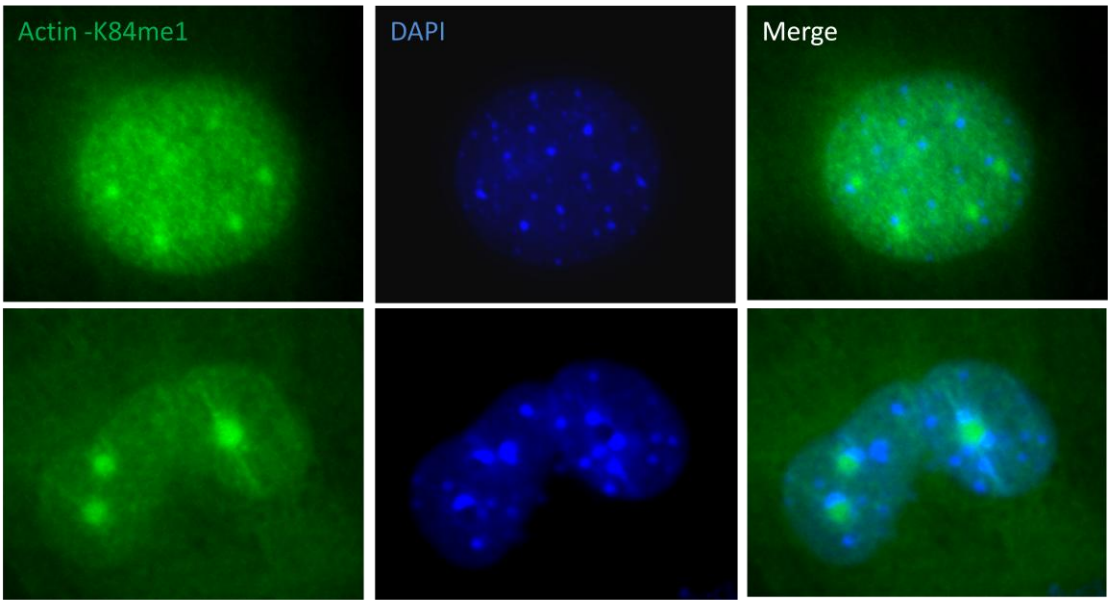

Figure 10: K84me1 accumulates in euchromatic regions in the nucleus in ALKBH4 depleted cells. *Alkbh4*$^{\Delta/\Delta}$ MEF cells immunostained with anti actin-K84me1. DNA counterstained with DAPI. (Anja Nilsen, unpublished).

4.2 ALKBH1

The molecular function of ALKBH1 is still not well described. Several studies have been conducted in respect to this issue, and some of the results and conclusions are conflicting. The first reports on ALKBH1 suggested a DNA repair mechanism similar to *E.coli* AlkB (Wei et al., 1996). Other studies have claimed that ALKBH1 displays AP lyase activity (Muller et al., 2010).

Three independent studies of *Alkbh1*$^{-/-}$ mice did not support the suggested role for ALKBH1 in DNA repair. While phenotypes associated with some DNA repair deficiencies include increased frequency of cancer or neurodegenerative diseases, ALKBH1 deficient mice have severe developmental failures (Paper III; Pan et al., 2008, Muller et al., 2013).

In paper III, we describe phenotypic defects of the *Alkbh1*$^{-/-}$ mouse strain and relate the findings to a role for ALKBH1 in differentiation and development of cells in tissues of ectodermal origin. ALKBH1 deficient embryos displayed delayed ossification of the sternum and skull, neural tube defects, malformation of limbs and unilateral eye development. Interestingly, these defects showed an incomplete penetrance, as only a subset of the knockout embryos had these phenotypic traits. The inconsistent phenotype might be a result of polygeny (Glazier et al., 2002), and the irregular patterns of inheritance might be caused by dependency upon modifier genes and gene dosage.

Bone morphogenetic proteins (BMPs) are a family of proteins that plays an important role during embryonic development on the embryonic patterning and early skeletal formation (Chen et al, 2004). Mutations in genes encoding BMPs result in variable phenotypes, like eye developmental defects and a number of skeletal defects with incomplete penetrance (Wyatt et al., 2010; Wordinger and Clark, 2007; Dudley et al., 1995), similar to the defects observed in *Alkbh1*$^{-/-}$ embryos. We found that several BMPs were aberrantly expressed in *Alkbh1*$^{-/-}$ embryos, which might cause the abnormal phenotype observed during embryonical development.

We observed a skewed sex-ratio distribution of *Alkbh1*$^{-/-}$ mice, with 3-4 male pups born for every female. Breedings with heterozygous and knockout *Alkbh1* showed that paternal inheritance of the targeted allele was more critical than maternal transmission considering the survival of the offspring. Biased sex ratios have been

reported as a consequence of sex chromosomal distorters (Taylor and Ingvarsson, 2003), and we speculated if silencing or pairing of the sex chromosomes could be influenced in the *Alkbh1*$^{-/-}$ mice. However, we found that ALKBH1 deficient promeiotic spermatocytes display normal formation of the XY body, which indicates normal segregation of the sex chromosomes. We found that ALKBH1 is highly expressed in testes, and the *Alkbh1* knockout mice have reduced testicular weight and increased level of apoptosis in haploid cell types in aged mice. It is possible that ALKBH1 depletion affects the maintenance of male post-meiotic X chromosome inactivation, resulting in increased cell death of round and elongating spermatids, and also sex-ratio distortion caused by improper silencing of the paternal X chromosome during early development. Epigenetic abnormalities in the chromatin code around sex-chromosomes in postmeiotic spermatocytes and spermatids may result in misexpression of X and Y-linked genes and subsequently sex-ratio distortion in favor of males. Various histone modifications in histone H2A and histone H3K4 in secondary spermatocytes and spermatids are controlled by the ubiquitin conjugating enzyme HR6B, contributing to the maintenance of X-chromosome silencing in postmeiotic cells (Baarends et al., 2007). Increased spermatid expression of multicopy X and Y genes are associated with deletions in the Y-chromosome (MSYq–) in mice. Moreover, these mice display aberrations in the histone code of the round spermatid sex chromosome and centromeric heterochromatin, in addition to sex-ratio distortions (Reynard and Turner, 2009). As previously described, ALKBH1 is found to exhibit demethylase activity on histone H2A (Ougland et al., 2012), and it is plausible to think that it has a role in generating a proper histone modification pattern necessary for male post-meiotic sex chromosome inactivation and paternal X-chromosome inactivation during early development. Also, sex-ratio distortions may be caused by transmission distortions of a specific allele in the resulting zygote. For instance, sperm bearing the Robertsonian (6.16) translocation have an impaired fertilizing ability and these mice exhibit sex ratio distortions in favor of male offspring (Aranha and Martin-DeLeon, 1995).

Recently, an in depth study of the *Alkbh1*$^{-/-}$ mice described in paper III was published focusing on the different expression patterns of a specific PIWI-interacting RNA (piRNA) in wild-type and ALKBH1 deficient spermatogenic cells. piRNAs are a class of small non-coding RNAs expressed in the germ line of many animal species found to be involved in regulatory mechanisms in spermatogenesis and transposon

silencing (Siomi et al., 2011). ALKBH1 deficiency results in derepression of a piRNA precursor transcript, and it is suggested that this is caused by aberrant histone H2A demethylation (Nordstrand et al., 2012).

Another ALKBH1 deficient model is also characterized with defects in development and cell differentiation (Pan et al, 2008), but there are differences in the tissues affected in this mouse model and the *Alkbh1*$^{-/-}$ mice described in paper III. Pan et al reported growth retardation and placental defects in which cells from trophoblast linages were reduced, and conclude that ALKBH1 plays a role in differentiation of trophoblast stem cells (Pan et al., 2008). However, a recently published study of the same *Alkbh1*$^{-/-}$ mouse strain generated by Pan *et al* report similar phenotypes as the *Alkbh1*$^{-/-}$ mouse stain decribed in paper III with regard to non-Mendelian inheritance, growth retardation and distorted sex-ratio (Muller et al., 2013). The differences observed in the two mouse models may be due to different gene targeting strategies used to generate *Alkbh1* deficient mice (Exon 6 in Paper III, Exon 3 in Pan *et al.* and Muller *et al.*), and it is possible that different variants of truncated ALKBH1 proteins have the ability to bind different interaction partners thus resulting in differences in the phenotype.

5. Conclusion and perspectives

Although the AlkB homologues exhibit with hydroxylation the same mode of action, they have been found to have a broad range of prime substrates: DNA, RNA and protein.

Prior to the ALKBH4 studies presented in paper I and paper II, the knowledge about this enzyme was very limited. We have provided increased understanding of the ALKBH4 enzyme and its biological and physiological significance. The results from our study in paper I show a role of ALKBH4 in modulation of actomyosin dynamics by being a regulator of the level of K84me1 in actin. Although we made extensive efforts to confirm demethylation activity of ALKBH4 on various actin-K84me1 substrates *in vitro*, ALKBH4 did not display robust activity under the conditions tested. Probably other, yet unknown, co-factors are needed in these *in vitro* assays to confirm a direct actin-K84me1 demethylation by ALKBH4.

Considering the embryonic lethality of *Alkbh4*$^{-/-}$ mice and the phenotype of the ALKBH4 depleted cell lines studied in paper I, it was surprising that the induction of ALKBH4 depletion in adult mice did not lead to a severe phenotype (paper II). Except for the prominent failure in spermatogenesis the mice appear to be normal. An explanation might be that the induction time of ALKBH4 depletion was too short for other phenotypic traits. Nevertheless, we report a novel role of ALKBH4 in spermatogenesis by being an important factor for the development of late premeiotic I stage cells and postmeiotic cells. Numerous unexplained cases of infertility in human males originate from defects in spermatogenesis (Matzuk and Lamb, 2002), and the results presented in this report could be important for understanding the mechanisms behind variants of male infertility. Further research is needed to elucidate the role of ALKBH4 in a physiological context and the inducible ALKBH4 mouse strain will be an invaluable tool in this respect.

The role of cytoplasmic ALKBH4 in migration should also be a subject for further investigations. Whether ALKBH4 is involved in actomyosin dynamics in specific sub-cellular compartments during cell movement and how actin polymerization/depolymerization and conformation is affected by ALKBH4 depletion should be further addressed. Also, the nuclear role of ALKBH4 and methylated K84-actin awaits closer examination.

In conclusion, the data presented in paper I, II and supplementary data presented in the discussion part in this thesis all point to an overall distribution of K84me1 in actin and suggests a global role for ALKBH4 in regulation of actomyosin dynamics, by being a modulator of actin-K84me1.

Our study of the *Alkbh1* deficient mouse presented in paper III revealed that this AlkB homologue is important for proper embryonic development. Also, *Alkbh1* mutant mice displayed higher level of apoptosis in spermatogenic cell types and sex-ratio distortion of offspring. Recent studies suggest that ALKBH1 is a histone H2A demethylase and link this activity to regulation of genes required for proper development of the mammalian nervous system (Ougland et al., 2012). More research is needed to study the mechanisms of ALKBH1 and its role in epigenetic regulation in spermatogenesis and embryogenesis.

In sum, despite the different primary substrates of ALKBH1 and ALKBH4, both ALKBH1 and ALKBH4 modulate protein post-translational modifications and are important factors during embryonic development and spermatogenesis.

Reference List

Aas,P.A., Otterlei,M., Falnes,P.O., Vagbo,C.B., Skorpen,F., Akbari,M., Sundheim,O., Bjoras,M., Slupphaug,G., Seeberg,E., and Krokan,H.E. (2003). Human and bacterial oxidative demethylases repair alkylation damage in both RNA and DNA. Nature *421*, 859-863.

Anderson,T.W., Vaughan,A.N., and Cramer,L.P. (2008). Retrograde flow and myosin II activity within the leading cell edge deliver F-actin to the lamella to seed the formation of graded polarity actomyosin II filament bundles in migrating fibroblasts. Mol Biol Cell *19*, 5006-5018.

Aranha,I.P. and Martin-DeLeon,P.A. (1995). Mouse chromosome 6 in Rb translocations: consequences in singly and doubly heterozygous males
7. Cytogenet. Cell Genet. *69*, 253-259.

Aravind,L. and Koonin,E.V. (2001). The DNA-repair protein AlkB, EGL-9, and leprecan define new families of 2-oxoglutarate- and iron-dependent dioxygenases. Genome Biol. *2*, RESEARCH0007.

Baarends,W.M., Wassenaar,E., Hoogerbrugge,J.W., Schoenmakers,S., Sun,Z.W., and Grootegoed,J.A. (2007). Increased phosphorylation and dimethylation of XY body histones in the Hr6b-knockout mouse is associated with derepression of the X chromosome
1. J. Cell Sci. *120*, 1841-1851.

Barr,F.A. and Gruneberg,U. (2007). Cytokinesis: placing and making the final cut. Cell *131*, 847-860.

Bedford,M.T. and Clarke,S.G. (2009). Protein arginine methylation in mammals: who, what, and why. Mol Cell *33*, 1-13.

Berg,J.S., Powell,B.C., and Cheney,R.E. (2001). A millennial myosin census
3999. Mol Biol Cell *12*, 780-794.

Berulava,T., Ziehe,M., Klein-Hitpass,L., Mladenov,E., Thomale,J., Ruther,U., and Horsthemke,B. (2012). FTO levels affect RNA modification and the transcriptome. Eur J Hum Genet.

Bjornstad,L.G., Zoppellaro,G., Tomter,A.B., Falnes,P.O., and Andersson,K.K. (2011). Spectroscopic and magnetic studies of wild-type and mutant forms of the Fe(II)- and 2-oxoglutarate-dependent decarboxylase ALKBH4. Biochem. J *434*, 391-398.

Bjornstad,L.G., Meza,T.J., Otterlei,M., Olafsrud,S.M., Meza-Zepeda,L.A., and Falnes,P.O. (2012). Human ALKBH4 interacts with proteins associated with transcription. PLoS. One. *7*, e49045.

Blessing,C.A., Ugrinova,G.T., and Goodson,H.V. (2004). Actin and ARPs: action in the nucleus. Trends Cell Biol *14*, 435-442.

Bork,P., Sander,C., and Valencia,A. (1992). An ATPase domain common to prokaryotic cell cycle proteins, sugar kinases, actin, and hsp70 heat shock proteins. Proc. Natl. Acad. Sci. U. S. A *89*, 7290-7294.

Bresnick,A.R. (1999). Molecular mechanisms of nonmuscle myosin-II regulation. Curr. Opin. Cell Biol *11*, 26-33.

Bunnell,T.M. and Ervasti,J.M. (2010). Delayed embryonic development and impaired cell growth and survival in Actg1 null mice
3. Cytoskeleton (Hoboken.) *67*, 564-572.

Bunnell,T.M., Burbach,B.J., Shimizu,Y., and Ervasti,J.M. (2011). beta-Actin specifically controls cell growth, migration, and the G-actin pool
2. Mol. Biol. Cell *22*, 4047-4058.

Cai,Y., Biais,N., Giannone,G., Tanase,M., Jiang,G., Hofman,J.M., Wiggins,C.H., Silberzan,P., Buguin,A., Ladoux,B., and Sheetz,M.P. (2006). Nonmuscle myosin IIA-dependent force inhibits cell spreading and drives F-actin flow. Biophys. J *91*, 3907-3920.

Carter,S.B. (1967). Haptotaxis and the mechanism of cell motility. Nature *213*, 256-260.

Cetica,V., Genitori,L., Giunti,L., Sanzo,M., Bernini,G., Massimino,M., and Sardi,I. (2009). Pediatric brain tumors: mutations of two dioxygenases (hABH2 and hABH3) that directly repair alkylation damage. J. Neurooncol. *94*, 195-201.

Chen,D., Zhao,M., and Mundy,G.R. (2004). Bone morphogenetic proteins
6. Growth Factors *22*, 233-241.

Cho,H.S., Suzuki,T., Dohmae,N., Hayami,S., Unoki,M., Yoshimatsu,M., Toyokawa,G., Takawa,M., Chen,T., Kurash,J.K., Field,H.I., Ponder,B.A., Nakamura,Y., and Hamamoto,R. (2011). Demethylation of RB regulator MYPT1 by histone demethylase LSD1 promotes cell cycle progression in cancer cells. Cancer Res *71*, 655-660.

Cho,H.S., Shimazu,T., Toyokawa,G., Daigo,Y., Maehara,Y., Hayami,S., Ito,A., Masuda,K., Ikawa,N., Field,H.I., Tsuchiya,E., Ohnuma,S., Ponder,B.A., Yoshida,M., Nakamura,Y., and Hamamoto,R. (2012). Enhanced HSP70 lysine methylation promotes proliferation of cancer cells through activation of Aurora kinase B. Nat Commun. *3*, 1072.

Choi,S.Y., Jang,J.H., and Kim,K.R. (2011). Analysis of differentially expressed genes in human rectal carcinoma using suppression subtractive hybridization. Clin. Exp. Med. *11*, 219-226.

Chuang,C.H., Carpenter,A.E., Fuchsova,B., Johnson,T., de,L.P., and Belmont,A.S. (2006). Long-range directional movement of an interphase chromosome site
7. Curr. Biol. *16*, 825-831.

Chuikov,S., Kurash,J.K., Wilson,J.R., Xiao,B., Justin,N., Ivanov,G.S., McKinney,K., Tempst,P., Prives,C., Gamblin,S.J., Barlev,N.A., and Reinberg,D. (2004). Regulation of p53 activity through lysine methylation. Nature *432*, 353-360.

Church,C., Moir,L., McMurray,F., Girard,C., Banks,G.T., Teboul,L., Wells,S., Bruning,J.C., Nolan,P.M., Ashcroft,F.M., and Cox,R.D. (2010). Overexpression of Fto leads to increased food intake and results in obesity. Nat. Genet. *42*, 1086-1092.

Clark,K., Langeslag,M., Figdor,C.G., and van Leeuwen,F.N. (2007). Myosin II and mechanotransduction: a balancing act
2274. Trends Cell Biol *17*, 178-186.

Conti,M.A., Even-Ram,S., Liu,C., Yamada,K.M., and Adelstein,R.S. (2004). Defects in cell adhesion and the visceral endoderm following ablation of nonmuscle myosin heavy chain II-A in mice
3132. J Biol Chem *279*, 41263-41266.

Cooke,H.J. and Saunders,P.T. (2002). Mouse models of male infertility. Nat. Rev. Genet. *3*, 790-801.

Cooke,R. (1997). Actomyosin interaction in striated muscle
6034. Physiol Rev. *77*, 671-697.

Dantan-Gonzalez,E., Rosenstein,Y., Quinto,C., and Sanchez,F. (2001). Actin monoubiquitylation is induced in plants in response to pathogens and symbionts 1. Mol. Plant Microbe Interact. *14*, 1267-1273.

de Lanerolle,P. and Serebryannyy,L. (2011). Nuclear actin and myosins: life without filaments. Nat. Cell Biol. *13*, 1282-1288.

de Lanerolle,P. (2012). Nuclear actin and myosins at a glance. J. Cell Sci. *125*, 4945-4949.

Dominguez,R. and Holmes,K.C. (2011). Actin structure and function 10 6073. Annu. Rev. Biophys. *40*, 169-186.

Dominissini,D., Moshitch-Moshkovitz,S., Schwartz,S., Salmon-Divon,M., Ungar,L., Osenberg,S., Cesarkas,K., Jacob-Hirsch,J., Amariglio,N., Kupiec,M., Sorek,R., and Rechavi,G. (2012). Topology of the human and mouse m6A RNA methylomes revealed by m6A-seq. Nature *485*, 201-206.

Dudley,A.T., Lyons,K.M., and Robertson,E.J. (1995). A requirement for bone morphogenetic protein-7 during development of the mammalian kidney and eye 1. Genes Dev. *9*, 2795-2807.

Duncan,T., Trewick,S.C., Koivisto,P., Bates,P.A., Lindahl,T., and Sedgwick,B. (2002). Reversal of DNA alkylation damage by two human dioxygenases. Proc. Natl. Acad. Sci. U. S. A *99*, 16660-16665.

Ea,C.K. and Baltimore,D. (2009). Regulation of NF-kappaB activity through lysine monomethylation of p65. Proc. Natl. Acad. Sci. U. S. A *106*, 18972-18977.

Edwards,K.A. and Kiehart,D.P. (1996). Drosophila nonmuscle myosin II has multiple essential roles in imaginal disc and egg chamber morphogenesis. Development *122*, 1499-1511.

Emoto,K., Kobayashi,T., Yamaji,A., Aizawa,H., Yahara,I., Inoue,K., and Umeda,M. (1996). Redistribution of phosphatidylethanolamine at the cleavage furrow of dividing cells during cytokinesis. Proc. Natl. Acad. Sci. U. S. A *93*, 12867-12872.

Emoto,K. and Umeda,M. (2000). An essential role for a membrane lipid in cytokinesis. Regulation of contractile ring disassembly by redistribution of phosphatidylethanolamine. J Cell Biol *149*, 1215-1224.

Emoto,K., Inadome,H., Kanaho,Y., Narumiya,S., and Umeda,M. (2005). Local change in phospholipid composition at the cleavage furrow is essential for completion of cytokinesis. J Biol Chem *280*, 37901-37907.

Falnes,P.O., Johansen,R.F., and Seeberg,E. (2002). AlkB-mediated oxidative demethylation reverses DNA damage in Escherichia coli. Nature *419*, 178-182.

Falnes,P.O. and Rognes,T. (2003). DNA repair by bacterial AlkB proteins 244. Res. Microbiol. *154*, 531-538.

Falnes,P.O., Bjoras,M., Aas,P.A., Sundheim,O., and Seeberg,E. (2004). Substrate specificities of bacterial and human AlkB proteins. Nucleic Acids Res. *32*, 3456-3461.

Fang,J., Feng,Q., Ketel,C.S., Wang,H., Cao,R., Xia,L., Erdjument-Bromage,H., Tempst,P., Simon,J.A., and Zhang,Y. (2002). Purification and functional characterization of SET8, a nucleosomal histone H4-lysine 20-specific methyltransferase. Curr. Biol. *12*, 1086-1099.

Favot,L., Hall,S.M., Haworth,S.G., and Kemp,P.R. (2005). Cytoplasmic YY1 is associated with increased smooth muscle-specific gene expression: implications for neonatal pulmonary hypertension. Am. J Pathol. *167*, 1497-1509.

Fawcett,D.W., Ito,S., and SLAUTTERBACK,D. (1959). The occurrence of intercellular bridges in groups of cells exhibiting synchronous differentiation. J. Biophys. Biochem. Cytol. *5*, 453-460.

Field,S.J., Pinder,J.C., Clough,B., Dluzewski,A.R., Wilson,R.J., and Gratzer,W.B. (1993). Actin in the merozoite of the malaria parasite, Plasmodium falciparum
1. Cell Motil. Cytoskeleton *25*, 43-48.

Fomproix,N. and Percipalle,P. (2004). An actin-myosin complex on actively transcribing genes. Exp. Cell Res *294*, 140-148.

Fu,D., Brophy,J.A., Chan,C.T., Atmore,K.A., Begley,U., Paules,R.S., Dedon,P.C., Begley,T.J., and Samson,L.D. (2010). Human AlkB homolog ABH8 Is a tRNA methyltransferase required for wobble uridine modification and DNA damage survival. Mol. Cell Biol. *30*, 2449-2459.

Fu,D., Jordan,J.J., and Samson,L.D. (2013). Human ALKBH7 is required for alkylation and oxidation-induced programmed necrosis. Genes Dev. *27*, 1089-1100.

Fu,Y., Dai,Q., Zhang,W., Ren,J., Pan,T., and He,C. (2010). The AlkB domain of mammalian ABH8 catalyzes hydroxylation of 5-methoxycarbonylmethyluridine at the wobble position of tRNA. Angew. Chem. Int. Ed Engl. *49*, 8885-8888.

Gao,W., Li,L., Xu,P., Fang,J., Xiao,S., and Chen,S. (2011). Frequent down-regulation of hABH2 in gastric cancer and its involvement in growth of cancer cells. J. Gastroenterol. Hepatol. *26*, 577-584.

Gauss-Muller,V., Kleinman,H.K., Martin,G.R., and Schiffmann,E. (1980). Role of attachment factors and attractants in fibroblast chemotaxis. J. Lab Clin. Med. *96*, 1071-1080.

Gerken,T., Girard,C.A., Tung,Y.C.L., Webby,C.J., Saudek,V., Hewitson,K.S., Yeo,G.S.H., McDonough,M.A., Cunliffe,S., McNeill,L.A., Galvanovskis,J., Rorsman,P., Robins,P., Prieur,X., Coll,A.P., Ma,M., Jovanovic,Z., Farooqi,I.S., Sedgwick,B., Barroso,I.s., Lindahl,T., Ponting,C.P., Ashcroft,F.M., O'Rahilly,S., and Schofield,C.J. (2007). The Obesity-Associated FTO Gene Encodes a 2-Oxoglutarate-Dependent Nucleic Acid Demethylase. Science *318*, 1469-1472.

Giannone,G., Dubin-Thaler,B.J., Rossier,O., Cai,Y., Chaga,O., Jiang,G., Beaver,W., Dobereiner,H.G., Freund,Y., Borisy,G., and Sheetz,M.P. (2007). Lamellipodial actin mechanically links myosin activity with adhesion-site formation. Cell *128*, 561-575.

Gieni,R.S. and Hendzel,M.J. (2009). Actin dynamics and functions in the interphase nucleus: moving toward an understanding of nuclear polymeric actin
1. Biochem. Cell Biol. *87*, 283-306.

Glazier,A.M., Nadeau,J.H., and Aitman,T.J. (2002). Finding genes that underlie complex traits
2. Science *298*, 2345-2349.

Glotzer,M. (2005). The Molecular Requirements for Cytokinesis. Science *307*, 1735-1739.

Greenbaum,M.P., Yan,W., Wu,M.H., Lin,Y.N., Agno,J.E., Sharma,M., Braun,R.E., Rajkovic,A., and Matzuk,M.M. (2006). TEX14 is essential for intercellular bridges and fertility in male mice. Proc. Natl. Acad. Sci. U. S. A *103*, 4982-4987.

Greenbaum,M.P., Ma,L., and Matzuk,M.M. (2007). Conversion of midbodies into germ cell intercellular bridges. Dev. Biol. *305*, 389-396.

Guo,S. and Kemphues,K.J. (1996). A non-muscle myosin required for embryonic polarity in Caenorhabditis elegans. Nature *382*, 455-458.

Gupton,S.L. and Waterman-Storer,C.M. (2006). Spatiotemporal feedback between actomyosin and focal-adhesion systems optimizes rapid cell migration. Cell *125*, 1361-1374.

Haller,K., Rambaldi,I., Daniels,E., and Featherstone,M. (2004). Subcellular localization of multiple PREP2 isoforms is regulated by actin, tubulin, and nuclear export. J Biol Chem *279*, 49384-49394.

Hausinger,R.P. (2004). FeII/alpha-ketoglutarate-dependent hydroxylases and related enzymes. Crit Rev. Biochem. Mol. Biol. *39*, 21-68.

He,Y., Korboukh,I., Jin,J., and Huang,J. (2012). Targeting protein lysine methylation and demethylation in cancers
1. Acta Biochim. Biophys. Sin. (Shanghai) *44*, 70-79.

Heath,J.P. and Holifield,B.F. (1991). Cell locomotion: new research tests old ideas on membrane and cytoskeletal flow. Cell Motil. Cytoskeleton *18*, 245-257.

Herman,I.M. (1993). Actin isoforms
6033. Curr. Opin. Cell Biol. *5*, 48-55.

Hess,R.A. and Renato de,F.L. (2008). Spermatogenesis and cycle of the seminiferous epithelium. Adv. Exp. Med. Biol *636*, 1-15.

Hodge,T. and Cope,M.J. (2000). A myosin family tree
6035. J. Cell Sci. *113 Pt 19*, 3353-3354.

Hofmann,W.A., Vargas,G.M., Ramchandran,R., Stojiljkovic,L., Goodrich,J.A., and de,L.P. (2006). Nuclear myosin I is necessary for the formation of the first phosphodiester bond during transcription initiation by RNA polymerase II. J Cell Biochem. *99*, 1001-1009.

Hofmann,W.A. (2009). Cell and molecular biology of nuclear actin. Int. Rev. Cell Mol. Biol. *273*, 219-263.

Huang,J., Perez-Burgos,L., Placek,B.J., Sengupta,R., Richter,M., Dorsey,J.A., Kubicek,S., Opravil,S., Jenuwein,T., and Berger,S.L. (2006). Repression of p53 activity by Smyd2-mediated methylation. Nature *444* , 629-632.

Huang,J., Sengupta,R., Espejo,A.B., Lee,M.G., Dorsey,J.A., Richter,M., Opravil,S., Shiekhattar,R., Bedford,M.T., Jenuwein,T., and Berger,S.L. (2007). p53 is regulated by the lysine demethylase LSD1. Nature *449*, 105-108.

Huang,J., Dorsey,J., Chuikov,S., Perez-Burgos,L., Zhang,X., Jenuwein,T., Reinberg,D., and Berger,S.L. (2010). G9a and Glp methylate lysine 373 in the tumor suppressor p53. J Biol Chem *285*, 9636-9641.

Hurley,J.H. (1996). The sugar kinase/heat shock protein 70/actin superfamily: implications of conserved structure for mechanism
6030. Annu. Rev. Biophys. Biomol. Struct. *25*, 137-162.

Jaalouk,D.E. and Lammerding,J. (2009). Mechanotransduction gone awry. Nat Rev Mol Cell Biol *10*, 63-73.

Jay,P.Y., Pham,P.A., Wong,S.A., and Elson,E.L. (1995). A mechanical function of myosin II in cell motility. J. Cell Sci. *108 (Pt 1)*, 387-393.

Jia,G., Yang,C.G., Yang,S., Jian,X., Yi,C., Zhou,Z., and He,C. (2008). Oxidative demethylation of 3-methylthymine and 3-methyluracil in single-stranded DNA and RNA by mouse and human FTO. FEBS Lett. *582*, 3313-3319.

Jia,G., Fu,Y., Zhao,X., Dai,Q., Zheng,G., Yang,Y., Yi,C., Lindahl,T., Pan,T., Yang,Y.G., and He,C. (2011). N6-Methyladenosine in nuclear RNA is a major substrate of the obesity-associated FTO. Nat Chem Biol *7*, 885-887.

Kataoka,H., Yamamoto,Y., and Sekiguchi,M. (1983). A new gene (alkB) of Escherichia coli that controls sensitivity to methyl methane sulfonate. J. Bacteriol. *153*, 1301-1307.

Kierszenbaum,A.L. and Tres,L.L. (1974). Nucleolar and perichromosomal RNA synthesis during meiotic prophase in the mouse testis. J. Cell Biol. *60*, 39-53.

Kilpelainen,T.O., Qi,L., Brage,S., Sharp,S.J., Sonestedt,E., Demerath,E., Ahmad,T., Mora,S., Kaakinen,M., Sandholt,C.H., Holzapfel,C., Autenrieth,C.S., Hypponen,E., Cauchi,S., He,M.A., Kutalik,Z., Kumari,M., Stancakova,A., Meidtner,K., Balkau,B., Tan,J.T., Mangino,M., Timpson,N.J., Song,Y.Q., Zillikens,M.C., Jablonski,K.A., Garcia,M.E., Johansson,S., Bragg-Gresham,J.L., Wu,Y., van Vliet-Ostaptchouk,J.V., Onland-Moret,N.C., Zimmermann,E., Rivera,N.V., Tanaka,T., Stringham,H.M., Silbernagel,G., Kanoni,S., Feitosa,M.F., Snitker,S., Ruiz,J.R., Metter,J., Larrad,M.T.M., Atalay,M., Hakanen,M., Amin,N., Cavalcanti-Proenca,C., Grontved,A., Hallmans,G., Jansson,J.O., Kuusisto,J., Kahonen,M., Lutsey,P.L., Nolan,J.J., Palla,L., Pedersen,O., Perusse,L., Renstrom,F., Scott,R.A., Shungin,D., Sovio,U., Tammelin,T.H., Ronnemaa,T., Lakka,T.A., Uusitupa,M., Rios,M.S., Ferrucci,L., Bouchard,C., Meirhaeghe,A., Fu,M., Walker,M., Borecki,I.B., Dedoussis,G.V., Fritsche,A., Ohlsson,C., Boehnke,M., Bandinelli,S., van Duijn,C.M., Ebrahim,S., Lawlor,D.A., Gudnason,V., Harris,T.B., Sorensen,T.I.A., Mohlke,K.L., Hofman,A., Uitterlinden,A.G., Tuomilehto,J., Lehtimaki,T., Raitakari,O., Isomaa,B., Njolstad,P.R., Florez,J.C., Liu,S.M., Ness,A., Spector,T.D., Tai,E.S., Froguel,P., Boeing,H., Laakso,M., Marmot,M., Bergmann,S., Power,C., Khaw,K.T., Chasman,D., Ridker,P., Hansen,T., Monda,K.L., Illig,T., Jarvelin,M.R., Wareham,N.J., Hu,F.B., Groop,L.C., Orho-Melander,M., Ekelund,U., Franks,P.W., and Loos,R.J.F. (2011). Physical Activity Attenuates the Influence of FTO Variants on Obesity Risk: A Meta-Analysis of 218,166 Adults and 19,268 Children. Plos Medicine *8*.

Kim,W., Bennett,E.J., Huttlin,E.L., Guo,A., Li,J., Possemato,A., Sowa,M.E., Rad,R., Rush,J., Comb,M.J., Harper,J.W., and Gygi,S.P. (2011). Systematic and quantitative assessment of the ubiquitin-modified proteome
4. Mol. Cell *44*, 325-340.

Kontaki,H. and Talianidis,I. (2010). Lysine methylation regulates E2F1-induced cell death. Mol Cell *39*, 152-160.

Korvald,H., Molstad Moe,A.M., Cederkvist,F.H., Thiede,B., Laerdahl,J.K., Bjoras,M., and Alseth,I. (2011). Schizosaccharomyces pombe Ofd2 is a nuclear 2-oxoglutarate and iron dependent dioxygenase interacting with histones
6027. PLoS. One. *6*, e25188.

Kudryashova,E., Kudryashov,D., Kramerova,I., and Spencer,M.J. (2005). Trim32 is a ubiquitin ligase mutated in limb girdle muscular dystrophy type 2H that binds to skeletal muscle myosin and ubiquitinates actin
5. J. Mol. Biol. *354*, 413-424.

Kukalev,A., Nord,Y., Palmberg,C., Bergman,T., and Percipalle,P. (2005). Actin and hnRNP U cooperate for productive transcription by RNA polymerase II. Nat Struct. Mol Biol *12*, 238-244.

Kunizaki,M., Hamamoto,R., Silva,F.P., Yamaguchi,K., Nagayasu,T., Shibuya,M., Nakamura,Y., and Furukawa,Y. (2007). The lysine 831 of vascular endothelial growth factor receptor 1 is a novel target of methylation by SMYD3. Cancer Res *67*, 10759-10765.

Kurahashi,H., Kogo,H., Tsutsumi,M., Inagaki,H., and Ohye,T. (2012). Failure of homologous synapsis and sex-specific reproduction problems. Front Genet. *3*, 112.

Kurowski,M.A., Bhagwat,A.S., Papaj,G., and Bujnicki,J.M. (2003). Phylogenomic identification of five new human homologs of the DNA repair enzyme AlkB
243. BMC. Genomics *4*, 48.

Lachner,M. and Jenuwein,T. (2002). The many faces of histone lysine methylation. Curr. Opin. Cell Biol *14*, 286-298.

Lando,D., Balmer,J., Laue,E.D., and Kouzarides,T. (2012). The S. pombe histone H2A dioxygenase Ofd2 regulates gene expression during hypoxia
6028. PLoS. One. *7*, e29765.

Lauffenburger,D.A. and Horwitz,A.F. (1996). Cell migration: a physically integrated molecular process
7. Cell *84*, 359-369.

Lee,D.H., Jin,S.G., Cai,S., Chen,Y., Pfeifer,G.P., and O'Connor,T.R. (2005). Repair of methylation damage in DNA and RNA by mammalian AlkB homologues
6026. J. Biol. Chem. *280*, 39448-39459.

Li,Q. and Sarna,S.K. (2009). Nuclear myosin II regulates the assembly of preinitiation complex for ICAM-1 gene transcription. Gastroenterology *137*, 1051-60, 1060.

Lindsay,A.J. and McCaffrey,M.W. (2009). Myosin Vb localises to nucleoli and associates with the RNA polymerase I transcription complex
5. Cell Motil. Cytoskeleton *66*, 1057-1072.

Lu,T., Jackson,M.W., Wang,B., Yang,M., Chance,M.R., Miyagi,M., Gudkov,A.V., and Stark,G.R. (2010). Regulation of NF-kappaB by NSD1/FBXL11-dependent reversible lysine methylation of p65. Proc. Natl. Acad. Sci. U. S. A *107*, 46-51.

MacQueen,A.J. and Hochwagen,A. (2011). Checkpoint mechanisms: the puppet masters of meiotic prophase
1. Trends Cell Biol. *21*, 393-400.

Mahadevaiah,S.K., Bourc'his,D., de Rooij,D.G., Bestor,T.H., Turner,J.M., and Burgoyne,P.S. (2008). Extensive meiotic asynapsis in mice antagonises meiotic silencing of unsynapsed chromatin and consequently disrupts meiotic sex chromosome inactivation. J. Cell Biol. *182*, 263-276.

Mailand,N., Bekker-Jensen,S., Faustrup,H., Melander,F., Bartek,J., Lukas,C., and Lukas,J. (2007). RNF8 ubiquitylates histones at DNA double-strand breaks and promotes assembly of repair proteins
4. Cell *131*, 887-900.

Matzuk,M.M. and Lamb,D.J. (2002). Genetic dissection of mammalian fertility pathways. Nat. Cell Biol. *4 Suppl*, s41-s49.

Maupin,P. and Pollard,T.D. (1986). Arrangement of actin filaments and myosin-like filaments in the contractile ring and of actin-like filaments in the mitotic spindle of dividing HeLa cells. J Ultrastruct. Mol Struct. Res *94*, 92-103.

McBride,A.E. and Silver,P.A. (2001). State of the arg: protein methylation at arginine comes of age. Cell *106*, 5-8.

McDonald,D., Carrero,G., Andrin,C., de,V.G., and Hendzel,M.J. (2006). Nucleoplasmic beta-actin exists in a dynamic equilibrium between low-mobility polymeric species and rapidly

diffusing populations
1. J. Cell Biol. *172*, 541-552.

Miller,C.J., Cheung,P., White,P., and Reisler,E. (1995). Actin's view of actomyosin interface
1. Biophys. J. *68*, 50S-54S.

Mitchison,T.J. and Cramer,L.P. (1996). Actin-based cell motility and cell locomotion
1. Cell *84*, 371-379.

Mogensen,J., Klausen,I.C., Pedersen,A.K., Egeblad,H., Bross,P., Kruse,T.A., Gregersen,N., Hansen,P.S., Baandrup,U., and Borglum,A.D. (1999). Alpha-cardiac actin is a novel disease gene in familial hypertrophic cardiomyopathy
1
6074. J. Clin. Invest *103*, R39-R43.

Muller,T.A., Meek,K., and Hausinger,R.P. (2010). Human AlkB homologue 1 (ABH1) exhibits DNA lyase activity at abasic sites. DNA Repair (Amst) *9*, 58-65.

Muller,T.A., Andrzejak,M.M., and Hausinger,R.P. (2013). A covalent protein-DNA 5'-product adduct is generated following AP lyase activity of human ALKBH1 (AlkB homologue 1)
1. Biochem. J. *452*, 509-518.

Muller,T.A., Yu,K., Hausinger,R.P., and Meek,K. (2013). ALKBH1 Is Dispensable for Abasic Site Cleavage during Base Excision Repair and Class Switch Recombination. PLoS. One. *8*, e67403.

Munsie,L., Caron,N., Atwal,R.S., Marsden,I., Wild,E.J., Bamburg,J.R., Tabrizi,S.J., and Truant,R. (2011). Mutant huntingtin causes defective actin remodeling during stress: defining a new role for transglutaminase 2 in neurodegenerative disease. Hum. Mol. Genet. *20*, 1937-1951.

Murakami,K., Yasunaga,T., Noguchi,T.Q., Gomibuchi,Y., Ngo,K.X., Uyeda,T.Q., and Wakabayashi,T. (2010). Structural basis for actin assembly, activation of ATP hydrolysis, and delayed phosphate release
1. Cell *143*, 275-287.

Nemethova,M., Auinger,S., and Small,J.V. (2008). Building the actin cytoskeleton: filopodia contribute to the construction of contractile bundles in the lamella. J Cell Biol *180*, 1233-1244.

Nishioka,K., Chuikov,S., Sarma,K., Erdjument-Bromage,H., Allis,C.D., Tempst,P., and Reinberg,D. (2002). Set9, a novel histone H3 methyltransferase that facilitates transcription by precluding histone tail modifications required for heterochromatin formation. Genes Dev. *16*, 479-489.

Nordstrand,L.M., Furu,K., Paulsen,J., Rognes,T., and Klungland,A. (2012). Alkbh1 and Tzfp repress a non-repeat piRNA cluster in pachytene spermatocytes
1. Nucleic Acids Res. *40*, 10950-10963.

Normand,G. and King,R.W. (2010). Understanding cytokinesis failure. Adv. Exp. Med. Biol. *676*, 27-55.

Nowak,G., Pestic-Dragovich,L., Hozak,P., Philimonenko,A., Simerly,C., Schatten,G., and de,L.P. (1997). Evidence for the presence of myosin I in the nucleus. J Biol Chem *272*, 17176-17181.

Nyman,T., Schuler,H., Korenbaum,E., Schutt,C.E., Karlsson,R., and Lindberg,U. (2002). The role of MeH73 in actin polymerization and ATP hydrolysis
6. J. Mol. Biol. *317*, 577-589.

Obrdlik,A., Kukalev,A., Louvet,E., Farrants,A.K., Caputo,L., and Percipalle,P. (2008). The histone acetyltransferase PCAF associates with actin and hnRNP U for RNA polymerase II transcription. Mol Cell Biol *28*, 6342-6357.

Oda,T., Iwasa,M., Aihara,T., Maeda,Y., and Narita,A. (2009). The nature of the globular- to fibrous-actin transition
43. Nature *457*, 441-445.

Ougland,R., Lando,D., Jonson,I., Dahl,J.A., Moen,M.N., Nordstrand,L.M., Rognes,T., Lee,J.T., Klungland,A., Kouzarides,T., and Larsen,E. (2012). ALKBH1 is a histone H2A dioxygenase involved in neural differentiation
6024. Stem Cells *30*, 2672-2682.

Pan,Z., Sikandar,S., Witherspoon,M., Dizon,D., Nguyen,T., Benirschke,K., Wiley,C., Vrana,P., and Lipkin,S.M. (2008). Impaired placental trophoblast lineage differentiation in Alkbh1(-/-) mice
5978. Dev. Dyn. *237*, 316-327.

Pederson,T. and Aebi,U. (2002). Actin in the nucleus: what form and what for? J. Struct. Biol. *140*, 3-9.

Percipalle,P. and Farrants,A.K. (2006). Chromatin remodelling and transcription: be-WICHed by nuclear myosin 1. Curr. Opin. Cell Biol *18*, 267-274.

Pestic-Dragovich,L., Stojiljkovic,L., Philimonenko,A.A., Nowak,G., Ke,Y., Settlage,R.E., Shabanowitz,J., Hunt,D.F., Hozak,P., and de,L.P. (2000). A myosin I isoform in the nucleus. Science *290*, 337-341.

Philimonenko,V.V., Zhao,J., Iben,S., Dingova,H., Kysela,K., Kahle,M., Zentgraf,H., Hofmann,W.A., de,L.P., Hozak,P., and Grummt,I. (2004). Nuclear actin and myosin I are required for RNA polymerase I transcription. Nat Cell Biol *6*, 1165-1172.

Phillips,B.T., Gassei,K., and Orwig,K.E. (2010). Spermatogonial stem cell regulation and spermatogenesis
1. Philos. Trans. R. Soc. Lond B Biol. Sci. *365*, 1663-1678.

Piekny,A., Werner,M., and Glotzer,M. (2005). Cytokinesis: welcome to the Rho zone. Trends Cell Biol. *15*, 651-658.

Piekny,A.J. and Glotzer,M. (2008). Anillin is a scaffold protein that links RhoA, actin, and myosin during cytokinesis. Curr. Biol *18*, 30-36.

Pollard,T.D. and Borisy,G.G. (2003). Cellular motility driven by assembly and disassembly of actin filaments. Cell *112*, 453-465.

Pollard,T.D. (2010). Mechanics of cytokinesis in eukaryotes
4. Curr. Opin. Cell Biol. *22*, 50-56.

Ponti,A., Machacek,M., Gupton,S.L., Waterman-Storer,C.M., and Danuser,G. (2004). Two distinct actin networks drive the protrusion of migrating cells. Science *305*, 1782-1786.

Pranchevicius,M.C., Baqui,M.M., Ishikawa-Ankerhold,H.C., Lourenco,E.V., Leao,R.M., Banzi,S.R., dos Santos,C.T., Roque-Barreira,M.C., Espreafico,E.M., and Larson,R.E. (2008). Myosin Va phosphorylated on Ser1650 is found in nuclear speckles and redistributes to nucleoli upon inhibition of transcription. Cell Motil. Cytoskeleton *65*, 441-456.

Procaccio,V., Salazar,G., Ono,S., Styers,M.L., Gearing,M., Davila,A., Jimenez,R., Juncos,J., Gutekunst,C.A., Meroni,G., Fontanella,B., Sontag,E., Sontag,J.M., Faundez,V., and Wainer,B.H. (2006). A mutation of beta -actin that alters depolymerization dynamics is

associated with autosomal dominant developmental malformations, deafness, and dystonia 2. Am. J. Hum. Genet. *78*, 947-960.

Qi,T., Tang,W., Wang,L., Zhai,L., Guo,L., and Zeng,X. (2011). G-actin participates in RNA polymerase II-dependent transcription elongation by recruiting positive transcription elongation factor b (P-TEFb). J Biol Chem *286*, 15171-15181.

Raghavan,M., Lindberg,U., and Schutt,C. (1992). The use of alternative substrates in the characterization of actin-methylating and carnosine-methylating enzymes. Eur. J. Biochem. *210*, 311-318.

Razafsky,D. and Hodzic,D. (2009). Bringing KASH under the SUN: the many faces of nucleo-cytoskeletal connections. J Cell Biol *186*, 461-472.

Reynard,L.N. and Turner,J.M. (2009). Increased sex chromosome expression and epigenetic abnormalities in spermatids from male mice with Y chromosome deletions 1. J. Cell Sci. *122*, 4239-4248.

Ridley,A.J., Schwartz,M.A., Burridge,K., Firtel,R.A., Ginsberg,M.H., Borisy,G., Parsons,J.T., and Horwitz,A.R. (2003). Cell migration: integrating signals from front to back 1. Science *302*, 1704-1709.

Ringvoll,J., Nordstrand,L.M., Vagbo,C.B., Talstad,V., Reite,K., Aas,P.A., Lauritzen,K.H., Liabakk,N.B., Bjork,A., Doughty,R.W., Falnes,P.O., Krokan,H.E., and Klungland,A. (2006). Repair deficient mice reveal mABH2 as the primary oxidative demethylase for repairing 1meA and 3meC lesions in DNA. EMBO J. *25*, 2189-2198.

Rodgers,B.D. (2005). Insulin-like growth factor-I downregulates embryonic myosin heavy chain (eMyHC) in myoblast nuclei. Growth Horm. IGF. Res *15*, 377-383.

Roeder,G.S. and Bailis,J.M. (2000). The pachytene checkpoint 1. Trends Genet. *16*, 395-403.

Rubenstein,P.A. (1990). The functional importance of multiple actin isoforms 6032. Bioessays *12*, 309-315.

Russel,L.D., Ettlin,R.A.S.H.A.E., and Clegg,E.D. (1990). Histological and Histopathological Evaluation of the Testis. Clearwater: Cache River Press; 1990. Clearwater: Cache River Press).

Russell,L.D., Vogl,A.W., and Weber,J.E. (1987). Actin localization in male germ cell intercellular bridges in the rat and ground squirrel and disruption of bridges by cytochalasin D. Am. J. Anat. *180*, 25-40.

Saha,S., Wong,C.C., Xu,T., Namgoong,S., Zebroski,H., Yates,J.R., III, and Kashina,A. (2011). Arginylation and methylation double up to regulate nuclear proteins and nuclear architecture in vivo. Chem. Biol. *18*, 1369-1378.

Sanger,J.M. and Sanger,J.W. (1980). Banding and polarity of actin filaments in interphase and cleaving cells. J Cell Biol *86*, 568-575.

Sanger,J.M., Mittal,B., Dome,J.S., and Sanger,J.W. (1989). Analysis of cell division using fluorescently labeled actin and myosin in living PtK2 cells. Cell Motil. Cytoskeleton *14*, 201-219.

Schroder,R.R., Manstein,D.J., Jahn,W., Holden,H., Rayment,I., Holmes,K.C., and Spudich,J.A. (1993). Three-dimensional atomic model of F-actin decorated with Dictyostelium myosin S1. Nature *364*, 171-174.

Schwarzacher,H.G. and Wachtler,F. (1993). The nucleolus. Anat. Embryol. (Berl) *188*, 515-536.

Schweitzer,J.K. and Souza-Schorey,C. (2004). Finishing the job: cytoskeletal and membrane events bring cytokinesis to an end. Exp. Cell Res *295*, 1-8.

Sedgwick,B., Robins,P., and Lindahl,T. (2006). Direct Removal of Alkylation Damage from DNA by AlkB and Related DNA Dioxygenases. In Methods in Enzymology
DNA Repair, Part A, a.P.M.Judith Campbell, ed. Academic Press), pp. 108-120.

Sedgwick,B., Bates,P.A., Paik,J., Jacobs,S.C., and Lindahl,T. (2007). Repair of alkylated DNA: Recent advances. DNA Repair *6*, 429-442.

Sellers,J.R. (2000). Myosins: a diverse superfamily. Biochim. Biophys. Acta *1496*, 3-22.

Shawlot,W., Deng,J.M., Fohn,L.E., and Behringer,R.R. (1998). Restricted beta-galactosidase expression of a hygromycin-lacZ gene targeted to the beta-actin locus and embryonic lethality of beta-actin mutant mice. Transgenic Res. *7*, 95-103.

Shi,X., Kachirskaia,I., Yamaguchi,H., West,L.E., Wen,H., Wang,E.W., Dutta,S., Appella,E., and Gozani,O. (2007). Modulation of p53 function by SET8-mediated methylation at lysine 382. Mol Cell *27*, 636-646.

Shi,Y. (2004). Histone demethylation mediated by the nuclear amine oxidase homolog LSD1.

Shimada,K., Nakamura,M., Anai,S., De,V.M., Tanaka,M., Tsujikawa,K., Ouji,Y., and Konishi,N. (2009). A novel human AlkB homologue, ALKBH8, contributes to human bladder cancer progression. Cancer Res. *69*, 3157-3164.

Shmerling,D. (2005). Strong and ubiquitous expression of transgenes targeted into the beta-actin locus by Cre/lox cassette replacement.

Siomi,M.C., Sato,K., Pezic,D., and Aravin,A.A. (2011). PIWI-interacting small RNAs: the vanguard of genome defence
2. Nat. Rev. Mol. Cell Biol. *12*, 246-258.

Small,J.V. and Resch,G.P. (2005). The comings and goings of actin: coupling protrusion and retraction in cell motility
1. Curr. Opin. Cell Biol. *17*, 517-523.

Solberg,A., Robertson,A.B., Aronsen,J.M., Rognmo,O., Sjaastad,I., Wisloff,U., and Klungland,A. (2013). Deletion of mouse Alkbh7 leads to obesity. J. Mol. Cell Biol. *5*, 194-203.

Songe-Moller,L., van den,B.E., Leihne,V., Vagbo,C.B., Kristoffersen,T., Krokan,H.E., Kirpekar,F., Falnes,P.O., and Klungland,A. (2010). Mammalian ALKBH8 possesses tRNA methyltransferase activity required for the biogenesis of multiple wobble uridine modifications implicated in translational decoding. Mol. Cell Biol. *30*, 1814-1827.

Steigemann,P. and Gerlich,D.W. (2009). Cytokinetic abscission: cellular dynamics at the midbody. Trends Cell Biol. *19*, 606-616.

Subramanian,K., Jia,D., Kapoor-Vazirani,P., Powell,D.R., Collins,R.E., Sharma,D., Peng,J., Cheng,X., and Vertino,P.M. (2008). Regulation of estrogen receptor alpha by the SET7 lysine methyltransferase. Mol Cell *30*, 336-347.

Svitkina,T.M., Verkhovsky,A.B., McQuade,K.M., and Borisy,G.G. (1997). Analysis of the actin-myosin II system in fish epidermal keratocytes: mechanism of cell body translocation. J Cell Biol *139*, 397-415.

Taniguchi,S., Kawano,T., Kakunaga,T., and Baba,T. (1986). Differences in expression of a variant actin between low and high metastatic B16 melanoma
3
6076. J. Biol. Chem. *261*, 6100-6106.

Tasaki,M., Shimada,K., Kimura,H., Tsujikawa,K., and Konishi,N. (2011). ALKBH3, a human AlkB homologue, contributes to cell survival in human non-small-cell lung cancer. Br. J. Cancer *104*, 700-706.

Taylor,D.R. and Ingvarsson,P.K. (2003). Common features of segregation distortion in plants and animals
1. Genetica *117*, 27-35.

Terman,J.R. and Kashina,A. (2013). Post-translational modification and regulation of actin
5987. Curr. Opin. Cell Biol. *25* , 30-38.

Tres,L.L. (2005). XY chromosomal bivalent: nucleolar attraction
4. Mol. Reprod. Dev. *72*, 1-6.

Trewick,S.C., Henshaw,T.F., Hausinger,R.P., Lindahl,T., and Sedgwick,B. (2002). Oxidative demethylation by Escherichia coli AlkB directly reverts DNA base damage. Nature *419*, 174-178.

Tsujikawa,K., Koike,K., Kitae,K., Shinkawa,A., Arima,H., Suzuki,T., Tsuchiya,M., Makino,Y., Furukawa,T., Konishi,N., and Yamamoto,H. (2007). Expression and sub-cellular localization of human ABH family molecules. J. Cell Mol. Med. *11*, 1105-1116.

Tsukada,Y., Fang,J., Erdjument-Bromage,H., Warren,M.E., Borchers,C.H., Tempst,P., and Zhang,Y. (2006). Histone demethylation by a family of JmjC domain-containing proteins. Nature *439*, 811-816.

Tullio,A.N., Accili,D., Ferrans,V.J., Yu,Z.X., Takeda,K., Grinberg,A., Westphal,H., Preston,Y.A., and Adelstein,R.S. (1997). Nonmuscle myosin II-B is required for normal development of the mouse heart
4602. Proc. Natl. Acad. Sci. U. S. A *94*, 12407-12412.

Tullio,A.N., Bridgman,P.C., Tresser,N.J., Chan,C.C., Conti,M.A., Adelstein,R.S., and Hara,Y. (2001). Structural abnormalities develop in the brain after ablation of the gene encoding nonmuscle myosin II-B heavy chain
4006. J Comp Neurol. *433*, 62-74.

van den Born,E., Vagbo,C.B., Songe-Moller,L., Leihne,V., Lien,G.F., Leszczynska,G., Malkiewicz,A., Krokan,H.E., Kirpekar,F., Klungland,A., and Falnes,P.O. (2011). ALKBH8-mediated formation of a novel diastereomeric pair of wobble nucleosides in mammalian tRNA. Nat. Commun. *2*, 172.

van,W.E., Krieger,E., Kemperman,M.H., De Leenheer,E.M., Huygen,P.L., Cremers,C.W., Cremers,F.P., and Kremer,H. (2003). A mutation in the gamma actin 1 (ACTG1) gene causes autosomal dominant hearing loss (DFNA20/26)
6
6075. J. Med. Genet. *40*, 879-884.

Vartiainen,M.K., Guettler,S., Larijani,B., and Treisman,R. (2007). Nuclear actin regulates dynamic subcellular localization and activity of the SRF cofactor MAL. Science *316*, 1749-1752.

Vavylonis,D., Wu,J.Q., Hao,S., O'Shaughnessy,B., and Pollard,T.D. (2008). Assembly mechanism of the contractile ring for cytokinesis by fission yeast. Science *319*, 97-100.

Verkhovsky,A.B., Svitkina,T.M., and Borisy,G.G. (1999). Self-polarization and directional motility of cytoplasm
6. Curr. Biol. *9*, 11-20.

Vicente-Manzanares,M., Webb,D.J., and Horwitz,A.R. (2005). Cell migration at a glance. J. Cell Sci. *118*, 4917-4919.

Vicente-Manzanares,M., Zareno,J., Whitmore,L., Choi,C.K., and Horwitz,A.F. (2007). Regulation of protrusion, adhesion dynamics, and polarity by myosins IIA and IIB in migrating cells. J Cell Biol *176*, 573-580.

Vicente-Manzanares,M., Ma,X., Adelstein,R.S., and Horwitz,A.R. (2009). Non-muscle myosin II takes centre stage in cell adhesion and migration. Nat Rev Mol Cell Biol *10*, 778-790.

Vijayasarathy,C. and Rao,B.S. (1987). Partial purification and characterisation of S-adenosylmethionine:protein-histidine N-methyltransferase from rabbit skeletal muscle. Biochim. Biophys. Acta *923*, 156-165.

Vogl,A.W., Vaid,K.S., and Guttman,J.A. (2009). The Sertoli Cell Cytoskeleton Molecular Mechanisms in Spermatogenesis. C.Y.Cheng, ed. Springer New York), pp. 186-211.

Vreugde,S., Ferrai,C., Miluzio,A., Hauben,E., Marchisio,P.C., Crippa,M.P., Bussi,M., and Biffo,S. (2006). Nuclear myosin VI enhances RNA polymerase II-dependent transcription. Mol Cell *23*, 749-755.

Wang,H., Cao,R., Xia,L., Erdjument-Bromage,H., Borchers,C., Tempst,P., and Zhang,Y. (2001). Purification and functional characterization of a histone H3-lysine 4-specific methyltransferase. Mol. Cell *8*, 1207-1217.

Wegner,A. and Isenberg,G. (1983). 12-fold difference between the critical monomer concentrations of the two ends of actin filaments in physiological salt conditions
6031. Proc. Natl. Acad. Sci. U. S. A *80*, 4922-4925.

Wei,Y.F., Carter,K.C., Wang,R.P., and Shell,B.K. (1996). Molecular cloning and functional analysis of a human cDNA encoding an Escherichia coli AlkB homolog, a protein involved in DNA alkylation damage repair
5977. Nucleic Acids Res. *24*, 931-937.

Westbye,M.P., Feyzi,E., Aas,P.A., Vagbo,C.B., Talstad,V.A., Kavli,B., Hagen,L., Sundheim,O., Akbari,M., Liabakk,N.B., Slupphaug,G., Otterlei,M., and Krokan,H.E. (2008). Human AlkB homolog 1 is a mitochondrial protein that demethylates 3-methylcytosine in DNA and RNA
6. J. Biol. Chem. *283*, 25046-25056.

Wolfe,B.A. and Gould,K.L. (2005). Split decisions: coordinating cytokinesis in yeast. Trends Cell Biol. *15*, 10-18.

Wordinger,R.J. and Clark,A.F. (2007). Bone morphogenetic proteins and their receptors in the eye
2. Exp. Biol. Med. (Maywood.) *232*, 979-992.

Wu,J.Q. and Pollard,T.D. (2005). Counting cytokinesis proteins globally and locally in fission yeast. Science *310*, 310-314.

Wu,Q., Saunders,R.A., Szkudlarek-Mikho,M., Serna,I.L., and Chin,K.V. (2010). The obesity-associated Fto gene is a transcriptional coactivator. Biochem. Biophys. Res Commun. *401*, 390-395.

Wu,S.S., Xu,W., Liu,S., Chen,B., Wang,X.L., Wang,Y., Liu,S.F., and Wu,J.Q. (2011). Down-regulation of ALKBH2 increases cisplatin sensitivity in H1299 lung cancer cells. Acta Pharmacol. Sin. *32*, 393-398.

Wyatt,A.W., Osborne,R.J., Stewart,H., and Ragge,N.K. (2010). Bone morphogenetic protein 7 (BMP7) mutations are associated with variable ocular, brain, ear, palate, and skeletal anomalies
1. Hum. Mutat. *31*, 781-787.

Xu,G., Paige,J.S., and Jaffrey,S.R. (2010). Global analysis of lysine ubiquitination by ubiquitin remnant immunoaffinity profiling
1. Nat. Biotechnol. *28*, 868-873.

Yang,J., Huang,J., Dasgupta,M., Sears,N., Miyagi,M., Wang,B., Chance,M.R., Chen,X., Du,Y., Wang,Y., An,L., Wang,Q., Lu,T., Zhang,X., Wang,Z., and Stark,G.R. (2010). Reversible methylation of promoter-bound STAT3 by histone-modifying enzymes. Proc. Natl. Acad. Sci. U. S. A *107*, 21499-21504.

Yang,X.D., Huang,B., Li,M., Lamb,A., Kelleher,N.L., and Chen,L.F. (2009). Negative regulation of NF-kappaB action by Set9-mediated lysine methylation of the RelA subunit. EMBO J. *28*, 1055-1066.

Yao,X., Grade,S., Wriggers,W., and Rubenstein,P.A. (1999). His(73), often methylated, is an important structural determinant for actin. A mutagenic analysis of HIS(73) of yeast actin
1. J. Biol. Chem. *274*, 37443-37449.

Ye,J., Zhao,J., Hoffmann-Rohrer,U., and Grummt,I. (2008). Nuclear myosin I acts in concert with polymeric actin to drive RNA polymerase I transcription. Genes Dev. *22*, 322-330.

Zhao,K., Wang,W., Rando,O.J., Xue,Y., Swiderek,K., Kuo,A., and Crabtree,G.R. (1998). Rapid and phosphoinositol-dependent binding of the SWI/SNF-like BAF complex to chromatin after T lymphocyte receptor signaling. Cell *95*, 625-636.

Zheng,G., Dahl,J., Niu,Y., Fedorcsak,P., Huang,C.M., Li,C., V+Ñgb++,C., Shi,Y., Wang,W.L., Song,S.H., Lu,Z., Bosmans,R., Dai,Q., Hao,Y.J., Yang,X., Zhao,W.M., Tong,W.M., Wang,X.J., Bogdan,F., Furu,K., Fu,Y., Jia,G., Zhao,X., Liu,J., Krokan,H., Klungland,A., Yang,Y.G., and He,C. (2013). ALKBH5 Is a Mammalian RNA Demethylase that Impacts RNA Metabolism and Mouse Fertility. Mol. Cell *49*, 18-29.

Zhou,M. and Wang,Y.L. (2008). Distinct pathways for the early recruitment of myosin II and actin to the cytokinetic furrow. Mol Biol Cell *19*, 318-326.

Appendices; Papers and Manuscript

I Li MM*, Nilsen A*, Shi Y*, Fusser M, Ding YH, Fu Y, Liu B, Niu Y, Wu YS, Huang CM,Olofsson M, Jin KX, Lv Y, Xu XZ, He C, Dong MQ, Rendtlew Danielsen JM, Klungland A,Yang YG, ALKBH4-dependent demethylation of actin regulates actomyosin dynamics. *Nat Commun*, 4, 1832 (2013)
* shared first authorship

II Nilsen A, Gregains G, Fusser M, Fedorcsak PZ, Klungland A, ALKBH4 depletion in male germ cells leads to spermatogenic defects. Manuscript.

III Nordstrand LM, Svärd J[#], Larsen E[#], Nilsen A[#], Ougland R[#], Furu K[#], Lien GF, Rognes T, Namekawa SH, Lee JT, Klungland A, Mice lacking Alkbh1 display sex-ratio distortion and unilateral eye defects. *PLoS ONE* 5, e13827 (2010).
[#] shared 2nd authorship

nature COMMUNICATIONS

ARTICLE

Received 2 Aug 2012 | Accepted 10 Apr 2013 | Published 14 May 2013

DOI: 10.1038/ncomms2863 OPEN

ALKBH4-dependent demethylation of actin regulates actomyosin dynamics

Ming-Ming Li[1,2,*], Anja Nilsen[3,*], Yue Shi[1,2,*], Markus Fusser[3], Yue-He Ding[4], Ye Fu[5], Bo Liu[6], Yamei Niu[1], Yong-Sheng Wu[1], Chun-Min Huang[1], Maria Olofsson[3], Kang-Xuan Jin[1,2], Ying Lv[1,2], Xing-Zhi Xu[6], Chuan He[5], Meng-Qiu Dong[4], Jannie M. Rendtlew Danielsen[1,7], Arne Klungland[3,8] & Yun-Gui Yang[1,2]

Regulation of actomyosin dynamics by post-transcriptional modifications in cytoplasmic actin is still poorly understood. Here we demonstrate that dioxygenase ALKBH4-mediated demethylation of a monomethylated site in actin (K84me1) regulates actin–myosin interaction and actomyosin-dependent processes such as cytokinesis and cell migration. ALKBH4-deficient cells display elevated K84me1 levels. Non-muscle myosin II only interacts with unmethylated actin and its proper recruitment to and interaction with actin depend on ALKBH4. ALKBH4 co-localizes with the actomyosin-based contractile ring and midbody via association with methylated actin. ALKBH4-mediated regulation of actomyosin dynamics is completely dependent on its catalytic activity. Disorganization of cleavage furrow components and multinucleation associated with ALKBH4 deficiency can all be restored by reconstitution with wild-type but not catalytically inactive ALKBH4. Similar to actin and myosin knock-out mice, homozygous Alkbh4 mutant mice display early embryonic lethality. These findings imply that ALKBH4-dependent actin demethylation regulates actomyosin function by promoting actin-non-muscle myosin II interaction.

[1] Genome Structure and Stability Group, BIG CAS-OSLO Genome Research Cooperation, Disease Genomics and Individualized Medicine Laboratory, Beijing Institute of Genomics, Chinese Academy of Sciences, No. 1-7 Beichen West Road, Chaoyang District, Beijing 100101, China. [2] University of Chinese Academy of Sciences, 19A Yuquan Road, Beijing 100049, China. [3] Clinic for Diagnostics and Intervention and Institute of Medical Microbiology, BIG CAS-OSLO Genome Research Cooperation, Oslo University Hospital Rikshospitalet, Oslo 0027, Norway. [4] National Institute of Biological Sciences, Beijing 102206, China. [5] Department of Chemistry and Institute for Biophysical Dynamics, The University of Chicago, 929 East 57th Street, Chicago, Illinois 60637, USA. [6] Beijing Key Laboratory of DNA Damage Response, College of Life Sciences, Capital Normal University, Beijing 100048, China. [7] The Novo Nordisk Foundation Center for Protein Research, Ubiquitin Signalling Group, Faculty of Health Sciences, Blegdamsvej 3b, 2200 Copenhagen, Denmark. [8] Institute of Basic Medical Sciences, University of Oslo, PO Box 1018, Blindern, NO-0315 Oslo, Norway. * These authors contributed equally to this work. Correspondence and requests for materials should be addressed to Y.-G.Y. (email: ygyang@big.ac.cn) or to A.K. (email: arne.klungland@rr-research.no).

Actin is one of the most abundant proteins in eukaryotic cells. It exists both as monomeric (G-actin) and filamentous (F-actin) actin, and the switch between these two states is highly dynamic. Dynamic actin filament networks are involved in a large variety of cellular functions, including lamellipodium formation, cell motility and cytokinesis[1]. The actin networks are maintained through coordinated actions of a large number of regulatory proteins that modulate filament assembly and disassembly, as well as through contractility driven by myosin II motor proteins[2,3]. The process of defining the plane and position of the cleavage furrow during cytokinesis requires communication between microtubules and the actin cortex and it eventually results in F-actin and NM II assembling into the contractile ring[4,5]. The contractile ring is a highly dynamic structure with a rapid turnover of both F-actin and NM II (refs 6,7). Accumulation of F-actin in the contractile ring may occur by nucleation in the furrow or by transport of pre-existing actin filaments nucleated elsewhere[8,9]. NM II is the major motor protein involved in cytokinesis and its movement along F-actin as well as F-actin depolymerization is required for furrow ingression[10,11]. Various post-translational modifications (PTMs) have been identified in actin, including N-terminal arginylation, acetylated aspartate residues, phosphorylated tyrosine residues, and methylated histidine and lysine residues[12–16]. However, how these actin PTMs are involved in the regulation of actomyosin dynamics remains largely unknown.

The superfamily of Fe(II) and 2-oxoglutarate (2OG, α-ketoglutarate)-dependent dioxygenases (PF03171) belongs to the non-heme iron protein family, which can hydroxylate inactivated C-H groups. This class of enzymes can catalyse the demethylation of a variety of substrates[17,18]. In *E. coli*, the Fe(II)/2OG dioxygenase AlkB catalyses demethylation of various types of methyl modified DNA bases following exposure to methylating agents[19,20]. Based on sequence homology within the catalytic domain of *E. coli* AlkB, 9 human AlkB homologs have been identified, ALKBH1-8 and the somewhat less conserved FTO (refs 21,22). Like *E. coli* AlkB, ALKBH2 and ALKBH3 have been shown to possess DNA repair activity *in vivo*[23]. We have recently demonstrated that FTO and ALKBH5 are RNA m^6A (N^6-methyl-adenosine) demethylases[24,25]. Demethylation of m^6A appears to be involved in energy homeostasis and implies important roles for FTO and ALKBH5 in obesity, type II diabetes and fertility[25–29]. The AlkB domain of ALKBH8 has been shown to hydroxylate modified uridine in the wobble-position of certain tRNA isoacceptors[30,31]. ALKBH1 is the first human AlkB homologue shown to hydroxylate proteins. Like the *S. pombe* homologue, ALKBH1 catalyses demethylation of histone H2A *in vivo* and has been proposed to be involved in neural differentiation[32,33]. These findings suggest a very wide functional diversity of mammalian AlkB proteins, with substrates ranging from DNA and RNA to protein. Although ALKBH4 has been demonstrated to decarboxylate 2OG *in vitro*[34], its substrate and biological function in mammalian cells are currently unknown.

In the present study, we show that ALKBH4 mediates demethylation of actin K84me1 and thereby regulates the actin–myosin II interaction. In addition, we demonstrate that deletion of ALKBH4 is embryonically lethal and depletion leads to defects in cytokinesis and cell motility.

Results

Deletion of *Alkbh4* causes embryonic lethality in mice. To investigate the biological function of ALKBH4, we generated conditional *Alkbh4* gene-targeted mice with LoxP sites flanking exons 2 and 3 of the endogenous *Alkbh4* locus. These exons includes conserved residues presumed to constitute the Fe(II)-binding cluster and residues required for binding to the 5-carboxylate of the 2-oxoglutarate co-substrate[35,36] (Fig. 1a and Supplementary Fig. S1a). The resultant $Alkbh4^{+/L}$ (*L* refers to the floxed allele) mice were crossed with mice ubiquitously expressing Cre-recombinase to generate the *Alkbh4* null allele ($Alkbh4^{-}$) (Supplementary Fig. S1a–c). Heterozygous $Alkbh4^{+/L}$ and $Alkbh4^{+/-}$ mice develop normally, with no apparent phenotype. However, $Alkbh4^{+/-}$ intercrosses failed to give rise to homozygous $Alkbh4^{-/-}$ offspring, and the Mendelian distribution between wild-type (WT) and heterozygous genotypes indicated that disruption of *Alkbh4* results in embryonic lethality (Fig. 1b).

ALKBH4 associates with the contractile ring and midbody. Interestingly, immunofluorescence microscopy, using ALKBH4 antibodies generated for this study (Supplementary Fig. S1d,e) revealed a pronounced accumulation of ALKBH4 at contractile ring and midbody structures, as determined by co-localization of endogenous or overexpressed ALKBH4 with the contractile ring/midbody component F-actin (Fig. 1c,d) and anillin, an actomyosin scaffold protein and cleavage furrow marker (Fig. 1e). This staining pattern was also observed in $Alkbh4^{+/+}$ *Cre* mouse embryonic fibroblast (MEF) cells (Fig. 1f). Consistent with the immunofluorescence analysis, purification of contractile ring and midbody structures from human MRC5 cells demonstrated that a pool of ALKBH4 co-fractionated with the contractile ring and midbody proteins NM II, actin, α-tubulin and Plk1 (Fig. 1g). Taken together, these data suggest that ALKBH4 could be a novel factor involved in cytokinesis. This was further substantiated by mass spectrometric analysis of affinity-purified Flag-GFP-ALKBH4 protein complexes identifying the two key components of the actomyosin-based contractile ring, actin and NM II (Supplementary Fig. S2a and Supplementary Table S1). These interactions were confirmed by endogenous and exogenous co-immunoprecipitation of ALKBH4 and actin or NM II (Fig. 2a,b), suggesting that ALKBH4 indeed is a *bona fide* component of the actomyosin network. Furthermore, the fact that incubation with magnesium and ATP prevents co-precipitation of NM II with ALKBH4 implies that the interaction between ALKBH4 and NM II is mediated by actin (Fig. 2a).

Novel actin K84me1 regulates ALKBH4–actomyosin interaction. A previously reported two-dimensional gel-electrophoresis approach, followed by immunoblotting using a pan-reactive anti-methyl-lysine mouse monoclonal antibody, revealed the existence of lysine-methylated actin proteins. However, no exact sites were identified[16]. Interestingly, the mass spectrometric analysis of ALKBH4 interacting proteins indicates that monomethylated actin (K84me1) was pulled down with ALKBH4 (Supplementary Table S1). To further validate and investigate this observation, we generated an actin-K84me1 antibody that specifically recognizes K84-monomethylated actin (Supplementary Fig. S2b). We then purified HA-β-actin from human 293T cells, digested with Asp-N/Arg-C and enriched for potential K84me1 species by peptide immunoprecipitation using the actin-K84me1 antibody, and analysed by mass spectrometry. This mass spectrometry analysis confirmed that actin is indeed methylated on K84 (Supplementary Fig. S2c,d and Supplementary Table S2). We then speculated that ALKBH4 might specifically interact with actin K84me1 and/or actin K84me1 might be an *in vivo* substrate of ALKBH4. By employing two different methylation-deficient actin mutants (K84A and K84R), we confirmed that actin is methylated on lysine 84 *in vivo* (Fig. 2c). We next examined the methylation profile between F-actin and G-actin in 293T cells. Interestingly, we found that under untreated conditions methylated actin

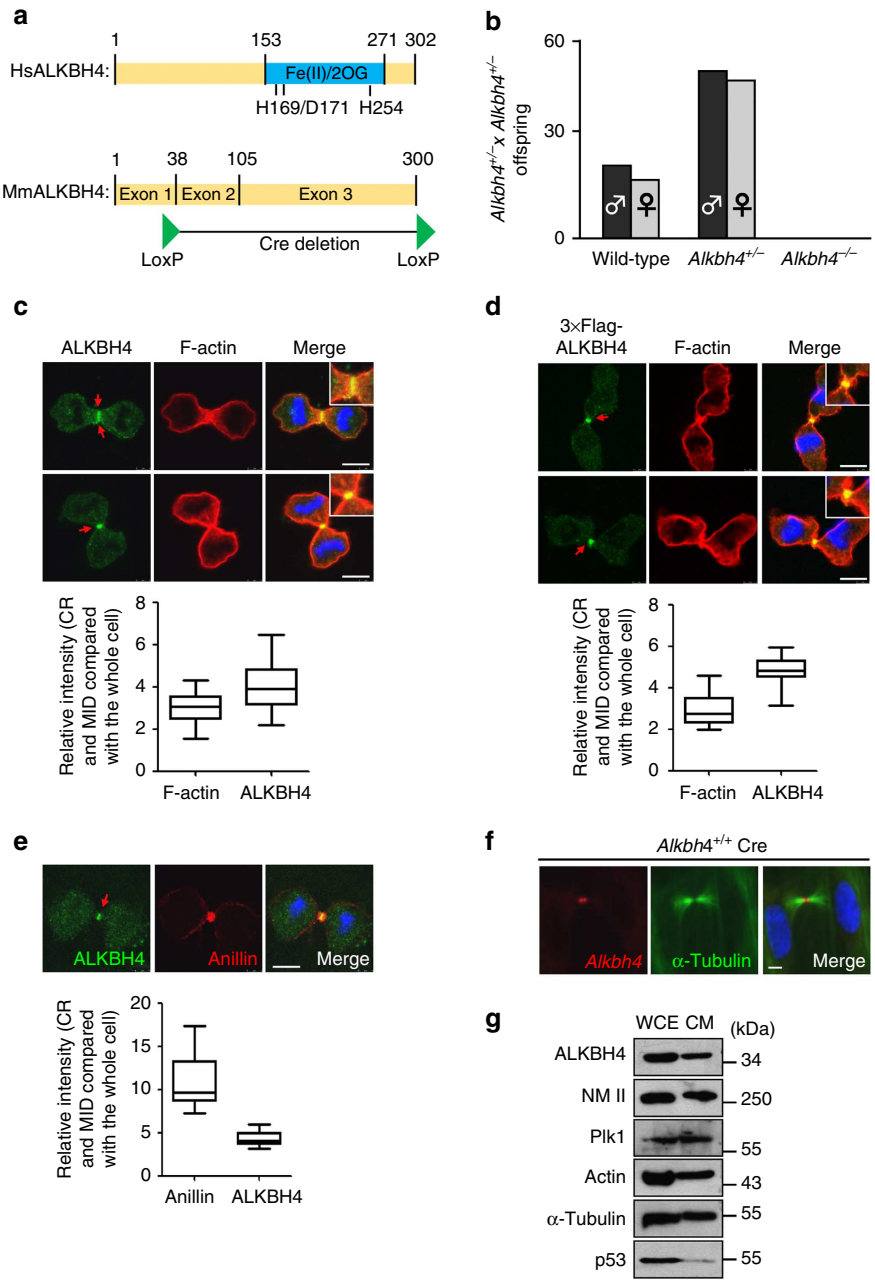

Figure 1 | Deletion of Alkbh4 causes embryonic lethality in mice and ALKBH4 associates with the contractile ring and midbody. (**a**) Schematic diagram showing human (upper panel) and mouse (lower panel) ALKBH4 protein structure with conserved catalytic amino acids within the dioxygenase domain (upper panel) and deleted exons in the *Alkbh4* knock-out allele (lower panel). (**b**) There were no homozygous *Alkbh4*$^{-/-}$ offspring from heterozygous *Alkbh4*$^{+/-}$ intercrosses. Mendelian distribution of WT and knock-out alleles indicated by the ratio 1:2:(1), WT: Het:(KO). +: WT allele; −: knock-out allele. (**c**) Endogenous ALKBH4 immunostaining in MRC5 cells with anti-ALKBH4 and F-actin staining with phalloidin. DNA was visualized by DAPI. Scale bars, 10 μm. Quantification of signal intensity (accumulation of protein) on the contractile ring (CR) and midbody (MID) relative to the whole cell (lower panel). (50 cells per condition per experiment). In box-and-whisker plot plotted by Prism5 software, median means 50% of cells is greater than this value, upper quartile or lower quartile means 25% cells is greater or less than this value and maximum or minimum means greatest or least value. (**d**) MRC5 cells stably expressing 3 × Flag-ALKBH4 were fixed and immunostained with anti-Flag and Phalloidin (F-actin). DNA was visualized by DAPI. Scale bars, 10 μm. Quantification of signal intensity (accumulation of protein) on the contractile ring (CR) and midbody (MID) relative to the whole cell (lower panel). (50 cells per condition per experiment). (**e**) MRC5 cells were fixed and immunostained with anti-ALKBH4 and anti-anillin (midbody marker). DNA was visualized by DAPI. Scale bars, 10 μm. Quantification of signal intensity (accumulation of protein) on the contractile ring (CR) and midbody (MID) relative to the whole cell (lower panel). (50 cells per condition per experiment). (**f**) MEF cells were fixed and immunostained with antibodies against ALKBH4 and α-tubulin (α-tub). DNA was visualized by DAPI. (**g**) MRC5 cells were sequentially synchronized with thymidine and nocodazole; and whole-cell extracts (WCE) and contractile ring/midbody (CM) fractions were analysed by immunoblotting with the indicated antibodies. Full-length blots are presented in Supplementary Fig. S7. Scale bars in all panels, 10 μm.

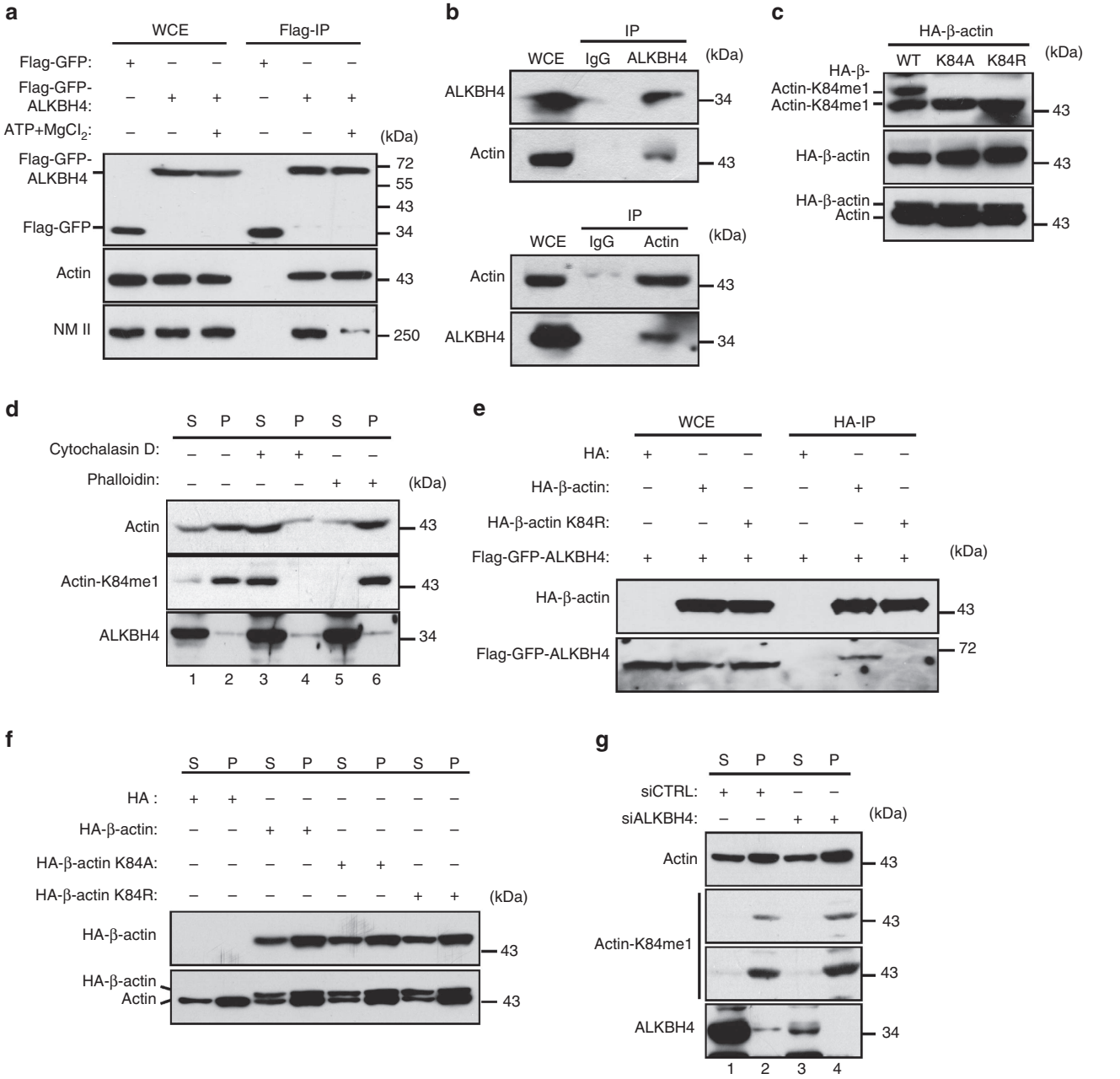

Figure 2 | Interaction of ALKBH4 with the actomyosin network and identification of actin K84 monomethylation. (**a**) Association between Flag-GFP-ALKBH4 and NM II assessed in 293T cells by immunoprecipitation. 293T cells were transfected with Flag-GFPor Flag-GFP-ALKBH4 constructs as indicated and lyisted in NET buffer, which didn't contain EDTA. In all, 2 mM ATP and 2 mM $MgCl_2$ were added into NET buffer freshly. WCE, whole-cell extract. (**b**) Association between endogenous ALKBH4 and actin assessed in MRC5 cells by co-immunoprecipitation analysis of ALKBH4 and actin using indicated antibodies. (**c**) WCEs from 293T cells transfected with HA-β-actin WT, K84A or K84R were immunoblotted with the indicated antibodies. (**d**) Detection of free and filamentous actin by actin fractionation. Semi-confluent 293T cells were treated with or without 1 μg ml^{-1} CCD and 1 μg ml^{-1} phalloidin for 30 min at 37 °C as indicated. Soluble free G-actin (S) and insoluble filamentous F-actin (P). (**e**) 293T cells were co-transfected with Flag-GFP-ALKBH4 either WT or K84R HA-β-actin as indicated and lysates were subjected to HA immunoprecipitation. Immunoprecipitates and WCE were immunoblotted with the indicated antibodies. (**f**) Forty-eight hours after transfection with the indicated DNA constructs, 293T cells were lysed and subjected to F-actin fractionation. Fractions were analysed by immunoblotting with the indicated antibodies. (**g**) Forty-eight hours after transfection with the indicated siRNAs, 293T cells were lysed and subjected to F-actin fractionation assay. Fractions were analysed by immunoblotting with the indicated antibodies. Full-length blots in all panels are presented in Supplementary Fig. S7.

preferentially exists as F-actin (Fig. 2d, lanes 1, 2). After forced disassembly of F-actin into G-actin by F-actin depolymerizing drug cytochalasin D (CCD), high levels of K84me1 G-actin were detected (Fig. 2d, lanes 3, 4). This suggests that methylated actin rapidly polymerize into filaments under physiological conditions and/or that demethylation preferentially takes place after filament formation. The expected shift in the F/G-actin ratio following treatment with either CCD (Fig. 2d, lanes 3, 4) or the F-actin stabilizing drug phalloidin (Fig. 2d, lanes 5, 6) confirmed efficient fractionation. Immunoblot analyses revealed that substitution of lysine 84 to arginine or alanine or treatment with the global methylation inhibitor AdOx (adenosine-2′, 3′-dialdehyde)

abolished the actin–ALKBH4 interaction (Figs 2e,3g and Supplementary Fig. S3a,b). This demonstrates that methylation of actin is required for efficient binding to ALKBH4. Mutation of lysine 84 to arginine and especially alanine results in a dramatic charge change that could impact the overall properties of actin. To determine if the mutants had retained functionality we tested their ability to polymerize into actin filaments. The F/G-actin fractionation showed that the distribution of G-actin and F-actin were similar in WT, K84A and K84R cells, demonstrating that both mutants could be readily incorporated into actin filaments *in vivo* (Fig. 2f). This is consistent with previous findings in yeast, showing that the K84A mutation had no effect on polymerization[37]. Furthermore, AdOx treatment did not affect actin's ability to form filaments (Supplementary Fig. S3c). In accordance with our previous data showing a strong interaction between ALKBH4 and actin as well as a clear co-localization of ALKBH4 with F-actin, we observed that, though most ALKBH4 was found in the soluble fraction, a fraction of ALKBH4 sedimented into the insoluble fraction with F-actin (Fig. 2g).

ALKBH4 promotes actin-NM II binding via actin demethylation. Though no natural substrate for ALKBH4 has yet been described, we reasoned that as ALKBH4 binds to methylated actin, accumulates at the contractile ring and midbody during cytokinesis, and possesses dioxygenase activity *in vitro*[34], ALKBH4 might mediate the removal of the methyl group on actin K84. To test this hypothesis, we first investigated if the level of actin-K84me1 correlated with expression of ALKBH4. Indeed, ALKBH4 depletion was accompanied by a dramatic increase in actin-K84me1 (Fig. 3a, lane 1 versus 2). Importantly, the increase in methylation was completely prevented by complementation with WT ALKBH4, but not by ALKBH4 containing a mutated catalytic domain (H169A/D171A/H254A (HDH)) (Fig. 3a, lanes 3–5). Additionally, overexpression of WT ALKBH4 but not the HDH ALKBH4 mutant resulted in a decrease in actin-K84me1 (Fig. 3b). Consistent with our findings in human cells, 4-hydroxytamoxifen (4-OHT) treatment of $Alkbh4^{L/L}$ MEF cells (designated $Alkbh4^{\Delta/\Delta}$) resulted in depletion of ALKBH4 and a pronounced increase in actin methylation (Fig. 3c).

It has previously been observed that a substrate may not readily dissociate from a catalytically inactive enzyme[38]. In accordance with this and the possibility of actin being an ALKBH4 substrate, we observed that the actin–ALKBH4 interaction was stronger after disruption of the dioxygenase domain in ALKBH4 (Fig. 3d). These different independent pieces of *in vivo* data presented above makes a strong indication that the actin K84me1 demethylation is dependent on ALKBH4.

X-ray crystallography and NMR have previously been used to predict the region of actin that binds to NM II (ref. 39). Interestingly, actin K84 is located within the predicted NM II interacting region, which made us speculate that methylation of K84 may influence the actin-NM II interaction. Intriguingly, and in contrast to ALKBH4 that preferentially binds to methylated actin, NM II does not interact with K84me1 (Fig. 3e). Furthermore, employing a methylation-deficient actin mutant, K84R, or inhibiting methylation by AdOx both resulted in increased NM II–actin interaction (Fig. 3f,g and Supplementary Fig. S3b,d), suggesting that ALKBH4-dependent demethylation of actin-K84me1 promotes binding of NM II to F-actin in the actomyosin network.

The ALKBH4–actomyosin interaction is mediated by actin. To better understand the functional interplay between components of the actomyosin network, we tested how depletion or inhibition of one component would affect the interaction of the other two. Consistent with the data that non-methylated actin interacts better with NM II, the NM II–actin interaction was greatly decreased in both ALKBH4-deficient MEF cells and human cells (Fig. 4a,b). NM II depletion did not influence the binding of ALKBH4 to actin (Fig. 4c and Supplementary Fig. S3e). Furthermore, treatment with the specific NM II inhibitor blebbistatin that inhibits myosin II's ability to release phosphate and to bind tightly to actin filaments only affected the NM II–actin interaction but not the interaction between ALKBH4 and actin (Fig. 4d and Supplementary Fig. S3f)[40]. Due to the high cellular abundance of actin we could not achieve efficient actin depletion. However, CCD treatment significantly impaired the binding of NM II to both actin and ALKBH4 (Fig. 4e and Supplementary Fig. S3g), suggesting that filamentous actin mediates the interaction between ALKBH4 and NM II in the ALKBH4–actomyosin complex. This is also consistent with the observation that incubation with magnesium and ATP prevents co-precipitation of ALKBH4 and NM II (Fig. 2a).

ALKBH4 deficiency affects cleavage furrow organization. The interaction of ALKBH4 with the actomyosin network and its ability to mediate demethylation of actin K84me1 suggest that ALKBH4 has an important role in cytokinesis. Strikingly, anillin and NM II failed to localize properly in ALKBH4-depleted cells during cytokinesis (Fig. 5a,b). The accumulation of the kinases Plk1 and aurora B at the midbody was also severely affected (Fig. 5a,b and Supplementary Fig. S4a,b), suggesting that ALKBH4-deficient cells have a defect in cleavage furrow formation. To investigate if ALKBH4 might also be important for other aspects of actomyosin dynamics than cytokinesis, we decided to study its impact on cell migration. Indeed, we observed a dramatic reduction in the migration ability of $Alkbh4^{\Delta/\Delta}$ compared with $Alkbh4^{L/L}$ MEF cells (Fig. 5c and Supplementary Fig. S4c), using the scratch assay method[41]. The cells were kept in low-serum medium to avoid proliferation and cell count after 24 h showed similar cell numbers between 4-OHT treated and untreated MEFs (Supplementary Fig. S4d).

Defects in the organization of the cleavage furrow may result in cytokinesis failure and formation of multinucleated cells. Indeed, ALKBH4-deficient cells, which exhibit clear defects in the organization of the cleavage furrow (Fig. 5a,b), also exhibited a dramatic increase in the frequency of multinucleation (Fig. 5d and Supplementary Fig. S4e). Multinucleated cells can result from cytokinesis failure or from a cell fusion event[42]. To distinguish between these possibilities, we followed cell division by live cell imaging, which confirmed that multinucleation observed after ALKBH4 depletion originated from aborted cytokinesis (Supplementary Fig. S5a and Supplementary Movies 1–3). Importantly, ALKBH4-deficient cells required much longer time to exit mitosis (Supplementary Fig. S5b). In many cases, cytokinesis eventually failed resulting in refusion of the two new partly separated daughter cells or apoptosis. This is consistent with FACS analyses showing a significant increase in apoptosis and hyperploid cells following ALKBH4 depletion (Fig. 6a and Supplementary Fig. S5c,d). In addition, we observed that a portion of ALKBH4-depleted cells had more than two centrosomes (Supplementary Fig. S6a). The increase in centrosome number is likely a consequence of polyploidy caused by cells failing to go through cytokinesis.

Collectively, these data indicate that ALKBH4 depletion, in addition to impairing the function of the contractile ring and hence disorganize the cleavage furrow, most likely affect a broader range of actomyosin-related functions in the cell.

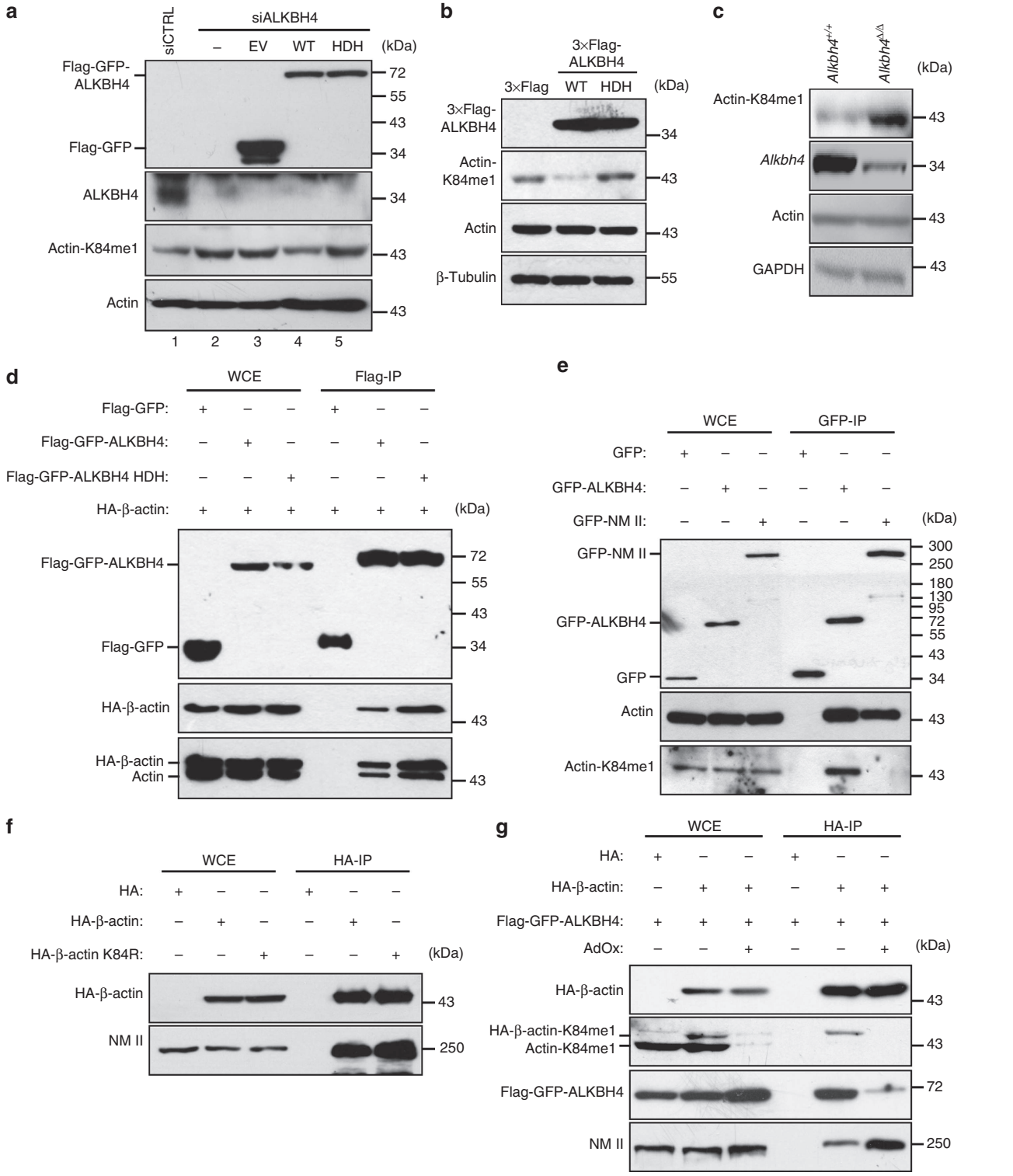

Figure 3 | ALKBH4 mediates demethylation of K84me1 actin *in vivo* regulating actomyosin interaction. (**a**) U2OS cells were simultaneously transfected with siCTRL or ALKBH4 siRNA, together with the indicated siRNA insensitive Flag-GFP-ALKBH4 constructs lysed, 48 h later cells were analysed by immunoblotting analysis using the indicated antibodies. (**b**) U2OS cells were transfected with WT or catalytically inactive ALKBH4 (HDH) and lysates were immunoblotted with the indicated antibodies. (**c**) Control *Alkbh4*$^{+/+}$*Cre* (*Alkbh4*$^{+/+}$) and *Alkbh4*$^{L/L}$*Cre* MEF (*Alkbh4*$^{\Delta/\Delta}$) cells were lysed and analysed by immunoblotting with the indicated antibodies. (**d**) 293T cells were co-transfected with Flag-GFP-ALKBH4 WT or HDH and HA-β-actin as indicated and lysates were subjected to Flag immunoprecipitation and immunoblotted with the indicated antibodies. (**e**) 293T/GFP-NM II or 293T/GFP-ALKBH4 stable cell lysates were subjected to GFP immunoprecipitation. Immunoprecipitates and WCEs were immunoblotted with the indicated antibodies. (**f**) 293T cells were transfected with WT or K84R HA-β-actin as indicated and lysates were subjected to HA immunoprecipitation. Immunoprecipitates and WCEs were immunoblotted with the indicated antibodies. Quantification of signal intensity of K84R relative to WT. (**g**) Forty-eight hours after transfection with the indicated DNA constructs, 293T cells were treated with 20 μM AdOx (adenosine-2′, 3′-dialdehyde) for 24 h, lysed and subjected to HA immunoprecipitation. Immunoprecipitates were analysed by immunoblotting with the indicated antibodies. Full-length blots in all panels are presented in Supplementary Fig. S7.

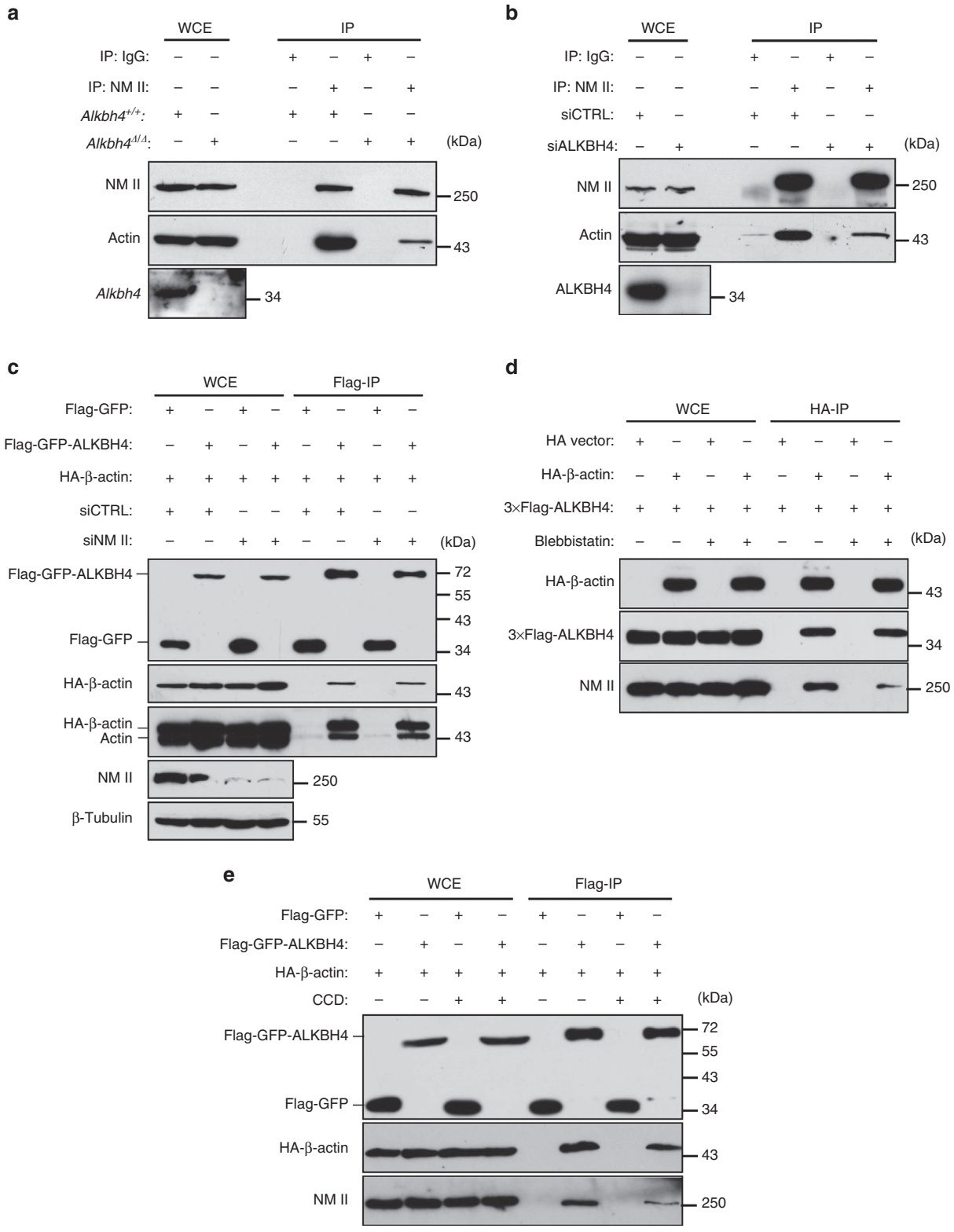

Figure 4 | The ALKBH4-Actomyosin interaction is mediated by actin. (**a**) Seventy-two hours after induction with 0.5 μM 4-OHT Control *Alkbh4*$^{+/+}$*Cre* (*Alkbh4*$^{+/+}$) and *Alkbh4*$^{L/L}$*Cre* (*Alkbh4*$^{\Delta/\Delta}$) MEF cells were lysed and subjected to NM II immunoprecipitation. Immunoprecipitates were analysed by immunoblotting with the indicated antibodies. (**b**) Forty-eight hours after transfection with the indicated siRNAs, 293T cells were lysed and subjected to NM II immunoprecipitation and subsequently immunoblotted with the indicated antibodies. (**c**) Forty-eight hours after transfection with the indicated siRNAs and DNA constructs, 293T cells were lysed and subjected to Flag immunoprecipitation. Immunoprecipitates were analysed by immunoblotting with the indicated antibodies. (**d**) Forty-eight hours after transfection with the indicated DNA constructs, 293T cells were treated with 5 μM Blebbistatin for 5 h, lysed and subjected to HA immunoprecipitation. Immunoprecipitates were analysed by immunoblotting with the indicated antibodies. (**e**) Forty-eight hours after transfection with the indicated DNA constructs, 293T cells were treated with 1 μg ml^{-1} cytochalasin D (CCD) for 1.5 h, lysed and subjected to Flag immunoprecipitation. Immunoprecipitates were analysed by immunoblotting with the indicated antibodies. Full-length blots in all panels are presented in Supplementary Fig. S7.

Complementation with WT ALKBH4 rescues cytokinesis defects. We next tested if reconstitution with WT and/or HDH-mutant ALKBH4 could rescue the cytokinesis-associated defects observed in ALKBH4-deficient cells. Cells were collected 48 h after simultaneous transfection with a combination of ALKBH4 small interfering RNA (siRNA) and ALKBH4 WT or ALKBH4 HDH. Complementation with WT, but not catalytically inactive ALKBH4, prevented multinucleation (Fig. 6b and Supplementary

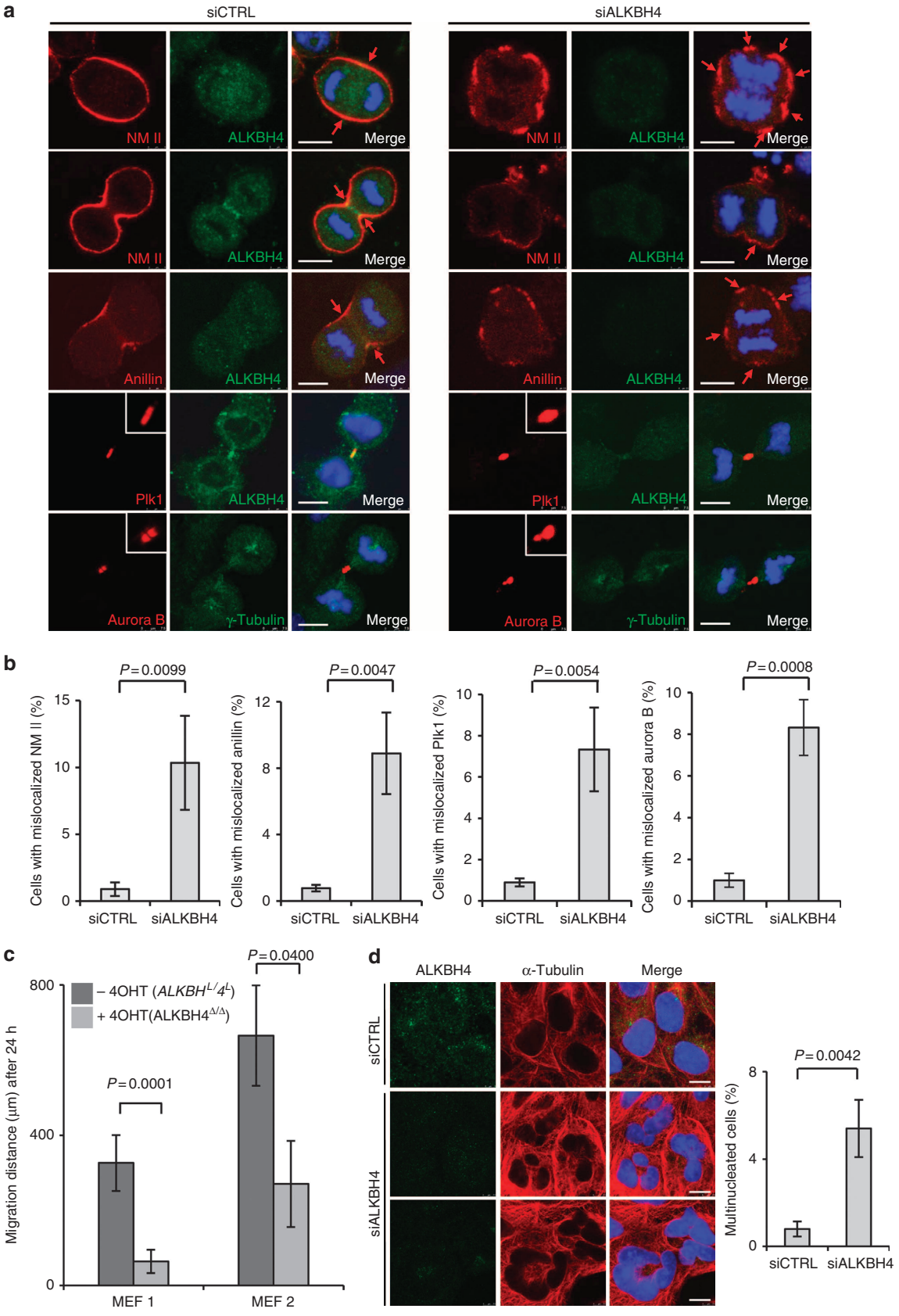

Fig. S6b) mislocalization of anillin, NM II, aurora B and Plk1 (Fig. 6c). Actually, overexpression of the HDH mutant in ALKBH4-depleted cells resulted in an even higher incidence of multinucleation (Fig. 6b) and cleavage furrow disorganization (Fig. 6c) compared with complementation with empty vector, suggesting that catalytically inactive ALKBH4 has a dominant-negative effect with regard to the ALKBH4 deficiency-associated phenotypes.

Discussion

In the present study, we have identified a novel post-translational modification on actin, K84 monomethylation, regulated by the previously uncharacterized dioxygenase ALKBH4. Though proteomic analysis using a pan-reactive anti-methyl lysine antibody previously suggested that actin might be methylated, no actual methylated residues were identified[16]. Our data demonstrate that ALKBH4-mediated demethylation of actin-K84me1 is important for maintaining actomyosin dynamics supporting normal cytokinesis and cell migration. It is not the first time PTMs of actin has been implicated in regulating cellular functions. Actin arginylation and H73me1 methylation have previously been proposed to regulate intracellular distribution of actin and polymer formation, respectively[43,44].

The interaction between the two major components of the actomyosin complex, actin and NM II, is regulated by ALKBH4-dependent demethylation of actin and is decreased in ALKBH4-deficient cells (Fig. 4a,b). These findings are further supported by the fact that NM II can bind more K84R mutant than WT actin (Fig. 3f and Supplementary Fig. S3c). In contrast, ALKBH4 specifically binds to the K84 methylated form of actin (Fig. 2e and Fig. 3e), and catalytically inactive ALKBH4 binds actin stronger than WT (Fig. 3d).

We have attempted to test the *in vitro* demethylase activity of recombinant ALKBH4 or Flag-tagged ALKBH4 purified from human cells using either synthesized methylated peptide or HA-tagged β-actin purified from 293T cells. Unfortunately, these purified ALKBH4 proteins did not display vigorous demethylation/hydroxylation under any of the experimental settings examined. This most likely reflects a need for some unknown cofactors or that the F-actin conformation in the *in vitro* experiments is incompatible with efficient ALKBH4 demethylase activity. Despite the difficulties of showing *in vitro* activity of ALKBH4, the different independent *in vivo* data presented above makes actin a strong candidate substrate of the ALKBH4 dioxygenase activity.

The reduced cell migration together with the severe problems associated with cytokinesis in ALKBH4-deficient human and murine cells suggest that ALKBH4-dependent demethylation of actin K84 has a very important role in regulating the actin–NM II interaction and actomyosin function. The facts that (1) cell motility and cytokinesis depend on proper actin–NM II interaction, (2) the actin–NM II interaction is compromised in ALKBH4-deficient cells and (3) NM II accumulation at the contractile ring and midbody is disturbed in ALKBH4-depleted cells, all point to a role of ALKBH4-mediated actin demethylation in promoting the recruitment of NM II to the cleavage furrow, and actin-NM II dependent structures in general. Actin fractionation revealed that, under physiological conditions, methylation of actin is preferentially observed on actin filaments and not monomeric actin.

With regard to actomyosin dynamics in relation to cytokinesis our findings are consistent with the following model (Fig. 7); upon recruitment to the contractile ring and midbody via interaction with methylated actin, ALKBH4 mediates demethylation of actin K84me1 and thus creates a binding site for NM II. Consecutive demethylation of actin moieties in the actin filament could then allow dynamic sliding of NM II along the actin filaments and mediate contraction of the contractile ring, resulting in cleavage furrow ingression and subsequent abscission.

Similarly to the previously described embryonic lethality of homozygous actin or NM II knock-out mice[45–48], homozygous *Alkbh4* knockout was also found to be embryonically lethal (Fig. 1a,b). This is in accordance with an essential function of ALKBH4 in regulating actomyosin function and supports our findings of an important role of ALKBH4 in cytokinesis. However, the fact that not all cells appear to have severe cytokinesis defects might suggest that ALKBH4-mediated actin demethylation and perhaps demethylation of yet unknown targets might be important not only for proper cytokinesis but for a far wider range of cellular functions.

No homozygous actin deletions or nonsense mutations have been described in humans, probably because, like in mice, such deletions or mutations would be lethal. However, several missense mutations have been associated with human diseases including mental retardation and developmental malformations[49–51]. In mice, such mutations have been associated with tumourigenesis and metastasis[52]. Identification of ALKBH4 as a new regulator of actomyosin function opens up the possibility that ALKBH4 might also be targeted by mutations in developmental diseases and cancer. In conclusion, we propose that the key purpose of actin methylation and demethylation mediated by ALKBH4 is to create 'handles' for NM II, to 'hold on to' when 'climbing' along the actin filament thereby generating contraction of the actomyosin network (Fig. 7).

Methods

Plasmids and protein purification. The human *ALKBH4* gene was subcloned into p3 × flag-CMV14 (Sigma), pEGFP-c1b or pGEX-5x-2 (GE Healthcare)[53]. The human *β-actin* gene was subcloned into pcDNA3-HA (Invitrogen) and pCMV-GFP-MyoII-B was ordered from Addgene. Mutations were introduced using the QuickChange site-directed mutagenesis kit (Stratagene). Recombinant GST-ALKBH4 protein was expressed in *E. coli* strain BL21(DE3) and purified as described in the commercial available instructions.

Cell culture and antibodies. Human MRC5 and 293T cells were cultured in RPMI 1640 at 37 °C, 5% CO2 with 10% fetal bovine serum and 1% (w/v) penicillin/streptomycin (Sigma). Human U2OS cells were grown in Dulbecco's modified Eagle's medium with 10% fetal bovine serum. Cells were treated with the following

Figure 5 | ALKBH4 deficiency interferes with cleavage furrow organization and cell migration. (**a**) MRC5 cells were treated with ALKBH4 or CTRL siRNA for 48 h, fixed and immunostained with the indicated antibodies and DAPI. Scale bar, 10 μm. (**b**) Quantification of cells with mislocalised anillin, NM II, aurora B and Plk1 (shown in **a**). The histograms represent the mean of three independent experiments (500 cells per condition per experiment). *P*-values were calculated using a two-tailed *t*-test. Error bars indicate s.d. (**c**) Migration assays were performed with a monolayer of confluent *Alkbh4*$^{\Delta/\Delta}$*Cre* or control (*Alkbh4*$^{L/L}$*Cre*) MEF cells. The migration distances from the edges of the wound were calculated from the time point when the scratch was made (0 h) and 24 h later (illustrated in Supplementary Fig. S4c). Assays were run with primary MEFs derived from two different embryos. *P*-values were calculated using a two-tailed *t*-test. Error bars represent s.d. from multiple reading points. (**d**) MRC5 cells were treated with ALKBH4 or CTRL siRNA for 48 h, fixed and immunostained with the indicated antibodies and DAPI(left). Scale bar, 10 μm. Quantification of multinucleated cells (right). Histogram represents the mean of three independent experiments (500 cells per condition per experiment). *P*-values were calculated using a two-tailed *t*-test. Error bars indicate s.d.

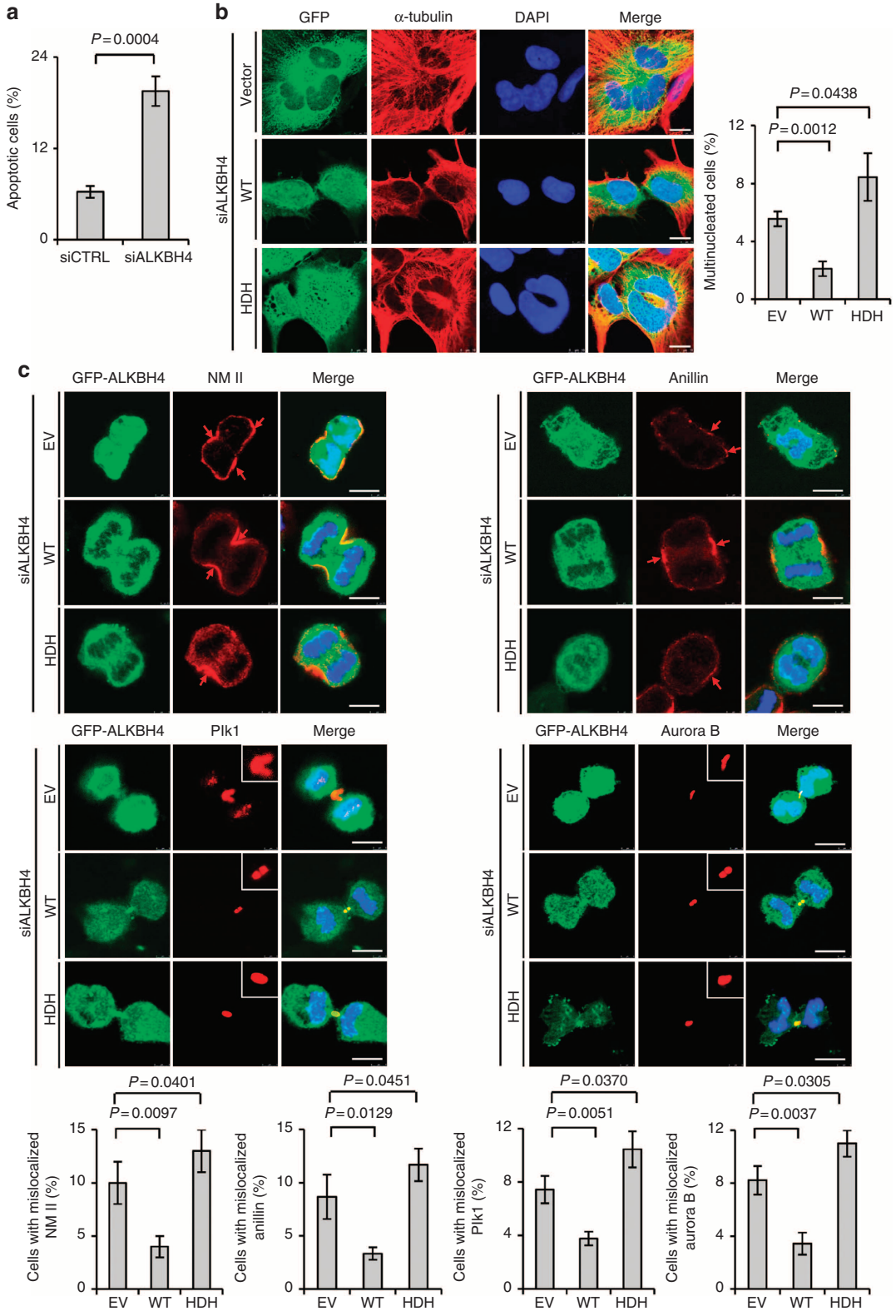

Figure 6 | Complementation with WT but not HDH ALKBH4 can rescue defects associated with cytokinesis failure. (**a**) Quantification of apoptotic cells (MRC5) following treatment with CTRL or ALKBH4 siRNA for 48 h. Quantification is based on three independent experiments (30,000 cells per condition per experiment). *P*-values were calculated using a two-tailed *t*-test. Error bars indicate s.d. (**b**) MRC5 cells were simultaneously treated with CTRL or ALKBH4 siRNA and the indicated siRNA insensitive Flag-GFP-ALKBH4 constructs for 48 h then analysed by immunofluorecence with the indicated antibodies. Quantification is based on three independent experiments (300 cells per condition per experiment). *P*-values were calculated using a two-tailed *t*-test. Error bars indicate s.d. (**c**) As in (**b**). Quantification of anillin, NM II, Plk1 and aurora B, mislocalization following treatment with CTRL or ALKBH4 siRNA and the indicated siRNA insensitive Flag-GFP-ALKBH4. Quantification is based on three independent experiments (300 cells per condition per experiment). *P*-values were calculated using a two-tailed *t*-test. Error bars indicate s.d.

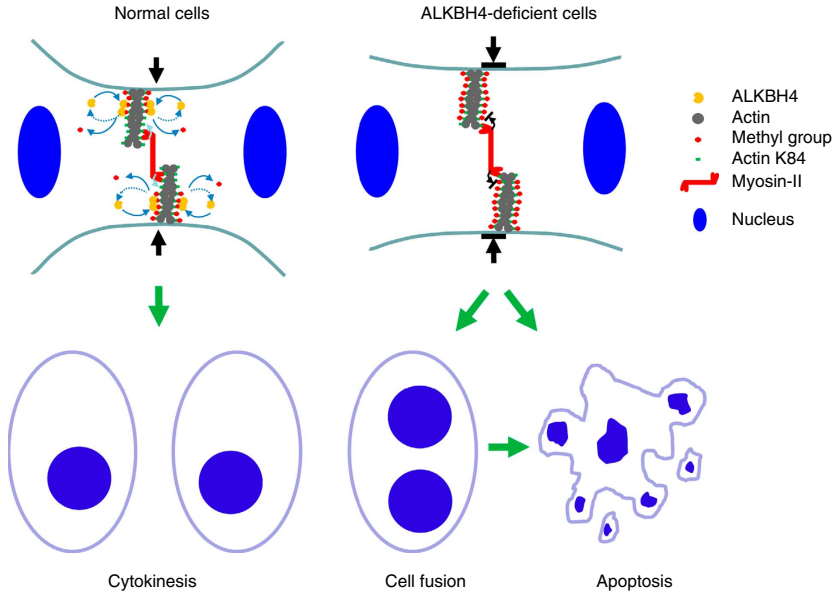

Figure 7 | Schematic model. The schematic describes a proposed model for the role of ALKBH4 in the regulation of actomyosin dynamics and cleavage furrow ingression during cytokinesis, and that ALKBH4 deficiency leads to cytokinesis failure or apoptosis (see discussion section for detailed explanation).

drugs: Nocodazole (Sigma), Cytochalasin D (Sigma) and Blebbistatin (Sigma) at the indicated periods of time and concentrations.

The following antibodies were used in the study: Abcam: rabbit-anti-Histone H3 phosphor-S10, mouse-anti-p53, mouse-anti-myosin-II, mouse-anti-GAPDH. Invitrogen: F-actin (phalloidin-Texas Red). Sigma: mouse-anti-β-tubulin, mouse-anti-γ-tubulin, mouse-anti-α-tubulin, mouse-anti-actin, mouse-anti-flag, rabbit-anti-flag. Santa Cruz: rabbit polyclonal anti-actin, goat-anti-anillin, mouse-anti-Plk1. CWbiotech: rabbit-anti-HA, mouse-anti-GFP. Bethyl: rabbit-anti-aurora B. ALKBH4: no. 1, generated using purified recombinant GST-ALKBH4 protein (AbMax Biotechnology), ALKBH4: no. 2 generated using human synthetic peptide (101QSGRKKQDYGPK112) (CWbiotech). Rabbit polyclonal anti-actin K84-monomethylated antibody (anti-actin K84me1) was generated using a synthetic peptide with monomethylated lysine 84 (77TNWDDMEm**K**IWHHTFY91) as immunogen (New England Peptide, Boston, USA).

Plasmid transfection and RNA interference. DNA transfections were carried out using polyetylenimine or Lipofectamine 2000 (Invitrogen). siRNA duplexes (GenePharma, China) were transfected into cells using Lipofectamine RNAiMAX (Invitrogen) according to the manufacturer's instructions.

For ALKBH4 rescue experiments, cells were co-transfected with 1 μg of plasmid DNA and 60 pmol siRNA using Lipofectamine 2000. The following siRNA sequences were used in the study: ALKBH4 no. 1: 5′-GAUCCCGGGAUU GAAAUGA-3′, ALKBH4 no. 2: 5′-GGGAUUGAAAUGAGGAGCA-3′, ALKBH4 no. 3: 5′-GGGAUCAUUUGAGCUUAAA-3′. NM II no. 1: 5′-GGGCCAA CAUUGAAACAUA-3′, NM II no. 2: 5′-GUGCUACAGUUUGGAAATA-3′, NM II n3: 5′-CUCGGGAUGAGGUGAUUAA-3′, Scrambled siRNA (siCTRL): 5′-UUCUCCGAACGUGUCACGU-3′.

Immunofluorescence analysis. Cells seeded onto coverslips were fixed with methanol or 4% paraformaldehyde on ice, then permeabilized with 0.1% Triton X-100 and 0.05% NP-40 on ice. After pre-blocking the coverslips were first incubated with primary antibody, then fluorescent dye-conjugated secondary antibody and mounted with DAPI-containing mounting medium (Vector Laboratories, Burlingame, CA). Confocal images were acquired and analysed on Leica TCS SP5 (Leica) equipped with HCX PL APO 63 × 1.4 oil CS immersion objective (Leica).

Immunoprecipitation. Whole-cell extract was generated by lysing cells in NET buffer (50 mM Tris-HCl pH7.4, 150 mM NaCl, 5 mM EDTA, 0.1% NP-40 and protease inhibitors) followed by sonication using a SonicDismembrator (Fisher Scientific) (1 min, with 10 s-on and 20 s-off cycles). When using CCD treatment, CCD was added to the NET buffer. Anti-Flag M2 affinity gel (Sigma), anti-HA affinity gel (Sigma) and anti-GFP-Trap-A beads (ChromoTek) were used for immunoprecipitations.

Identification of methylation sites by mass spectrometry. HA-tagged β-actin was immunoprecipitated from 293T cells 48 h after transfection, eluted from the beads with 100 mM glycine pH 2.5, and immediately neutralized with Tris buffer. The proteins were then precipitated with four volumes of cold acetone, air dried and resuspended in 8 M urea, 100 mM Tris, pH 8.5. After reduction (5 mM TCEP, 20 min, RT) and alkylation (10 mM iodoacetamide, 15 min, RT), the sample was diluted to 2 M urea, 100 mM Tris pH 8.5, followed by Asp-N (Roche, Cat. No. 11420488001) digestion (1:50 enzyme:substrate, 37 °C, O/N), Asp-N inactivation (0.5 mM EDTA for 2 min), and Arg-C (Roche, Cat. No. 11370529001) digestion (1:50 enzyme:substrate, 37 °C, 8 h with 5 mM DTT and 8.5 mM $CaCl_2$). The digestion was quenched with 5% formic acid and the peptides were desalted and re-dissolved in the NET buffer. Methylated β-actin peptides were further enriched by IP using actin K84me1 antibody. After elution (with 100 mM glycine, pH 2.5) and desalting, the enriched peptides were analysed on an Easy-nLC 1000 UPLC (Thermo Fisher Scientific) coupled to a Q Exactive mass spectrometer (Thermo Fisher Scientific). Peptides were loaded on a pre-column (75 μm ID packed with 8 cm 10 μm-C18 resin) and separated on an analytical 75 μm ID column packed with 11 cm 3 μm-C18 resin (pre-column: ODS-AQ 12 nM S-10 μm (YMC Co., Ltd), analytical column: Luna 3 μm 100 Å resin (*Phenomenex*)) with anacetonitrile gradient from 0–25% in 60 min and 25–80% in another 7 min at a flow rate of 200 nl min^{-1}. Spectra were acquired in a data-dependent mode: the 10 most intense ions of +2, +3 or +4 charge from each full scan ($R = 70{,}000$) were isolated for HCD MS2 ($R = 17{,}500$) at NEC 27 with a dynamic exclusion time of 150 s. For peptide identification, the MS2 spectra were searched against an EPI-IPI human database (forward + reversed sequences) using Prolucid with 50 p.p.m. mass accuracy for both precursor and fragment ions and considering carbamidomethylation on Cys as a fixed modification and mono-, di- or tri-methylation at Lys as differential modifications[54]. Search results were filtered using DTASelect 2.0 with 10 p.p.m. mass accuracy for precursor mass and a 1% FDR cutoff at the spectral level[55]. The β-actin K84me1 spectra presented in the figures were annotated using pLabel, requiring 20 p.p.m. accuracy for fragment ions[56]. The data files have been uploaded to http://www.peptideatlas.org/ with the access number: PASS00132 and password: WW685h.

Time-lapse microscopy. Cells were placed in a 37 °C heated microscope chamber and observed under differential interference contrast. Images were acquired every 2 min with Olympus IX81 microscope, equipped with Olympus × 40 dry lens and processed using Andor iQ2.7 image browser software.

FACS analyses. For cell cycle analysis the Cycle test Plus DNA reagent kit was applied according to the manufacturer's instructions (Becton-Dickinson). FACS analysis was carried out on a FACSAria III equipped with FACSDiva software 6.0 (Becton-Dickinson) and Modfit LT software (version 3.1, BD). Apoptotic cells were detected by staining with annexin-PI using the Annexin V-FITC and PI Apoptosis Detection Kit (Jiamay Biotech) and analysed by flow cytometry.

Midbody isolation. Midbody purification was performed according to the protocol developed by Mullins and McIntosh and Sellitto and Kuriyama[57,58].

F-actin fractionation assay. The ratio of F-actin versus G-actin in cells was analysed using an F-actin/G-actin *in vivo* assay kit (Cytoskeleton) based on the manufacturer's protocol.

Generation of conditionally targeted Alkbh4 mice. Gene targeting vector containing ALKBH4 exon 2 and exon 3 was constructed by cloning genomic ALKBH4 fragments into the pCR4-TOPO vector (Invitrogen) from BAC clone bMQ 337L22 BAC clone (Geneservice). Two LoxP sites were inserted, flanking an inserted neomycin-resistance gene cassette and the exon 2 and exon 3 regions. A Diphteria Toxin A (*DTA*) gene was used for negative selection. The targeting vector was linearized with *Nru*I and electroporated into 129Sv/Pas ES cells. ES cells were selected with 200 μg ml^{-1} G418. Positive ES cell clones were injected into C57BL/6N blastocysts. Chimeric mice ($Alkbh4^{+/L}$) were crossed with a C56BL/6 Cre-deleter mouse strain (GenOway) to generate heterozygous conventional knock-out mice.

Southern blotting assay. Genomic DNA was digested with *Spe*I/*Pci*I and hybridized using an external 524 bp probe (Ext 5′probe) located upstream of the 5′ homology sequence and an internal 399 bp probe (Int 3′probe) located within the 3′ homology sequence of the targeting vector. Pre-hybridization and hybridization: 4 × SSC, 1% SDS, 0.5% skimmed milk, 20 mM EDTA, 100 μg ml^{-1} hering sperm, at 65 °C for 18 h. Washings: two times 3 × SSC, 1% SDS at 65 °C for 15 min, then two times 0.5 × SSC, 1% SDS at 65 °C for 15 min. Primers used: external 5′ probe: 5′-TCGCTAAGGCCCGCTGCCGGGGAGC-3′ and 5′-AAATGCAGAGATC TCGGCGT-3′. Internal 3′ probe: 5′-TAGTACAGGCTGGCCTCAAAAT-3′ and 5′-ATCACCAGAACCACCATGAGG-3′.

Isolation and culture of MEFs. Mice homozygous for the recombined allele ($Alkbh4^{L/L}$) were bred with a mouse line ubiquitously expressing the Cre-ER transgene (mouseline: B6. Cg-Tg (CAG-cre/Esr1) 5 Amc J^{-1}, Jackson Laboratory), inducible by tamoxifen, to generate $Alkbh4^{L/L}Cre$ mouse strain. MEFs were isolated from 12.5–13.5 dpc embryos according to protocol described[59], and grown in Dulbeccos modified Eagle's medium supplemented with 10% fetal calf serum, 1% GlutaMAX (Invitrogen) and 1% PenStrep (Invitrogen). *Alkbh4* deletion in $Alkbh4^{L/L}Cre$ cell lines was accomplished by 0.5 μM 4-hydroxytamoxifen (4-OHT, Sigma H6278) treatment in MEF culture medium for 4 days. $Alkbh4^{+/+}Cre$ primary MEF cell lines were used as control cells for the experiments. Primary MEF cell lines (up to passage 5) were used in the experiments.

Cell scratch assay. The migration assay was performed as described[41]. Cell counting experiments were performed by plating equal numbers (10^5) of primary $Alkbh4^{L/L}Cre$ MEFs, treated or untreated with 4-OHT in each well of six-well plates containing low-serum medium (0.5% FBS), and the cells were counted every 24 h using a hemocytometer.

Genotyping. Mice were PCR genotyped with the following primer sets: WT allele (+), Alkbh4-2+ and Alkbh4-4- (340 bp); recombined allele (L), Alkbh4-2+ and Alkbh4-NEO (1,003 bp); knock-out allele (−) or Cre-ER-mediated ΔL, Alkbh4-2+ and Alkbh4-2- (550 bp). Expand long template kit PCR kit (Roche) was used with 10 pmol forward and reverse primers. Primer sequences: Alkbh4-2+: 5′-AGTTGCTTTAGTTCCAAGAAGAGCATCGG-3′, Alkbh4-2-: 5′-GCCT CCCAAAACTTGGTATCACAAACC-3′, Alkbh4-4-: 5′-TGAGCTGCTGA CGTGCTTAACC-3′, Alkbh4-NEO-: 5′-TCTCACCTTGCTCCTGCCGAGA AAGTATC-3′.

Statistical analysis. Two-tailed *t*-tests in grouped analyses of Prism5 software were applied. *P*-value <0.05 was considered significant.

References

1. Reichl, E. M. *et al.* Interactions between myosin and actin crosslinkers control cytokinesis contractility dynamics and mechanics. *Curr. Biol.* **18,** 471–480 (2008).
2. Pollard, T. D. & Borisy, G. G. Cellular motility driven by assembly and disassembly of actin filaments. *Cell* **112,** 453–465 (2003).
3. Veigel, C. & Schmidt, C. F. Moving into the cell: single-molecule studies of molecular motors in complex environments. *Nat. Rev. Mol. Cell Biol.* **12,** 163–176 (2011).
4. Barr, F. A. & Gruneberg, U. Cytokinesis: placing and making the final cut. *Cell* **131,** 847–860 (2007).
5. Steigemann, P. & Gerlich, D. W. Cytokinetic abscission: cellular dynamics at the midbody. *Trends Cell Biol.* **19,** 606–616 (2009).
6. Murthy, K. & Wadsworth, P. Myosin-II-dependent localization and dynamics of F-actin during cytokinesis (vol 15, pg 724, 2005). *Curr. Biol.* **15,** 883–883 (2005).
7. Yumura, S. Myosin II dynamics and cortical flow during contractile ring formation in Dictyostelium cells. *J. Cell Biol.* **154,** 137–145 (2001).
8. Cao, L. G. & Wang, Y. L. Mechanism of the formation of contractile ring in dividing cultured animal-cells.1. Recruitment of preexisting actin-filaments into the cleavage furrow. *J. Cell Biol.* **110,** 1089–1095 (1990).
9. Cao, L. G. & Wang, Y. L. Mechanism of the formation of contractile ring in dividing cultured animal-cells.2. Cortical movement of microinjected actin-filaments. *J. Cell Biol.* **111,** 1905–1911 (1990).
10. Pollard, T. D. Mechanics of cytokinesis in eukaryotes. *Curr. Opin. Cell Biol.* **22,** 50–56 (2010).
11. Fededa, J. P. & Gerlich, D. W. Molecular control of animal cell cytokinesis. *Nat. Cell Biol.* **14,** 440–447 (2012).
12. Kashina, A. *et al.* Arginylation of beta-actin regulates actin cytoskeleton and cell motility. *Science* **313,** 192–196 (2006).
13. Abe, A., Saeki, K., Yasunaga, T. & Wakabayashi, T. Acetylation at the N-terminus of actin strengthens weak interaction between actin and myosin. *Biochem. Biophys. Res. Commun.* **268,** 14–19 (2000).
14. Heibeck, T. H. *et al.* An extensive survey of tyrosine phosphorylation revealing new sites in human mammary epithelial cells. *J. Proteome. Res.* **8,** 3852–3861 (2009).
15. Johnson, P., Harris, C. I. & Perry, S. V. 3-Methylhistidine in actin and other muscle proteins. *Biochem. J.* **105,** 361–370 (1967).
16. Iwabata, H., Yoshida, M. & Komatsu, Y. Proteomic analysis of organ-specific post-translational lysine acetylation and -methylation in mice by use of anti-acetyllysine and -methyllysine mouse monoclonal antibodies. *Proteomics* **5,** 4653–4664 (2005).
17. Costas, M., Mehn, M. P., Jensen, M. P. & Que, L. Dioxygen activation at mononuclear nonheme iron active sites: enzymes, models, and intermediates. *Chem. Rev.* **104,** 939–986 (2004).
18. Schofield, C. J. & Zhang, Z. Structural and mechanistic studies on 2-oxoglutarate-dependent oxygenases and related enzymes. *Curr. Opin. Struct. Biol.* **9,** 722–731 (1999).
19. Falnes, P. O., Johansen, R. F. & Seeberg, E. AlkB-mediated oxidative demethylation reverses DNA damage in Escherichia coli. *Nature* **419,** 178–182 (2002).
20. Trewick, S. C., Henshaw, T. F., Hausinger, R. P., Lindahl, T. & Sedgwick, B. Oxidative demethylation by Escherichia coli AlkB directly reverts DNA base damage. *Nature* **419,** 174–178 (2002).
21. Gerken, T. *et al.* The obesity-associated FTO gene encodes a 2-oxoglutarate-dependent nucleic acid demethylase. *Science* **318,** 1469–1472 (2007).
22. Kurowski, M. A., Bhagwat, A. S., Papaj, G. & Bujnicki, J. M. Phylogenomic identification of five new human homologs of the DNA repair enzyme AlkB. *BMC Genomics* **4,** 48 (2003).
23. Duncan, T. *et al.* Reversal of DNA alkylation damage by two human dioxygenases. *Proc. Natl Acad. Sci. USA* **99,** 16660–16665 (2002).
24. Jia, G. *et al.* N6-methyladenosine in nuclear RNA is a major substrate of the obesity-associated FTO. *Nat. Chem. Biol.* **7,** 885–887 (2011).
25. Zheng, G. *et al.* ALKBH5 is a mammalian RNA demethylase that impacts RNA metabolism and mouse fertility. *Mol. Cell* **49,** 18–29 (2013).
26. Dina, C. *et al.* Variation in FTO contributes to childhood obesity and severe adult obesity (vol 39, pg 724, 2007). *Nat. Genet.* **39,** 1285–1285 (2007).
27. Frayling, T. M. *et al.* A common variant in the FTO gene is associated with body mass index and predisposes to childhood and adult obesity. *Science* **316,** 889–894 (2007).
28. Scott, L. J. *et al.* A genome-wide association study of type 2 diabetes in Finns detects multiple susceptibility variants. *Science* **316,** 1341–1345 (2007).
29. Scuteri, A. *et al.* Genome-wide association scan shows genetic variants in the FTO gene are associated with obesity-related traits. *PLoS Genet.* **3,** e115 (2007).
30. Fu, D. *et al.* Human AlkB homolog ABH8 is a tRNA methyltransferase required for wobble uridine modification and DNA damage survival. *Mol. Cell. Biol.* **30,** 2449–2459 (2010).
31. van den Born, E. *et al.* ALKBH8-mediated formation of a novel diastereomeric pair of wobble nucleosides in mammalian tRNA. *Nat. Commun.* **2,** 172 (2011).
32. Lando, D., Balmer, J., Laue, E. D. & Kouzarides, T. The S. pombe histone H2A dioxygenase Ofd2 regulates gene expression during hypoxia. *PloS one* **7,** e29765 (2012).
33. Ougland, R. *et al.* ALKBH1 is a histone H2A dioxygenase involved in neural differentiation. *Stem Cells* **30,** 2672–2682 (2012).
34. Bjornstad, L. G., Zoppellaro, G., Tomter, A. B., Falnes, P. O. & Andersson, K. K. Spectroscopic and magnetic studies of wild-type and mutant forms of the Fe(II)- and 2-oxoglutarate-dependent decarboxylase ALKBH4. *Biochem. J.* **434,** 391–398 (2011).
35. Valegard, K. *et al.* The structural basis of cephalosporin formation in a mononuclear ferrous enzyme. *Nat. Struct. Mol. Biol.* **11,** 95–101 (2004).
36. Lee, D. H. *et al.* Repair of methylation damage in DNA and RNA by mammalian AlkB homologues. *J. Biol. Chem.* **280,** 39448–39459 (2005).
37. Miller, C. J., Cheung, P., White, P. & Reisler, E. Actin's view of actomyosin interface. *Biophys. J.* **68,** 50S–54S (1995).
38. Mailand, N. *et al.* RNF8 ubiquitylates histones at DNA double-strand breaks and promotes assembly of repair proteins. *Cell* **131,** 887–900 (2007).

39. McGough, A. F-actin-binding proteins. *Curr. Opin. Struct. Biol.* **8,** 166–176 (1998).
40. Straight, A. F. *et al.* Dissecting temporal and spatial control of cytokinesis with a myosin II inhibitor. *Science* **299,** 1743–1747 (2003).
41. Liang, C. C., Park, A. Y. & Guan, J. L. In vitro scratch assay: a convenient and inexpensive method for analysis of cell migration *in vitro*. *Nat. Protoc.* **2,** 329–333 (2007).
42. Ganem, N. J., Storchova, Z. & Pellman, D. Tetraploidy, aneuploidy and cancer. *Current Opin. Genet. Dev.* **17,** 157–162 (2007).
43. Karakozova, M. *et al.* Arginylation of beta-actin regulates actin cytoskeleton and cell motility. *Science* **313,** 192–196 (2006).
44. Nyman, T. *et al.* The role of MeH73 in actin polymerization and ATP hydrolysis. *J. Mol. Biol.* **317,** 577–589 (2002).
45. Shawlot, W., Deng, J. M., Fohn, L. E. & Behringer, R. R. Restricted beta-galactosidase expression of a hygromycin-lacZ gene targeted to the beta-actin locus and embryonic lethality of beta-actin mutant mice. *Transgenic Res.* **7,** 95–103 (1998).
46. Uren, D. *et al.* Gene dosage affects the cardiac and brain phenotype in nonmuscle myosin II-B-depleted mice. *J. Clin. Invest.* **105,** 663–671 (2000).
47. Shmerling, D. *et al.* Strong and ubiquitous expression of transgenes targeted into the beta-actin locus by cre/lox cassette replacement. *Genesis* **42,** 229–235 (2005).
48. Bunnell, T. M., Burbach, B. J., Shimizu, Y. & Ervasti, J. M. Beta-actin specifically controls cell growth, migration, and the G-actin pool. *Mol. Biol. Cell* **22,** 4047–4058 (2011).
49. Mogensen, J. *et al.* Alpha-cardiac actin is a novel disease gene in familial hypertrophic cardiomyopathy. *J. Clin. Invest.* **103,** R39–R43 (1999).
50. van Wijk, E. *et al.* A mutation in the gamma actin 1 (ACTG1) gene causes autosomal dominant hearing loss (DFNA20/26). *J. Med. Genet.* **40,** 879–884 (2003).
51. Procaccio, V. *et al.* A mutation of beta-actin that alters depolymerization dynamics is associated with autosomal dominant developmental malformations, deafness, and dystonia. *Am. J. Human Genet.* **78,** 947–960 (2006).
52. Taniguchi, S., Kawano, T., Kakunaga, T. & Baba, T. Differences in expression of a variant actin between low and high metastatic B16-melanoma. *J. Biol. Chem.* **261,** 6100–6106 (1986).
53. Yang, Y.G., Lindahl, T. & Barnes, D. E. Trex1 exonuclease degrades ssDNA to prevent chronic checkpoint activation and autoimmune disease. *Cell* **131,** 873–886 (2007).
54. Xu, T. *et al.* ProLuCID, a fast and sensitive tandem mass spectra-based protein identification program. *Mol. Cell. Proteomics* **5,** S174 (2006).
55. Tabb, D. L., McDonald, W. H. & Yates, III J. R. DTASelect and contrast: tools for assembling and comparing protein identifications from shotgun proteomics. *J. Proteome Res.* **1,** 21–26 (2002).
56. Yang, B. *et al.* Identification of cross-linked peptides from complex samples. *Nat. Met.* **9,** 904–906 (2012).
57. Mullins, J. M. & McIntosh, J.R. Isolation and initial characterization of the mammalian midbody. *J. Cell Biol.* **94,** 654–661 (1982).
58. Sellitto, C. & Kuriyama, R. Distribution of a matrix component of the midbody during the cell cycle in Chinese hamster ovary cells. *J. Cell Biol.* **106,** 431–439 (1988).
59. Xu, J. Preparation, culture, and immortalization of mouse embryonic fibroblasts. *Curr. Protocols Mol. Biol.* Chapter 28, Unit **28,** 1 (2005).

Acknowledgements

This work was supported by the 973 programs (2011CB510103, 2012CB518302 to Y.-G.Y. and 2010CB835203 to M.-Q.D.), China Natural Science Foundation (31071185 to Y.-G.Y; 31250110215, 31150110143 to J.R.M.D.), the CAS Young Foreign Fellow Award (2010Y2SB14 to J.R.M.D.), Danish Medical Research Council (J.M.R.D), the CAS '100-talents' Professor Program (Y.-G.Y.), the CAS Senior Foreign Research Fellow Award (2011T1S21 to A.K.), and MLS, University of Oslo. We are grateful to Linda Tveteråas and Guro F. Lien for technical assistance. We thank T. Lindahl for providing reagents, GenOway, Lyon, France for knock-out mice service; The Norwegian Transgenic Center (NTS); and the Center for Comparative studies at Oslo University Hospital for the service provided.

Author contributions

Y.-G.Y., A.K. designed the experiments. Y.-G.Y., J.M.R.D, A.K., M.-M.L. and A.N. wrote the paper. M.-M.L. and Y.S. performed most of the experiments with the assistance of Y.-H.D., Y.F., B.L., Y.N., Y.-S.W, J.M.R.D. M.-Q.D., C.-M.H., K.-X.J., Y.L. and C.H. A.N. generated and characterized knock-out mice and MEFs with the assistance of M.F. and M.O. X.X. provided reagents. All authors participated in interpreting the results.

Additional information

Accession codes: Mass spectrometry data have been uploaded to Peptide Atlas under accession code PASS00132.

Supplementary Information accompanies this paper at http://www.nature.com/naturecommunications

Competing financial interests: The authors declare no competing financial interests.

Reprints and permission information is available online at http://npg.nature.com/reprintsandpermissions/

How to cite this article: Li, M.-M. *et al.* ALKBH4-dependent demethylation of actin regulates actomyosin dynamics. *Nat. Commun.* 4:1832 doi: 10.1038/ncomms2863 (2013).

ALKBH4-dependent Demethylation of the Novel Actin K84me1 Modification Regulates Actomyosin Dynamics

Ming-Ming Li[1,7#], Anja Nilsen[2#], Yue Shi[1,7#], Markus Fusser[2], Yue-He Ding[3], Ye Fu[4], Bo Liu[5], Yamei Niu[1], Yong-Sheng Wu[1], Chun-Min Huang[1], Maria Olofsson[2], Kang-Xuan Jin[1,7], Ying Lv[1,7], Xing-Zhi Xu[5], Chuan He[4], Meng-Qiu Dong[3], Jannie M. Rendtlew Danielsen[1,6], Arne Klungland[2,8*], Yun-Gui Yang[1,7*]

[1]Genome Structure & Stability Group, BIG CAS-OSLO Genome Research Cooperation, Disease Genomics and Individualized Medicine Laboratory, Beijing Institute of Genomics, Chinese Academy of Sciences, No.1-7 Beichen West Road, Chaoyang District, Beijing 100101, P. R. China

[2]Centre for Molecular Biology and Neuroscience and Institute of Medical Microbiology, BIG CAS-OSLO Genome Research Cooperation, Oslo University Hospital Rikshospitalet, Oslo 0027, Norway

[3]National Institute of Biological Sciences, Beijing 102206, P. R. China

[4]Department of Chemistry and Institute for Biophysical Dynamics, The University of Chicago, 929 East 57th Street, Chicago, Illinois 60637, USA

[5]Beijing Key Laboratory of DNA Damage Response, College of Life Sciences, Capital Normal University, Beijing 100048, P. R. China

[6]The Novo Nordisk Foundation Center for Protein Research, Ubiquitin Signalling Group, Faculty of Health Sciences, Blegdamsvej 3b, 2200, Copenhagen, Denmark

[7]University of Chinese Academy of Sciences, 19A Yuquan Road, Beijing 100049, P. R. China

[8]Institute of Basic Medical Sciences, University of Oslo, PO Box 1018, Blindern, NO-0315 Oslo, Norway.

[#]These authors contributed equally to this work.

*Correspondence and requests for materials should be addressed to Yun-Gui Yang (e-mail: ygyang@big.ac.cn) or Arne Klungland (e-mail: arne.klungland@rr-research.no)

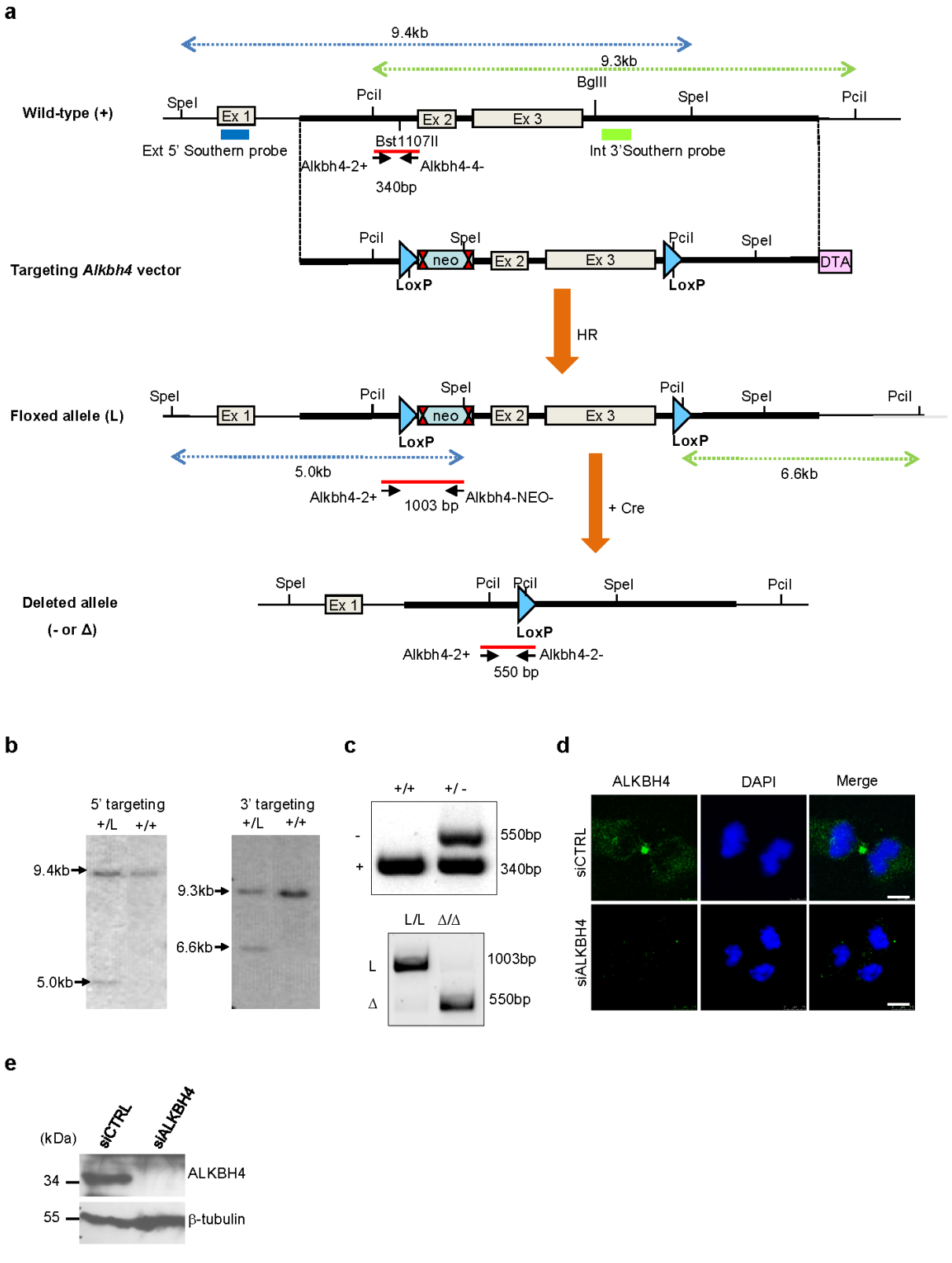

Supplementary Figure S1. Strategies for *Alkbh4* knock-out and genotyping and ALKBH4 antibody testing. a, Schematic presentation of *Alkbh4* gene-targeting and genotyping strategy, showing wild-type allele (WT); gene-targeting vector; floxed allele (L); and the Cre mediated

deletion of exons 2 and 3 allele (germline:- or inducible: Δ). Deletion of exon 2 and 3 removes the dioxygenase domain of *Alkbh4* and will invalidate the catalytic domain of both long (AK008083) and short (BC022729) isoforms of Alkbh4. The genomic region of interest was amplified as three fragments from AB2.2 ES cell DNA in the bMQ 337L22 BAC clone (Geneservice). An approx. 4.2 kb sized 5' fragment containing sequences from exon 1 to part of intron 3 was amplified with primers 5'-TTAGAGCCCAAGACTTCCAAGTTCC-3'/ 5'-CAGCACACAGGATAGAAATCCAACC-3'. This subclone was used to generate the 5' small homology arm of the targeting vector. An approx. 3.1 kb sized 3' fragment containing the exons 2 and 3 sequences was amplified with primers 5'-GCTATTGTGGGTCTTTGCTGGTTCC-3'/ 5'-TCTGCACACAGAAACACAAGCCTCC-3'. This fragment was used to generate the proximal part of the 3' long homology arm. An approx. 4.8 kb sized 3' fragment containing part of the exon 3 and downstream sequences was amplified with primers 5'-TTCAGGGAGCTGTCCAGTGAGTTCC-3'/ 5'-TCACTGGAAACTGCTGGAGCCTACC-3'. This subclone was used to generate the distal part of the 3' long homology arm of the targeting vector. The three PCR fragments were subcloned into pCR4-TOPO vector (Invitrogen). A 3510 bp sized SpeI/Bst1107I fragment of the short homology arm was inserted into a G140 vector (Genoway) upstream of the LoxP-FRT-Neomycin-FRT (linearized with AvrII/PmeI). A 3758 bp sized NheI-HpaI fragment from this construct was inserted into a pGA1 vector (Genoway) with inserted polylinker (restriction sites PacI-NruI-XbaI-HpaI-SpeI-AvrII-Bst1107I-NheI-NotI-AscI) linearized with XbaI-HpaI. A synthetic LoxP fragment was inserted into the BglII site downstream exon 3 of the distal part of the distal long homology arm to generate the distal LoxP site. This insertion destroyed the BglII site and introduced PciI and AspI sites. The proximal long arm was joined to the distal long arm by insertion of a 3722bp sized AatII-PmeI fragment isolated from the distal long arm into the proximal long arm cut with AatII-PmlII. A 5887bp sized Bst1107I-SpeI fragment isolated from the long homology arm was inserted into the short homology arm plasmid, linearized with Bst1107I-NheI. The final targeting vector was completed by insertion of a Diphteria Toxin A negative selection cassette at the 3'end long homology arm via AscI-NotI. FRT sites indicated in figure by red ⧖. The targeting vector was linearized with NruI and electroporated into 129Sv/Pas ES cells. ES cells were selected with 200 μg/ml G418. Homologous recombination in ES cells was verified by Southern blot analysis. The Southern blot screening was based on a SpeI and

PciI digestion of genomic DNA and hybridization using an external 524 bp probe (Ext 5'probe) located upstream of the 5' homology sequence and an internal 399 bp probe (Int 3'probe) located within the 3' homology sequence of the targeting vector. Blue- and green- dashed double-end arrow lines representing southern-blotting products using 5'-probe and 3'-probe, to distinguish WT (+) allele from floxed allele (L), respectively. DNA fragments detected by these probes are shown in figure. Ex: exon. **b**, ES cells were injected into C57BL/6N blastocysts and chimeras were bred with C56BL/6 mice to make a germline transmissible *Alkbh4* floxed allele ($Alkbh4^{L}$). Floxed mice were mated with a C56BL/6 Cre-deleter mouse strain (Genoway) to excise the floxed region and generate germline transmissable knock-out allele (-). Mice homozygous for the recombined allele ($Alkbh4^{L/L}$) were bred with tamoxifen-inducible Cre-ER mice to generate $Alkbh4^{L/L}Cre$ mouse strain for the inducible deletion (Δ) of *Alkbh4* in MEF cells. PCR strategy for genotyping: PCR products shown as red lines with corresponding primer sets. Product size shown as indicated. **c**, Representative images of PCR genotyping of *Alkbh4* wild-type ($Alkbh4^{+/+}$) and heterozygous conventional/germline knockout mice ($Alkbh4^{+/-}$) and Cre-mediated conversion of *Alkbh4* floxed gene ($Alkbh4^{L/L}$) to *Alkbh4* deleted ($Alkbh4^{\Delta/\Delta}$) obtained from 4-OHT induced $Alkbh4^{L/L}Cre$ MEF cells. **d**, MRC5 cells were treated with CTRL or ALKBH4 siRNA for 48 h, fixed and immunostained with ALKBH4 antibody (#1) and DAPI. Scale bars, 10 μm. **e**, MRC5 cells were treated with CTRL or ALKBH4 siRNA for 48 h, lysed and analyzed by immunoblotting with the ALKBH4 (#2) and β-tubulin antibodies.

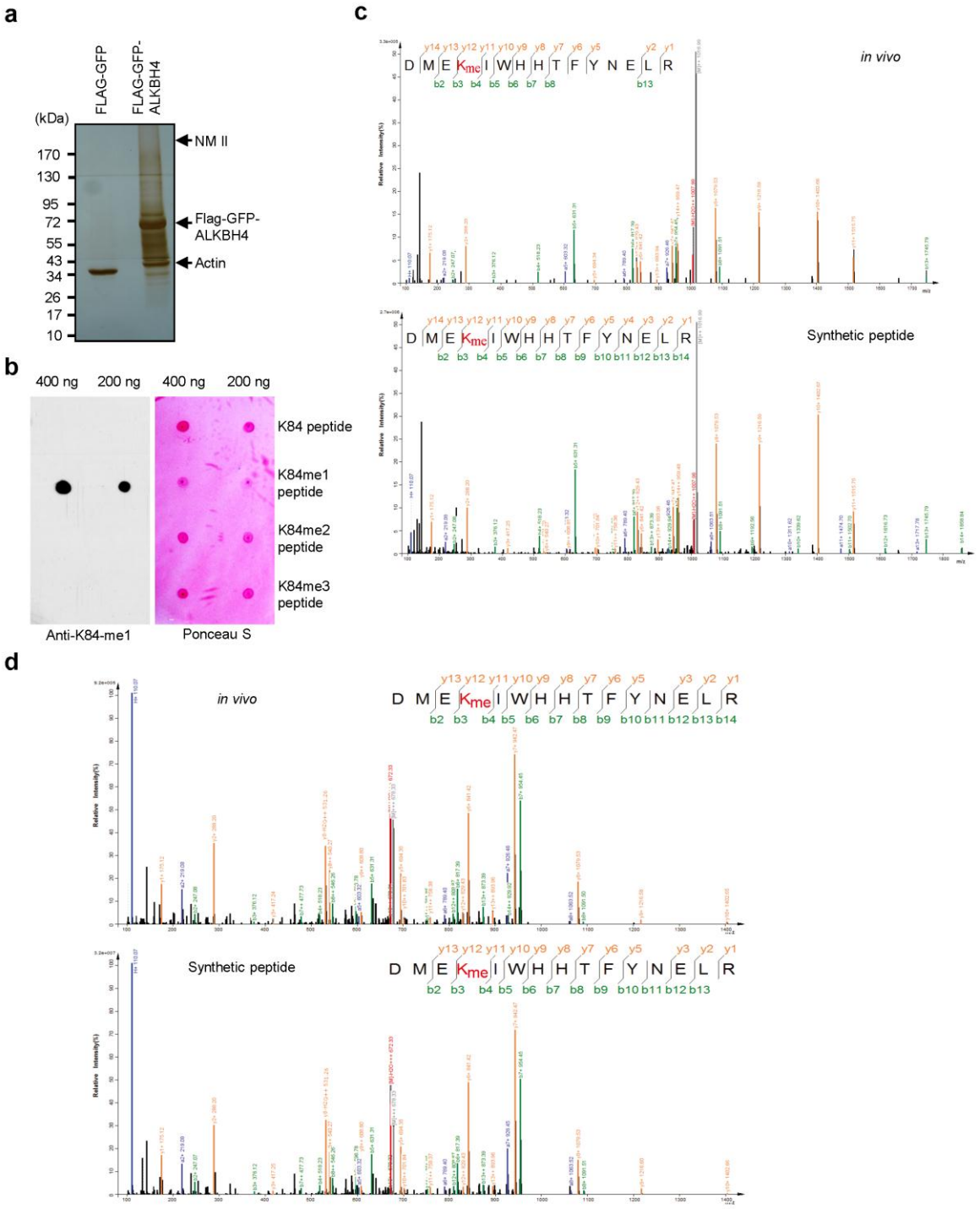

Supplementary Figure S2. Mass spectrometry analysis based screening for ALKBH4 interacting partners and methylated peptide. a, Silver staining of Flag immunoprecipitates from 293T cells transfected with Flag-GFP or Flag-GFP-ALKBH4. NM II and actin were identified in ALKBH4 specific bands by mass spectrometric (MS) analysis. **b**, Specificity of the actin-K84me1 antibody was verified by dot-blotting of non-, mono-, di- and tri-methylated actin peptides synthesized by New England Peptide. **c-d**, High-resolution and high-mass-accuracy fragmentation

spectra of a doubly (**c**) and triply (**d**) charged β-actin peptide that is mono-methylated at K84 are shown. The one originated from the HA-β-actin immunoprecipitated from 293T cells indicated as *in vivo* (upper panel) matched well with that of a synthetic peptide (lower panel).

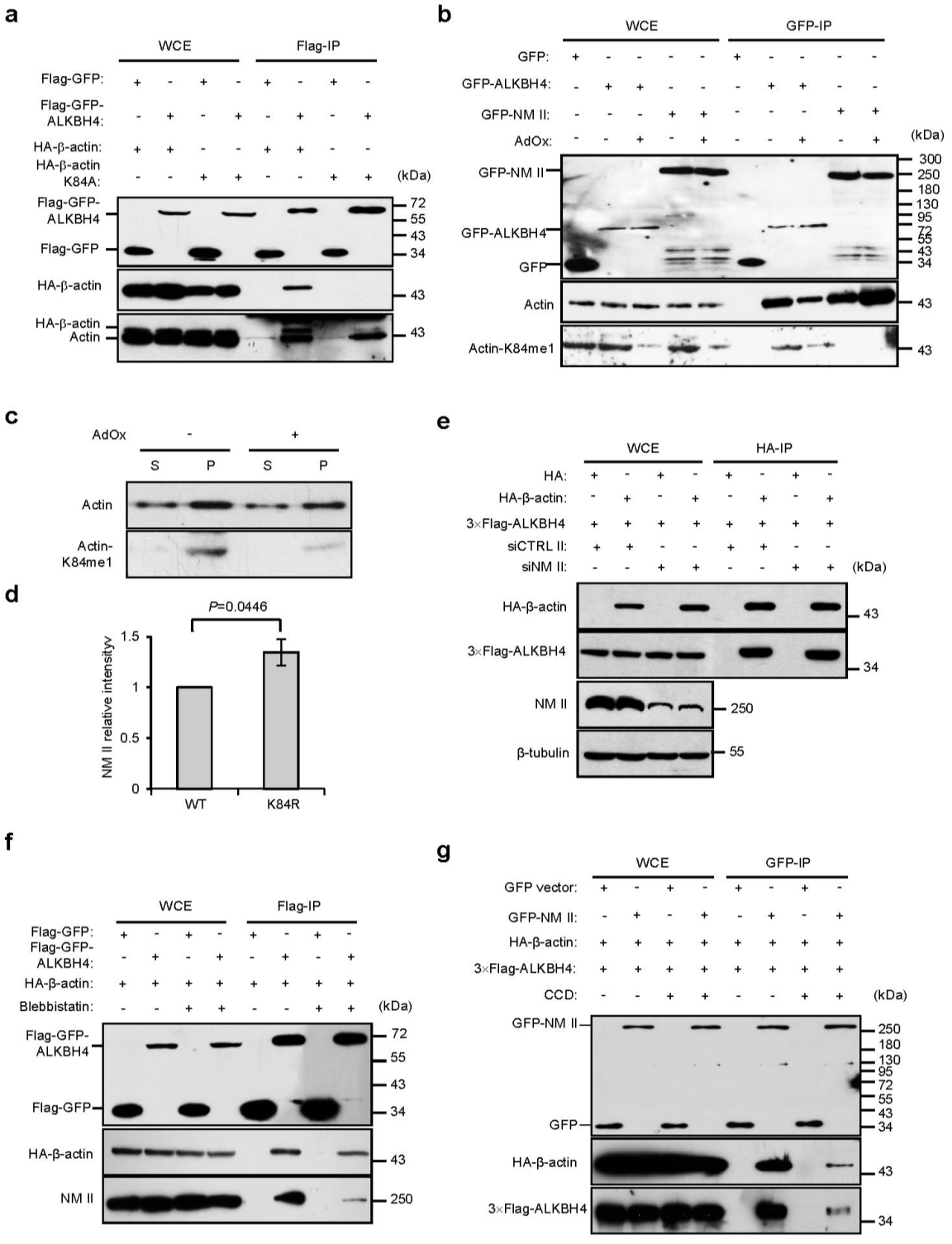

Supplementary Figure S3. Actin mediates the ALKBH4-Actomyosin interaction. a, 293T cells were co-transfected with Flag-GFP-ALKBH4 and HA-β-actin WT or K84A as indicated and lysates were subjected to Flag immunoprecipitation. Immunoprecipitates and WCEs were immunoblotted with the indicated antibodies. **b,** 293T /GFP-NM II or 293T/GFP-ALKBH4 stable cell were treated

with 20 μM AdOx (Adenosine-2′, 3′-dialdehyde) for 24 h, lysed and subjected to GFP immunoprecipitation. Immunoprecipitates were analyzed by immunoblotting with the indicated antibodies. **c,** Detection of free and filamentous actin by actin fractionation. 293T cells were treated with 20 μM AdOx for 24 h. Fractions were analyzed by immunoblotting with the indicated antibodies. **d**, Quantification of signal intensity of K84R relative to WT from three independent experiments. 293T cells were transfected with WT or K84R HA-β-actin as indicated and lysates were subjected to HA immunoprecipitation. **e,** 48 h after transfection with the indicated siRNAs and DNA constructs, 293T cells were lysed and subjected to HA immunoprecipitation. Immunoprecipitates were analyzed by immunoblotting with the indicated antibodies. **f**, 48 h after transfection with the indicated DNA constructs, 293T cells were treated with 5μM Blebbistatin for 5 h, lysed and subjected to Flag immunoprecipitation. Immunoprecipitates were analyzed by immunoblotting with the indicated antibodies. **g**, 48 h after transfection with the indicated DNA constructs, 293T cells were treated with 1 μg/ml CytochalasinD (CCD) for 1.5 h, lysed and subjected to GFP immunoprecipitation. Immunoprecipitates were analyzed by immunoblotting with the indicated antibodies.

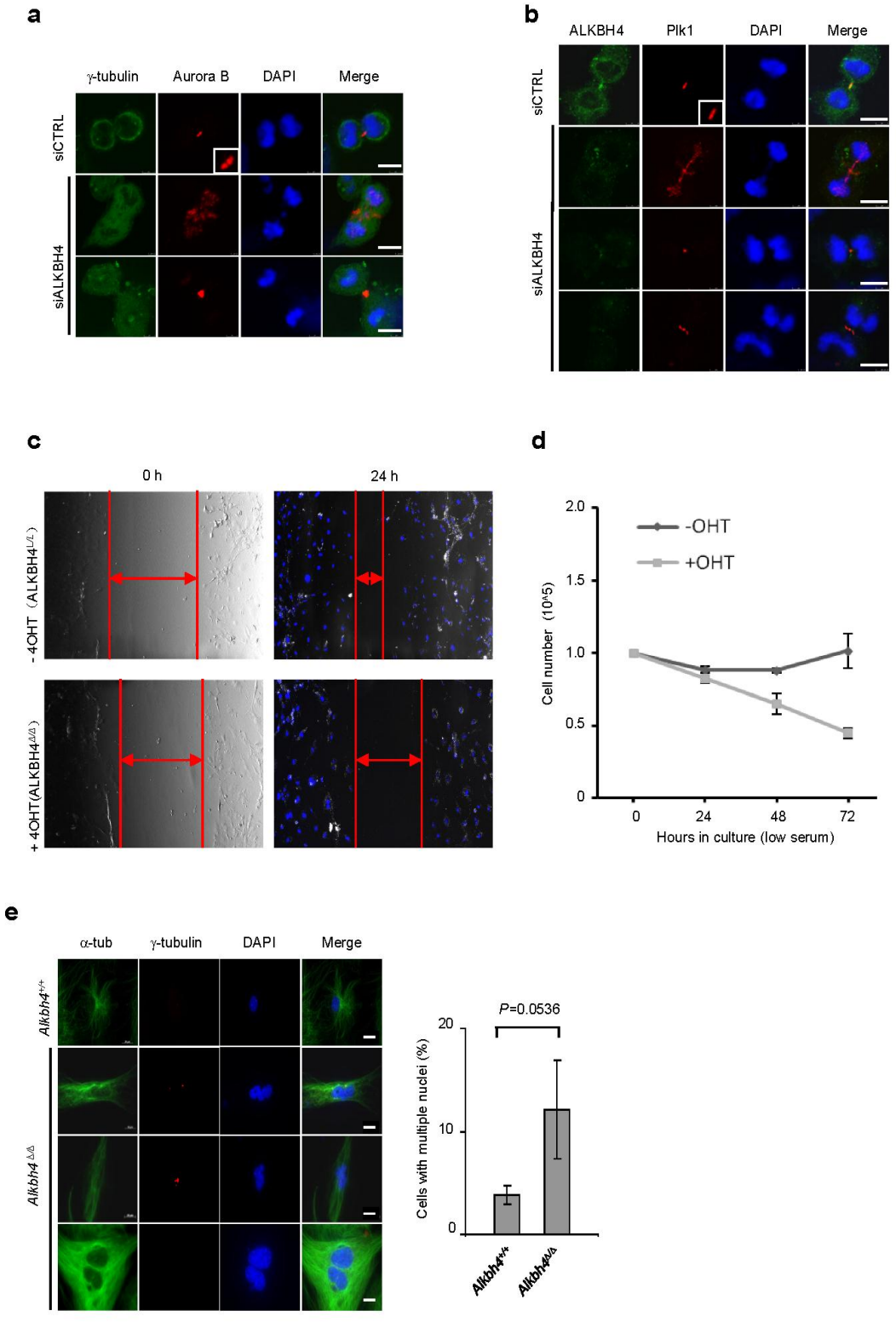

Supplementary Figure S4. Cellular phenotypes associated with ALKBH4 deficiency. a-b, MRC5 cells treated with ALKBH4 or CTRL siRNA were immunostained with γ-tubulin and Aurora B (**a**) or Plk1 and ALKBH4 (**b**). Scale bars, 10 μm. **c**, Representative images of scratch assay with primary *Alkbh4*$^{L/L}$*Cre* MEF cells untreated (*Alkbh4*$^{L/L}$) or treated with 4-OHT (*Alkbh4*$^{\Delta/\Delta}$). Pictures

were taken at time 0 h when the scratch was made and 24 h later with matched reference points. The images acquired were analyzed by measuring the distances between the borders of the scratches (red arrows). **d**, *Alkbh4*$^{L/L}$*Cre* MEF cells, 4-OHT-treated *(Alkbh4*$^{\Delta/\Delta}$) and untreated (*Alkbh4*$^{L/L}$), show approximately the same amount of cells after 24h in low serum medium, but *Alkbh4*$^{\Delta/\Delta}$ cells start to die off at 48h and on. Cell count of *Alkbh4*$^{L/L}$*Cre* MEF cells, untreated (-OHT) or treated with 4-OHT (+ OHT), replated in low serum medium (0.5%) and harvested at the indicated time points (n = 2, two different primary MEF cell lines). **e**, *Alkbh4*$^{+/+}$*Cre* (*Alkbh4*$^{+/+}$) and *Alkbh4*$^{L/L}$*Cre* (*Alkbh4*$^{\Delta/\Delta}$) MEF cells were treated with 4-OHT and immunostained with the indicated antibodies and DAPI, scale bars 20 μm. Histogram represents the mean of three independent experiments (300 cells/condition/experiment). *P* value was calculated using a two-tailed *t*-test. Error bars indicate s.d.

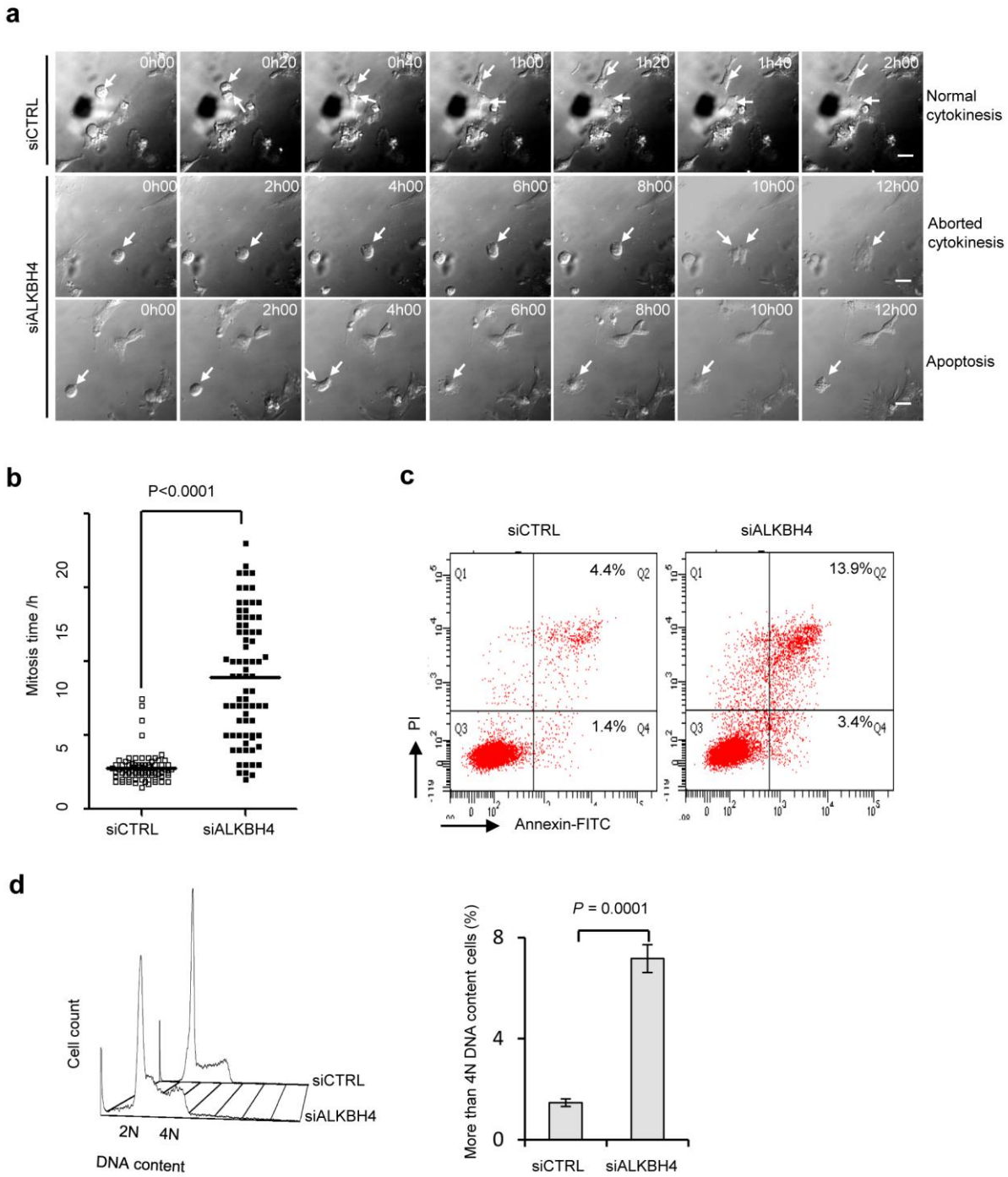

Supplementary Figure S5 ALKBH4 deficiency leads to increased cell death, mitotic index. a, Representative images of successful and failed cytokinesis and apoptosis in MRC5 cells treated with ALKBH4 or CTRL siRNA for 48 h; see Supplementary Movies 1, 2 and 3, respectively. Time is indicated in hours and minutes. Scale bars: 20 μm. **b**, Measurement of live cell mitotic length for ALKBH4 proficient and deficient cells (80 cells/condition/experiment for each genotype). **c**, MRC5 cells were treated with CTRL or ALKBH4 siRNA for 48 h, stained with annexin V and propidium iodide (PI) and analysed by flow cytometry. **d**, MRC5 cells treated with CTRL or ALKBH4 siRNA

for 48 h were stained with propidium iodide (PI) and analysed by flow cytometry. Quantification of > 4N DNA content cells is based on three independent experiments (30,000 cells/condition/experiment).

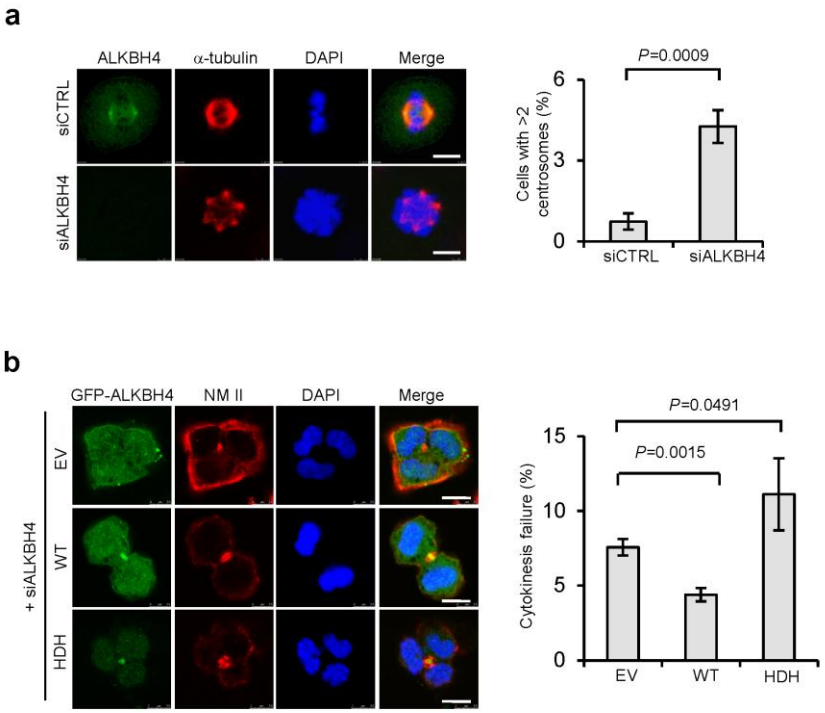

Supplementary Figure S6. ALKBH4 deficiency leads to centrosome supernumerary and cytokinesis failure. a, MRC5 cells treated with ALKBH4 or CTRL siRNA were immunostained with α-tubulin and ALKBH4. Graph represents the mean of three independent experiments (300 cells/condition/experiment). *P* value was calculated using a two-tailed *t*-test. Error bars indicate s.d. Scale bars, 10 μm. **b**, MRC5 cells were simultaneously transfected with ALKBH4 siRNA and the indicated siRNA insensitive Flag-GFP-ALKBH4 constructs for 48 h, fixed and immunostained with the NM II antibody and DAPI. EV, empty vector. Quantification was based on three independent experiments (100 cells/condition/experiment). *P* value was calculated using a two-tailed *t*-test. Error bars indicate s.d. Scale bars, 10 μm.

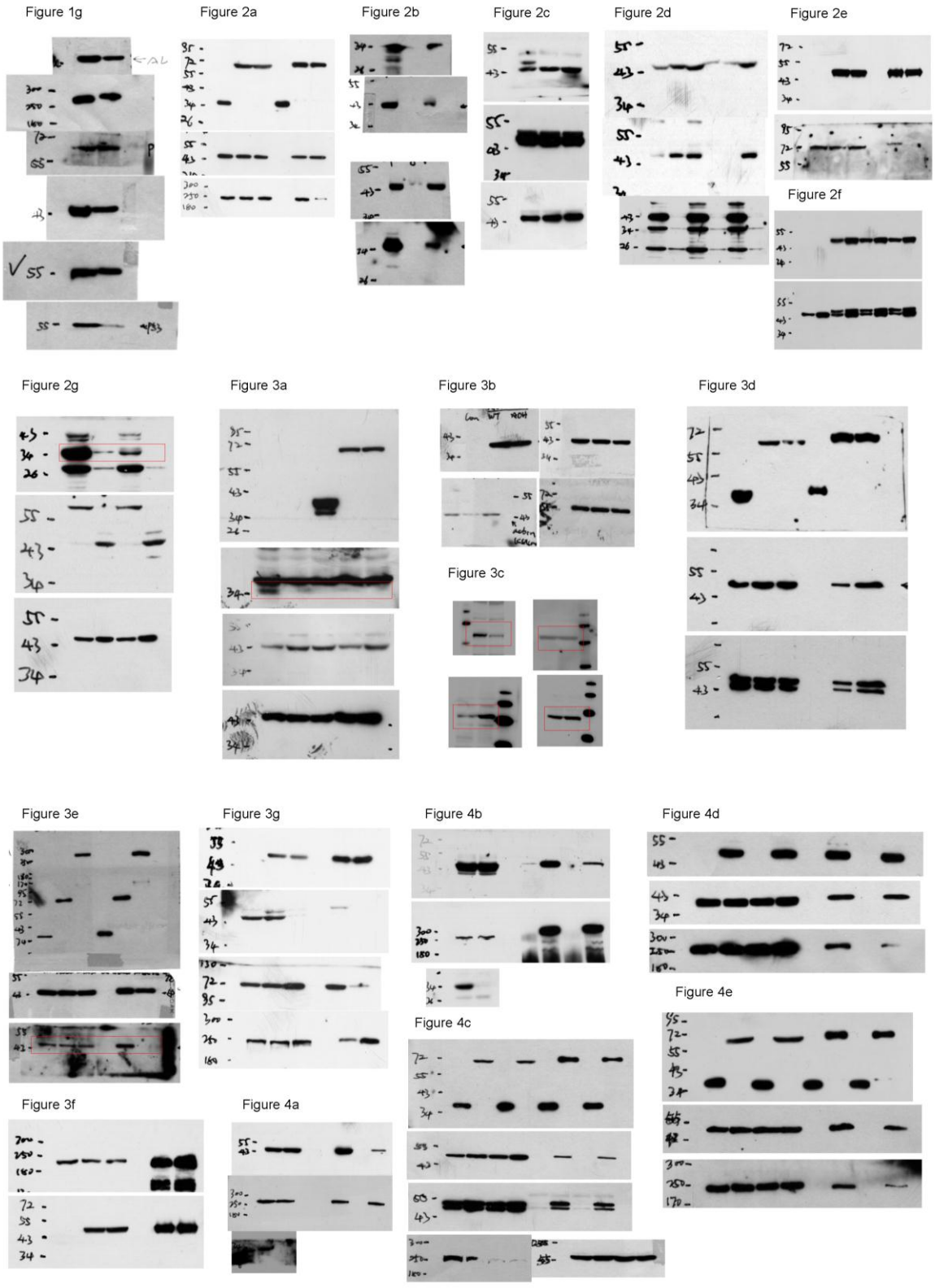

Supplementary Figure S7. Full scans of the key immunoblots.

Supplementary Table S1. A full list of all identified proteins from ALKBH4 pull down

Accession #	Coverage	Peptides	#AAs	MW [Da]	Score	Description
IPI:IPI00033770.5	**66.23**	**42**	**302**	**33816**	**149.50**	**Isoform 1 of Alkylated DNA repair protein alkB homolog 4**
IPI:IPI00220327.3	36.34	35	644	65978	123.11	Keratin, type II cytoskeletal 1
IPI:IPI00304925.5	35.88	26	641	70009	95.03	Heat shock 70 kDa protein 1
IPI:IPI00009865.2	29.01	28	593	59475	94.77	Keratin, type I cytoskeletal 10
IPI:IPI00021439.1	**50.13**	**23**	**375**	**41710**	**76.43**	**Actin, cytoplasmic 1**
IPI:IPI00021304.1	17.21	16	645	65825	54.12	Keratin, type II cytoskeletal 2 epidermal
IPI:IPI00514530.5	29.76	14	289	32254	43.89	Putative uncharacterized protein ACTA1
IPI:IPI00396485.3	14.72	11	462	50109	38.53	Elongation factor 1-alpha 1
IPI:IPI00019359.3	17.82	11	623	62092	35.95	Keratin, type I cytoskeletal 9
IPI:IPI00796776.1	11.11	8	567	60089	25.56	cDNA FLJ54081, highly similar to Keratin, type II cytoskeletal 5
IPI:IPI00554648.3	6.21	5	483	53671	17.99	Keratin, type II cytoskeletal 8
IPI:IPI00384444.5	5.72	5	472	51589	17.43	Keratin, type I cytoskeletal 14
IPI:IPI00465248.5	9.91	3	434	47139	9.34	Isoform alpha-enolase of Alpha-enolase
IPI:IPI00908770.1	8.20	2	317	35897	7.55	cDNA FLJ53063, highly similar to Tubulin beta-7 chain
IPI:IPI00074893.1	2.13	2	892	97202	7.28	Zinc finger protein 512B
IPI:IPI00007856.1	**1.03**	**1**	**1941**	**222906**	**6.52**	**Myosin-2**
IPI:IPI00647809.1	5.42	3	295	32624	6.50	Chromosome 9 open reading frame 156
IPI:IPI00888126.1	6.59	2	364	39567	6.49	similar to pyruvate kinase, muscle
IPI:IPI00028091.3	2.39	2	418	47341	6.29	Actin-related protein 3
IPI:IPI00218161.1	4.68	2	449	51221	5.67	Isoform 3 of High affinity cAMP-specific and IBMX-insensitive 3',5'-cyclic phosphodiesterase 8A
IPI:IPI00641244.1	11.34	2	97	10670	5.50	11 kDa protein
IPI:IPI00387111.5	12.26	2	106	11490	5.37	Uncharacterized protein ENSP00000333154
IPI:IPI00794605.1	7.45	1	161	17596	4.89	18 kDa protein
IPI:IPI00027547.2	12.73	1	110	11277	4.58	Dermcidin
IPI:IPI00867509.1	2.09	1	527	58910	4.34	Coronin-1C_i3 protein

IPI:IPI00641825.2	33.33	1	30	3640	3.96	Phospholipase C, beta 1
IPI:IPI00166202.3	3.06	1	589	65478	3.73	C-type lectin, superfamily member 13
IPI:IPI00873681.2	2.03	1	493	56946	3.66	57 kDa protein
IPI:IPI00305289.2	1.23	1	1056	119085	2.76	Kinesin-like protein KIF11
IPI:IPI00645641.2	3.83	1	784	87525	2.59	cDNA FLJ58439
IPI:IPI00410582.3	3.74	1	294	34172	2.54	Isoform Gamma of Tripartite motif-containing protein 4
IPI:IPI00470589.2	0.83	1	1560	166617	2.48	Isoform 2 of NHR domain-containing protein KIAA1787
IPI:IPI00742780.1	1.78	1	563	65730	2.19	FLJ00279 protein (Fragment)
IPI:IPI00908896.1	6.29	1	159	16839	2.17	cDNA FLJ54533, highly similar to Heterogeneous nuclear ribonucleoprotein H
IPI:IPI00413955.2	1.75	1	744	81740	2.14	cDNA FLJ11853 fis, clone HEMBA1006758, highly similar to Homo sapiens protocadherin beta 13 (PCDH-beta13) mRNA
IPI:IPI00910316.1	1.56	1	514	56646	2.01	cDNA FLJ54333, highly similar to T-complex protein 1 subunit epsilon

Supplementary Table S2. β-actin K84 mono-methylation was identified with a total of 26 spectra of +2, +3, or +4 charge states from a HA-β-actin immunoprecipitated sample indicated as *in vivo*. Only high-confidence search results are shown after filtering.

Sequence	Xcorr	DeltCN	Confident %	Obs[M+H+]	Calc[M+H+]	Δm(PPM)	SpR	Probility Score	Ion % Matched	Spectra count	Charge State
D.DMEK(14.0157)IWHHTFYNELR.V	4.9339	0.4761	100.00%	2032.979	2032.9698	4.5	1	7.71	65.20%	13	3
D.DMEK(14.0157)IWHHTFYNELR.V	3.8567	0.3748	99.20%	2033.9806	2032.9698	3.6	1	5.4	36.40%	4	4
D.DMEK(14.0157)IWHHTFYNELR.V	5.9979	0.3611	98.30%	2034.9766	2032.9698	0	1	6.27	71.40%	9	2

ALKBH4 Depletion in Male Germ Cells leads to Spermatogenic Defects

Anja Nilsen [1], Gareth Greggains [2], Markus Fusser [1], Peter Fedorcsak [2#] , Arne Klungland [1,3#]

[1] Institute of Medical Microbiology, Oslo University Hospital Rikshospitalet, University of Oslo, Norway

[2] Section for Reproductive Medicine, Department of Gynecology, Oslo University Hospital, Rikshospitalet and Institute of Clinical Medicine, University of Oslo, Oslo, Norway

[3] Institute of Basic Medical Sciences, University of Oslo, Oslo, Norway

[#] Correspondence should be addressed to A.K. (arne.klungland@rr-research.no) or P.F. (peter.fedorcsak@medisin.uio.no)

ABSTRACT

ALKBH4, an AlkB homologue in the 2OG and Fe2+ dependent hydroxylase family, has previously been shown to regulate the level of monomethylated lysine-84 in actin and thereby indirectly influences the ability of non-muscular myosin II to bind actin filaments. ALKBH4 modulates fundamental processes including cytokinesis and cell motility, and its depletion is lethal during early preimplantation embryo stage.

The aim of this study was to investigate the effect of ALKBH4 deficiency in a physiological context, using inducible *Alkbh4* knockout mice. Here, we report that ALKBH4 is essential for the development of spermatocytes during the prophase of meiosis, and that ALKBH4 depletion leads to insufficient establishment of the synaptonemal complex. We also show that ALKBH4 is localized in nucleolar structures of Sertoli cells and in nuclear foci in spermatogonia and primary spermatocytes.

INTRODUCTION

The nine mammalian homologues of the *E. coli* DNA demethylase AlkB, ALKBH1 to ALKBH8 and FTO, display diverse enzymatic activities. ALKBH1-3,-5,-8 and FTO are oxidative demethylases acting on methyl groups of nucleic acids (Aravind and Koonin, 2001; Westbye et al., 2008; Jia et al., 2008; Ringvoll et al., 2006; Songe-Moller et al., 2010; Aas et al., 2003; Zheng et al., 2013), whereas ALKBH1 also exhibits hydroxylase activity on methylated histone H2A (Ougland et al., 2012). .

We have recently described that ALKBH4 interacts with a mono-methylated lysine (K84me1) in actin. Depletion of ALKBH4 both in primary and in transformed cell cultures resulted in increased levels of actin-K84me1, suggesting that ALKBH4 is a K84me1-actin demethylase. Notably, non-muscular myosin II is unable to interact with actin-K84me1, and consequently, depletion of ALKBH4 results in major cellular defects, including failure of cytokinesis, reduced cell migration and increased cell death{Li, 2013 5968 /id}. Accordingly, we have shown that loss of ALKBH4 is lethal during early embryonic development (Li et al., 2013). ALKBH4 is expressed both in the cytoplasm and in the nucleus of interphase cells (Tsujikawa et al., 2007; Li et al., 2013), and accumulates in the midbody during cytokinesis (Li et al., 2013). Based on protein interaction studies and visualization of ectopically expressed ALKBH4 in nucleoli in somatic cells, a role for ALKBH4 in gene transcription has also been proposed (Bjornstad et al., 2012).

Male germ cells undergo DNA synthesis, homologous chromosome pairing and recombination during the prophase of meiosis. Chromosomal pairing and homologous recombination are facilitated by the synaptonemal complex (SC), a zipper-like protein structure that assembles between bivalents during meiotic

prophase (Zickler and Kleckner, 1999; Page and Hawley, 2004). The diversity of errors that might occur during the meiotic prophase are monitored by multiple molecular checkpoints (reviewed in (MacQueen and Hochwagen, 2011)).

The chromosomes are actively repositioned during the meiotic prophase. Before zygotene, the telomeres associate with the nuclear envelope (NE) in meiosis-specific complexes. During zygotene, these ends cluster into a localized area of the NE (the bouquet) while, at early pachytene, the ends redistribute throughout the nuclear periphery (Zickler, 1998; Bass, 2003; Scherthan, 2007; Harper et al., 2004). In the diplonema, separation of the homologous chromosomes begins, which is completed during diakinesis. The spermatocyte then enters two meiotic divisions to form spermatids, which go through a differentiation phase called spermiogenesis (Hess and Renato de, 2008).

The somatic Sertoli cells provide the structural support for the germinal epithelium and the physiological environment for spermatocyte development. Germ cells are attached to Sertoli cells by actin-based adherence junctions (ectoplasmic specialization, ES), which assist in the translocation of early spermatocytes towards the lumen of seminiferous tubuli (Vogl et al., 2009).

Concluding the cytokinesis during mitosis, the midbody structure is abscised to separate the two cells (Glotzer, 2005). During meiosis, however, dividing germ cells do not abscise the midbody and stay connected through a stable syncytium linking the cytoplasm of generations of daughter cells {Fawcett, 1959 4 /id}.

To investigate the physiological role of ALKBH4 and circumvent embryonic lethality of *Alkbh4* deletion, we depleted ALKBH4 in mice using a tamoxifen-inducible *Alkbh4*$^{L/L}$ *CreEsr* strain. Here, we report that ALKBH4 depletion leads to a marked loss of male germ cells during meiotic prophase and disorganization

of the synaptonemal complex. Moreover, we describe the nuclear localization pattern of ALKBH4 in mitotic and premeiotic male germ cells in addition to the Sertoli cells.

RESULTS

Characterization of *Alkbh4*$^{\Delta/\Delta}$ mice

Based on our previous study, which show the requirement of ALKBH4 in cell proliferation and migration, we wanted to study the effect of ALKBH4 depletion in juvenile mice which are still developing and have a higher rate of cell proliferation compared to adult mice. The inducible knockout genotype *Alkbh4*$^{L/L}$ *CreEsr* have been described previously (Li et al., 2013). In this study, 4 week old *Alkbh4*$^{L/L}$ *CreEsr* mice were treated with tamoxifen to delete *Alkbh4* (designated *Alkbh4*$^{\Delta/\Delta}$). *Alkbh4*$^{L/L}$ and *Alkbh4*$^{+/+}$ *CreEsr* mice were used as controls and exposed to the same treatment as *Alkbh4*$^{L/L}$ *CreEsr* mice (Figure S1 a,b,c). The body weight gain of *Alkbh4*$^{\Delta/\Delta}$ mice was not altered compared to control mice (Figure S2 a). The testes of 2 weeks-induced *Alkbh4*$^{\Delta/\Delta}$ mice were significantly smaller than in *Alkbh4*$^{L/L}$ and *Alkbh4*$^{+/+}$ *CreEsr* mice and in *Alkbh4*$^{\Delta/\Delta}$ mice treated with tamoxifen for 1 week (Figure 1a). Despite ablation of the *Alkbh4* gene (Figure S1 b), the other organs appeared normal at macroscopic inspection. The weight of the spleen, another highly proliferative organ, was not affected by the depletion of ALKBH4 (Figure S2 b). The reduced sizes of testes in *Alkbh4*$^{\Delta/\Delta}$ mice lead us to examine the testicular histology in detail. The diameter of the seminiferous tubuli was significantly reduced in *Alkbh4*$^{\Delta/\Delta}$ mice (Figure 1b, right panel). We observed degeneration of the germinal epithelium marked by loss of germ cells, disruption of the organized germ cell layers, and luminal dislocation of primary spermatocytes (Figure 1c, right panel).

Increased germ cell apoptosis upon ALKBH4 depletion in mice

To assess whether the reduced tubular diameter and loss of germinal epithelium were associated with either a reduced entry of cells in spermatogenesis or increased cell

death, we performed a 2 hour-pulse of 5-bromo-2'-deoxyuridine (BrdU)-incorporation and terminal deoxynucleotidyl transferase (TdT)-mediated dUTP nick end labeling (TUNEL) experiments. The amount of preleptotene spermatocytes, which were identified in stage VII-VIII tubuli by their basal localization and increased BrdU labeling indicative of DNA synthesis, was similar among the control and *Alkbh4*$^{\Delta/\Delta}$ testis (Figure 2 a). The amount of apoptotic cells, identified as TUNEL positive nuclei, was increased (p= 0.056) in *Alkbh4*$^{\Delta/\Delta}$ testes compared to controls (Figure 2 b). Apoptotic nuclei were most prevalent in the primary spermatocyte layer of stage VI-XII tubuli, indicating loss of pachytene spermatocytes (Figure 2 b).

Stage-specific loss of testicular germ cells in *Alkbh4*$^{\Delta/\Delta}$ mice

The stages of meiotic prophase were assessed in sections immunolabeled for γH2Ax and counterstained with DAPI (Figure 3a). In stage IX tubuli, severe depletion of pachytene spermatocytes and spermatids (S9) was observed in *Alkbh4*$^{\Delta/\Delta}$ mice after 2 weeks of tamoxifen treatment compared to tamoxifen-treated *Alkbh4*$^{L/L}$ and *Alkbh4* $^{\Delta/\Delta}$ mice treated with tamoxifen for 1 week (n >10 tubuli per section, 6 sections per group). The absolute amount of leptotene spermatocytes was unchanged (Figure 3b). The absolute number of counted Sertoli cells was marginally increased in *Alkbh4*$^{\Delta/\Delta}$ tubuli (Figure 3b), but increased proliferation of these cells was not observed in BrdU labelling experiments (data not shown).

Comprehensive assessment of germ cell density in *Alkbh4*$^{\Delta/\Delta}$ and tamoxifen-treated *Alkbh4*$^{L/L}$ mice revealed comparable number of premeiotic spermatogonia, preleptotene and leptotene spermatocytes . Severe lack of pachytene spermatocytes was noted in *Alkbh4*$^{\Delta/\Delta}$ mice, especially at the late pachytene stage, and depletion of subsequent meiotic stages was apparent (Figure 3c). In normal testis, the average ratio

of spermatocytes to round and elongated spermatids is approximately 1:2:2 (Kerr et al., 2006). The amount of round spermatids was around the half of expected in ALKBH4-depleted testis (Figure 3 c), indicating further loss of germ cells around or during the meiotic divisions. Careful examination of sectioned stage XII tubuli, where the meiotic divisions take place, did not reveal consistently abnormal or asymmetric metaphases. Metaphase stage cells isolated from stage XII tubuli using the trans-illumination method were also labelled with anti-β-tubulin to visualize the metaphase spindle, but consistent morphological defects were not observed (data not shown).

Disordered synaptonemal complex in ALKBH4-deficient pachytene spermatocytes

Synaptonemal complex protein 3 (SYCP3) is one of the major components in the SC. This meiosis-specific protein is essential for the axial element assembly along the chromosomes and it is necessary for accurate synapsis formation (reviewed in Fraune et al., 2012).

In *Alkbh4*$^{L/L}$ leptonema, intranuclear aggregates of SYCP3 were detected. In the leptonema/zygonema transition, the aggregates decreased in size, and smaller foci/short stretches of SYCP3 in the SCs appeared. The mature SCs, formed along the entire chromosome axes in pachynema, were apparent as longer SYCP3-positive threads. At the diakinesis stage of meiosis, SYCP3 was removed from chromosome arms, but was maintained in smaller foci (corresponding to paired centromeres) (Figure 4). These observations are in agreement with previously reported SYCP3-staining pattern in mouse spermatocytes (Boateng et al., 2013; Schertan et al., 1996).

In *Alkbh4*$^{\Delta/\Delta}$ mice (tamoxifen-treated for 2 weeks), the SCs developed normally in leptotene and leptotene/zygotene stages, and occasionally, spermatocytes

progressed beyond the diakinesis stage with apparently normal SCs (Figure 4). In pachytene stage, an increased proportion of spermatocytes lost the organized SCs, which appeared as shorter SYCP3-positive segments, diffuse cytoplasmatic SYCP3 signal and weaker SYCP3 signal in the SCs. Moreover, in a fraction of the affected spermatocytes we observed SYCP3 staining as condensed protein fragments under the nuclear membrane. The nuclei of these cells were shrunken and the cells dislocated towards the lumen, indicative of cell death.

ALKBH4 localizes to the nucleoli in Sertoli cells and in nuclear patches in mitotic and premeiotic germ cells

Selective loss of pachytene spermatocytes in *Alkbh4*$^{\Delta/\Delta}$ mice led us to examine the expression of ALKBH4 protein throughout spermatogenesis (Figure 5, upper panel). We have previously characterized the localization of ALKBH4 in the cleavage furrow during cytokinesis (Li et al., 2013). We were not able to assess a detailed cytoplasmic localization pattern for ALKBH4 in the testis sections studied in this report. However, in the nuclei of Sertoli cells, spermatogonia, and zygotene and pachytene spermatocytes of wild-type mice, ALKBH4 localized to distinct structures in euchromatin, often in close association with heterochromatin. In Sertoli cells, a single ALKBH4-rich structure was observed in each nucleus. In spermatogonia, ALKBH4 was distributed in fine granular patches under the nuclear envelope. In preleptotene (Pl) and early leptotene (L_{early}) spermatocytes, ALKBH4 formed 3 to 8 diffuse threads and patches per nucleus. During the late leptotene (L_{late}) to the mid-pachytene (P_{mid}) stages, the number of ALKBH4-rich patches decreased and localized in the periphery of the nucleus. Expression of ALKBH4 diminished during the late pachynema (P_{late}) and diakinesis (Figure 5, lower panel). In *Alkbh4*$^{\Delta/\Delta}$ mice treated with tamoxifen for

one and two weeks, an overall decrease of ALKBH4-specific immunofluorescence was observed compared to the *Alkbh4*$^{L/L}$ samples (Figure S3).

We speculated if the ALKBH4 positive structures in the nuclei could be related to nucleolar compartments, as has been reported previously for ectopically expressed ALKBH4 in cell culture studies (Bjornstad et al., 2012). Co-immunostaining with anti-ALKBH4 and anti-Fibrillarin (a nucleolar marker) verified the localization of ALKBH4 in the nucleoli in Sertoli cells (Figure S4).

DISCUSSION

In this study, we used an inducible knockout approach to disrupt the *Alkbh4* gene in mice to reveal its function in a physiological context. Considering the embryonically lethal phenotype of the *Alkbh4* $^{-/-}$ mice, failure of cytokinesis and increased cell death after depletion of ALKBH4 previously described (Li et al., 2013), it was surprising that the induced mutant mice were viable with general normal appearance except for disruption of spermatogenesis. This leads us to hypothesize that ALKBH4 might play a distinct role in development, both in embryogenesis and in gametogenesis.

We found that depletion of ALKBH4 in mice does not seem to influence the entry of germ cells in meiosis, but ALKBH4 is required for successful completion of the meiotic prophase. Indeed, spermatogenesis was arrested at the pachytene stage in *Alkbh4*$^{\Delta/\Delta}$ mice, indicated by a reduced density of pachytene spermatocytes, increased rate of apoptosis, as well as dispersion of the organized synaptonemal complex. The gradual loss of nuclear ALKBH4 towards the late pachytene phase also supports the notion that *Alkbh4* has a specific function during the prophase of meiosis.

Although the molecular defects leading to meiotic arrest at pachynema in *Alkbh4*$^{\Delta/\Delta}$ mice are unknown, the disordered axial elements seen after depletion of ALKBH4 lead us to propose that the loss of cells at the pachytene stage was related to a failure of SC formation, with subsequent activation of pachytene checkpoint control mechanisms and apoptosis (Hermo et al., 2010). A fraction of ALKBH4-depleted spermatocytes did nevertheless complete meiosis, but these surviving cells gave rise to lower than expected number of haploid spermatids, suggesting that lack of ALKBH4 affects spermatogenesis beyond the pachytene stage, as well. We have previously described ALKBH4 as a modulator of specific actin-myosin dynamics in the cytoplasm via regulation of the K84me1-level in actin in cell culture (Li et al.,

2013). Interestingly, in this study we found ALKBH4 to localize in distincteuchromatic aggregates/patches in the nucleus of spermatogenic cells and in the nucleolus of Sertoli cells, which may support the involvement of ALKBH4 in regulation of specific actin dynamics in the nucleus required for normal development of premeiotic and postmeiotic germ cells via regulation of the K84me1 modification. In the cell nucleus, actin interacts with many different proteins involved in chromatin structure and function (Olave et al., 2002; Farrants, 2008), transcription initiation and elongation (Hofmann et al., 2004; Grummt, 2006; Qi et al., 2011), and RNA processing (Percipalle, 2009; Saitoh et al., 2004). In the early stages of premeiotic spermatocytes (preleptotene and mid-leptotene) ALKBH4 is found in several threads and patches in the nucleus. From late leptonema to mid-pachynema, the number of patches decreases. Interestingly, ALKBH4 does not seem to be present as aggregates in the nuclei of late pachytene and metaphase cell types. One possibility is that these structures are nucleolar organizing regions (NORs), nuclear structures engaged in ribosome biogenesis (Schwarzacher and Wachtler, 1993) associated with several autosomal bivalents in meiotic prophase spermatocytes (Kierszenbaum and Tres, 1974). At middle pachytene the NORs detach from their autosomal bivalents and associates close to the XY chromosomal pair (termed the XY-body), The nucleolus associated to the XY pair appears transcriptionally inactive (Tres, 2005). We could not detect ALKBH4- aggregates nearby the XY-body in pachytene stage spermatocytes, which also reflects the possibility that ALKBH4 is predominantly present at transcriptionally active sites.

Organization of the chromosomes and timed homologous recombination events during the prophase of meiosis requires highly organized cell machinery. Actin has been shown to be involved in many nuclear processes in yeast meiocytes, such as

pairing of chromosomal homologues, formation of synaptonemal complex and telomeric organization/bundling in zygotene stage cells which could be a network of both nuclear and cytoplasmic actin interaction in these processes (Koszul and Kleckner, 2009; Lui et al., 2013; Scherthan, 2007). The role of actin dynamics during mammalian spermatogenesis, however, remains to be explored (Hess and Renato de, 2008; Xiao and Yang, 2007). Studies of long-range interphase chromosome movements in mammalian somatic cells show dependency on nuclear actin and myosin (Chuang, 2006). In mammalian primary spermatocytes, actin may also play a part in the process of homologous chromosome pairing and formation of the synaptonemal complex. It is possible that many of the same processes could relate to mammalian meiotic cells, with ALKBH4 as an important modulator.

In conclusion, we report a role of ALKBH4 in spermatogenesis, by being an important factor for the development of premeiotic I stage cells and postmeiotic cells. A majority of unexplained cases of reproduction problems in human originate from defects in gametogenesis, and the results presented in this report could be important for understanding the mechanisms lying behind infertility.

MATERIALS AND METHODS

Ethics

All experimental procedures were approved by the Norwegian Animal Research Authority in accordance with institutional rules and national legislation. Mice were housed in the minimal disease unit under barrier conditions.

Alkbh4 $^{L/L}$ *Cre* mice and controls

We have described the DNA sequence in the *Alkbh4* allele flanked by *LoxP* (*Alkbh4* $^{L/L}$) previously (Li et al., 2013). *Alkbh4* $^{L/L}$ mice were mated with *CreEsr* transgenic mice (Hayashi and McMahon, 2002) (Jackson Laboratories, West Grove, PA) to create the inducible knockout genotype *Alkbh4* $^{L/L}$ *CreEsr* .

Deletion of *Alkbh4* (herein termed *Alkbh4* $^{\Delta/\Delta}$) in *Alkbh4* $^{L/L}$ *Cre-ER* mice was achieved by daily i.p injection of tamoxifen (Sigma) (1mg /20g bodyweight) in corn oil for 7 or 14 consecutive days. Injections started in 4-week-old mice (Figure S1 a). *Alkbh4* $^{L/L}$ mice injected with tamoxifen were used as controls. Tamoxifen-injected *Alkbh4* $^{+/+}$ *CreEsr* mice were used as additional control to assess the effect of the activated Cre recombinase. The genotype was determined by standard PCR methods as described previously (Li et al., 2013).

Histopathology

Testes were fixed in 10% neutral buffered formalin and embedded in paraffin. Sections (4 µm) were fixed on slides, deparafinized and rehydrated in 100-70% ethanol. The slides were stained with hematoxylin and eosin (Richard-Allan Scientific) according to standard protocols. After dehydration, the slides were washed

in Clear Rite 3 and mounted using Mounting medium 4111 (Richard-Allan Scientific). Images of stained sections were acquired using AxioCam ICc1 camera on an Axio Observer.Z1 microscope (Carl Zeiss).

Histological analysis

Tissues were fixed in 10% neutral buffered formalin and embedded in paraffin. For histology, tissue sections were stained with hematoxylin and eosin (H&E) according to standard protocols and examined by light microscopy. For immunohistochemistry, tissue sections were deparaffinized, rehydrated, and subjected to heat-induced epitope retrieval in Tris-EDTA buffer (10mM Tris, 1mM EDTA, pH 9). The sections were permeabilized with 0.1% Triton-x 100 in TBS-T (TBS with 0.1% Tween) for 15 min at room temperature and blocked with 0.5% BSA, 0.5% goat serum in TBST for 1 hour at room temperature. Slides were incubated with polyclonal rabbit-anti ALKBH4 (1:500, #282 (Li et al., 2013) overnight at 4ºC, followed by incubation with 0.3% H_2O_2 for 10 minutes, incubation with secondary antibody, and staining according to the EnVision + HRP kit (DAKO, K4010). For immunofluorescence, tissue section were prepared as described above and permeabilized with 0.5% triton-x 100 in TBST for 10 min at room temperature and blocked with 0.5% dried milk + 0.5% serum (normal serum from the same species as secondary antibodies) in TBST for 1 hour at room temperature. Slides were incubated with primary antibody for 1 hour or overnight at 4ºC before incubation with secondary antibody. DAPI (1 µg/ml) was used as counterstain and Mowiol 4-88 (Polysciences) was used for mounting. Primary antibodies used: goat-anti yH2A.x (1:500, Abcam), rabbit polyclonal anti-ALKBH4 (1:1000,#282), anti-SYCP3 (20mg/ml, LifeSpan Biosciences), anti-Fibrillarin (1:100, Santa Cruz). Secondary antibodies: donkey-anti-goat-Alexa 488/594 (1:500,

Invitrogen), goat anti-rabbit-Alexa 488 (1:500, Invitrogen). Images of stained sections were acquired using AxioCam MRRev3 camera on an Axio Observer.Z1 microscope (Carl Zeiss).

BrdU labeling

To observe BrdU (5-bromo-2-deoxyuridine) incorporation in testis, mice were injected i.p with 1 mg BrdU (Sigma) and sacrificed after 2 hours. Staining of testis sections were done according to protocol described (BrdU protocol, Abcam). Rat-anti BrdU (1:100, Abcam) was used as primary antibody, and goat anti-rat Alexa594 (1:500, Invitrogen) was used as secondary antibody. Sections were counterstained with DAPI and mounted with Mowiol. Images of stained sections were acquired using AxioCam MRRev3 camera on an Axio Observer.Z1 microscope (Carl Zeiss).

Apoptosis detection

The *In Situ* Cell Death Detection Kit, TMR red, (Roche) was used for TUNEL labeling of testis sections according to protocol described (Roche). Sections were counterstained with DAPI and mounted with Mowiol. Images of stained sections were acquired using AxioCam MRRev3 camera on an Axio Observer.Z1 microscope (Carl Zeiss).

Immunoblotting

Testes were collected and snap frozen in liquid nitrogen and stored at -80 C until used. Whole protein extracts from testis were made by homogenizing and lysing tissue in RIPA (RadioImmunoPrecipitation Assay) buffer (50mM Tris HCl pH 8, 150 mM NaCl, 1% NP-40, 0.5% sodium deoxycholate, 0.1% SDS) added complete

protease inhibitor cocktail (Roche) with a bead based homogenization system (Lysing Matrix, MP Biomedicals).Protein concentration was determined using the Bradford assay. Equal amounts of total protein were separated by SDS-PAGE, transferred to a PVDF membrane and immunoblotted with the following primary antibodies: rabbit anti-ALKBH4 (#282, 1:500), goat anti α-tubulin (1:8000, Sigma). HRP-labeled secondary antibodies were detected using the SuperSignal West Dura substrate (Thermo Scientific) and ChemiDoc XRS+ System (Bio-Rad).

Reference List

Aas,P.A., Otterlei,M., Falnes,P.O., Vagbo,C.B., Skorpen,F., Akbari,M., Sundheim,O., Bjoras,M., Slupphaug,G., Seeberg,E., and Krokan,H.E. (2003). Human and bacterial oxidative demethylases repair alkylation damage in both RNA and DNA. Nature *421*, 859-863.

Aravind,L. and Koonin,E.V. (2001). The DNA-repair protein AlkB, EGL-9, and leprecan define new families of 2-oxoglutarate- and iron-dependent dioxygenases. Genome Biol. *2*, RESEARCH0007.

Bass,H.W. (2003). Telomere dynamics unique to meiotic prophase: formation and significance of the bouquet. Cell Mol. Life Sci. *60*, 2319-2324.

Bjornstad,L.G., Meza,T.J., Otterlei,M., Olafsrud,S.M., Meza-Zepeda,L.A., and Falnes,P.O. (2012). Human ALKBH4 interacts with proteins associated with transcription. PLoS. One. *7*, e49045.

Boateng,K.A.; Bellani,M.A.; Gregoretti,I.V.; Pratto,F.; Camerini-Otero,R.D.(2013). Homologous pairing preceding SPO11-mediated double-strand breaks in mice. Dev. Cell. *24, 196-205.*

Chuang,C.H. (2006). Long-Range Directional Movement of an Interphase Chromosome Site.

de Lanerolle,P. (2012). Nuclear actin and myosins at a glance. J. Cell Sci. *125*, 4945-4949.

Dominguez,R. and Holmes,K.C. (2011). Actin structure and function. Annu. Rev. Biophys. *40*, 169-186.

Farrants,A.K. (2008). Chromatin remodelling and actin organisation. FEBS Lett. *582*, 2041-2050.

Fawcett,D.W., Ito,S., and Slautterback,D. (1959). The occurrence of intercellular bridges in groups of cells exhibiting synchronous differentiation. J. Biophys. Biochem. Cytol. *5*, 453-460.

Fraune,J.; Schramm,S.; Alsheimer,M.; Benavente,R. (2012). The mammalian synaptonemal complex: protein components, assembly and role in meiotic recombination. Exp. Cell Res. *318, 1340-1346*.

Glotzer,M. (2005). The Molecular Requirements for Cytokinesis. Science *307*, 1735-1739.

Grummt,I. (2006). Actin and myosin as transcription factors. Curr. Opin. Genet Dev. *16*, 191-196.

Harper,L., Golubovskaya,I., and Cande,W.Z. (2004). A bouquet of chromosomes. J. Cell Sci. *117*, 4025-4032.

Hayashi,S. and McMahon,A.P. (2002). Efficient recombination in diverse tissues by a tamoxifen-inducible form of Cre: a tool for temporally regulated gene activation/inactivation in the mouse. Dev. Biol. *244*, 305-318.

Hermo,L., Pelletier,R.M., Cyr,D.G., and Smith,C.E. (2010). Surfing the wave, cycle, life history, and genes/proteins expressed by testicular germ cells. Part 1: Background to spermatogenesis, spermatogonia, and spermatocytes. Microsc. Res. Tech. *73*, 241-278.

Hess,R.A. and Renato de,F.L. (2008). Spermatogenesis and cycle of the seminiferous epithelium. Adv. Exp. Med. Biol *636*, 1-15.

Hofmann,W.A., Stojiljkovic,L., Fuchsova,B., Vargas,G.M., Mavrommatis,E., Philimonenko,V., Kysela,K., Goodrich,J.A., Lessard,J.L., Hope,T.J., Hozak,P., and de,L.P. (2004). Actin is part of pre-initiation complexes and is necessary for transcription by RNA polymerase II. Nat. Cell Biol. *6*, 1094-1101.

Jia,G., Yang,C.G., Yang,S., Jian,X., Yi,C., Zhou,Z., and He,C. (2008). Oxidative demethylation of 3-methylthymine and 3-methyluracil in single-stranded DNA and RNA by mouse and human FTO. FEBS Lett. *582*, 3313-3319.

Kerr,J.B., Loveland,K.L., O`Bryan,M.K., and de Kretzer,D.M. (2006). Cytology of the Testis and Intrinsic Control Mechanisms. In Knobil and Neill's Physiology of Reproduction , (St Louis: Academic Press), pp. 827-947.

Kierszenbaum,A.L. and Tres,L.L. (1974). Nucleolar and perichromosomal RNA synthesis during meiotic prophase in the mouse testis. J. Cell Biol. *60*, 39-53.

Koszul,R. and Kleckner,N. (2009). Dynamic chromosome movements during meiosis: a way to eliminate unwanted connections? Trends Cell Biol. *19*, 716-724.

Li,M.M., Nilsen,A., Shi,Y., Fusser,M., Ding,Y.H., Fu,Y., Liu,B., Niu,Y., Wu,Y.S., Huang,C.M., Olofsson,M., Jin,K.X., Lv,Y., Xu,X.Z., He,C., Dong,M.Q., Rendtlew Danielsen,J.M., Klungland,A., and Yang,Y.G. (2013). ALKBH4-dependent demethylation of actin regulates actomyosin dynamics. Nat. Commun. *4*, 1832.

Lui,D.Y., Cahoon,C.K., and Burgess,S.M. (2013). Multiple opposing constraints govern chromosome interactions during meiosis. PLoS. Genet. *9*, e1003197.

MacQueen,A.J. and Hochwagen,A. (2011). Checkpoint mechanisms: the puppet masters of meiotic prophase. Trends Cell Biol. *21*, 393-400.

Olave,I.A., Reck-Peterson,S.L., and Crabtree,G.R. (2002). Nuclear actin and actin-related proteins in chromatin remodeling. Annu. Rev. Biochem. *71*, 755-781.

Ougland, R. ALKBH1 is a histone H2A dioxygenase involved in neural differentiation. 2012. Lando, D., Jonson, I, Dahl, J. A., Moen, M. N., and Nordstrand, L. M.
Ref Type: Generic

Page,S.L. and Hawley,R.S. (2004). The genetics and molecular biology of the synaptonemal complex. Annu. Rev. Cell Dev. Biol. *20*, 525-558.

Percipalle,P. (2009). The long journey of actin and actin-associated proteins from genes to polysomes. Cell Mol. Life Sci. *66*, 2151-2165.

Qi,T., Tang,W., Wang,L., Zhai,L., Guo,L., and Zeng,X. (2011). G-actin participates in RNA polymerase II-dependent transcription elongation by recruiting positive transcription elongation factor b (P-TEFb). J Biol Chem *286*, 15171-15181.

Ringvoll,J., Nordstrand,L.M., Vagbo,C.B., Talstad,V., Reite,K., Aas,P.A., Lauritzen,K.H., Liabakk,N.B., Bjork,A., Doughty,R.W., Falnes,P.O., Krokan,H.E., and Klungland,A. (2006). Repair deficient mice reveal mABH2 as the primary oxidative demethylase for repairing 1meA and 3meC lesions in DNA. EMBO J. *25*, 2189-2198.

Saitoh,N., Spahr,C.S., Patterson,S.D., Bubulya,P., Neuwald,A.F., and Spector,D.L. (2004). Proteomic analysis of interchromatin granule clusters. Mol. Biol. Cell *15*, 3876-3890.

Scherthan,H. (2007). Telomere attachment and clustering during meiosis. Cell Mol. Life Sci. *64*, 117-124.

Scherthan,H.; Weich,S.; Schwegler,H.; Heyting,C.; Harle,M.; Cremer,T. (1996). Centromere and telomere movements during early meiotic prophase of mouse and man are associated with the onset of chromosome pairing. J.Cell Biol. *134, 1109-1125.*

Schwarzacher,H.G. and Wachtler,F. (1993). The nucleolus. Anat. Embryol. (Berl) *188*, 515-536.

Songe-Moller,L., van den,B.E., Leihne,V., Vagbo,C.B., Kristoffersen,T., Krokan,H.E., Kirpekar,F., Falnes,P.O., and Klungland,A. (2010). Mammalian ALKBH8 possesses tRNA methyltransferase activity required for the biogenesis of multiple wobble uridine modifications implicated in translational decoding. Mol. Cell Biol. *30*, 1814-1827.

Tres,L.L. (2005). XY chromosomal bivalent: nucleolar attraction. Mol Reprod. Dev. *72*, 1-6.

Tsujikawa,K., Koike,K., Kitae,K., Shinkawa,A., Arima,H., Suzuki,T., Tsuchiya,M., Makino,Y., Furukawa,T., Konishi,N., and Yamamoto,H. (2007). Expression and sub-cellular localization of human ABH family molecules. J. Cell Mol. Med. *11*, 1105-1116.

Vogl,A.W., Vaid,K.S., and Guttman,J.A. (2009). The Sertoli Cell Cytoskeleton
Molecular Mechanisms in Spermatogenesis. C.Y.Cheng, ed. Springer New York), pp. 186-211.

Westbye,M.P., Feyzi,E., Aas,P.A., Vagbo,C.B., Talstad,V.A., Kavli,B., Hagen,L., Sundheim,O., Akbari,M., Liabakk,N.B., Slupphaug,G., Otterlei,M., and Krokan,H.E. (2008). Human AlkB homolog 1 is a mitochondrial protein that demethylates 3-methylcytosine in DNA and RNA. J. Biol. Chem. *283*, 25046-25056.

Xiao,X. and Yang,W.X. (2007). Actin-based dynamics during spermatogenesis and its significance. J. Zhejiang. Univ Sci. B *8*, 498-506.

Zheng,G., Dahl,J., Niu,Y., Fedorcsak,P., Huang,C.M., Li,C., V+Ñgb++,C., Shi,Y., Wang,W.L., Song,S.H., Lu,Z., Bosmans,R., Dai,Q., Hao,Y.J., Yang,X., Zhao,W.M., Tong,W.M., Wang,X.J., Bogdan,F., Furu,K., Fu,Y., Jia,G., Zhao,X., Liu,J., Krokan,H., Klungland,A., Yang,Y.G., and He,C. (2013). ALKBH5 Is a Mammalian RNA Demethylase that Impacts RNA Metabolism and Mouse Fertility. Mol. Cell *49*, 18-29.

Zickler,D. (1998). The leptotene-zygotene transition of meiosis.

Zickler,D. and Kleckner,N. (1999). Meiotic chromosomes: integrating structure and function. Annu. Rev. Genet. *33*, 603-754.

FIGURE LEGENDS

Figure 1. Loss of Alkbh4 reduces the size of testes and the diameter of seminiferious tubuli

The phenotype of testis of tamoxifen-treated mice with genotypes *Alkbh4*$^{L/L}$ (Control), CreEsr (Control) and *Alkbh4* $^{\Delta/\Delta}$. **a)** Right panel, representative testis from control and *Alkbh4* $^{\Delta/\Delta}$ mice after tamoxifen treatment before and one week tamoxifen tratement (0-1 week), and after deletion of *Alkbh4* with tamoxifen treatment for 2 weeks. Left panel, average testis/body weight ratio of 4-5 weeks old mice before and after 1 week of treatment with tamoxifen (0-1 week), and 6 weeks old mice treated with tamoxifen for 2 weeks (0-1 week: *Alkbh4*$^{L/L,}$ n=3; CreEsr, n=1; *Alkbh4*$^{\Delta/\Delta}$,n=3. 2 weeks*:* *Alkbh4*$^{L/L,}$ n=5; *CreEsr*, n=6; *Alkbh4* $^{\Delta/\Delta}$,n=6). Data are expressed as mean ± SEM. **b)** Right panel, histological overview of representative control and *Alkbh4* $^{\Delta/\Delta}$ testis after 2 weeks of tamoxifen induction (HE stain, x 25 magnification). Left panel, decreased diameter of seminiferous tubuli in *Alkbh4*$^{\Delta/\Delta}$ mice after 2 weeks tamoxifen treatment compared to control mice (n= 100 tubuli/animal, 2 animals/genotype/timepoint. 0-1 week CreEsr N/A). Data are expressed as mean ± SEM. **c)** High magnification view (x 630) of testis section in b). Statistical analysis was performed using the non-paired, two-tailed Student's test: *p<0.05.

Figure 2

Maintained DNA synthesis and increased apoptosis in testes of *Alkbh4*$^{\Delta/\Delta}$ mice

a) Left panel, epifluorescence microscopy of BrdU labelled testicular sections in 6 weeks old mice treated with tamoxifen for 2 weeks, indicating comparable density of S-phase cells in control and *Alkbh4* $^{\Delta/\Delta}$ mice. DNA was visualized by DAPI staining. Right panel, quantification of the increased BrdU positive cells/ stage VIII tubulus in

sections (n=10 tubuli/animal, 2 animals/genotype) in testes of *Alkbh4*$^{\Delta/\Delta}$ compared to *Alkbh4*$^{L/L}$ mice. All data expressed as means ± SEM.

b) Left panel, epifluorescence microscopy of TUNEL-stained testicular sections in 6 weeks old mice treated with tamoxifen for 2 weeks. TUNEL identifies increased proportion of apoptotic germ cells in *Alkbh4*$^{\Delta/\Delta}$ mice compared to control (*Alkbh4* $^{L/L}$). DNA was counterstained with DAPI. Right panel, quantification of the increased number of TUNEL positive cells/tubulus in sections (n = 40 tubuli/animal, 3 animals/genotype) in testes of *Alkbh4*$^{\Delta/\Delta}$ compared to *Alkbh4*$^{L/L}$ mice. All data expressed as means ± SEM.

Figure 3

Stage-specific arrest of spermatogenesis in *Alkbh4*$^{\Delta/\Delta}$ mice

a) Immunofluoresence labeling of histological sections for anti-γH2A.X (red) with DAPI (blue) counterstain, where Sertoli cells (Se), leptotene (L) and pachytene (P) spermatocytes and round spermatids (S9) can be distinguished. **b)** Mean cell density per cross-section of stage IX (n >10 tubuli per histological section, total of 6 sections) from control (*Alkbh4*$^{L/L}$*) and Alkbh4* $^{\Delta/\Delta}$ mice treated with tamoxifen for one or two weeks shows severe depletion of pachytene spermatocytes and S9 round spermatids after 2 weeks of tamoxifen treatment in *Alkbh4*$^{\Delta/\Delta}$ mice. Statistical analysis was performed using the non-paired, two-tailed Student's test: *$p<0.05$. **c)** Mean cell density at selected stages (I, VIII, IX) of spermatogenesis in *Alkbh4*$^{\Delta/\Delta}$ mice indicates depletion of cells at pachynema and all subsequent stages. Dashed lines indicate cell types in tubular stages not counted (late leptonema to early pachynema, late pachynema to secondary spermatocyte S1).

Figure 4

Pachytene spermatocytes in *Alkbh4*$^{\Delta/\Delta}$ mice fail to maintain synaptonemal complex. Upper panels, immunofluorescence labeling of histological sections for SYCP3 (red) and DAPI (blue counterstain) allows distinguishing leptotene (L) spermatocytes, cells at leptonema-zygonema transition (L/Z), as well as pachytene (P) and diakinesis-stage (D) spermatocytes by the characteristic development of the synaptonemal complex (SC). Lower panels, among pachytene spermatocytes in *Alkbh4*$^{\Delta/\Delta}$ mice, cells with disordered SC can be observed (arrows). Scale bars, 10 µm.

Figure 5

Nuclear localization of ALKBH4 in seminiferous tubuli.

Upper panels, overview of the spermatogenic cycle in mouse testis with immunofluorescence labeling for ALKBH4 (green), γH2A.x (red) and DNA (DAPI, blue). Lower panels, ALKBH4 shows nucleolar localization in Sertoli cells. During the meiotic prophase, ALKBH4 is distributed in diffuse nuclear patches throughout preleptotene (Pl), leptotene (L), and zygotene (Z) stages, and disappears towards late pachynema (P). Scale bar, 10 µm.

a)


Alkbh4 L/L
Alkbh4 Δ/Δ
0-1 week
2 weeks

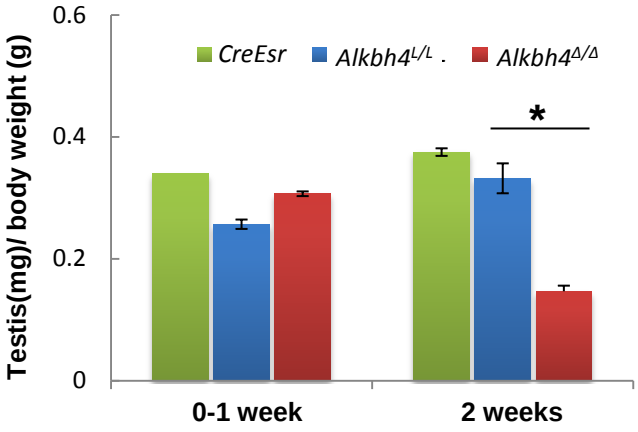
Testis(mg)/ body weight (g)
0.6
0.4
0.2
0
CreEsr
Alkbh4 L/L
Alkbh4 Δ/Δ
*
0-1 week
2 weeks

b)

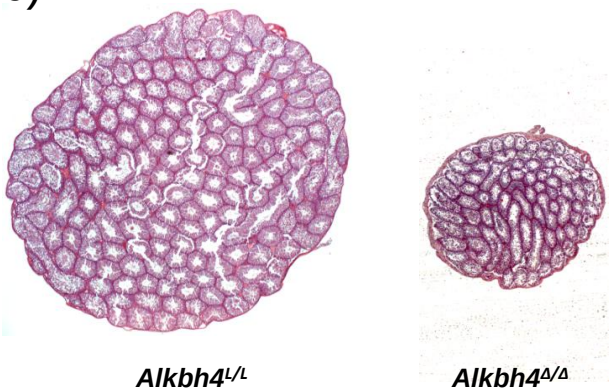
Alkbh4 L/L
Alkbh4 Δ/Δ

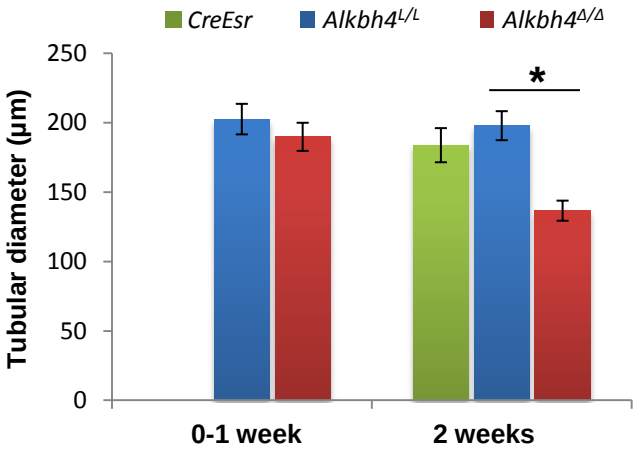
Tubular diameter (µm)
250
200
150
100
50
0
CreEsr
Alkbh4 L/L
Alkbh4 Δ/Δ
*
0-1 week
2 weeks

c)

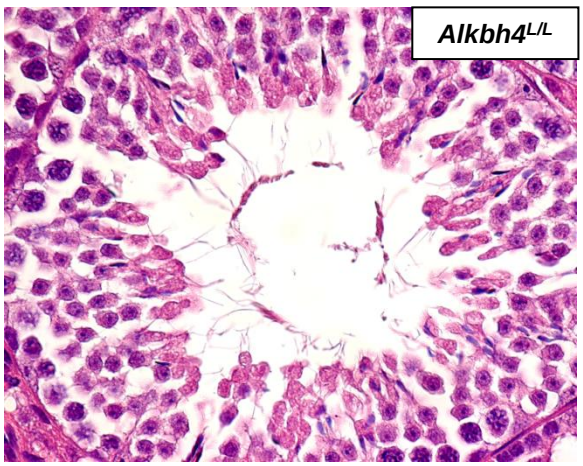
Alkbh4 L/L

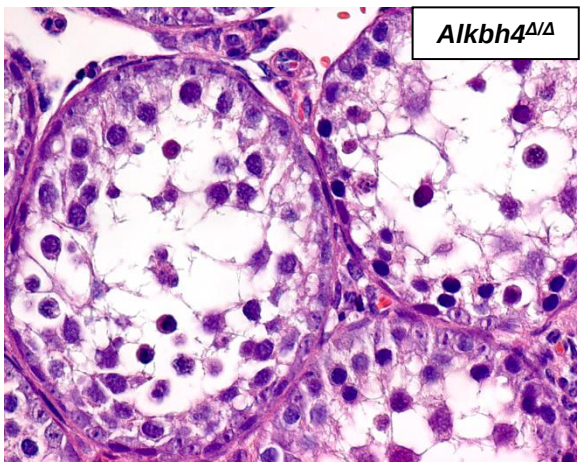
Alkbh4 Δ/Δ

a)

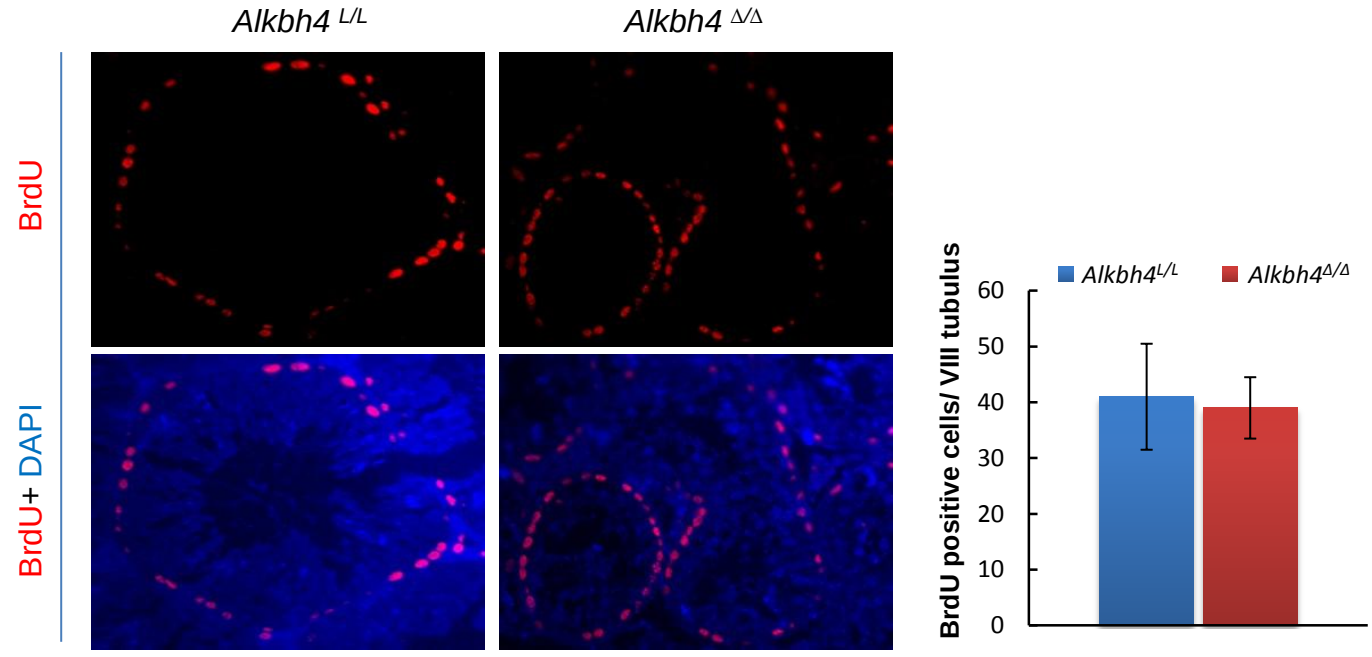
Alkbh4 L/L
Alkbh4 Δ/Δ
BrdU
BrdU+ DAPI
BrdU positive cells/ VIII tubulus
Alkbh4L/L
Alkbh4Δ/Δ
60
50
40
30
20
10
0

b)

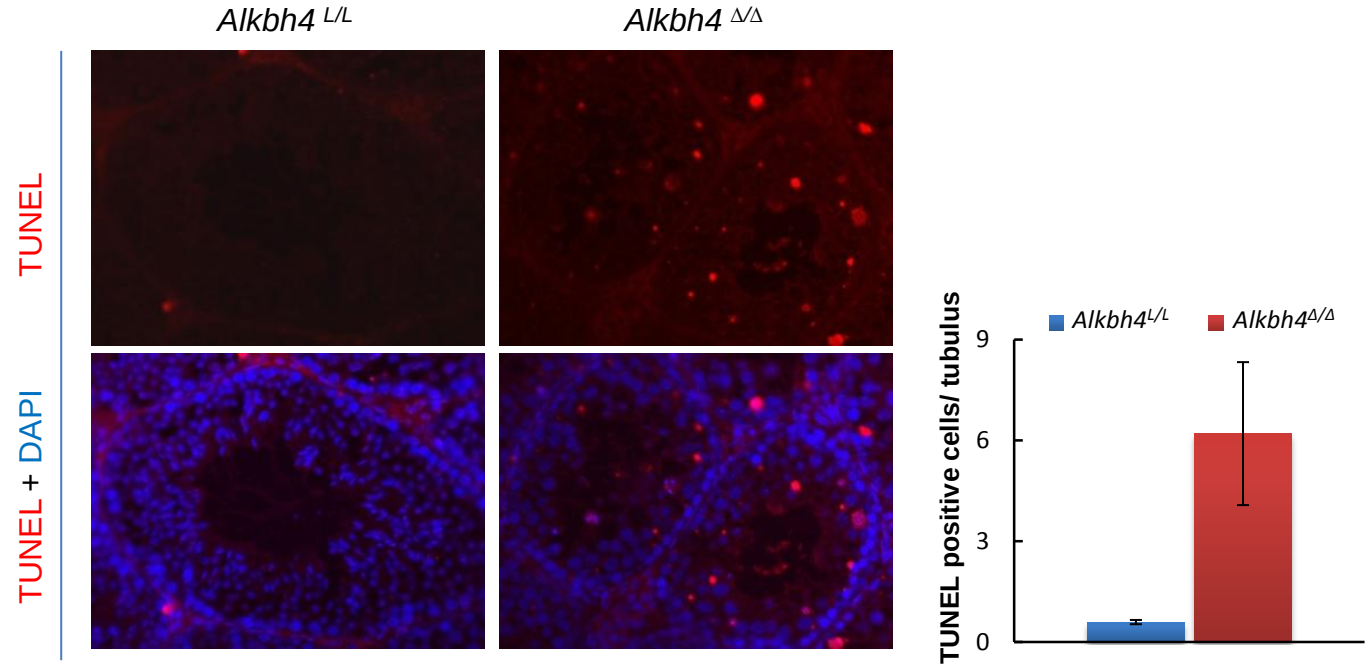
Alkbh4 L/L
Alkbh4 Δ/Δ
TUNEL
TUNEL + DAPI
TUNEL positive cells/ tubulus
Alkbh4L/L
Alkbh4Δ/Δ
9
6
3
0

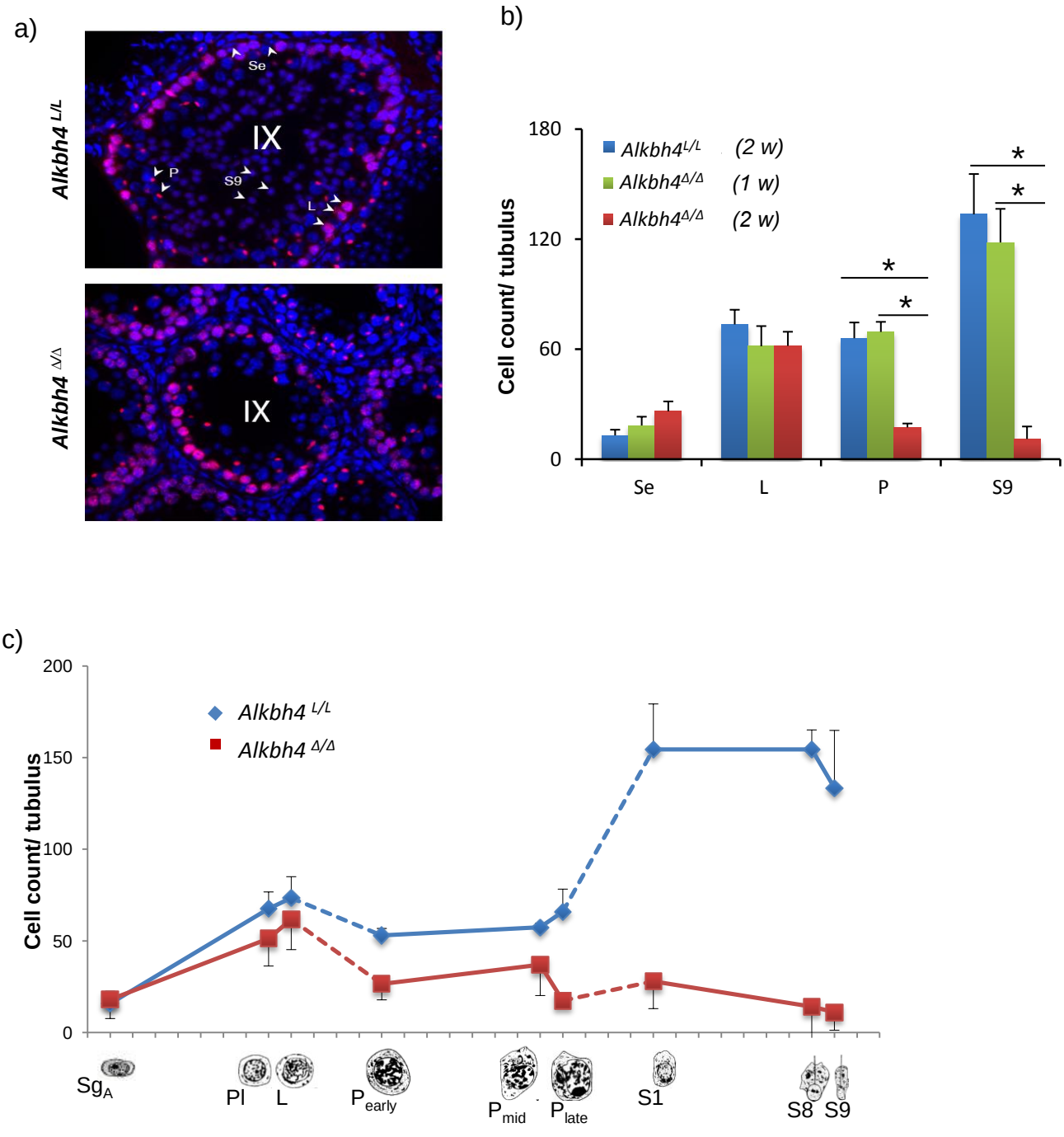
a)
Alkbh4 L/L
Alkbh4 Δ/Δ
Se
P
S9
L
IX
IX
b)
Alkbh4L/L (2 w)
Alkbh4Δ/Δ (1 w)
Alkbh4Δ/Δ (2 w)
Cell count/ tubulus
180
120
60
0
*
*
*
*
Se
L
P
S9
c)
Alkbh4 L/L
Alkbh4 Δ/Δ
Cell count/ tubulus
200
150
100
50
0
SgA
Pl
L
Pearly
Pmid
Plate
S1
S8
S9

Figure 4

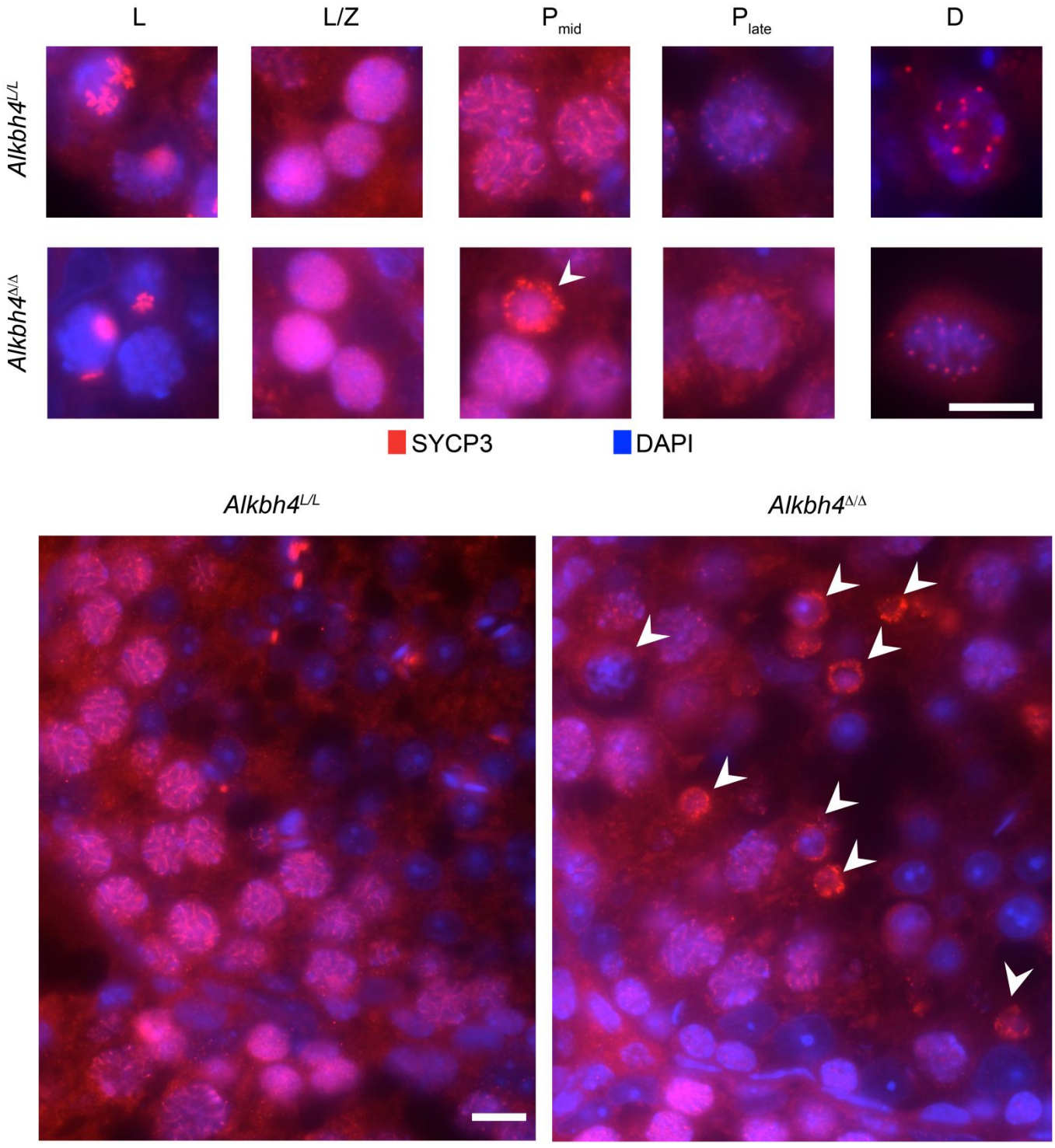
L
L/Z
P mid
P late
D
Alkbh4L/L
Alkbh4Δ/Δ
SYCP3
DAPI
Alkbh4L/L
Alkbh4Δ/Δ

Figure 5

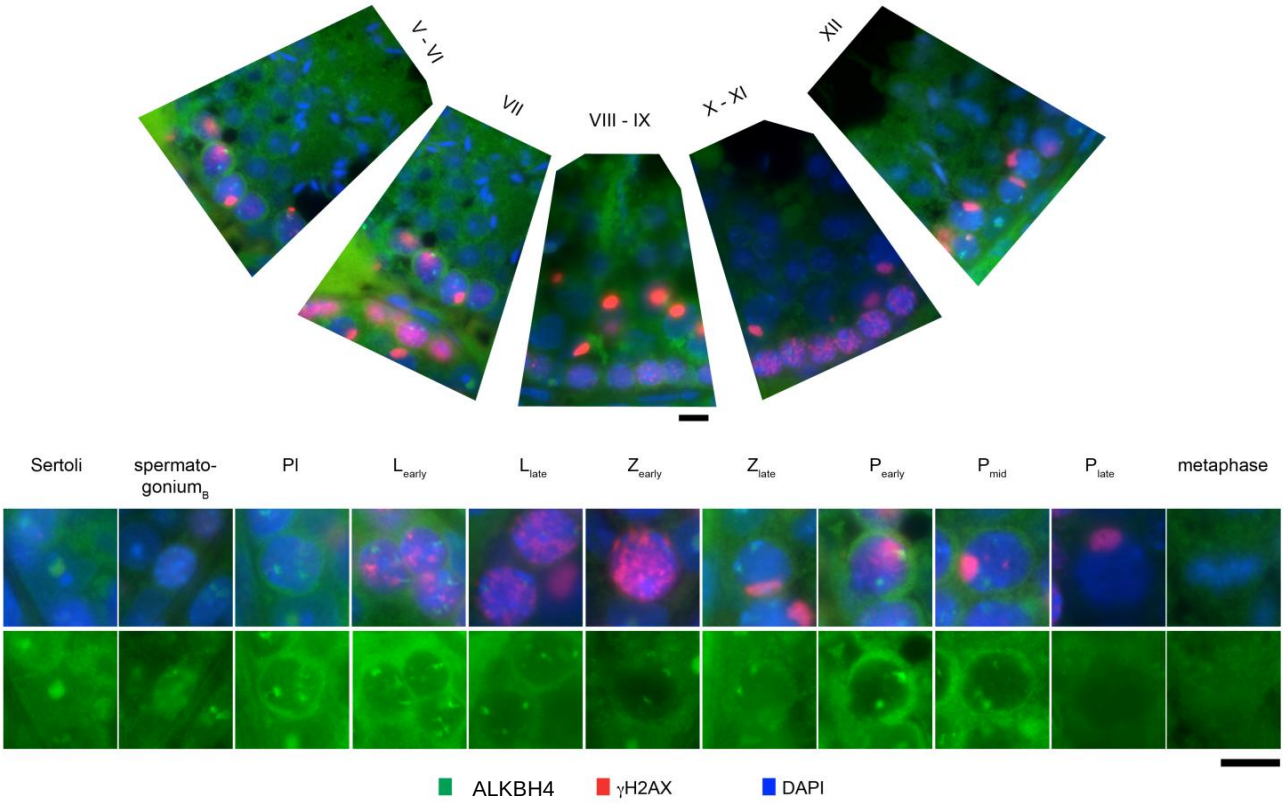
V - VI
VII
VIII - IX
X - XI
XII
Sertoli
spermato-gonium$_B$
PI
L$_{early}$
L$_{late}$
Z$_{early}$
Z$_{late}$
P$_{early}$
P$_{mid}$
P$_{late}$
metaphase
ALKBH4
γH2AX
DAPI

SUPPLEMENTARY FIGURE LEGENDS

Supplementary figure 1.
Outline of tamoxifen treatment and suppression of *Alkbh4* detected by PCR and Western blot.
a) Schematic outline of TAM treatment in of *Alkbh4$^{L/L}$ CreEsr* and control mice day 0 to 14 with indicated time-points for sampling.
b) Cre-mediated recombination of the LoxP-flanked DNA sequence in selected organs of *Alkbh4$^{\Delta/\Delta}$* mice after 2 weeks of tamoxifen treatment detected by PCR.
c) Depletion of ALKBH4 in whole-testis extracts of *Alkbh4$^{\Delta/\Delta}$* mice after 2 weeks of tamoxifen treatment detected by Western blot.

Supplementary figure 2.
Depletion of ALKBH4 does not alter weight gain and relative weight of spleen in mice.
a) *Alkbh4$^{\Delta/\Delta}$* mice have similar weight gain during tamoxifen treatment as control mice. Weight gain (gram) in 6 weeks old male and female mice shown after treatment with tamoxifen for two weeks (Male: *CreEsr,* n=5*; Alkbh4$^{L/L,}$* n=9*; Alkbh4$^{\Delta/\Delta}$* ,n=9. Female*: CreEsr,* n/a; *Alkbh4$^{L/L,}$* n=11; *Alkbh4 $^{\Delta/\Delta}$* ,n=12). Data are expressed as mean ± SD.
b) Weight of spleen relative to body weight is not affected by loss of ALKBH4. *(CreEsr,* 3; *Alkbh4$^{L/L,}$* n=4; *Alkbh4 $^{\Delta/\Delta}$* ,n=6). Data are expressed as mean ± SD.

Supplementary figure 3.
Reduced expression of ALKBH4 in *Alkbh4$^{\Delta/\Delta}$ mice.*
a) Immunohistochemical labelling of testis sections show lower levels of ALKBH4 in testis from *Alkbh4$^{\Delta/\Delta}$* mice treated with tamoxifen for 1 week. Left panels show sections of *Alkbh4$^{L/L}$* testes . Right panels show sections of *Alkbh4$^{\Delta/\Delta}$* testes.
b) Immunofluorescent staining of ALKBH4 in *Alkbh4$^{L/L}$* (left panel) and *Alkbh4$^{\Delta/\Delta}$* (right panel) testes from mice treated with tamoxifen for 2 weeks.

Supplementary figure 4.
Immunofluorescent labeling of Sertoli cell with anti-ALKBH4 (green) and anti-Fibrillarin (red) show nucleolar localization (arrow). DNA counterstained with DAPI.

a)

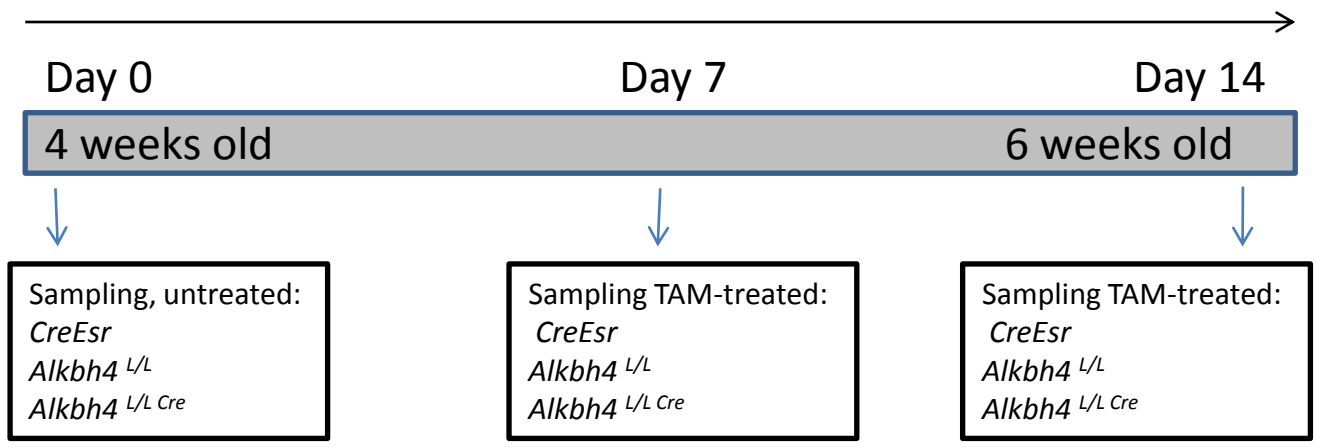
Day 0
Day 7
Day 14
4 weeks old
6 weeks old
Sampling, untreated:
CreEsr
Alkbh4 L/L
Alkbh4 L/L Cre
Sampling TAM-treated:
CreEsr
Alkbh4 L/L
Alkbh4 L/L Cre
Sampling TAM-treated:
CreEsr
Alkbh4 L/L
Alkbh4 L/L Cre

b)

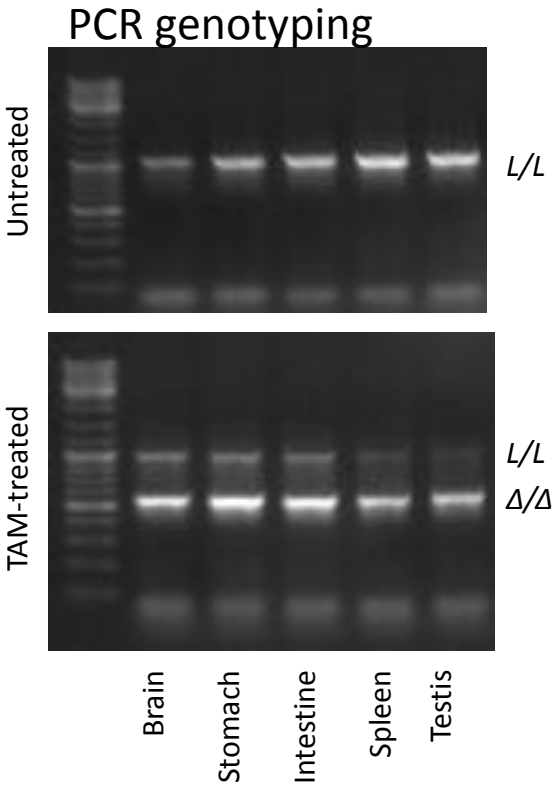
PCR genotyping
Untreated
L/L
TAM-treated
L/L
Δ/Δ
Brain
Stomach
Intestine
Spleen
Testis

c)

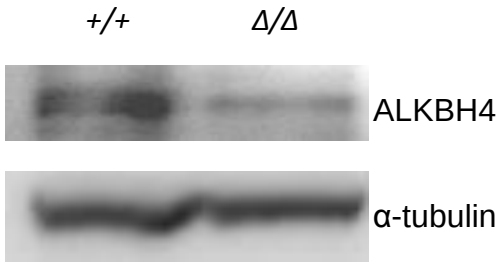
+/+
Δ/Δ
ALKBH4
α-tubulin

a)

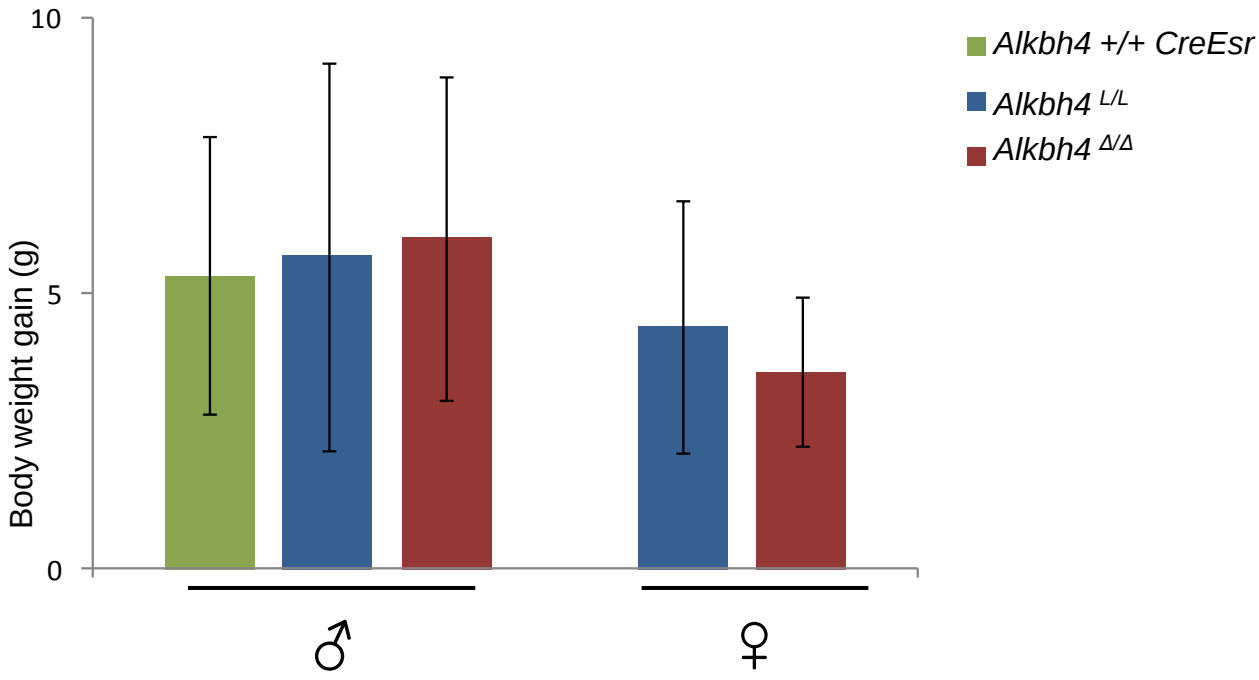
10
5
0
Body weight gain (g)
♂
♀
Alkbh4 +/+ CreEsr
Alkbh4 L/L
Alkbh4 Δ/Δ

b)

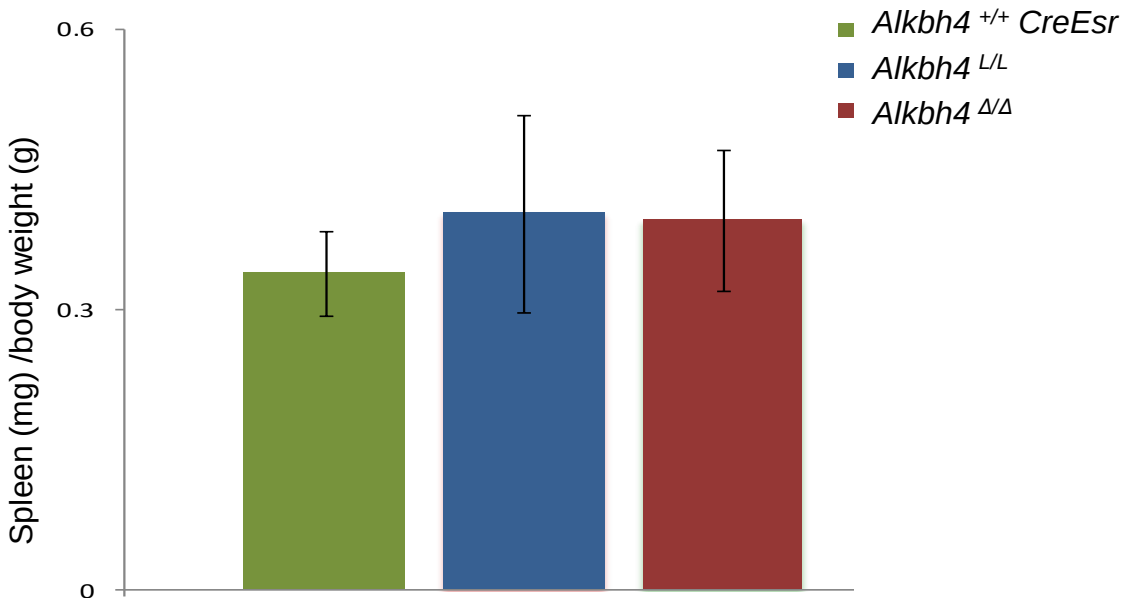
0.6
0.3
0
Spleen (mg) /body weight (g)
Alkbh4 +/+ CreEsr
Alkbh4 L/L
Alkbh4 Δ/Δ

a)

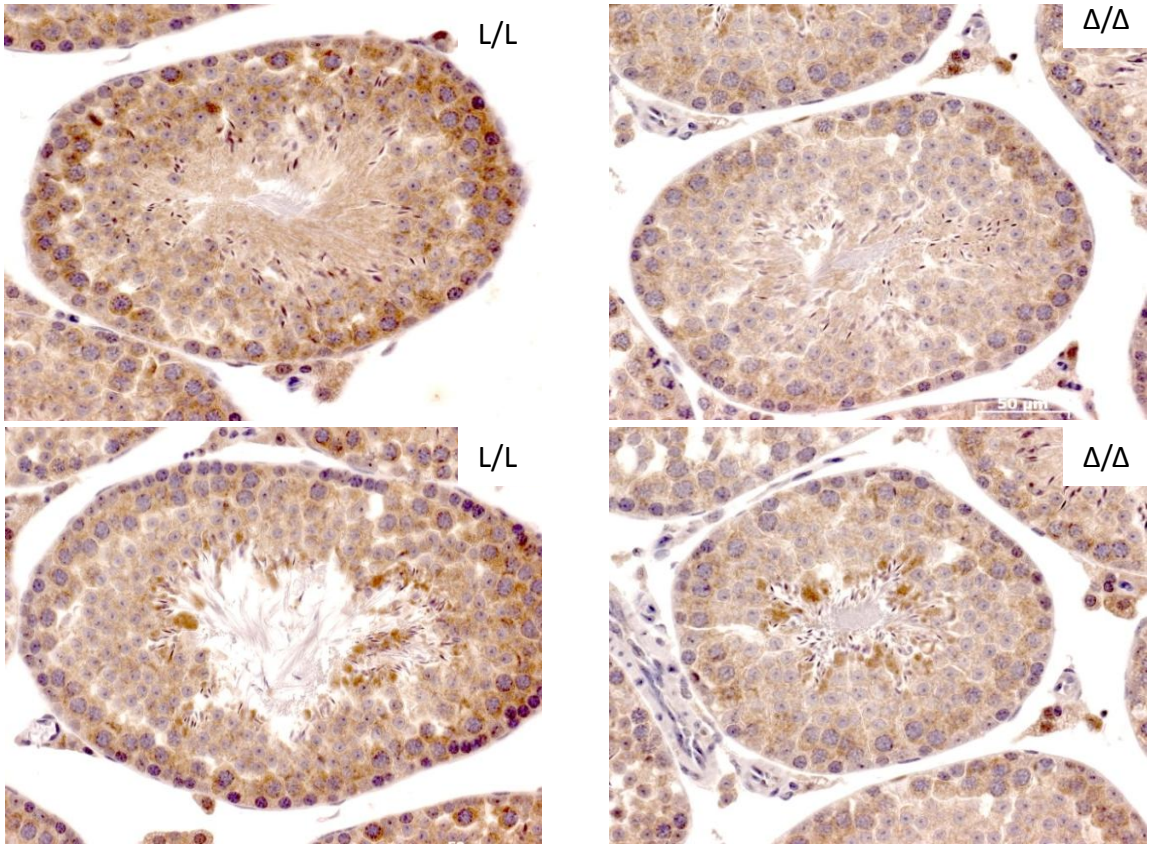

b)

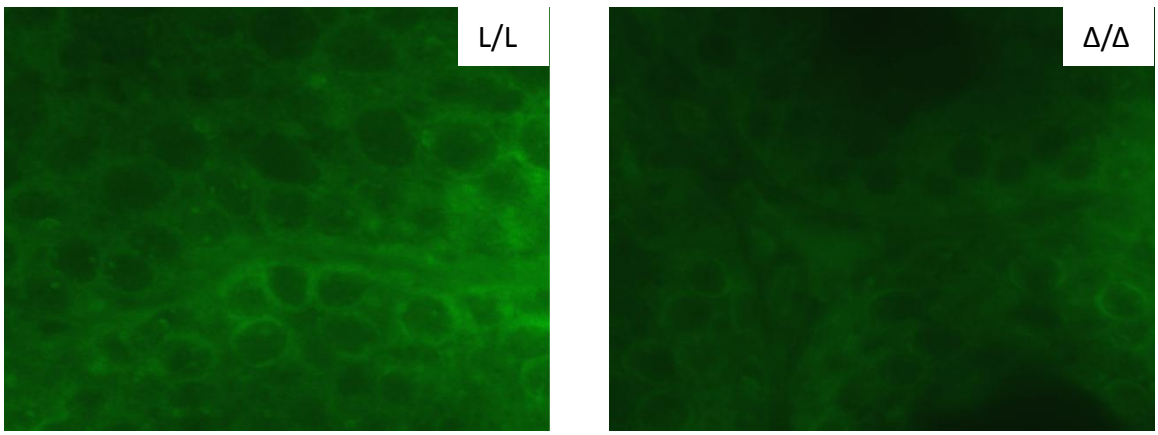

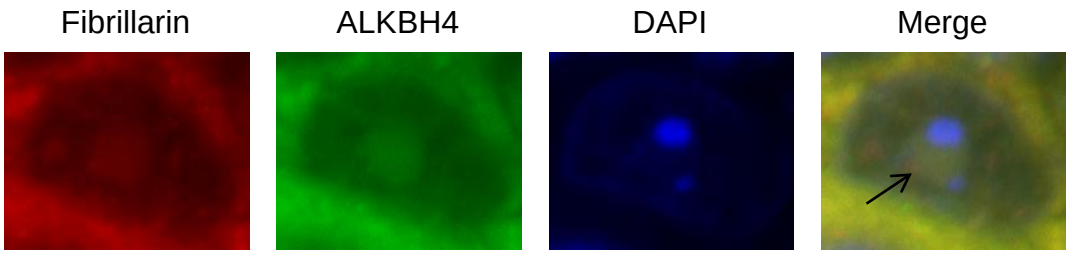
Fibrillarin
ALKBH4
DAPI
Merge

OPEN ACCESS Freely available online

PLoS one

Mice Lacking Alkbh1 Display Sex-Ratio Distortion and Unilateral Eye Defects

Line M. Nordstrand[1], Jessica Svärd[1☯], Elisabeth Larsen[1,2☯], Anja Nilsen[1☯], Rune Ougland[1,2☯], Kari Furu[1☯], Guro F. Lien[1], Torbjørn Rognes[1,3], Satoshi H. Namekawa[2], Jeannie T. Lee[2,5], Arne Klungland[1,4]*

1 Centre for Molecular Biology and Neuroscience, Institute of Medical Microbiology, Oslo University Hospital and University of Oslo, Oslo, Norway, **2** Department of Molecular Biology, Massachusetts General Hospital, Boston, Massachusetts, United States of America, **3** Department of Informatics, University of Oslo, Oslo, Norway, **4** Institute of Basic Medical Sciences, University of Oslo, Oslo, Norway, **5** Howard Hughes Medical Institute, Massachusetts General Hospital, Boston, Massachusetts, United States of America

Abstract

Background: *Eschericia coli* AlkB is a 2-oxoglutarate- and iron-dependent dioxygenase that reverses alkylated DNA damage by oxidative demethylation. Mouse AlkB homolog 1 (Alkbh1) is one of eight members of the newly discovered family of mammalian dioxygenases.

Methods and Findings: In the present study we show non-Mendelian inheritance of the *Alkbh1* targeted allele in mice. Both *Alkbh1*$^{-/-}$ and heterozygous *Alkbh1*$^{+/-}$ offspring are born at a greatly reduced frequency. Additionally, the sex-ratio is considerably skewed against female offspring, with one female born for every three to four males. Most mechanisms that cause segregation distortion, act in the male gametes and affect male fertility. The skewing of the sexes appears to be of paternal origin, and might be set in the pachythene stage of meiosis during spermatogenesis, in which *Alkbh1* is upregulated more than 10-fold. In testes, apoptotic spermatids were revealed in 5–10% of the tubules in *Alkbh1*$^{-/-}$ adults. The deficiency of *Alkbh1* also causes misexpression of *Bmp2*, *4* and *7* at E11.5 during embryonic development. This is consistent with the incompletely penetrant phenotypes observed, particularly recurrent unilateral eye defects and craniofacial malformations.

Conclusions: Genetic and phenotypic assessment suggests that Alkbh1 mediates gene regulation in spermatogenesis, and that Alkbh1 is essential for normal sex-ratio distribution and embryonic development in mice.

Citation: Nordstrand LM, Svärd J, Larsen E, Nilsen A, Ougland R, et al. (2010) Mice Lacking Alkbh1 Display Sex-Ratio Distortion and Unilateral Eye Defects. PLoS ONE 5(11): e13827. doi:10.1371/journal.pone.0013827

Editor: Joseph Najbauer, City of Hope National Medical Center, United States of America

Received May 10, 2010; **Accepted** October 14, 2010; **Published** November 3, 2010

Funding: This work was supported by the National Program in Functional Genomics (FUGE) sponsored by the Norwegian Research Council, the Norwegian Cancer Society and the European Union program 'DNA repair'. The funders had no role in study design, data collection and analysis, decision to publish, or preparation of the manuscript.

Competing Interests: The authors have declared that no competing interests exist.

* E-mail: arne.klungland@rr-research.no

☯ These authors contributed equally to this work.

Introduction

The *Eschericia coli* (*E. coli*) DNA repair enzyme AlkB demethylates e.g. 1-methyladenine (1-meA) to adenine – generating succinate and formaldehyde – in the presence of iron as cofactor and 2-oxoglutarate as cosubstrate [1,2]. To date, eight AlkB homologs have been identified in the mammalian genome [3]. Except for Alkbh5, all the remaining proteins have been identified throughout the animal kingdom, suggesting fundamental roles in biological processes [4]. Two of these homologs, ALKBH2 and ALKBH3 in humans (Alkbh2 and Alkbh3 in mice), are similar to *E. coli* AlkB in that they efficiently repair damaged nucleic acids in the presence of iron and 2-oxoglutarate *in vitro* [5–9]. In mice, Alkbh2 is the major, probably only, dioxygenase that repairs 1-meA DNA *in vivo* and mice lacking Alkbh2 accumulate 1-meA in the genome during ageing [10]. This year, two groups reported that Alkbh8 is a tRNA methyltransferase required for the final step in the biogenesis of mcm^{5}U [11,12]. ALKBH8 plays important roles in the survival and progression of human bladder cancer both *in vitro* and *in vivo* [13]. A likely ninth AlkB homolog, the obesity-associated Fto protein, was shown to have potential to demethylate 3-methylthymine (3-meT) [14,15]. Crystal structure of the FTO protein recently confirmed this, and indicated that single-stranded RNA is the primary substrate of FTO [16]. Similarly, recombinant truncated Alkbh1 enzyme may demethylate 3-methylcytosine *in vitro* [17], but it remains unclear whether this activity is physiologically relevant.

All eight mammalian AlkB homologs contain the conserved iron- and 2-oxoglutarate dioxygenase domain. However, the region of *E. coli* AlkB that interacts with the nucleic acid substrate, the N-terminal nucleotide recognition lid, does not share sequence similarity with the mammalian homologs. Therefore, one cannot exclude the possibility that the targets of such proteins are not nucleic acids, but other macromolecules such as proteins. Since JmjC histone demethylases remove methyl groups from histones using the same mechanism as *E. coli* AlkB, it has been suggested that Alkbh1, 4 and 7 might be involved in histone/protein demethylation [18,19]. However, for Alkbh1 we, and others, have been unable to identify DNA/histone demethylation activity

[6,7,20,21]. In 2008 a paper on Alkbh1 was published by Pan et al, where a gene-targeting study in mice showed that Alkbh1 localizes to nuclear euchromatin and functions in epigenetic regulation of gene expression [20]. Their study demonstrated impaired placental trophoblast lineage differentiation in *Alkbh1*$^{-/-}$ mice, and a strong interaction of Alkbh1 with Mrj, an essential placental gene that mediates gene repression by recruitment of class II histone deacetylases (HDAC) [20].

In the present study we attempt to elucidate the role of Alkbh1 by targeted deletion in C57/BL6 mice. We demonstrate that *Alkbh1* deficiency in mice results in apoptosis in adult testes and sex-ratio distortion of offspring, most likely caused by defects in the pachytene stage during spermatogenesis. An incompletely penetrant phenotype apparent during embryonic development is consistent with *Bmp2*, *4* and *7* misexpression. Although many mechanistic aspects of Alkbh1 function remain to be revealed, these results show that Alkbh1 is crucial for normal embryonic development and viability in mice, and plays an important role during spermatogenesis.

Materials and Methods

Generation of *Alkbh1* Targeted Mice

A specific 360-bp murine probe of exon 6 in the *Alkbh1* gene was amplified from mouse genomic DNA by polymerase chain reaction (PCR) and used to screen a 129 SvJ mouse genomic library (Stratagene). To generate the targeting construct, we subcloned fragments from a ~14-kb genomic clone on both sides of neomycin *(neo)* in the pGT-N38 vector (New England Biolabs). Homologous arms consisting of a 3.0-kb MfeI/HindIII fragment and a 3.7-kb BsrGI fragment facilitated removal of a 3.8-kb HindIII/BsrGI fragment including exon 6 and replacement with the *neo* cassette. The targeting construct was electroporated into 129 SvJ embryonic stem (ES) cells, and transfectants were selected in geneticin (G418) and expanded for further analysis. Chimaeric mice were produced by microinjection of one targeted ES cell clone with normal karyotype into C57/BL6 blastocysts at embryonic day 3.5 (E3.5). We verified germline transmission of the targeted allele by Southern-blot analysis of ScaI-digested genomic DNA on the 5′ end and PCR analysis on the 3′ end. 5′ and 3′ homologous recombination in the F_1 generation were confirmed by PCR analysis. Heterozygous males were backcrossed for three generations onto C57/BL6 females. All mouse experiments were approved by the Norwegian Animal Research Authority (Ref. nr. 08/9940) and done in accordance with institutional guidelines at the Centre for Comparative Medicine at Oslo University Hospital. Animal work was conducted in accordance with the rules and regulations of the Federation of European Laboratory Animal Science Association's (FELASA).

Genotyping

For *Alkbh1* genotyping, ear-clip samples were degraded by incubation in PBND buffer (50 mM KCl, 10 mM Tris-HCl pH 8.3, 2.5 mM $MgCl_2$-$6H_2O$, 0.1 mg/ml gelatin, 0.45% v/v NP40, 0.45% v/v Tween 20) and 0.5 mg/ml proteinase K at 55°C over night. Samples were heated to 95°C for 10 min to inactivate proteinase K, and PCR amplified for 35 cycles with an annealing temperature of 60°C (see primers below). For sex genotyping of embryos, a small piece of tissue was obtained from the embryosac or -tail and washed three times in PBS to eliminate maternal contamination. The tissue was degraded by a 3-hour incubation, and subsequently treated as above. PCR analysis of *Sry* (Y-linked gene) was performed to determine maleness and *Rapsn* was used as an autosomal, internal control as described (Mouse Phenotypes, a Handbook of Mutatation Analysis, Cold Spring Harbor laboratory press, Chapter 3, page 40, 2005).

Primers wild-type allele (WT): 5′-AGTTATCAGGGCCATC-CAGGGAGGT-3′

5′-AACTGAGAGGTACAGGGAAGCATAA-3′

Primers targeted allele (KO): 5′-GCTTGCCGAATATCAT-GGTG-3′

5′-AACTGAGAGGTACAGGGAAGCATAA-3′

Whole-Mount *In Situ* Hybridization

We carried out whole-mount *in situ* hybridization on E9.5 to E12.5 embryos fixed in paraformaldehyde as described (Henrique et al. 1995). Mouse antisense and sense (control) RNA probes were prepared using DIG RNA labeling mix (Roche) together with T3 or Sp6 and T7 RNA polymerases (Roche). Templates for the labeling reaction were PCR products amplified from full-length mouse cDNA with T3, Sp6 or T7 promoters added to the PCR primers. For *Alkbh1* the template contained 465-bp of exon 6, for *Bmp2* 519-bp of exon 2–3 and for *Bmp7* 559-bp of exon 2–5. For *Bmp4*, linearized pSP72 plasmid with a 1550-bp insert was used as template. Embryos were examined on a SMZ1500 microscope (Nikon).

Quantitative Real-Time PCR (qPCR) Analysis

Total RNA was isolated from embryos, organs and germ cells using the Fast RNA Pro Green Kit (MP Biomedicals) according to the manufacturers protocol. Any DNA remnants were removed using TURBO DNase (Ambion) and cDNA was made using High Capacity cDNA Reverse Transcription Kit (Applied Biosystems). The quantitative PCR reactions were carried out on a StepOnePlus or 7500 Fast instrument using 50 ng cDNA, TaqMan® Fast Universal PCR Master Mix and appropriate TaqMan primers and probes (all from Applied Biosystems). Pre-designed primers and probes were used both for the target genes (*Alkbh1, Vav2, Mapk8, Ccdc80, Rest, and Hif1a*) and endogenous controls (*Gapdh, 18s* and *β-actin*). All samples were run in triplicates and with one technical parallel (2 runs per sample). The relative quantity was calculated using the equation $RQ = 2^{-\Delta\Delta CT}$, where RQ is the relative quantity of the target gene. ΔΔCT is the difference in CT-value between the target gene and the endogenous control minus the difference in CT-values between the reference gene and the endogenous control.

STAPUT Isolation of Testicular Cells

Male germ cells were isolated from testes using an adapted version of the STAPUT method [22]. Pachytene cells and round spermatids were isolated from six 12-week old males, while a total of sixty 10-day old males were sacrificed for the isolation of type A and type B spermatogonia. The testes were put in ice cold DMEM medium containing antibiotics and then carefully detunicated. The tubules were treated with DNaseI, collagenase, trypsin and hyaluronidase (all from Sigma-Aldrich) at 34°C to remove connective tissue and somatic cells, yielding a cell suspension of germinal cells in DMEM containing 0.5% BSA. The cell suspension was loaded into the cell loading chamber of the STAPUT apparatus and separated by sedimentation velocity at unit gravity in a 2–4% w/v BSA gradient in DMEM medium at 4°C for 2.5 hours. After sedimentation, 10 ml fractions were collected and checked under the microscope. Fractions containing pure germ cells were pooled and the cell number counted in a *Countess*® Automated Cell Counter (Invitrogen). Cells were spun down and the pellet was snap frozen in liquid nitrogen before placed in −70°C. An aliquot of isolated cells was fixed on SuperFrost Plus slides (VWR) using Cell Adherence Solution (Crystalgen, Lot no 425081) for microscopic analysis of purity.

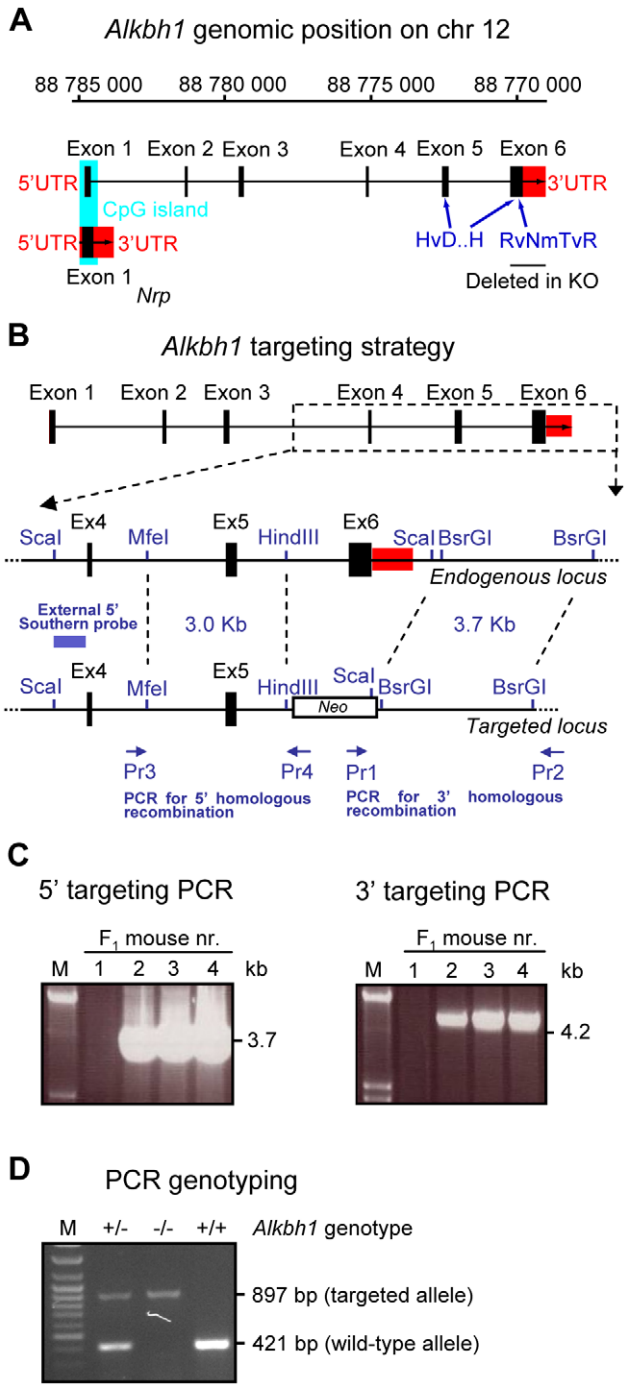

Figure 1. Targeted disruption of *Alkbh1* in embryonic stem cells and mice. (A) Schematic representation of the genomic region harboring the *Alkbh1* gene. Exon 6 is replaced by neomycin, thus maintaining the overlapping *Nrp* gene, and removing the conserved 2-oxoglutarate interaction domain (RvNmTvR) and parts of the iron-binding cluster (HvD…H) essential for enzymatic activity. A CpG island of 550 bp, shown in blue, is surrounding exon 1 (criteria used: Island size >200, GC Percent >50.0, Obs/Exp >0.6). The *Nrp* gene displays an overlap with exon 1 and is encoded as a forward frameshift to *Alkbh1* in the mouse. The 5′ and 3′ UTRs of *Alkbh1* and *Nrp* are shown in red. Coding exons are shown as black boxes. (B) Overview of the *Alkbh1* targeting strategy. Upper, schematic map of the genomic *Alkbh1* locus. Dashed lines point out the region used for homologous recombination. Middle, partial resctriction map of the endogenous *Alkbh1* locus participating in homologous recombination. Bottom, the targeted *Alkbh1* locus after correct integration of genomic fragments consisting of a 3.0-kb MfeI/HindIII fragment and a 3.7-kb BsrGI fragment on both sides of *Neo*, thereby replacing a 3.8-kb HindIII/BsrGI fragment including exon 6 with *Neo*. (C) PCR analysis for verification of 5′ and 3′ homologous recombination in the F_1 generation. The 3.7-kb 5′ targeted band (Pr3, Pr4) and the 4.2-kb 3′ targeted band (Pr1, Pr2) is present in F_1 mouse nr. 2, 3 and 4. M is the DNA marker. (D) PCR genotyping of the *Alkbh1* allele. The 421-bp wild-type band (WT) and the 897-bp targeted band (KO) is shown. M is the DNA marker.
doi:10.1371/journal.pone.0013827.g001

TUNEL Assay of Testes

We fixed testes from 3- and 9-month old animals in neutral-buffered formalin, progressively dehydrated them in a graded ethanol series, and embedded them in paraffin. Sections (4-µm) were deparaffinized and treated with proteinase K for 15 min and quenched in 3% hydrogen peroxide in PBS for 5 min at room temperature. Subsequently, nuclear staining in apoptotic cells was detected using ApopTag kit (Chemicon, http://www.chemicon.com) according to the manufacturers instruction. Sections were analysed on an Axioplan 2 microscope (Zeiss).

Immunofluorescent Staining of Testicular Cells

Testicular cells from 12-month old males were spread on SuperFrost Plus slides (VWR), progressively dehydrated in a graded ethanol series and dried completely. Slides were washed in 1× PBS and fixated in 4% PFA in PBS. Slides were blocked in 5% serum in PBS for 1 hour at room temperature and incubated with primary antibodies overnight at 4°C prior to detection with secondary antibodies. Primary antibodies used were rabbit anti-MacroH2A (1:500, Upstate) and mouse anti-FK2 (1:5000, Biomol). Secondary antibodies used were goat anti-rabbit Alexa Fluor 488 (green dye) (Invitrogen) and goat anti-mouse Alexa Fluor 594 (red dye) (Invitrogen), respectively. Single Z-sections were captured by Axioplan 2 microscope (Zeiss).

DNA Microarray Analysis

High quality of total RNA extracted from adult testes was verified on Agilent Bioanalyzer 2100 (RIN value between 9.8 and 10.0). 15 µg of biotinylated and fragmented cRNA was then hybridized onto the GeneChip Mouse Genome 430 2.0 Array (Affymetrix) according to manufacturers protocols (Affymetrix). QCs including scale factor, background, noise, spikes and RNA degradation were checked and validated using the yaqcaffy library (http://www.bioconductor.org/packages/2.3/%20bioc/vignettes/yaqcaffy/inst/doc/yaqcaffy.pdf).

Affymetrix raw data was generated with GCOS 1.4 (GeneChip Operating Software, Affymetrix), and the signal intensities of each probe set were normalized with the RMA (Robust Microarray Anlaysis) algorithm. To find differentially expressed genes, t-test with randomized variance was used as statistical test and the cut-off (p-value) was set to 0.05 with a FDR correction. Class comparison analysis was used to identify interesting genes. The signal in one group was always (i.e. for all the triplicate) higher or lower compared to the other group. Fold change for all the genes that passed the above criteria was computed and only the genes with ≥2-fold change were studied. The heatmap was generated using the GeneSpring GX 10 demoversion (Agilent). All data is MIAME compliant and the raw data has been deposited in a MIAME compliant database, the accession number is GSE22073.

Skeletal Staining

For skeletal analysis, skin and internal viscera of E18.5 embryos and newborn mice were removed. We then fixed the animals overnight in 95% ethanol and carried out Alcian blue 8GX

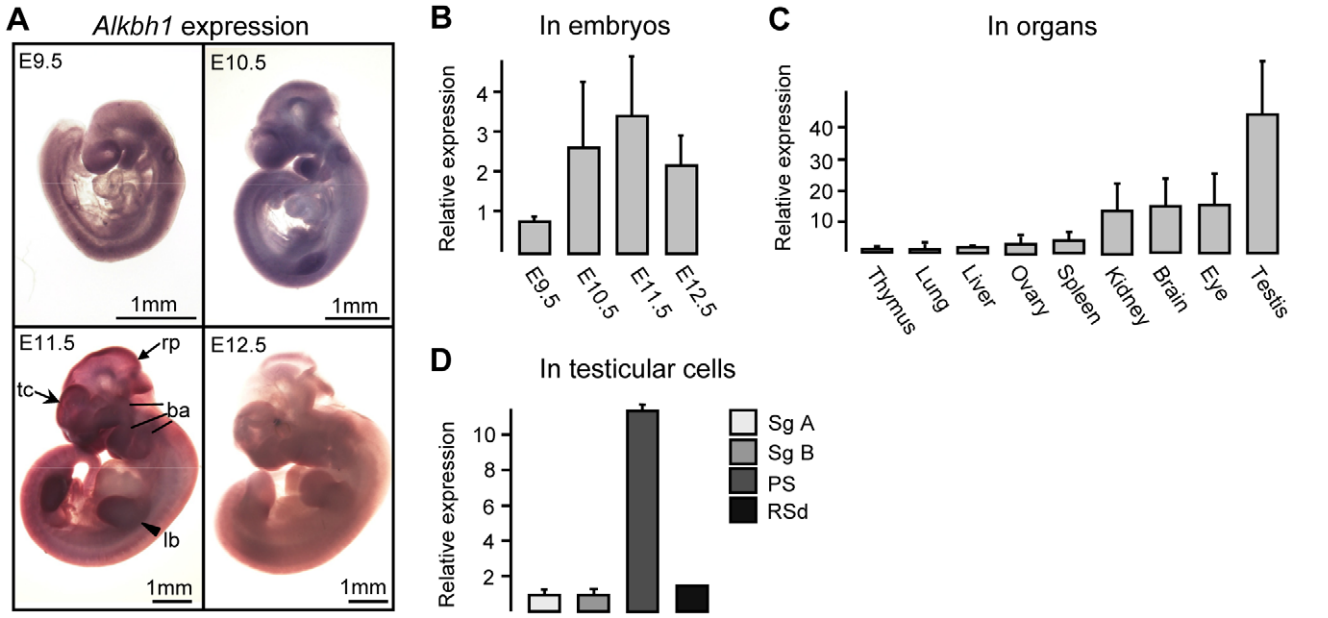

Figure 2. Expression of *Alkbh1* in embryos, organs and male germ cells. (A) Whole-mount *in situ* hybridization of *Alkbh1* between E9.5 and E12.5, side view. Peak expression is revealed at E11.5 in the telencephalon (tc) and frontonasal process, the maxillary and mandibular and hyoid arches (ba), the upper and lower limb buds (lb), and the midbrain and rhombomere 1 (r1) roof plates (rp). (B) Expression of *Alkbh1* between E9.5 and E12.5 by qPCR in RNA extracted from three - eight whole embryos. Peak expression at E11.5 is confirmed. Reference sample, E9.5 (RQ = 1.00); endogenous control, *Gapdh*. (C) Expression of *Alkbh1* in mouse organs by qPCR in RNA extracted from three - five 12-week old mice. Peak expression is shown in testis. Reference sample, thymus (RQ = 1.00); endogenous control, *18s*. (D) Expression of *Alkbh1* at different stages of spermatogenesis. Male germ cells from C57/BL6 mice were STAPUT sorted into type A spermatogonia (Sg A), type B spermatogonia (Sg B), pachytene spermatocytes (PS) and round spermatids (RSd), and analysed by qPCR after RNA extraction from the purified cell populations. Reference sample, type A spermatogonia (RQ = 1.00); endogenous control, *β-actin*.
doi:10.1371/journal.pone.0013827.g002

(Sigma) and Alizarin red S (Sigma) staining of cartilage and bone, respectively, as described (Manipulating the Mouse Embryo, 3rd edition, Cold Spring Harbor laboratory press, Chapter 16, Protocol 22, pages 699–700, 2003). The skeletons were photographed with a Nikon D80 camera.

Histological Analysis of Eyes

We fixed adult eyes in neutral-buffered formalin or paraformaldehyde added 20% absolute alcohol for 24 hours, progressively dehydrated them in a graded ethanol series, and embedded them in paraffin. Sections (4-µm) were deparaffinized, rehydrated and stained with hematoxylin and eosin. Sections were analysed on an AxioCam HRc microscope (Zeiss).

Results

Deletion of *Alkbh1* in Embryonic Stem Cells and Mice

To gain more insight into the role of the Alkbh1 dioxygenase we have generated mice lacking *Alkbh1*. Alkbh1 was the first mammalian AlkB homolog to be identified [23], and is the AlkB homolog most similar in sequence to *Eschericia coli (E. coli)* AlkB. The region of greatest similarity includes 107 amino acids, 37% of which are identical between the *E. coli* and mouse Alkbh1. The conserved RvNmTvR and HvD…H motifs of the 2-oxoglutarate and iron binding sites, respectively, are also present in both proteins. The conserved domains of Alkbh1 are encoded by exon 5 and 6 at the 3′ end of the mouse *Alkbh1* gene. To fully eliminate the activity of Alkbh1 and keep the overlapping *Nrp* gene intact, we substituted exon 6 with a neomycin-resistance gene cassette by homologous recombination in mouse embryonic stem cells (Figs. 1A–D). The expression of the *Nrp* gene was confirmed by qPCR (data not shown).

Expression Analysis of *Alkbh1* in Embryos, Organs and Male Germ Cells

The expression pattern of *Alkbh1* was analysed in embryos at different stages by whole-mount *in situ* hybridization (Fig. 2A) and by qPCR (Fig. 2B). Weak expression of *Alkbh1* was observed throughout the embryo at E8.5 (data not shown). As the cells migrate and differentiate during organogenesis the expression becomes more specific, and *Alkbh1* was detected in the spinal cord, forebrain and branchial arches at E9.5, and also in limb buds at E10.5 (Fig. 2A). Peak expression was detected at E11.5 in the frontonasal process including telencephalon (tc), maxillary, mandibular and hyoid arches (ba), upper and lower limb buds (lb), and midbrain and rhombomere 1 (r1) roof plates (rp) (Fig. 2A). *Alkbh1* expression decreased considerably from E11.5 to E12.5 (Fig. 2A–B). In adult organs, *Alkbh1* was highly expressed in testis (RQ = 44.0), with slightly lower expression in eye, brain and kidney (RQ = 16.0, 15.4, 14.4) (Fig. 2C). Moreover, the expression of *Alkbh1* was studied at different stages during spermatogenesis, and was found to be significantly elevated in the pachytene spermatocytes (PS) (RQ = 11.3) compared with spermatogonia A and B (Sg A, Sg B) and round spermatids (RSd) (RQ = 1.7) (Fig. 2D). This is the third stage of the prophase of meiosis I, in which synapsis is completed and homologous recombination occurs. Thus, Alkbh1 may have considerable potential for gene-function in embryonic development and in the pachytene stage during spermatogenesis.

Non-Mendelian Inheritance and Sex-Ratio Distortion in *Alkbh1* Targeted Mice

Mendelian inheritance, in which each parent contributes one of two possible alleles for a given trait, has a characteristic ratio of

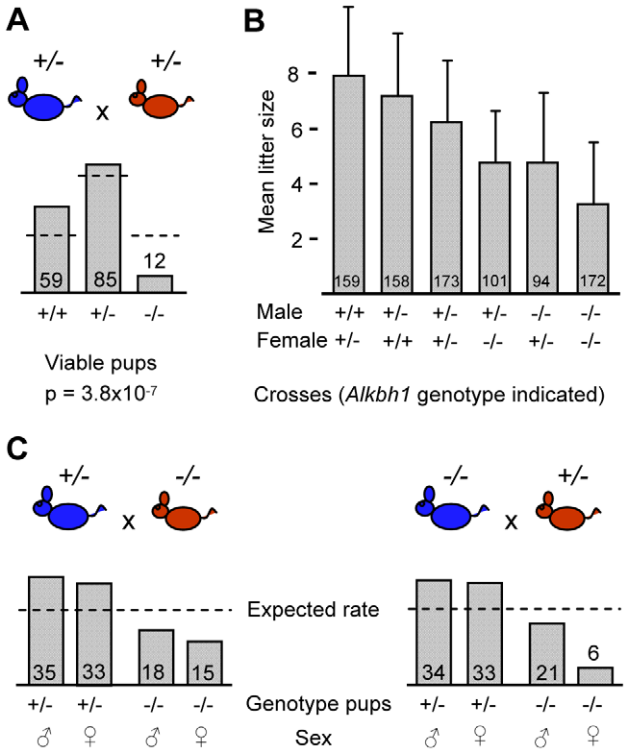

Figure 3. Non-Mendelian inheritance and sex-ratio distortion in *Alkbh1* targeted mice. (A) Offspring distribution of different genotypes at 1-month after crosses between heterozygous males (blue) and females (red) is shown (+ indicates wild-type *Alkbh1* allele and – indicates targeted *Alkbh1* allele). Mean number of pups per cross from 25 litters are represented. Dashed lines represent expected Mendelian distribution, and the χ^2-test was used to determine significance. (B) Average litter sizes from all crosses at 1-month of age are presented on the y-axis, while *Alkbh1* genotype of males and females used in the different crosses are indicated on the x-axis. The corresponding number of pups from more than 20 litters per cross are shown on the bars. (C) Left panel, crosses between heterozygous males (blue) and homozygous females (red). Right panel, crosses between homozygous males (blue) and heterozygous females (red). Offspring distribution of different *Alkbh1* genotypes at 1-month is shown. Mean number of pups per cross, calculated from 21 litters in the left panel and 20 litters in the right panel, are shown. Dashed lines represent expected sex-ratio distribution.
doi:10.1371/journal.pone.0013827.g003

1:2:1 after heterozygous crosses. Initial crosses of mice carrying either one or two targeted *Alkbh1* loci revealed non-Mendelian distribution. Therefore, we carried out extensive breeding analysis and genotyped more than 1400 *Alkbh1* mutant mice and embryos (Fig. 3). Following heterozygous breedings, the survival of $Alkbh1^{-/-}$ pups after 1 month was only 20% compared with wild-type littermates (Fig. 3A). In addition, the frequency of viable $Alkbh1^{+/-}$ mice was only 60% of the expected rate (Fig. 3A). The non-Mendelian distribution was clearly significant with a p-value of 3.8×10^{-7} (χ^2-test). A similar pattern was observed in $Alkbh1^{+/-}$ male x $Alkbh1^{-/-}$ female crosses, $p=5\times10^{-4}$ (χ^2-test) and $Alkbh1^{-/-}$ male x $Alkbh1^{+/-}$ female crosses, $p=3.7\times10^{-5}$ (χ^2-test) (Fig. 3C). In general, the average litter size decreased as the number of targeted alleles in the parental generation increased (Fig. 3B). The mean litter size was 9.2 for wild-type crosses, 6.2 for heterozygous crosses and 3.2 for homozygous crosses (Fig. 3B). Notably, paternal inheritance of the targeted allele seemed to be more critical than maternal transmission for the survival of offspring. Another evident phenotype was the growth retardation observed in viable $Alkbh1^{-/-}$ mice compared with wild-type littermates (Fig. S1).

One process of non-Mendelian inheritance is segregation distortion. There are a number of mechanisms that can cause segregation distortion, and both autosomal sex-ratio distortion as well as segregation distortion of the sex chromosomes exist [24]. In $Alkbh1^{+/-}$ male x $Alkbh1^{-/-}$ female crosses, the ratio of female to male homozygous offspring at 1 month was approximately 1:1 (Fig. 3C, left panel). In $Alkbh1^{-/-}$ male x $Alkbh1^{+/-}$ female crosses, the ratio of homozygous $Alkbh1^{-/-}$ pups was significantly skewed against females, with one female born for every three to four males (Fig. 3C, right panel). The survival of $Alkbh1^{-/-}$ male pups was 60% compared with $Alkbh1^{+/-}$ pups, whereas the proportion of viable $Alkbh1^{-/-}$ female pups was only 18%, $p=7.1\times10^{-5}$ (χ^2-test) (Fig. 3C, right panel). Following heterozygous crosses, the survival of $Alkbh1^{-/-}$ offspring was significantly reduced, 30% of the males and just 10% of the females survived compared with wild-type littermates, $p=1.4\times10^{-6}$ (χ^2-test) (data not shown). A sex-ratio distortion was also seen in mid-stage $Alkbh1^{-/-}$ embryos (E10–E12.5) after heterozygous breedings (17 litters), with 89% male and 60% female embryos present compared with wild-type embryos (data not shown).

Spermatogenic Defects in *Alkbh1* Deficient Testis

Reduced testis weight was observed in $Alkbh1^{-/-}$ males at 12-week and 12-month of age, constituting three-quarters and two-thirds the mean weight of testis from wild-type littermates, respectively (Fig. 4A). TUNEL staining of testes from 12-week old wild-type and $Alkbh1^{-/-}$ males were histologically indistinguishable and showed no apoptotic cells (data not shown). On the other hand, extensive apoptosis and reduced number of germ cells were revealed in 5–10% of the seminiferous tubules in 9-month old $Alkbh1^{-/-}$ males (Fig. 4B, Fig. S2). In $Alkbh1^{-/-}$ testes, no apoptosis was detected in the spermatogonia (Sg) located at the edges of the tubules and in the meiotic spermatocytes (Sc) residing mostly in the two to three subbasal layers (Fig. 4B, Fig. S2). However, numerous apoptotic and degraded cells were seen in the subbasal regions corresponding to spermatocytes and spermatids, as well as in degenerating round and elongating spermatids (Sd) in the more luminal layers of the tubules (Fig. 4B, Fig. S2). In wild-type, a few apoptotic cells were occasionally located mainly at the basal layer of the seminiferous tubules (Fig. 4B, Fig. S2). To better define the basis for arrest in germ cells and the sex-ratio distortion, we focused on the XY-body in the pachytene stage of meiosis. The XY-body is a condensed chromatin structure containing the sex chromosomes, which is thought to be essential for meiotic progression. In mid-pachynema the XY-body forms a spherical structure near the nuclear periphery [25]. Two different markers against XY-bodies were used, macroH2A and FK2, however visible sex-bodies were readily identified in pachytene spermatocytes from 12-month old wild-type and $Alkbh1^{-/-}$ testes (Fig. 4C). MacroH2A recognizes the sex chromatin, and FK2 detects the abundant ubiquitination of H2A in the XY-body. We also did antibody staining against several specific stages throughout spermatogenesis, but no significant differences between wild-type and $Alkbh1^{-/-}$ mice were revealed (Fig. S3). The fact that sex-body formation is not impaired in *Alkbh1*-null males does not exclude the hypothesis of an epigenetic and silencing defect of the paternal X chromosome in those mice. Another possibility is that the skewing of the sexes in $Alkbh1^{-/-}$ mice is related to autosomal sex-ratio distortion. It is well known that most mechanisms that affect segregation distortion act in the male gametes and affect male fertility [24].

Expression Profiling in Wild-Type and $Alkbh1^{-/-}$ Testis

Due to the pivotal role of Alkbh1 in mouse survival and potentially in germ cells, we searched for Alkbh1-regulated genes

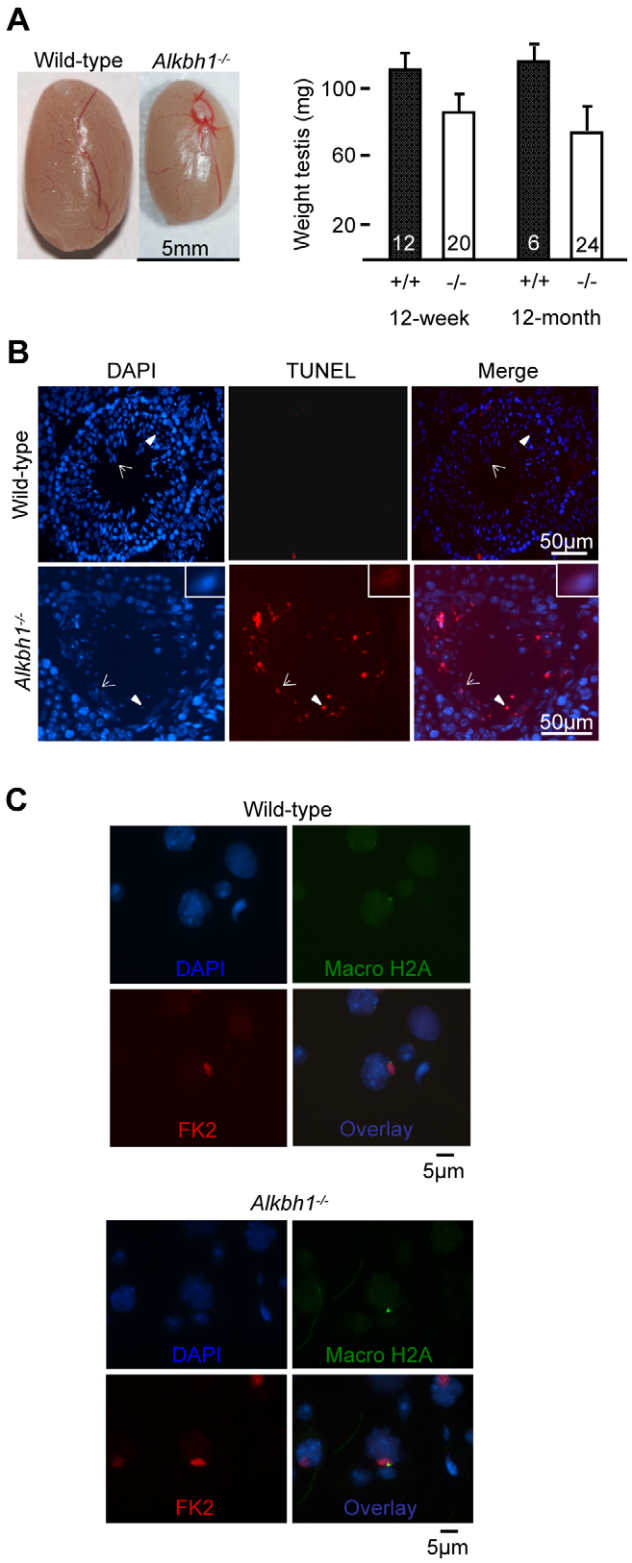

Figure 4. Spermatogenic defects in *Alkbh1* deficient testis. (A) Left panel, representative testis from 12-month old wild-type and *Alkbh1*$^{-/-}$ males. Right panel, average testis weight (mg) from 12-week old wild-type (110.6±10.4 mg, $n=12$) and *Alkbh1*$^{-/-}$ (85.6±8.4 mg, $n=20$) males, and 12-month old wild-type (114.4±8.9 mg, $n=6$) and *Alkbh1*$^{-/-}$ (74.3±12.1 mg, $n=24$) males. (B) TUNEL staining (middle panel) and DAPI staining (left panel) of testis sections from 9-month old wild-type and *Alkbh1*$^{-/-}$ mice, showing apoptosis in *Alkbh1*$^{-/-}$ round (arrowhead) and elongating (arrow) spermatids, and in degenerated germ cells in the subbasal layers of the tubules (middle and right panel). Closer view of one apoptotic elongating spermatid is shown in the lower panels. (C) Double immunostaining of XY-bodies in mid-pachytene cells. Testicular cells from 12-month old wild-type and *Alkbh1*$^{-/-}$ males were spread and stained with two different markers against XY-bodies. MacroH2A (green), FK2 (red) and DAPI (blue). (Magnifications: (B) ×20, (C) ×20).
doi:10.1371/journal.pone.0013827.g004

in adult testes. Microarray analysis of whole testes from 12-week old males identified 25 genes that were differentially expressed in *Alkbh1*$^{-/-}$ versus wild-type, using the class comparison strategy (Fig. 5A). *Ptpro* were also statistically significantly upregulated in *Alkbh1*$^{-/-}$ testes (Table S1; All data is deposited in GEO, accession number GSE22073). The function of PTPRO in adult testis has not been explored, but Avraham et al found expression of PTPRO in testis in humans [26]. Ptpro is suggested to be involved in the differentiation and axonogenesis of central and peripheral nervous system neurons, where it is in position to regulate phosphotyrosine levels in intracellular signaling cascades [27]. qPCR was performed on selected genes, to verify the class comparison analysis (Fig. 5B). Upregulation of *Vav2* and *Ccdc80* was confirmed in *Alkbh1*$^{-/-}$ versus wild-type whole testes. Vav2 is a guanine nucleotide exchange factor important for the formatin of adherens junctions between Sertoli cells and spermatids in testis, as well as in the formation of synapses in neurons [28]. The function of Ccdc80, also known as steroid sensitive gene 1, has not been studied in testis, but is supposed to be expressed in this organ according to its EST profile in the Unigene database (http://www.ncbi.nlm.nih.gov/UniGene/ESTProfileViewer.cgi?uglist = Mm.181074). Ccdc80 is expressed in human mesenchymal stem cells and mouse embryo cartilage, suggesting a role in skeletogenesis [29]. Together, these findings point towards a role in regulating the expression of genes having diverse functions – in spermatogenesis, in the nervous system and in skeletogenesis, although the genes affected in the microarray analysis are merely indirect targets of the Alkbh1 protein.

Alkbh1 Deficiency Causes Unilateral Eye Development

The reduced viability of *Alkbh1* deficient mice and the expression pattern of *Alkbh1* during embryonic development prompted us to analyse embryos and mice at earlier developmental stages. Both *Alkbh1*$^{+/-}$ and *Alkbh1*$^{-/-}$ mice showed embryonic (E) and postnatal (P) lethality, ranging from E9.5 to P28 (data not shown). Both embryos and neonatal mice clearly displayed an incompletely penetrant defect of small (microphthalmia) or missing (anophthalmia) eyes, and most often in the right eye (unilateral) (Fig. 6A, D). Eye malformations such as microphthalmia and anophthalmia occur in the mouse if eye morphogenesis is disrupted during the critical stages between E9.5 and E13.5 [30]. Small or missing eyes were observed in 18% of *Alkbh1*$^{-/-}$ embryos ($n=7/39$) and 9% of *Alkbh1*$^{+/-}$ embryos ($n=7/79$) at E11.5–E12.5. In surviving adults, eye defects were observed in 9% of *Alkbh1*$^{-/-}$ mice ($n=14/150$) and 0.5% of *Alkbh1*$^{+/-}$ mice ($n=1/198$). Eye defects varied from unilateral (one side) to bilateral (both sides) microphthalmia or anophthalmia, or unilateral microphthalmia in combination with unilateral anophthalmia (Fig. 6A, D). Intriguingly, the disturbed eye development affected the right eye more severely than the left eye, bearing resemblance to the histone arginine demethylase *Jmjd6* and the HMG box factor *Sox3* null phenotypes in mice [31–33].

To identify any abnormalities in addition to small or missing eyes, E18.5 embryos and newborn mice were analysed by skeletal

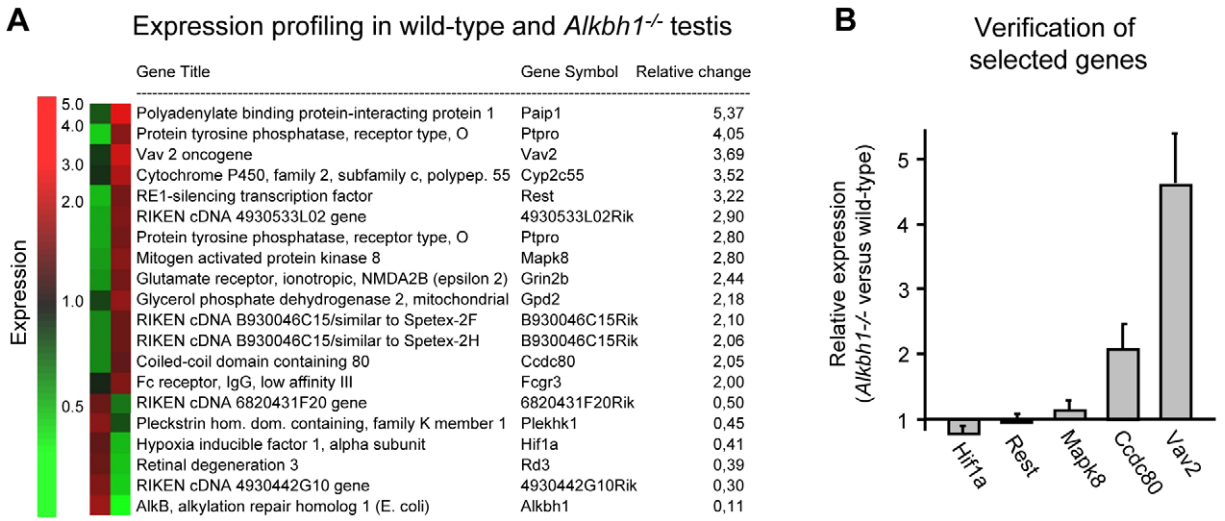

Figure 5. Expression profiling in wild-type and *Alkbh1*$^{-/-}$ adult testis. (A) Microarray analysis of whole testes from three wild-type and three *Alkbh1*$^{-/-}$ 12-week old males. Results are presented following class comparison analysis and visualized by GeneSpring v 6.0. (B) Verification of differentially expressed genes from the microarray analysis of wild-type and *Alkbh1*$^{-/-}$ testes. A selection of genes identified in the class comparison analysis (*Vav2*, *Mapk8*, *Ccdc80*, *Rest*, *Hif1a*) were checked for significance by qPCR. Upregulation of *Vav2* and *Ccdc80* were confirmed, while the differential expression of *Mapk8*, *Rest* and *Hif1a* were not found to be significant. On the RNA used for the microarray study. Reference sample, wild-type *Ccdc80* (RQ = 1.00); endogenous control, *18s*.
doi:10.1371/journal.pone.0013827.g005

staining of bone (Alizarin red) and cartilage (Alcian blue). Multiple defects were detected in the craniofacial, sternum and limb skeleton of mice lacking Alkbh1 (Figs. 6A–F). In the skull, reduced or missing intramembranous ossification resulted in enlarged sutures (Figs. 6B–C, F), while in the sternum, delayed ossification and aberrant fusion of the sternal bands were observed (Fig. 6E). Skeletal staining also showed assymetric shortening of the nasal bones, curving unilaterally in *Alkbh1*$^{-/-}$ mice causing mal-developed teeth (Fig. S4A), as well as reduced ossification in the phalanges (P) and the metatarsals (M) of the autopod of *Alkbh1*$^{-/-}$ newborns (Fig. S4B). The most crucial step in skeletal morphogenesis is the formation of mesenchymal condensations at E9.5 to E11.5 in mouse development [34]. The *Alkbh1* variable phenotype indicates incomplete condensation of mesenchymal cells during skeletogenesis.

Incomplete Penetrance of Unilateral Eye Defects

Penetrance is described as incomplete when a trait associated with a specific allele is expressed in a proportion of the population carrying the allele variant [35]. The eye phenotype associated with lack of the *Alkbh1* allele is characterized by incomplete penetrance (Fig. 7A–B). The *Alkbh1*$^{-/-}$ mouse in Fig. 7B has developed normally except for the deficiency of one eye. In contrast, the *Alkbh1*$^{-/-}$ embryo in Fig. 7A has gross developmental abnormalities, in addition to one small eye with only a residual mass of retinal cells, and one eye missing. The excessive brain tissue outside the skull is characteristic of a condition in which the neural tube fails to close, called exencephaly. Exencephaly is a neural tube defect (NTD), together with spina bifida (open spine) and anencephaly (open skull) [36]. At E10.5–E11.5, NTDs were observed in 23% of *Alkbh1*$^{+/-}$ embryos ($n = 12/52$) and 10% of *Alkbh1*$^{-/-}$ embryos ($n = 3/31$). The defects originated primarily from disrupted closure in the midbrain-hindbrain region (Fig. 7A) and upper spinal region, and were frequently associated with head and facial malformations (Fig. S4C). Around 50% of embryos with NTDs simultaneously displayed eye malformations ($n = 14/27$). The eye- and NTD-defects observed in *Alkbh1* mutants correspond with the expression pattern of *Alkbh1* seen in embryos and adult mice.

Gross morphological and histological analysis of adult *Alkbh1*$^{-/-}$ eyes revealed a range of serious deformities and size variations (Fig. 7C–D). Hematoxylin and eosin (HE) staining of paraffin-embedded sections showed that the lens was either completely missing or clearly smaller and displaced in the eye field (Fig. 7D). Furthermore, the lens fiber cells had lost their ordered lamination pattern, and swollen and liquefied fibers as well as vacuoles were seen throughout the lens (Fig. S4D). In retinal cells, there was a severe loss of organization even though all the retinal cells were present (Fig. 7D). In some areas, the neural retina (NR) was dysplastic with inclusions of rods and cones surrounded by outer nuclear layer cells (ONL), forming rosettes (Fig. 7E). In others, regions of thick layers of retinal pigment epithelium (RPE) cells were observed, with RPE cells appearing inside the NR layers in direct contact with the lens (Fig. 7E). Hence, Alkbh1 is important for growth and appropriate positioning and survival of lens and retinal cells.

Altered Expression of *Bmp*s in *Alkbh1* Deficient Embryos

Embryonic development and tissue regeneration are regulated by four major families of signaling molecules. One of the largest families is the bone morphogenetic proteins (Bmps) [37]. In skeletogenesis, Bmp signaling plays an important role in regulating chondrocyte differentiation and establishment of joint boundaries [38]. Current evidence indicates that Bmp2, Bmp4 and Bmp7 are the main source of Bmp signaling in vertebrate limb buds [39]. Similar signaling mechanisms are suggested for growth and regional specification of the forebrain, branchial arches and eye during development [40–42]. This prompted us to examine the expression of *Bmp2*, *Bmp4* and *Bmp7* in apparently normal *Alkbh1*$^{-/-}$ embryos at E11.5 (Fig. 8A). *Bmp2* and *Bmp7* were induced in the lateral telencephalon (tc) of *Alkbh1*$^{-/-}$ embryos, and expression of *Bmp2* also increased in the frontonasal process (Fig. 8A). Moreover, *Bmp4* and *Bmp7* became upregulated specifically in the maxillary and mandibular cleft, while *Bmp2* was upregulated throughout the maxillary, mandibular and hyoid

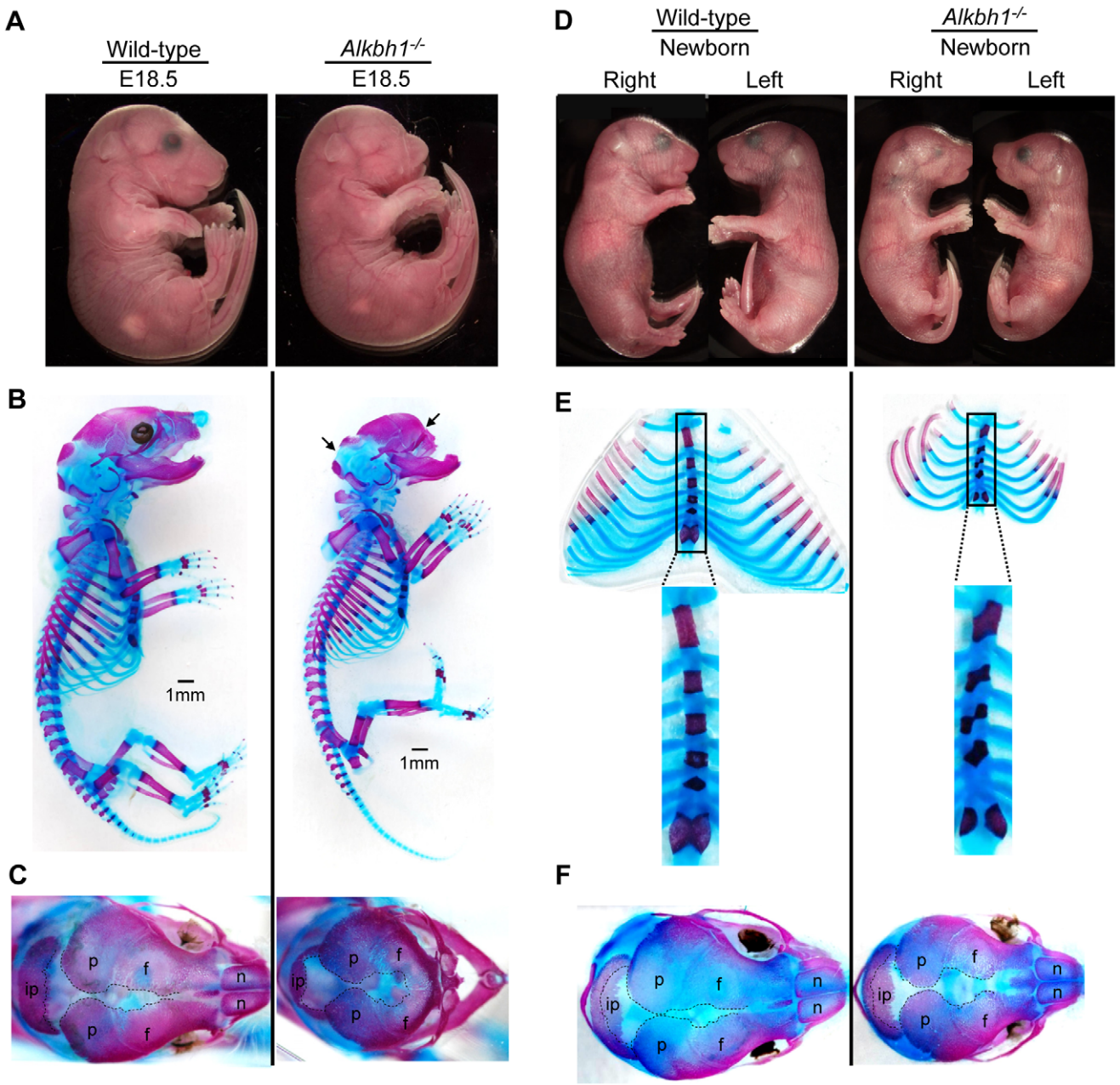

Figure 6. Eye and skeletal phenotype of *Alkbh1*$^{-/-}$ embryos and newborns, showing ossified areas in red and cartilage in blue. (A) Side view of embryos at E18.5. The *Alkbh1*$^{-/-}$ has a bilateral anophthalmic phenotype, a shortened snout and slightly reduced body size. (B) Skeletal staining of E18.5 embryos displaying missing nasal bones, shortened frontal bones and upward curving of the lower jaws in *Alkbh1*$^{-/-}$. (C) Dorsal view of the craniofacial skeleton of E18.5 embryos showing reduced ossification of the interparietal, parietal and frontal bones leading to bigger sutures in the skull of the *Alkbh1*$^{-/-}$. (D) Side view of newborn mice. The *Alkbh1*$^{-/-}$ has a unilateral microphthalmic eye phenotype and reduced body size. (E) Skeletal staining of the rib cage and sternum (in magnification) revealing delayed ossification and severe aberrant fusion of the sternal bands in *Alkbh1*$^{-/-}$ newborn mice. Interparietal, ip; parietal, p; frontal, f; nasal, n. (F) Dorsal view of the craniofacial skeleton of newborns demonstrating bigger sutures in the skull of *Alkbh1*$^{-/-}$.
doi:10.1371/journal.pone.0013827.g006

mesenchyme (Fig. 8A). In limb buds, *Bmp4* and *Bmp7* were highly upregulated in the apical ectodermal ridge (AER) and in two broader domains anteriorly and posteriorly (Fig. 8B). *Bmp2* expression disappeared from the posterior domain in hindlimb, and expression in AER of forelimb diffused proximally into the mesenchyme (lm) (Fig. 8B). The disrupted expression of *Bmp2*, *Bmp4* and *Bmp7* might be the cause of the somewhat smaller limb buds in *Alkbh1*$^{-/-}$ embryos. Regulation of these *Bmp* genes is important for AER formation, which is the major signaling center for limb outgrowth [37]. In general, both increased and decreased Bmp signaling can result in skeletal phenotypes [38].

Discussion

Our data point towards an important role of Alkbh1 in spermatogenesis and embryonic development. Several genes involved in spermatogenesis, in the nervous system and in skeletogenesis were found to be differentially expressed in

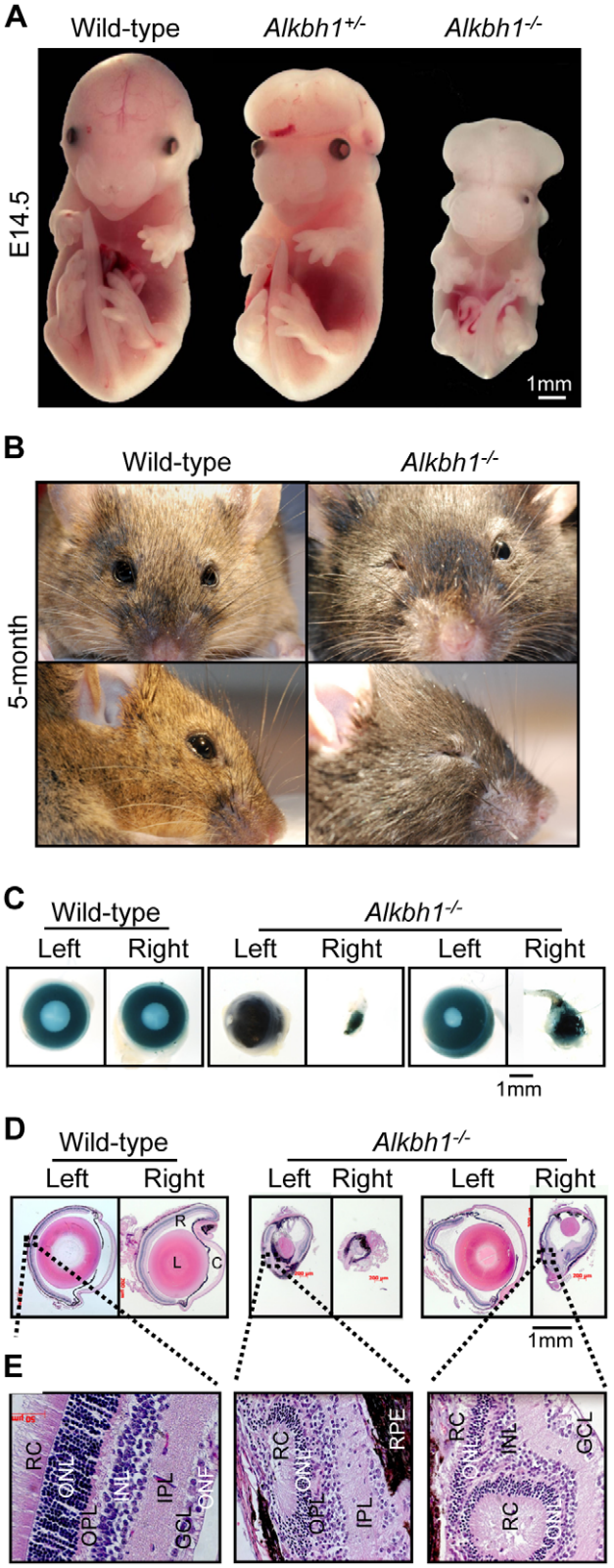

Figure 7. Incomplete penetrance of eye defects and exencephaly of *Alkbh1*$^{-/-}$ embryos and adults. (A) Frontal view of wild-type, *Alkbh1*$^{+/-}$, and *Alkbh1*$^{-/-}$ embryos at E14.5. The *Alkbh1*$^{+/-}$ and *Alkbh1*$^{-/-}$ embryos exhibit exencephaly in combination with a shortened, broad snout, while the *Alkbh1*$^{-/-}$ embryo also has a bilateral microphthalmic eye phenotype and severely reduced body size. (B) Frontal view and side view of wild-type and *Alkbh1*$^{-/-}$ adult mice. The *Alkbh1*$^{-/-}$ mouse has a unilateral microphthalmic eye malformation. (C) Whole-mount view of fixated eyes from wild-type and *Alkbh1*$^{-/-}$ adult mice demonstrating absent pupils and various degrees of eye malformations. (D) Histological analysis of paraffin-embedded eye sections. In *Alkbh1*$^{-/-}$ eyes, the lens is either missing or small and displaced in the eye field. Retinal cells appear degenerated or have lost their organized lamination pattern. R, retina; L, lens; C, cornea. (E) Closer view of the retina shown in d. Neural retinal cells are dysplastic with inclusions of rods and cones surrounded by outer nuclear layer cells. Retinal pigment epithelium cells are found inside the multi-layered neural retina. RC, rods and cones; ONL, outer nuclear layer; OPL, outer plexiform layer; INL, inner nuclear layer; IPL, inner plexiform layer; GCL, ganglion cell layer; ONF, optic nerve fibers. (Magnifications: (D) ×2,5, (E) ×40).
doi:10.1371/journal.pone.0013827.g007

Alkbh1$^{-/-}$ whole testes. Adult males deficient in *Alkbh1* exhibited dramatically increased levels of apoptosis in 5–10% of the seminiferous tubules of testes; in spermatids and in degenerated germ cells in the subbasal regions corresponding to spermatocytes and spermatids. The reduced number of all spermatogenic cells in the apoptotic tubules, might reflect an indirect effect of prolonged arrest in spermatids in the affected tubules. Similar nonspecific defects have been seen in *miwi*-null mice [43] and TRF2 mutants [44,45]. Most genes involved in spermatogenesis display pleiotropic and leaky mutant phenotypes, as presented in this paper. Targeted disruptions of genes resulting in a variable range of defects and incomplete penetrance of spermatogenesis is even the case for regulatory genes, such as those encoding RNA binding proteins DAZLA [46] and MVH [47], and cell cycle regulators HSP-70.2 [48,49] and cyclin A1 [50].

The sex-ratio distortion lead us to study the XY-bodies in pachytene spermatocytes from *Alkbh1*$^{-/-}$ testes, however visible XY-bodies were detected showing that X and Y chromosomes paired normally during male meiosis. This does not exclude the hypothesis of an epigenetic and silencing defect of the paternal X chromosome in those mice, which could explain the sex-ratio distortion observed. Moreover, embryonic and postnathal lethality seen in *Alkbh1*$^{-/-}$ mice seem to be of paternal origin and *Alkbh1*$^{-/-}$ males exhibit subfertility compared to wild-type males. Several characteristics of the *Alkbh1*$^{-/-}$ mice are comparable with those described for the *Jmjd1a* histone lysine demethylase and the *G9a* histone lysine methyltransferase mutant mice, although to a milder extent than demonstrated in the histone disrupted mouse models [51,52]. *Jmjd1a* deficiency caused extensive germ cell apoptosis and blocked spermatid elongation, resulting in small testes and infertility in male mice [51]. Inactivation of *G9a* in the germ-lineage resulted in sterility due to a drastic loss of mature gametes [52]. The specific upregulation of *Alkbh1* in the pachytene stage, together with the sex-ratio distortion, suggests a potential to regulate the expression of genes during meiosis in the germline. Future investigations will focus on the regulation of specific genes in pachytene spermatocytes isolated from *Alkbh1*$^{-/-}$ and wild-type testes.

Alkbh1 mutant mice displayed phenotypes of incomplete penetrance, including unilateral eye malformations, neural tube defects, and craniofacial and skeleton associated abnormalities. Around 10% of the *Alkbh1*$^{-/-}$ mice appeared relatively normal, whereas the most affected mice died early during embryogenesis. The phenotypes are similar to published results on the bone morphogenetic proteins (Bmps), such as haploinsufficiency of Bmp2 causing exencephaly comparable to Fig. 7A [53], and compound heterozygous mutants for Bmp2 and Bmp4 showing unilateral microphthalmia similar to Fig. 6–7 [54]. In addition, postnatal lethality and sex-ratio distortion against females have been shown in *Bmp4*$^{tm1/+}$ heterozygous at weaning [55]. Altogether, this led us to investigate the effect on Bmps, and the

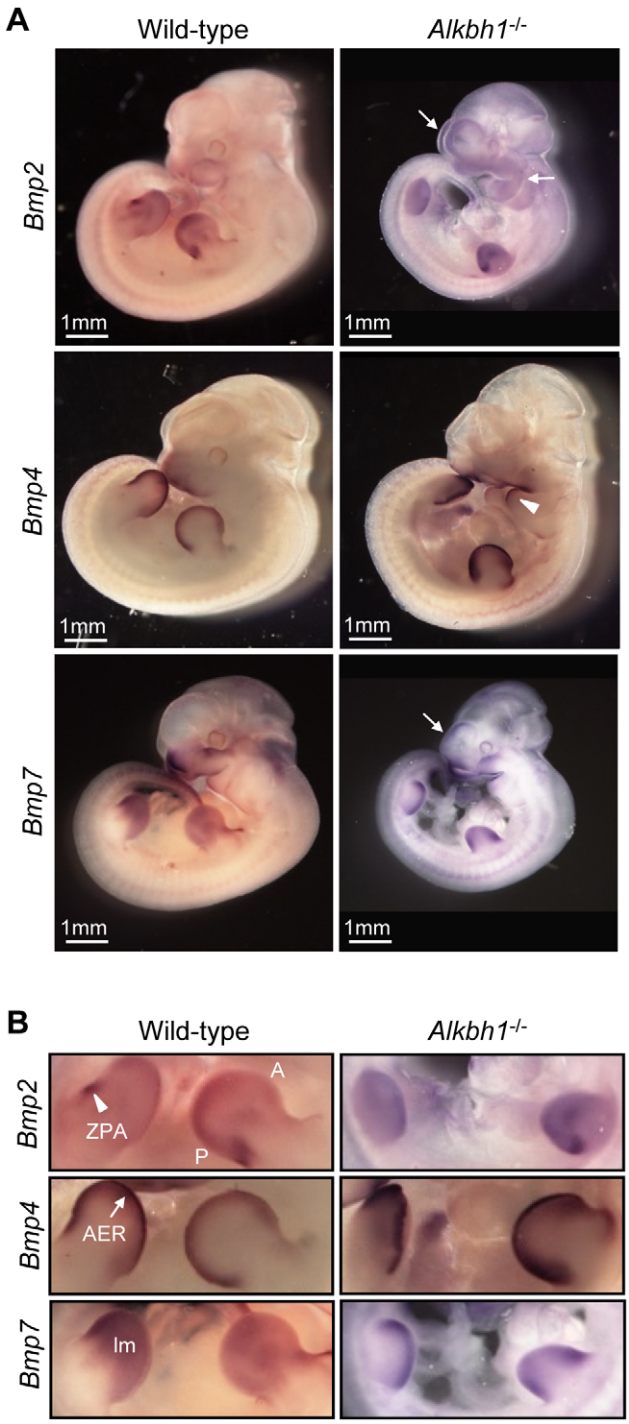

Figure 8. Misexpression of *Bmp2*, *Bmp4* and *Bmp7* in *Alkbh1* deleted embryos at E11.5. (A) Whole-mount *in situ* hybridization of *Bmp2*, *Bmp4* and *Bmp7* in *Alkbh1*$^{-/-}$ embryos at E11.5, side view. Altered expression is shown in the frontonasal process, the telencephalon (tc) and in the branchial arches (ba). (B) Closer view of the limbs from the whole-mount *in situ* hybridization of *Bmp2*, *Bmp4* and *Bmp7* in *Alkbh1*$^{-/-}$ embryos at E11.5, side view. The expression is altered in the zone of polarizing activity (ZPA), the apical ectodermal ridge (AER) and in the limb mesenchyme (lm). A, anterior; P, posterior.
doi:10.1371/journal.pone.0013827.g008

misexpression of *Bmp2*, *Bmp4* and *Bmp7* in *Alkbh1*$^{-/-}$ embryos at E11.5 might explain the inconsistent phenotypes presented. This is due to the critical dependence of gene dosage for proper Bmp function together with the expression- and function-overlap of the Bmps in different tissues [39,40]. Mouse models of Bmp4 and Bmp7 have shown that redundancy between Bmp4 and Bmp7 is not sufficient to prevent the eye phenotype to occur [40,41,56]. In the skull, signaling pathways involving Bmp2, Bmp4 and Bmp7 regulate mesenchymal condensation size, and intense expression of these signaling genes is necessary for closure of sutures [34]. In addition to modifier genes such as Bmps, genetic and epigenetic components can cause variable phenotypic outcomes from specific genes [57], leading to irregular patterns of inheritance as seen for the *Alkbh1* deficient mice. A recent paper has shown that the osteoblast-specific transcription factor Osterix is regulated by the JmjC histone demethylase NO66 [58]. Experiments in the chick embryo have revealed that epigenetic factors are required for the establishment of left-right asymmetries, together with the action of well-studied genetic and signaling mechanisms [59,60].

The reduced viability and developmental phenotypes apparent in our mouse model, was not reported in the *Alkbh1*-null mice generated by Pan et al [20]. However, they showed severe growth defects in *Alkbh1*$^{-/-}$ embryos and newborns in addition to placentas [20], and the growth retardation demonstrated in pups at four weeks of age are comparable with our data (Pan et al. Suppl. Fig. 2 and this paper Fig. S1). No obvious color variation (from red/pink to pale brown/bluish) or growth retardation was observed in *Alkbh1*$^{-/-}$ placentas compared to wild-type placentas. Our results are based on extensive breeding studies of *Alkbh1* targeted mice, which revealed a dramatic effect on lethality and sex-ratio in adult mice. We therefore sought to characterize testes and embryos in more detail, as well as the prominent abnormalities in eye development. The different mouse background chosen as well as the dissimilar targeting strategies deleting different parts of the *Alkbh1* gene (Exon 6 in our strain, Exon 3 in Pan et al) could be a possible explanation for the discrepancies in the penetrance of phenotypes in the two knockout mice models. Even so, together with the findings on Alkbh1 by Pan et al, these data suggest that the effect of *Alkbh1* deficiency is pleiotropic and dependent on cell type and/or stage of development.

Recent studies have recognized roles for 2-oxoglutarate dependent dioxygenases in histone and nucleic acid demethylation, as well as in signaling protein hydroxylation [19]. For the demethylating enzymes, several have been shown to carry out its reaction in a manner similar to the potential Alkbh1 mediated, iron- and 2-oxoglutarate dependent, hydroxylation [1,2,61]. Previously, mouse models for histone methyl transferases and histone demethylases have been characterized with multiple developmental defects [31–33,62]. Our working hypothesis, based on the variable developmental phenotype of *Alkbh1* deficient mice together with the localization of Alkbh1 to nuclear euchromatin [20], is that Alkbh1 possibly works as a histone demethylase during embryogenesis and spermatogenesis. We believe that the hydroxylation activity of Alkbh1 is dependent on yet undefined partners specific for the different stages/tissues where it has an important role, and this will be addressed in future studies for the pachytene stage of meiosis in male germ cells – when homologues chromosomes pair and crossing over can occur.

Supporting Information

Figure S1 Average body weight of *Alkbh1* targeted males and females. (A) 1-month old wild-type (19.0±2.0 g, $n = 45$) and *Alkbh1*$^{-/-}$ (14.6±3.8 g, $n = 48$) males, and 1-month old wild-type (17.7±1.7 g, $n = 43$) and *Alkbh1*$^{-/-}$ (14.8±2.2 g, $n = 33$) females. The average weight was 25% lower for *Alkbh1*$^{-/-}$ males than for wild-type males and 15% lower for *Alkbh1*$^{-/-}$ females than for wild-

type females. About one out of five *Alkbh1*$^{-/-}$ males showed more than 40% lower weight compared to wild-type males. (B) 9-month old wild-type (40.5±4.2 g, $n = 23$) and *Alkbh1*$^{-/-}$ (32.5±2.9 g, $n = 31$) males, and 9-month old wild-type (31.5±3.4 g, $n = 28$) and *Alkbh1*$^{-/-}$ (29.3±3.8 g, $n = 41$) females. The average weight of *Alkbh1*$^{-/-}$ males was 20% below that of wild-type males, and the average weight of *Alkbh1*$^{-/-}$ females was 7% below that of wild-type females. No weight difference was demonstrated between the *Alkbh1*$^{+/-}$ and wild-type (data not shown). +/+ (wild-type), black bars; −/− (*Alkbh1*$^{-/-}$), grey bars.
Found at: doi:10.1371/journal.pone.0013827.s001 (0.10 MB TIF)

Figure S2 Closer view of the DAPI and TUNEL staining of testis sections shown in Fig. 4. (A, B) Sections from 9-month old wild-type (left panel) and *Alkbh1*$^{-/-}$ (right panel) mice are presented. Apoptosis was detected in degenerating spermatids (Sd) in the luminal layers of *Alkbh1*$^{-/-}$ tubules, as well as in severely degraded cells in the subbasal regions corresponding to spermatocytes and spermatids. No apoptotic cells were seen in spermatogonia (Sg) and spermatocytes (Sc) in *Alkbh1*$^{-/-}$ mice, although the amount of all spermatogenic cells are reduced in the apoptotic tubules. (Magnification: ×20).
Found at: doi:10.1371/journal.pone.0013827.s002 (3.93 MB TIF)

Figure S3 Immunostaining with stage-specific antibodies against spermatogenic cells in *Alkbh1* deficient testes. (A) Testis sections from 12-month old wild-type and *Alkbh1*$^{-/-}$ males stained with TRA98 antibody specific for spermatogonia, which were present both in wild-type and mutant. Although several tubules showed spermatogonia not only in the first basal layer, but also in the subbasal layers in the *Alkbh1*$^{-/-}$ mice, no significant differences were detected when compared to wild-type. (B) Testis sections from 12-month old wild-type and *Alkbh1*$^{-/-}$ males stained with TRA369 specific for pachytene spermatocytes through elongating spermatids, which were present both in wild-type and mutant. (Magnification: ×20).
Found at: doi:10.1371/journal.pone.0013827.s003 (1.84 MB TIF)

Figure S4 Skeletal defects, eye defects in combination with NTD, and lens defects in *Alkbh1* targeted mice. (A) Craniofacial defects. Dorsal view of the craniofacial skeleton of adult mice showing assymetric shortening of the nasal bones, curving unilaterally in *Alkbh1*$^{-/-}$ mice causing mal-developed teeth ($n = 4$ *Alkbh1*$^{-/-}$; $n = 1$ *Alkbh1*$^{+/-}$). Ossified areas are shown in red and cartilage in blue. (B) Limb defects. Dorsal view of the autopod limb skeleton revealing reduced ossification in the phalanges (P) and the metatarsals (M) of the autopod of *Alkbh1*$^{-/-}$ newborns ($n = 4/4$ *Alkbh1*$^{-/-}$). Ossified areas are shown in black and cartilage in blue. (C) Eye defects and NTDs. Side view of embryos at E12.5. The *Alkbh1*$^{-/-}$ embryo has a bilateral microphthalmic eye phenotype in combination with a neural tube defect (NTD). The NTD is originating from disrupted closure in the upper spinal region, and is associated with head and facial malformations leading to a shortened, broad snout. In addition, a severe intracranial hemorrhage is visible. (D) Lens defects. Histological analysis of paraffin-embedded eye sections from adult mice. In *Alkbh1*$^{-/-}$ eyes the lens fiber cells have lost their ordered lamination pattern, and swollen and liquefied fibers as well as vacuoles are seen throughout the lens. (Magnification: ×10).
Found at: doi:10.1371/journal.pone.0013827.s004 (6.28 MB TIF)

Table S1 Statistically upregulated genes in *Alkbh1*$^{-/-}$ versus wild-type testes identified in the microarray analysis. Microarray analysis of RNA extracted from whole testes from three wild-type and three *Alkbh1*$^{-/-}$ 12-week old males identified 6 genes that were statistically upregulated in *Alkbh1*$^{-/-}$ versus wild-type. To find differentially expressed genes, t-test with randomized variance was used as statistical test and the cut-off (p-value) was set to 0.05 with a FDR correction.
Found at: doi:10.1371/journal.pone.0013827.s005 (0.22 MB TIF)

Acknowledgments

We are grateful to Hege Wiksèn, Cecilie G. Castellanos, Linda Ellevog and Gaute Nesse for excellent technical assistance. We thank IngenKO, Australia, The Norwegian Transgenic Center (NTS) and the Centre for Comparative Medicine at Oslo University Hospital for the excellent service they provided.

Author Contributions

Conceived and designed the experiments: LMN JTL AK. Performed the experiments: LMN JS EL AN RO KF GFL. Analyzed the data: LMN JS EL AN RO KF TR SHN JTL AK. Wrote the paper: LMN AK.

References

1. Trewick SC, Henshaw TF, Hausinger RP, Lindahl T, Sedgwick B (2002) Oxidative demethylation by Escherichia coli AlkB directly reverts DNA base damage. Nature 419: 174–178.
2. Falnes PO, Johansen RF, Seeberg E (2002) AlkB-mediated oxidative demethylation reverses DNA damage in Escherichia coli. Nature 419: 178–182.
3. Kurowski MA, Bhagwat AS, Papaj G, Bujnicki JM (2003) Phylogenomic identification of five new human homologs of the DNA repair enzyme AlkB. BMC Genomics 4: 48.
4. Falnes PO, Klungland A, Alseth I (2007) Repair of methyl lesions in DNA and RNA by oxidative demethylation. Neuroscience 145: 1222–1232.
5. Lee DH, Jin SG, Cai S, Chen Y, Pfeifer GP, et al. (2005) Repair of methylation damage in DNA and RNA by mammalian AlkB homologues. J Biol Chem 280: 39448–39459.
6. Duncan T, Trewick SC, Koivisto P, Bates PA, Lindahl T, et al. (2002) Reversal of DNA alkylation damage by two human dioxygenases. Proc Natl Acad Sci U S A 99: 16660–16665.
7. Aas PA, Otterlei M, Falnes PO, Vagbo CB, Skorpen F, et al. (2003) Human and bacterial oxidative demethylases repair alkylation damage in both RNA and DNA. Nature 421: 859–863.
8. Sedgwick B (2004) Repairing DNA-methylation damage. Nat Rev Mol Cell Biol 5: 148–157.
9. Monsen VT, Sundheim O, Aas PA, Westbye MP, Sousa MM, et al. (2010) Divergent {beta}-hairpins determine double-strand versus single-strand substrate recognition of human AlkB-homologues 2 and 3. Nucleic Acids Res, gkq518 [pii];10.1093/nar/gkq518 [doi].
10. Ringvoll J, Nordstrand LM, Vagbo CB, Talstad V, Reite K, et al. (2006) Repair deficient mice reveal mABH2 as the primary oxidative demethylase for repairing 1meA and 3meC lesions in DNA. EMBO J 25: 2189–2198.
11. Fu D, Brophy JA, Chan CT, Atmore KA, Begley U, et al. (2010) Human AlkB homolog ABH8 Is a tRNA methyltransferase required for wobble uridine modification and DNA damage survival. Mol Cell Biol 30: 2449–2459.
12. Songe-Moller L, van den BE, Leihne V, Vagbo CB, Kristoffersen T, et al. (2010) Mammalian ALKBH8 possesses tRNA methyltransferase activity required for the biogenesis of multiple wobble uridine modifications implicated in translational decoding. Mol Cell Biol 30: 1814–1827.
13. Shimada K, Nakamura M, Anai S, De VM, Tanaka M, et al. (2009) A novel human AlkB homologue, ALKBH8, contributes to human bladder cancer progression. Cancer Res 69: 3157–3164. 0008-5472.CAN-08-3530 [pii];10.1158/0008-5472.CAN-08-3530 [doi].
14. Gerken T, Girard CA, Tung YC, Webby CJ, Saudek V, et al. (2007) The obesity-associated FTO gene encodes a 2-oxoglutarate-dependent nucleic acid demethylase. Science 318: 1469–1472.
15. Boissel S, Reish O, Proulx K, Kawagoe-Takaki H, Sedgwick B, et al. (2009) Loss-of-function mutation in the dioxygenase-encoding FTO gene causes severe growth retardation and multiple malformations. Am J Hum Genet 85: 106–111. S0002-9297(09)00238-9 [pii];10.1016/j.ajhg.2009.06.002 [doi].
16. Han Z, Niu T, Chang J, Lei X, Zhao M, et al. (2010) Crystal structure of the FTO protein reveals basis for its substrate specificity. Nature 464: 1205–1209. nature08921 [pii];10.1038/nature08921 [doi].
17. Westbye MP, Feyzi E, Aas PA, Vagbo CB, Talstad VA, et al. (2008) Human AlkB homolog 1 is a mitochondrial protein that demethylates 3-methylcytosine in DNA and RNA. J Biol Chem 283: 25046–25056.
18. Sedgwick B, Robins P, Lindahl T (2006) Direct removal of alkylation damage from DNA by AlkB and related DNA dioxygenases. Methods Enzymol 408: 108–120.
19. Loenarz C, Schofield CJ (2008) Expanding chemical biology of 2-oxoglutarate oxygenases. Nat Chem Biol 4: 152–156.

20. Pan Z, Sikandar S, Witherspoon M, Dizon D, Nguyen T, et al. (2008) Impaired placental trophoblast lineage differentiation in Alkbh1(−/−) mice. Dev Dyn 237: 316–327.
21. Tsujikawa K, Koike K, Kitae K, Shinkawa A, Arima H, et al. (2007) Expression and sub-cellular localization of human ABH family molecules. J Cell Mol Med 11: 1105–1116.
22. Bellve AR (1993) Purification, culture, and fractionation of spermatogenic cells. Methods Enzymol 225: 84–113.
23. Kataoka H, Yamamoto Y, Sekiguchi M (1983) A new gene (alkB) of Escherichia coli that controls sensitivity to methyl methane sulfonate. J Bacteriol 153: 1301–1307.
24. Taylor DR, Ingvarsson PK (2003) Common features of segregation distortion in plants and animals. Genetica 117: 27–35.
25. Solari AJ (1974) The behavior of the XY pair in mammals. Int Rev Cytol 38: 273–317.
26. Avraham S, London R, Tulloch GA, Ellis M, Fu Y, et al. (1997) Characterization and chromosomal localization of PTPRO, a novel receptor protein tyrosine phosphatase, expressed in hematopoietic stem cells. Gene 204: 5–16.
27. Beltran PJ, Bixby JL, Masters BA (2003) Expression of PTPRO during mouse development suggests involvement in axonogenesis and differentiation of NT-3 and NGF-dependent neurons. J Comp Neurol 456: 384–395.
28. Kawakatsu T, Ogita H, Fukuhara T, Fukuyama T, Minami Y, et al. (2005) Vav2 as a Rac-GDP/GTP exchange factor responsible for the nectin-induced, c-Src- and Cdc42-mediated activation of Rac. J Biol Chem 280: 4940–4947.
29. Liu Y, Monticone M, Tonachini L, Mastrogiacomo M, Marigo V, et al. (2004) URB expression in human bone marrow stromal cells and during mouse development. Biochem Biophys Res Commun 322: 497–507.
30. Graw J (2003) The genetic and molecular basis of congenital eye defects. Nat Rev Genet 4: 876–888.
31. Rizzoti K, Lovell-Badge R (2007) SOX3 activity during pharyngeal segmentation is required for craniofacial morphogenesis. Development 134: 3437–3448.
32. Chang B, Chen Y, Zhao Y, Bruick RK (2007) JMJD6 is a histone arginine demethylase. Science 318: 444–447.
33. Bose J, Gruber AD, Helming L, Schiebe S, Wegener I, et al. (2004) The phosphatidylserine receptor has essential functions during embryogenesis but not in apoptotic cell removal. J Biol 3: 15.
34. Hall BK, Miyake T (2000) All for one and one for all: condensations and the initiation of skeletal development. Bioessays 22: 138–147.
35. Glazier AM, Nadeau JH, Aitman TJ (2002) Finding genes that underlie complex traits. Science 298: 2345–2349.
36. Copp AJ, Greene ND, Murdoch JN (2003) The genetic basis of mammalian neurulation. Nat Rev Genet 4: 784–793.
37. Robert B (2007) Bone morphogenetic protein signaling in limb outgrowth and patterning. Dev Growth Differ 49: 455–468.
38. Baldridge D, Shchelochkov O, Kelley B, Lee B (2010) Signaling pathways in human skeletal dysplasias. Annu Rev Genomics Hum Genet 11: 189–217. 10.1146/annurev-genom-082908-150158 [doi].
39. Bandyopadhyay A, Tsuji K, Cox K, Harfe BD, Rosen V, et al. (2006) Genetic analysis of the roles of BMP2, BMP4, and BMP7 in limb patterning and skeletogenesis. PLoS Genet 2: e216.
40. Ducy P, Karsenty G (2000) The family of bone morphogenetic proteins. Kidney Int 57: 2207–2214.
41. Ohkubo Y, Chiang C, Rubenstein JL (2002) Coordinate regulation and synergistic actions of BMP4, SHH and FGF8 in the rostral prosencephalon regulate morphogenesis of the telencephalic and optic vesicles. Neuroscience 111: 1–17.
42. Wordinger RJ, Clark AF (2007) Bone morphogenetic proteins and their receptors in the eye. Exp Biol Med (Maywood) 232: 979–992. 232/8/979 [pii];10.3181/0510-MR-345 [doi].
43. Deng W, Lin H (2002) miwi, a murine homolog of piwi, encodes a cytoplasmic protein essential for spermatogenesis. Dev Cell 2: 819–830.
44. Martianov I, Fimia GM, Dierich A, Parvinen M, Sassone-Corsi P, et al. (2001) Late arrest of spermiogenesis and germ cell apoptosis in mice lacking the TBP-like TLF/TRF2 gene. Mol Cell 7: 509–515.
45. Zhang D, Penttila TL, Morris PL, Teichmann M, Roeder RG (2001) Spermiogenesis deficiency in mice lacking the Trf2 gene. Science 292: 1153–1155.
46. Ruggiu M, Speed R, Taggart M, McKay SJ, Kilanowski F, et al. (1997) The mouse Dazla gene encodes a cytoplasmic protein essential for gametogenesis. Nature 389: 73–77.
47. Tanaka SS, Toyooka Y, Akasu R, Katoh-Fukui Y, Nakahara Y, et al. (2000) The mouse homolog of Drosophila Vasa is required for the development of male germ cells. Genes Dev 14: 841–853.
48. Dix DJ, Allen JW, Collins BW, Mori C, Nakamura N, et al. (1996) Targeted gene disruption of Hsp70-2 results in failed meiosis, germ cell apoptosis, and male infertility. Proc Natl Acad Sci U S A 93: 3264–3268.
49. Zhu D, Dix DJ, Eddy EM (1997) HSP70-2 is required for CDC2 kinase activity in meiosis I of mouse spermatocytes. Development 124: 3007–3014.
50. Liu D, Matzuk MM, Sung WK, Guo Q, Wang P, et al. (1998) Cyclin A1 is required for meiosis in the male mouse. Nat Genet 20: 377–380.
51. Liu Z, Zhou S, Liao L, Chen X, Meistrich M, et al. (2009) The Jmjd1a demethylase-regulated histone modification is essential for crem-regulated gene expression and spermatogenesis. J Biol Chem.
52. Tachibana M, Nozaki M, Takeda N, Shinkai Y (2007) Functional dynamics of H3K9 methylation during meiotic prophase progression. EMBO J 26: 3346–3359.
53. Castranio T, Mishina Y (2009) Bmp2 is required for cephalic neural tube closure in the mouse. Dev Dyn 238: 110–122.
54. Uchimura T, Komatsu Y, Tanaka M, McCann KL, Mishina Y (2009) Bmp2 and Bmp4 genetically interact to support multiple aspects of mouse development including functional heart development. Genesis 47: 374–384.
55. Dunn NR, Winnier GE, Hargett LK, Schrick JJ, Fogo AB, et al. (1997) Haploinsufficient phenotypes in Bmp4 heterozygous null mice and modification by mutations in Gli3 and Alx4. Dev Biol 188: 235–247.
56. Wyatt AW, Osborne RJ, Stewart H, Ragge NK (2010) Bone morphogenetic protein 7 (BMP7) mutations are associated with variable ocular, brain, ear, palate, and skeletal anomalies. Hum Mutat 31: 781–787. 10.1002/humu.21280 [doi].
57. van Heyningen V, Yeyati PL (2004) Mechanisms of non-Mendelian inheritance in genetic disease. Hum Mol Genet 13 Spec No 2: R225–R233.
58. Sinha KM, Yasuda H, Coombes MM, Dent SY, de CB (2010) Regulation of the osteoblast-specific transcription factor Osterix by NO66, a Jumonji family histone demethylase. EMBO J 29: 68–79. emboj2009332 [pii];10.1038/emboj.2009.332 [doi].
59. Raya A, Kawakami Y, Rodriguez-Esteban C, Ibanes M, Rasskin-Gutman D, et al. (2004) Notch activity acts as a sensor for extracellular calcium during vertebrate left-right determination. Nature 427: 121–128.
60. Wang S, Yu X, Zhang T, Zhang X, Zhang Z, et al. (2004) Chick Pcl2 regulates the left-right asymmetry by repressing Shh expression in Hensen's node. Development 131: 4381–4391.
61. Tsukada Y, Fang J, Erdjument-Bromage H, Warren ME, Borchers CH, et al. (2006) Histone demethylation by a family of JmjC domain-containing proteins. Nature 439: 811–816.
62. Li MO, Sarkisian MR, Mehal WZ, Rakic P, Flavell RA (2003) Phosphatidylserine receptor is required for clearance of apoptotic cells. Science 302: 1560–1563.

Figure S1

A

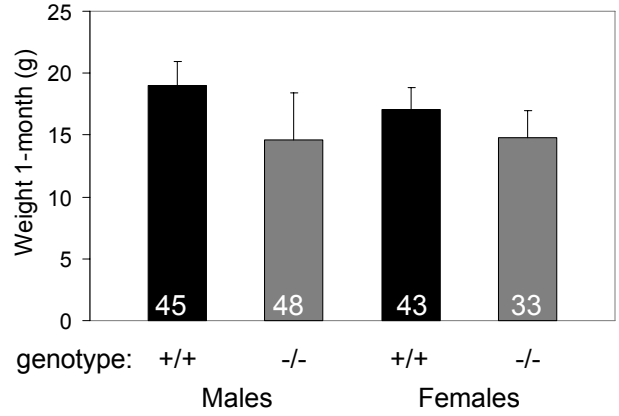
Weight 1-month (g)
25
20
15
10
5
0
45
48
43
33
genotype: +/+ -/- +/+ -/-
Males
Females

B

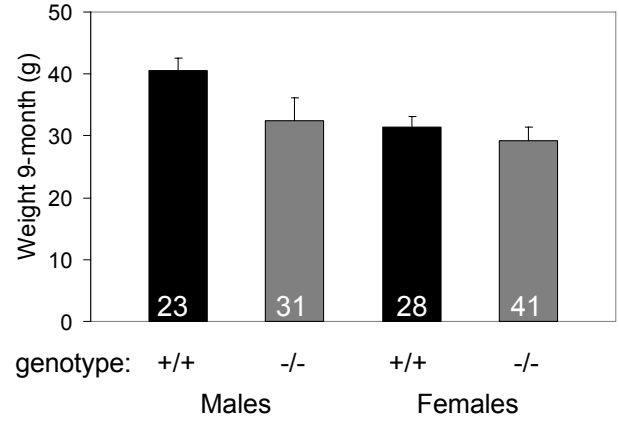
Weight 9-month (g)
50
40
30
20
10
0
23
31
28
41
genotype: +/+ -/- +/+ -/-
Males
Females

Figure S2

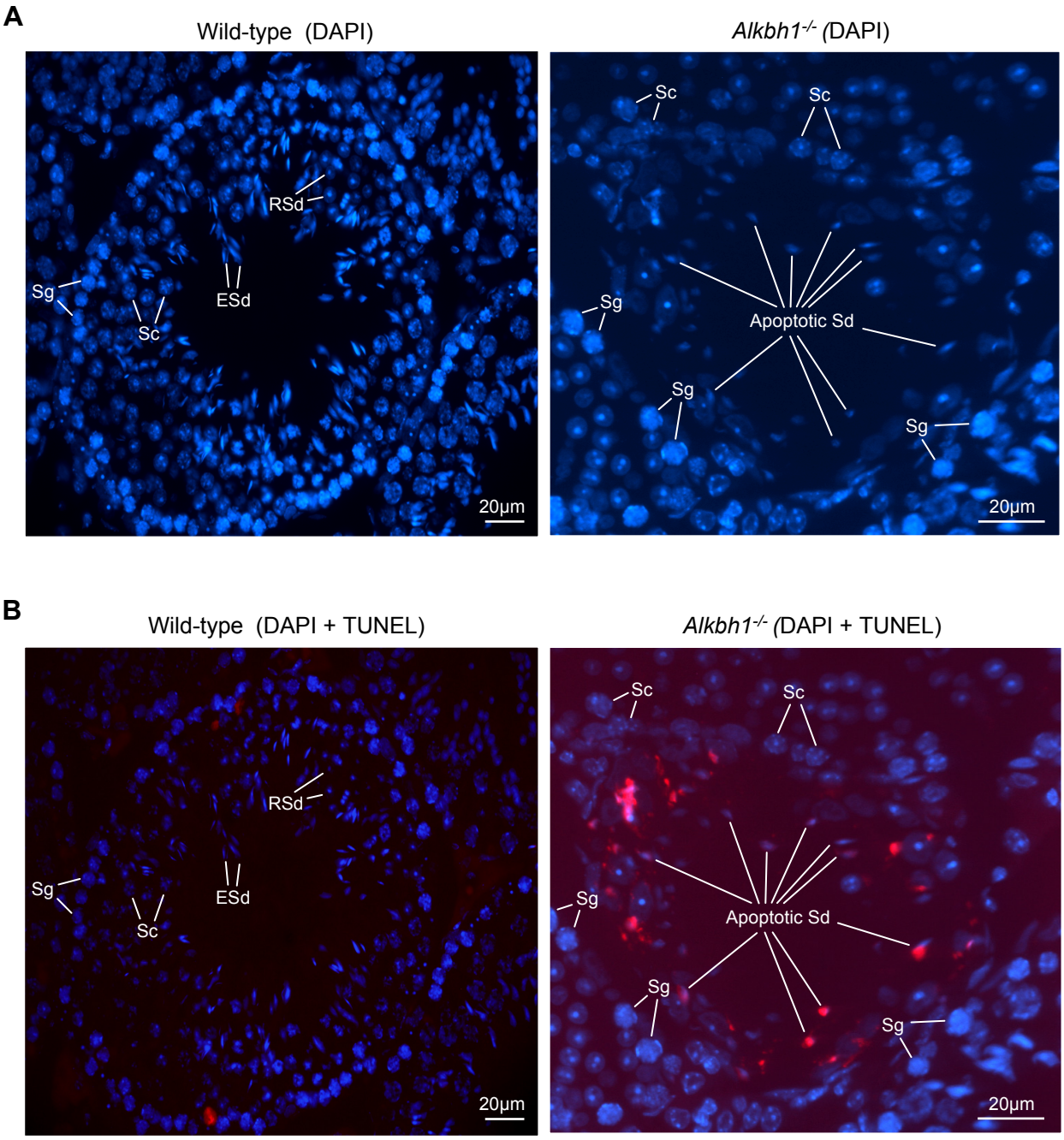
A
Wild-type (DAPI)
Alkbh1-/- (DAPI)
RSd
ESd
Sg
Sc
Apoptotic Sd
20μm
B
Wild-type (DAPI + TUNEL)
Alkbh1-/- (DAPI + TUNEL)

Figure S3

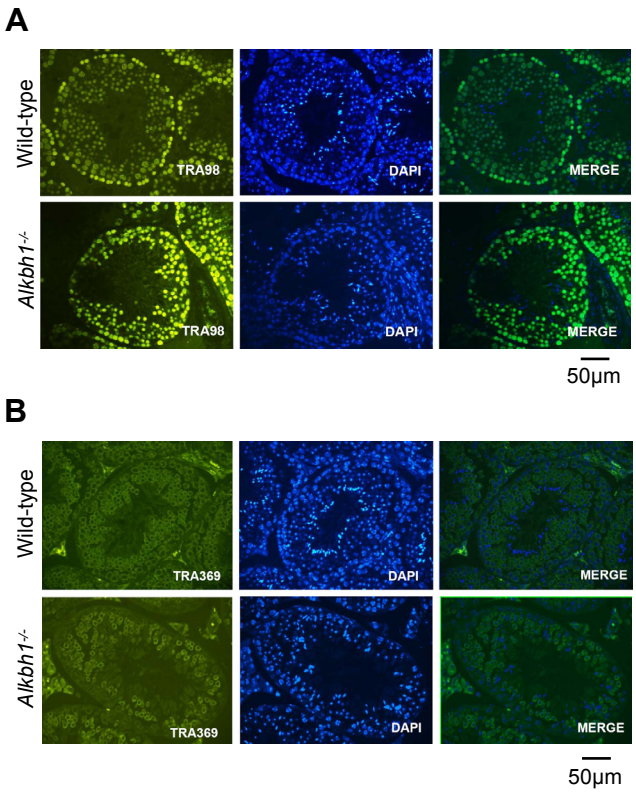
A
Wild-type
Alkbh1-/-
TRA98
DAPI
MERGE
TRA98
DAPI
MERGE
50μm
B
Wild-type
Alkbh1-/-
TRA369
DAPI
MERGE
TRA369
DAPI
MERGE
50μm

Figure S4

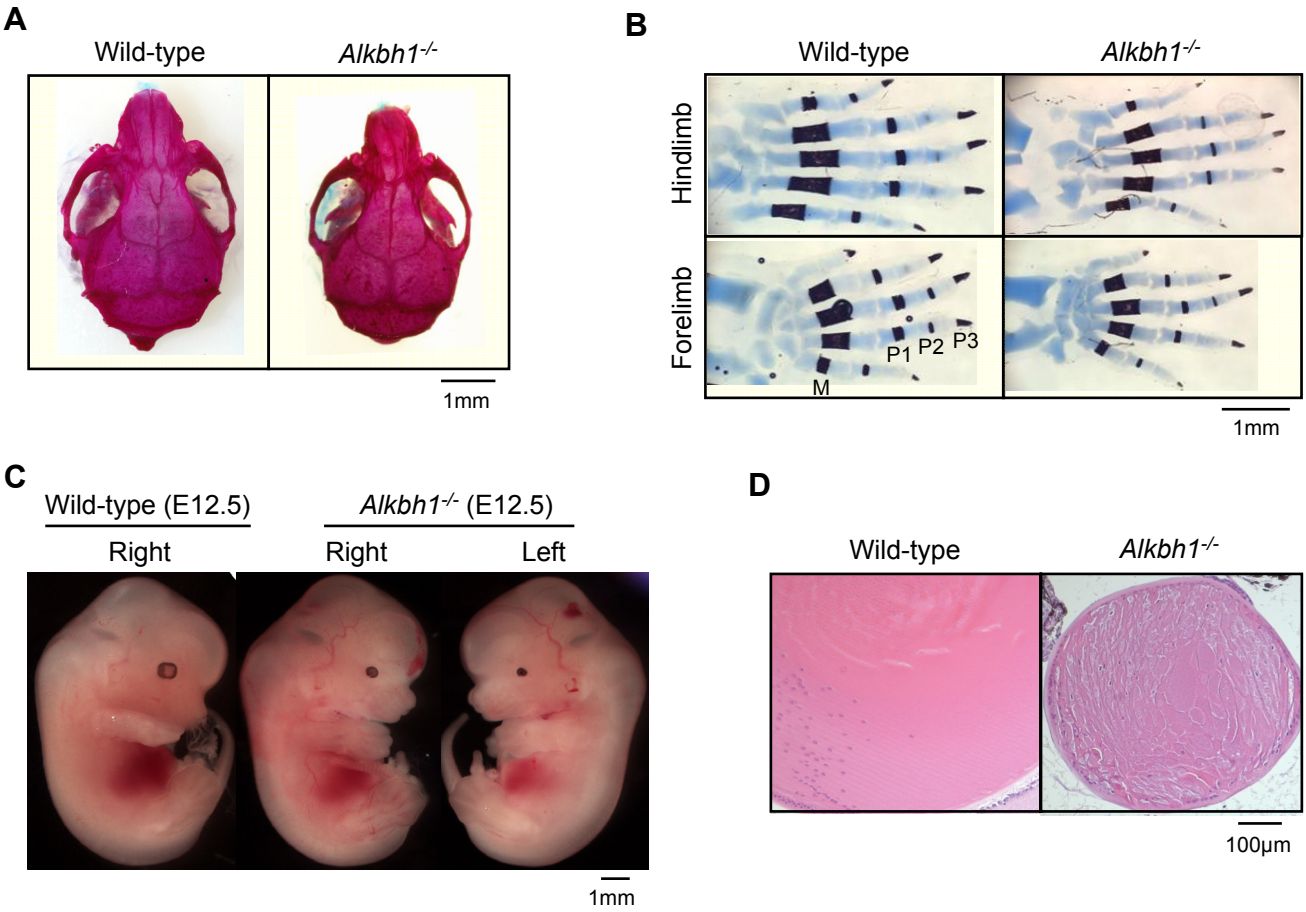
A
Wild-type
Alkbh1-/-
1mm
B
Wild-type
Alkbh1-/-
Hindlimb
Forelimb
P1 P2 P3
M
1mm
C
Wild-type (E12.5)
Alkbh1-/- (E12.5)
Right
Right
Left
1mm
D
Wild-type
Alkbh1-/-
100μm

Table S1

Parametric p-value	Parametric FDR corrected p-value	Geom mean of intensities in KO	Geom mean of intensities in WT	Ratio of geom means KO/WT	Probe set	Gene Symbol	Gene Title
8,40E-06	8,99E-06	64,6	23	2,809	1425863_a_at	Ptpro	Protein tyrosine phosphatase, receptor type, O
4,21E-05	3,59E-05	6430,3	3490,6	1,842	1429323_at	1700001E04Rik	RIKEN cDNA 1700001E04 gene
4,22E-05	4,49E-05	378	218,3	1,732	1431975_at	4930521O11Rik	RIKEN cDNA 4930521O11 gene
1,81E-05	2,70E-05	1732,1	1112,2	1,557	1429755_a_at	4933406F09Rik	RIKEN cDNA 4933406F09 gene
4,46E-05	5,39E-05	72,7	52,8	1,377	1451905_a_at	Mx1	Myxovirus (influenza virus) resistance 1